Sur la rupture des couches minces : une approche variationnelle

Andreés Alessandro León Baldelli

Thèse de Doctorat
de l'Université Pierre et Marie Curie


Discipline : Mécanique
École Doctorale de Sciences Mécaniques, Acoustique, Électronique et Robotique de Paris (SMAER)
présentée par :

Andrés A. León Baldelli

pour obtenir le grade de Docteur de l'Université Pierre et Marie Curie

---

On Fracture of Thin Films: a Variational Approach

Sur la rupture des couches minces : une approche variationnelle

---

dirigée par Jean-Jacques Marigo et Corrado Maurini
à l'Institut Jean le Rond d'Alembert

Soutenue le 23 septembre 2013
devant le jury composé de :

M. Kaushik Bhattacharya	rapporteur
M. Christian Dascalu	examinateur
M. Jean-Jacques Marigo	directeur de thèse
M. Corrado Maurini	co-directeur
M.me Maria Giovanna Mora	examinateur
M. Stéphane Pagano	rapporteur
M. Benoit Roman	examinateur
M. Stéphane Roux	examinateur

This page intentionally left blank.

Abstract

We study the problem of fracture in thin film systems subject to tensile stresses originated by mechanical loading or inelastic phenomena, due *e.g.* to thermal or moisture couplings. In such systems, homogeneous loads lead to the nucleation of interacting transverse and debonding cracks, producing auto-structuration of quasi-periodic crack networks and propagation of complex patterns showing robust morphological features. We tackle the problem of describing the irreversible evolution of fractures, covering the phases of crack nucleation, path selection and irreversible evolution in space and time.

Available literature results rely upon phenomenological models lacking rigorous derivation and are limited to simple geometrical settings. In addition, problems of nucleation of new cracks, mechanisms of path selection and irreversible, non-smooth evolution in space and time are not explored, due to the limitations of to classical theory of fracture mechanics.

We propose the derivation of a limit, asymptotic, reduced-dimension, global, variational, theory for fracture of thin films starting from three-dimensional brittle elasticity within the framework of variational fracture, using notions of variational convergence. We then introduce a regularization of the limit fracture problem, by the means of a damage gradient functional, suitable to the numerical solution by finite elements.

The proposed work allows to obtain a systematic understanding of the competition between various mechanisms including fracture and debonding; to rigorously establish a reduced, variational, asymptotic model, valid for thin films that is rich enough to capture the important physics of failure; and to tackle a detailed numerical study of the complex cracking and debonding patterns observed in thin film systems.

Keywords: fracture, variational mechanics, thin films, singular perturbation, asymptotic analysis, dimension reduction, Γ-convergence, damage models, finite elements.

Résumé

Nous étudions le problème de rupture des systèmes de couches minces soumis à contraintes de tension dues aux chargements mécaniques ou à d'autres phénomènes élastiques, associés *e.g.* à couplages thérmiques où humidité. Dans ces systèmes, chargements homogènes conduisent à la nucléation de fissures interagissantes transverses et de décollement, produisant l'auto-structuration de réseaux de fissures quasi-périodiques et la propagation de patterns complexes qui montrent caractéristiques morphologiques robustes. On s'intéresse à décrire l'évolution de ces fissures, en prenant en compte les phases de nucléation, sélection du trajet de fissure et évolution irreversible en espace et en temps.

Les résultats disponibles en littérature se basent sur des modèles phénoménologiques, dépourvus d'une dérivation rigoureuse, et sont limités à des cas géométriquement simples. Dans ces derniers, le problème de nucléation, les mécanismes de sélection du chemin de fissuration et l'évolution non régulière en espace et en temps ne sont pas explorés, à cause des limitations de la théorie classique de la mécanique de la rupture.

Nous proposons la dérivation d'une théorie variationnelle asymptotique, bidimensionnelle et globale, à partir d'un problème tridimensionnel d'élasticité fragile dans le cadre de l'approche variationnelle à la mécanique de la rupture, en faisant intervenir une notion de convergence variationnelle. Ensuite, nous introduisons une régularisation du problème faible de rupture par le moyen d'un modèle en gradient d'endommagement, adapté à la solution numérique *via* la méthode des éléments finis. Le travail proposé permet d'obtenir une compréhension des mécanismes couplés élastiques, de fissuration et décollement; d'établir un modèle asymptotique, réduit et variationnel, valable pour des systèmes de couches minces suffisamment riche pour capturer les mécanismes physiques essentiels; et d'aborder une étude détaillé des expériences numériques qui révèlent les patterns complexes de fissures observés dans les systèmes de couches minces.

Mots-clés: rupture, mécanique variationnelle, couches minces, perturbation singulières, analyse asymptotique, réduction de dimension, Γ-convergence, modèles d'endommagement, élements finis.

Riassunto

Studiamo il fenomeni di frattura in sistemi di film sottili soggetti a tensione derivante da carichi meccanici o altri processi inelastici, dovuti ad esempio ad accoppiamento termico o ad umidità. In questi sistemi, carichi omogenei conducono alla nucleazione di fessure interagenti, trasverse e di decoesione interfacciale, producendo un'auto-strutturazione di fratture quasi-periodiche e la propagazione di *pattern* complessi dalle proprietà morfologiche robuste. Affrontiamo il problema della descrizione dell'evoluzione irreversibile delle fratture, abbracciando le fasi di nucleazione, selezione del percorso di fessura ed evoluzione irreversibile in spazio e tempo.

Risultati precedenti in letteratura si basano su modelli fenomenologici, sprovvisti di derivazione rigorosa, e sono limitati a casi geometricamente semplici. Inoltre, il problema della nucleazione di nuove fessure, i meccanismi di selezione del percorso e la sua evoluzione non-regolare in spazio e tempo non sono esplorati a causa delle limitazioni della teoria classica della meccanica della frattura.

Proponiamo la derivazione di una teoria asintotica, a dimensione ridotta, globale e variazionale, per studiare la frattura dei film sottili usando nozioni di convergenza variazionale. Infine, introduciamo una regolarizzazione del problema di frattura, attraverso modelli di danno a gradiente, adatto alla soluzione numerica discretizzata. Il lavoro proposto permette di ottenere una comprensione della competizione tra elasticità, fessurazione trasversa e decoesione interfacciale; di stabilire un modello ridotto, variazionale ed asintotico, valido per film sottili fragili, sufficientemente ricco da catturare gli elementi essenziali della fisica della rottura; e di affrontare uno studio numerico dettagliato dei complessi *pattern* di frattura e decoesione osservati nei sistemi di film sottili.

Parole chiave: rottura, meccanica variazionale, film sottili, perturbazioni singolari, analisi asintotica, riduzione di dimensione, Γ-convergenza, modelli di danno, elementi finiti.

Resumen

Estudiamos los fenómenos de ruptura en sistemas de capas delgadas sometidos a tensión, originada por cargas mecánicas u otros procesos inélasticos, debidos, por ejemplo, a acoplamientos térmicos o humedad. En estos sistemas, cargas homogeneas conducen a la nucleación de grietas transversas y decohésion interfacial, produciendo un auto-estructuración de redes de grietas casi-periódicas y la propagación de *pattern* complejos caracterizados por propriedades morfológicas robustas. Describimos la evolución irreversible de las grietas, abrazando las fases de nucleación, de selección del trayecto y de evolución irreversible en espacio y tiempo.

Se han reportado resultados en la literatura basados en modelos fenomenológicos que carecen de derivacion rigurosa y se limitan a casos geométricamente simples. Además, debido a las limitaciones de la teoria clasica de la mecànica de la ruptura, no se exploran la fase de nucleacion de nuevas grietas, los mecanismos de selección del trayecto y la evolucion irregular en espacio y tiempo.

Proponemos la derivación de una teoria asintotica global, en dimensión reducida y variacional, para estudiar la ruptura de capas delgadas utilizando nociones de convergencia variacional. Por ultimo, introducimos una regularización de el problema límite de ruptura, por medio de modelos regularizados a gradiente de daño, adapta para la solución numérica discretizada. El trabajo propuesto permite de comprender la competición entre elasticidad, ruptura transversa y decoesión; de establecer un modelo reducido, variacional y asintotico, valido para sistemas de capas delgadas y suficientemente rico para capturar los elementos esenciales de la física de la ruptura. También permite realizar un estudio detallado de los complejos patterns de grietas y decoesión experimentalmente observados.

Palabras clave: ruptura, problema variacional, capas delgadas, perturbaciónes singulares, problema asintotico, reducción de dimension, Γ-convergencia, modelos de daño, elementos finitos.

Acknowledgements

It is my pleasure to thank those people who have been by my side during these enriching three years of life. First, I would like to thank my thesis directors, Jean-Jacques Marigo and Corrado Maurini. Jean-Jacques, it has been such a privilege working by your side, you enlightening the path. You are a constant inspiration for your theoretical depth, pedagogical wisdom and overwhelming passion. With patient dedication, you opened new eyes upon the interpretation of Nature. Corrado, with daily presence, you have has been a guide through this passionating and enlightening scientific journey.

To my directors goes my deepest esteem, as they always inspired me to give the best of myself.

I would like to thank the members of the scientific committee that has evaluated this work: M.G. Mora, B. Roman, C. Dascalu and S. Roux, and especially K. Bhattacharya and S. Pagano who have accepted to report on the thesis. I will make treasure of your comments and suggestions.

I have had the pleasure to work by the side of a number of scientists, a special mention goes to Blaise Bourdin, who has so warmly welcomed as I moved my first steps into the numerics. I also credit Jean-François Babadjian and Duvan Henao Manrique, for shedding light into the insights of variational convergence; and Benoit Roman and Joël Marthelot, for allowing me to "see" and "touch" an asymptotic limit. From your presence and support I have learned so much.

I would like to thank all the colleagues, professors and researchers at the "Institut Jean le Rond d'Alembert", where most of the work has been carried. In this work, all the illuminating discussions I had with you find their place. In particular, I am deeply indebted to Joël Frelat: you have been a precious friend and provided me invaluable support, since the eve of my thesis and in all of its facets.

Heartfelt thanks go to Marco Rivetti, Mélodie Monteil, Stéphane Monté and Federico Bianco: you are not only enriching colleagues, but most of all precious friends.

With Federico and Stefania, we shared such an important part of our lives, in time and space. Our indefatigable discussions and her unconditional love and support have turn an apartment into our *home*.

I greatly value the time spent with Aisling Ní Annaidh, Ata Mesgarnejad, Zubaer Hossain and Paul Sicsic: although short, it leaves a deep mark. Also, I owe so much to you, Michelle and Livia, for feeding me with your creativity along these years.

My words fail to express my emotion of seeing my beloved friends on the day of my defense: Giorgio, Umberto (we were kids!), Marta and Alessandra (Paris and I missed you), Sebastien (unexpected!), and Laura (folded in my pocket). That feeling is my greatest reward.

My last thanks go to my family, reunited for the important day of my defense: with my deepest love, this work is dedicated to you.

Was Vernünftig ist, das ist Wirklich;
und was Wirklich ist, das ist Vernünftig.

GWF Hegel,
Berlin, 1821

This page intentionally left blank.

Contents

Contents **v**

Preamble **1**
Notation . . . 13

1 Introduction to variational fracture **15**
1.1 Elements of variational fracture mechanics . . . 15
1.2 Variational fracture mechanics of thin films . . . 21
1.2.1 The general setting: three-dimensional brittle system . . . 21
1.2.2 The scalar case . . . 24
1.2.3 Static fracture problem . . . 24
1.2.4 Quasi-static evolution problem . . . 25

2 The one-dimensional film **27**
2.1 A simplified one-dimensional model . . . 30
2.1.1 Dimensional analysis . . . 32
2.2 The static problem: energy minimizers at fixed load . . . 33
2.2.1 The sound elastic film . . . 33
2.2.2 The debonding problem . . . 35
2.2.3 The transverse fracture problem . . . 40
2.2.4 Coupled transverse fracture and debonding . . . 42
2.3 The quasi-static evolution problem . . . 48
2.3.1 Evolution of transverse cracks . . . 48
2.3.2 Evolution of debonding . . . 49
2.3.3 Film subject to coupled transverse cracks and debonding . . . 50
2.3.4 Comments and extensions . . . 51
2.4 Conclusions of the chapter . . . 56
2.A Properties of the minimizers . . . 57

3 Derivation of the limit models **61**
3.1 A parametric asymptotic study in scalar elasticity . . . 65
3.1.1 Rescaling of the problem . . . 68
3.1.2 The open half space $\delta > 0$. . . . 71
3.1.3 The closed half space $\delta \leq 0$. . . . 71

3.1.4 The open half space $\delta < 0$. 72
3.1.5 The straight line $\delta = 0$. 75
3.1.6 The energy of the two-dimensional limit model 83
3.2 A reduced dimension theory for thin films in vector elasticity 85
3.2.1 Identification of the cascade problems 89
3.2.2 Comments and extensions 94
3.3 Brittle thin films in scalar elasticity 97
3.3.1 Constitutive assumptions 97
3.3.2 Variational formulation in SBV 98
3.4 Brittle thin films, application in two-dimensional vectorial elasticity . . . 107
3.4.1 The reduced limit energy in two-dimensional vectorial elasticity . 107
3.4.2 Nondimensionalization and free parameters 109
3.4.3 Formulation of the reduced problem 109
3.5 Conclusions of the chapter 111
3.A Proof of the dimensional reduction for scalar elasticity 113
3.B Spaces of functions with measure derivatives 120

4 Exploring crack patterns: numerical experiments **121**
4.1 The regularized energy 124
4.2 The regularized formulation 127
4.2.1 Mechanical interpretation of the regularized model with local minimization 130
4.3 Numerical experiments 131
4.3.1 Multiple cracking and debonding of a slender strip 131
4.3.2 Multiple cracking and debonding of a thin disk 139
4.3.3 Vinyl lettering on a metal substrate 144
4.3.4 *Ouverture*: a strongly coupled two-dimensional pattern 148
4.4 Conclusions of the chapter 150

Conclusions and perspectives **153**

A Scientific contribution **157**

References **158**

Preamble

Cracking of thin films systems is often experienced in everyday life. Ceramic painted artifacts, coated materials, stickers, paintings and muds are some of the physical systems that exhibit the appearance of complex networks of cracks, channeling through the topmost layer in the stack. In addition, the phenomenology is enriched by the possible interplay with mechanisms of spontaneous interfacial decohesion. Since the 1980's, when the technology of thin films started to have an extensive presence in industrial applications, a systematic study of fracture mechanics of film-substrate systems has begun. Thin films are grown on substrates for many technological applications. Examples include coatings as thermal barriers on superalloys in engines, silicon nitride films as environmental barriers on metals, polymers in microprocessors and thin films as optoelectronic materials on substrates in light-emitting diodes. The mechanical performance of thin films under severe environmental conditions often dictates design, and their integrity often ensures efficiency of the whole structure. Under these conditions, residual stresses may arise due to the deposition techniques or multi-physical couplings involving thermal effects, humidity and mechanical loadings, causing cracks to grow in the film, in the substrate, or both. An extensive review of common fracture patterns is given in [HS91]. Figure 1 illustrates the fracture of a thin film and its debonding from the substrate. A thin vinyl sticker is bonded onto a metal panel and exposed to atmospheric conditions. Among others effects, the incident radiation from the sun generates inelastic mismatch strains leading to transverse cracking and debonding. A closer examination leads to observe some properties. Cracks within the film are essentially transverse to the plane and completely cut the film along its thickness. In addition, although the corners and the associated stress concentration favor the growth of cracks, these are also present along smooth boundaries away from singular points. Debonding, where present, appears at the boundaries of the film and by the trace of glue left on the panel, one argues that the deformations are induced by inelastic shrinkage stresses, *i.e.* stresses are tensile.

The mechanical description. A vast share of the scientific literature has, ever since the first technological applications, focused on the description of the phenomenology induced by the fracture in thin film-substrate systems.

Let us picture the system of Figure 1 in its initial state, *i.e.* before cracks appear. If one is *sufficiently* away from the boundaries, the state of stress–and to some larger extent–the *state* of the system is reasonably supposed to be homogeneous. This is understood when inelastic strains are imposed as a consequence of a thermal load. Such

inelastic strains are due to a temperature change in circumstances where there exists a mismatch between the thermal expansion coefficients of the layers. Such stresses are constant provided that the system is in thermal equilibrium.

After cracks appear, the picture is much more complex. Cracks nucleate and propagate, intersect, coalesce and branch, further defining angles and directions, drawing shapes and forming patterns. The latter may be almost $1D$ or essentially $2D$, depending on the loading conditions and the symmetries of the system.

A vast literature based on approaches typical of classical linear fracture mechanics, ascribed to Griffith [Gri21], is devoted to give a theoretical insight and to interpret the observations.

The origin of stresses. The development of stresses in thin film systems is associated to different physical mechanisms; an overview is given in [Hut96]. Residual stresses in working conditions are often generated by the technological process of production or deposition of the layers. Sputtering, spraying, vapor or epitaxial deposition and spin coating may produce non-homogeneous residual stresses that are difficult to characterize. On the other hand, mechanical stresses during operating conditions of the final assembly are transferred from the structure, which carries the working loads, to the superficial layers. Since often the underlying structure is much more rigid than the coating films, it can be assumed, at a first order approximation, that the overlying thin film system is driven by an imposed displacement at the interface with the substrate. In this sense, the presence of the film system can be neglected, at a first order, in the elastic response of the structure under its loads. In addition, stresses also develop because of thermal effects. A change of temperature from the deposition conditions (a natural stress-free state) rises significant stresses when the film and the substrate have different thermal expansion coefficients. When such mismatch is important, thermal stresses can lead to extensive cracking and debonding, see [HS91], [FS09]. Stresses of thermal origin are easier to control and characterize. Indeed, in a system whose displacement at the boundaries is left free (hence natural stress-free boundary conditions are satisfied at equilibrium), the stress state is homogeneous away from the boundaries. The homogeneity, as it will be discussed in the following, although allows for an easy characterization of the stress state, it engenders important difficulties in the mechanical modeling of fracture processes. Also localized stresses can be obtained through *e.g.* instrumented indentation [FS09] leading to, for instance, annular concentric and star-shaped crack patterns [Rhe+01]. The compressive *vs* tensile nature of stresses determines different failure patterns. When stresses are compressive, the dominant mechanisms are related to bucking-driven delamination [CC00] and bulging, whereas when stresses are tensile, channel and surface cracking [YSE92], spalling and interface debonding [DTE88], [CK92], [YH03], [CE03] are common failure mechanisms, see [NE93], [Hut96] for a general overview of crack patterns.

Nucleation and the role of initial flaws. The first systematic studies of the problem of fracture in thin films lay within Griffith's classical theory of fracture mechanics [Gri21].

This theory provides a means to investigate the conditions under which an existing crack will propagate along a given path, essentially by the means of an energy balance. The propagation criterion has a clear interpretation in two-dimensions. Consider a body $\overline{\Omega} \subset \mathbb{R}^2$ under an applied displacement load parametrized by a scalar t along a portion $\partial_D\overline{\Omega}$ of its boundary, and with imposed force vanishing (to fix ideas) along the complement to the entire boundary $\partial_N\Omega = \partial\overline{\Omega} \setminus \partial_D\Omega$. Let the crack path be given, *i.e.* Γ is a known curve $\Gamma \subset \Omega$. The position of the crack tip along Γ can be parametrized by t, so that $l(t)$ identifies its position along the propagation. In correspondence to the equilibrium configuration, the elastic energy of the body $\mathcal{P}(t, l(t))$ is a function of the load and crack length. The classical Griffith's criterion states that the propagation of a preexisting crack, of initial length $a_0 > 0$, takes place whenever the elastic energy released for an infinitesimal crack advance, *i.e.* the quantity $-\partial\mathcal{P}(t, l(t))/\partial l(t)$, bounded from above by a constant *i.e.* the material toughness G_c, reaches its critical value. That is, when the equality $-\partial\mathcal{P}(t, l(t))/\partial l(t) = G_c$ is satisfied.

It is reasonable to assume that inhomogeneities exist in the film system at a sufficiently small scale. Within Griffith's theory, the existence of macroscopic cracks is assumed to derive from the growth of small-scale defects. The energy release rates associated to an initial flaw (of length a_0) are computed in [TPI00] for various crack configurations, generally in infinite or semi-infinite two-dimensional bodies. Considering a cross section of a film system, hence assuming underlying translational invariance with respect to one direction along the middle plane of the film, in [Beu92] the same type of results are obtained considering the elastic mismatch between the layer, accounted for by the Dundurs' parameters [Dun69]. Referring to Figure 2(a), the cited works focus on the computation of the energy release rate of an initial flaw of length a_0, along the prescribed vertical segment, for $a_0 \leq a \leq h_f$, where h_f is the thickness of the layer.

The formation of the first channel crack is associated to the putative "worst defect". However, since the control of the fine geometric features of initial flaws is out of reach, any criterion in which the knowledge of the fine details of the microscopic scale is necessary, not only is unusable from the practical standpoint, also contradicts with the macroscopic and global essence of Griffith's theory.

The analysis of the extension of small-scale cracks is therefore abandoned in favor of the study of the propagation of flaws fully developed along the thickness; that is, of macroscopic cracks approaching a free boundary, see Figure 2(b). Usable arguments, from an engineering standpoint, are constructed considering pre-existing macroscopic initial cracks. The computation of the energy release rates for channeling cracks (*i.e.* with $a_0 = h_f$) that elongate laterally within the film, starting from a free boundary, is performed in [HS91]. Moreover, the concept of "steady-state cracking" is first formulated. It is noted, in fact, that the energy release rate attains an asymptotic value as soon as a crack, starting from a free boundary, spans a length larger than several film thicknesses. The only length that explicitly appears in the propagation condition $-\partial\mathcal{P}(t, l(t))/\partial l(t) = G_c$ is then h_f. This allows the establishment of usable criteria for fail-safe design of multilayer composites with macroscopic initial cracks, identifying a "critical thickness" h_c, below which no crack is expected to extend when the system is subject to a given load. These criteria are usually stated with a relation of the following

type (see [HS91], [HS93]):

$$Z = G_c/(h_f {e_0}^2 E_f), \tag{1}$$

where e_0 is the intensity of the equi-biaxial inelastic (*e.g.* thermal) strain, E_f the Young modulus of the film and Z (or Ω_c as first labeled in [EDH88]) is a non-dimensional "cracking number" of order unity depending upon the elastic and brittle properties of the multilayer [LHE95]. Its value roughly classifies also the resulting fracture pattern [HS91], [YSE92]. Such criterion provides a design specification on the film thickness h_f against cracking with a given pattern Z, for loads up to e_0. Subsequently, [Suo01] derives the energy release rates computing singular crack tip fields for straight and kinking interfacial and channeling cracks, by the means of the celebrated Irwin's formula [Irw58] which relates local quantities computed around the crack tip to the global energy release rate. Such quantities are computed as functions of the Dundurs' parameters [Dun69], measuring the elastic mismatch between the layers.

The study of the propagation of fully developed cracks is soon enriched with new elements such as plastic yielding [BK96] and buckling [HS91], [SF93], [CC00]. FEM computations are performed in [BK96] to obtain results similar to [Beu92] accounting for perfect and hardening plasticity with a shear-lag model [Cox52].

Another important failure mechanism of film/substrate composites is extensive debonding due to residual stresses [YH03]. Since solving the problem of nucleation is out of reach, debonding is considered the consequence of kinking of a fully developed crack into a plane parallel to the layer interface. Analysis of debonding is tackled in [DTE88], [JHK90], [CK92], [NM96], [YH03]. The results of these studies provide debonding crack propagation criteria, local stress intensity factors, debonded areas and their shapes as a function of the applied load and elastic mismatch. In [VMA99] debonding due to compressive stresses (and buckling) is numerically simulated via a FEM approach upon the assumption of an ad-hoc initial distribution of debonded zones at the interface.

All the cited studies, intended to provide a design criterion in order to avoid cracking in multiple circumstances, rest on the postulated existence of macroscopic fully developed cracks. However, in [LHE95] it is experimentally proved that, although the suggested criterion can conservatively account for propagation of existing macroscopic cracks, it cannot capture the critical loads of a macroscopically homogeneous body, still being supposedly associated to flaws at sufficiently small scales. Hence, the apparent size effect associated to the film thickness, the essence of (1), does not explain macroscopic cracking in homogeneous bodies and the complete knowledge of initial flaws is claimed to be essential for the understanding onset of cracks. However, in these situations a robust novel feature emerges. The experimental campaign in [LHE95], shows that in situations where the state of the system is homogeneous at the macroscopic scale (*i.e.* no fully developed cracks exist), cracks form at loads much higher than those predicted by (1) and are robustly arranged in a periodic array, see Figure 3. A notion of macroscopic "pattern" appears, weakening the direct causal relation between the local microscopic nature of small scale defects and the emergent large-scale features. Owing to these observations, the presence of cracks, fully developed along the film thickness, perpendicular to the interface and already arranged into a macroscopic equi-distributed pattern, is taken

as starting assumption in [HS91], [TOG92], [Tho+11] to study the evolution of the crack spacing. Criteria of energy balance and maximum stress are used in [Hsu01] and [SSF00] to compare one-dimensional theoretical results for crack arrays to one- ad two-dimensional experiments, respectively. To this scenario [BM07] adds an elasto-plastic phenomenological law for the interface whereas [AJB02] is concerned with periodic arrays of cracks competing with an underlying periodic material structure.

The equi-distributed arrangement is only one of the most commonly observed crack patterns. The universal non-dimensional number Z [Eva89], [HS91] is used to roughly classify regimes of cracking: debonding, spalling, substrate damage, channeling and superficial cracks.

Intense efforts were hence spent to study the patterns themselves by the means of numeric techniques. The implementation of phenomenological spring-network models, whose pioneering work is [Mea87], has been exploited to attempt to simulate the evolution of crack patterns in thin films. More recently and in the same spirit, in [HSB96], [CB97], [LN00] and [Kit11], an elementary spring network with nearest-neighbor interactions represents the continuous system, the interaction with the substrate is accounted for by a discrete linear elastic potential. A different wake in numerics follows the works of [Hua+03] and [Lia03] which propose a numerical treatment of complex $2D$ crack patterns within the framework of XFEM. In all the works cited above, to palliate the inability of the classical theory of fracture to account for nucleation, one (or many) initial cracks (with a given size, distribution and shape), or a probabilistic dispersion of the relevant quantities (*e.g.* the toughness) via *ad hoc* PDF laws are needed to trigger cracking. Consequently, the fine mechanisms of nucleation leading to the macro-scale structure of the crack pattern are hidden within the properties of the probabilistic distribution of micro-scale inhomogeneities.

From the theoretical standpoint, [XH00] proposes a *reduced* two-dimensional effective model for thin film systems, further studying the propagation of some of the commonly observed crack patterns. Under suitable additional hypotheses, the authors investigate the steady-state propagation of single and array of cracks, illustrate the interaction between parallel or perpendicular neighboring cracks and show the existence of a particular solution which corresponds to an Archimedean-spiral-shaped crack, if sufficiently long macroscopic spiral-shaped initial cracks exist.

The theoretical works within the classical framework of linear fracture mechanics cited above, have dealt with the propagation (following the celebrated Griffith's criterion [Gri21]) of *pre-existing* cracks along *known* crack paths, the latter are either given explicitly or implicitly, by the means of additional *ad hoc* path selection (*i.e.* branching) criteria. However, the necessary assumptions of *a priori* knowledge of the crack path proper to the classical framework of fracture mechanics, not only hide the subtle mechanisms leading to emergence of crack patterns, but also constrain the analysis to very simple settings, forbidding the exploration and explanation of the observed complexity.

Indeed, the nucleation and the path selection phases are deeply related to the geometric features of the observed crack patterns, determining the non-homogeneous response, starting from a macroscopically homogeneous state. As the experimental evidence shows, at nucleation in a macroscopically homogeneous body, macroscopic

patterns emerge. The question whether such macroscopic patterns are dominated by microscopic (local) imperfections still remains open. In other words, notwithstanding the existence of microscopic defects, are those responsible of the macroscopic response or other mechanisms play this decisive role?

A global approach. From a different perspective, problems of localization (possibly with a notion of periodicity) and self-organization of patterns are much better understood in linear and nonlinear solid mechanics (*i.e.* without fractures) as the observable states selected by a stability criterion [Ngu00]. For instance, buckling in thin film systems [AB08a], [AB08b], [AB08c], localization of damage in softening materials [PMM11] focused reactive flows in geophysical systems [SL11], morphogenesis in nonlinearly elastic biological tissues [BG05], [BC13] are explained by this concept. In all such systems, size effects related to the existence of one (or several) internal length scales play an essential role in the stability properties of the admissible states. Consequently, localization, self-organization and the emergence of patterns are intimately linked to macroscopic size effects influencing the stability properties of the system. We may more reasonably suspect that the complexity of crack geometries (and all the phenomenology that ensues) springs rather from *global* structural properties than from *local* microscopic features. Indeed, thin film systems appear to belong to a wider class of systems encountered in nature. Consider the three examples in Figure 4.

The first image depicts the well known basaltic columns produced during the cooling and subsequent solidification lava flows [GMM09] by the propagation of a crack front along the vertical direction. Despite shrinking (due to the change of phase) can be accommodated vertically, on planes orthogonal to the thermal flow tensile stresses arise and are high enough to engender the extensive fracture front. As a consequence, columns appear as the fracture network propagates vertically, parallel to the direction of the thermal flow.

The second image depicts a glazed vase showing a crackled surface. Here, the aesthetic effect is produced by the differential inelastic deformations induced by the thermal treatment, leading the body to release its stored elastic energy by creating new free surfaces.

The last picture [Let+10], reports an example of fragmentation in a MEMS device. The thin film laying over a support under uni-axial tension shows a network of parallel cracks within the coating layer, perpendicular to the principal stress direction.

Although these three systems, and many others could be included in the list, evolve at different length scales, are characterized by different constitutive laws and multi-physical couplings, they all express a fundamental feature: the *existence of an intrinsic length scale*. This length scale fixes the diameter of the hexagonal cross section of the columns in Figure 4(a), the mean size of the cells at the surface of the vase in Figure 4(b) and the spacing of the quasi-periodic array of parallel cracks in Figure 4(c).

In all such systems, the presence of an intrinsic length scale appears as an essential and *global* feature manifested by the fracture processes, characterizing the regimes of

multiple cracking and leading to complex crack patterns that produce the periodic tessellation of the initially sound domain.

The existence of internal length scales and their consequences on the stability of admissible states are not only related, but, as it will be shown, are also necessary for the understanding of mechanisms of fracture in thin films.

The crack path is unknown. Since it is the crack pattern itself, with its complex phenomenology of nucleation and propagation, that essentially characterizes the multiple cracking and debonding regimes in thin film systems, it has to be taken into account as a genuine *unknown* of the problem. Instead of being postulated *a priori* or englobed within the fine properties of the ad hoc probabilistic distributions, its essential properties have to be obtained as an outcome of the study. This allows to identify the role of the interacting mechanisms that contribute to their determination.

The variational approach to fracture, as set forth in [FM98] and further developed in [BFM08], allows to naturally incorporate the crack path as an additional unknown to the elastic problem, and to handle the complexity of their evolution in time and space. More in general, this novel vision palliates the gaps in the classical theory of fracture mechanics related to the issues of nucleation, selection of crack paths and regularity of crack evolutions (in space and time), proposing a sound, global, macroscopic theory based on a rigorous mathematical variational formulation and springing from a basic principle of energy stability. It echoes the spirit of the seminal work of [Gri21] in which the crack propagation originates from an energy balance and is essentially opposite to the vision of the works that have followed the pioneering cited reference, which bring back the global energetic spirit to a local approach.

The key point in [FM98] and [BFM08] is showing that an energy argument can be used as a selection criterion among crack paths, with the quasi-static minimization of the energy of the system among admissible competitors (displacements and cracks). Assume that a body $\overline{\Omega}$ is in equilibrium under the load t applied its Dirichlet boundary $\partial_D\overline{\Omega}$ and is free at its complement $\partial_N = \partial\overline{\Omega} \setminus \partial_D\Omega$. The body may contain a crack Γ which defines the sound part of the body as the open set $\Omega \setminus \Gamma$. In this case the crack Γ is regarded as a genuine additional unknown to the displacement field u and both are sought as the pair minimizing the total energy of the body $E(u, \Gamma)$, among kinematically admissible displacements and cracks within Ω. The total energy comprises the term accounting for the elastic energy of the sound domain $P(u, \Gamma)$, and the energy associated to the crack surface $S(\Gamma)$, *i.e.* $E(u, \Gamma) = P(u, \Gamma) + S(\Gamma)$. The stability principle turns even more fruitful when it is confronted to the issue of nucleation and evolution. Suppose that at time t_0, the body is in the state just obtained as solution of the static problem, in particular let us denote the corresponding crack set by Γ_0. Hence, along a subsequent evolution, parametrized by $t \geq t_0$, the stability principle requires to the crack $\Gamma(t)$ to be a minimizer of the total energy, among all curves $\hat{\Gamma} \supseteq \Gamma(t)$, the last set inclusion reflects the irreversible character of fracture processes. In the last statement, we can confront to the problem of nucleation just by considering the admissible case $\Gamma_0 = \emptyset$. In this situation, with or without singularities, it is shown that a crack will necessarily

nucleate for a sufficiently high load, *viz.* in a finite time [BFM08]. Energy stability and irreversibility are the two first essential ingredients of this variational formulation. The third, a weak form of energy balance, provides a selection criterion among the linearly independent infinity of solutions that may be constructed with the first two criteria. The works [FM98], [BFM08] offer a deep, as much as wide, analysis of the general framework of variational fracture.

A wider perspective. The theory of variational fracture, of which a few threads will be sketched in the next Chapter, fits within the larger class of systems whose response along a loading process is independent of the rate of loading. Systems that behave as such are labeled *rate independent* and the general formulation, in a variational setting, of their associated evolution problems is studied in abstract detail in [Mie05]. Other than brittle fracture mechanics, it finds applications in the study of phase transformations in shape-memory alloys [MTL00], dry friction [EM06], micromagnetism [RK04], just to cite a few notable examples. Within this abstract framework it is possible to study, with the help of fine and rigorous mathematical tools, complex phenomena originating from simple and fundamental principles within a global view.

Let us turn the attention back to the films system. The "thinness" of such structures has a profound influence upon the mechanical modeling, mathematical analysis and computational experimentation. In the mechanical modeling of problems associated to thin film systems "small parameters" naturally appear. One of those is typically the ratio between the thickness and the diameter of the structure. A direct numerical approach to the solution of their associated problems proves to be extremely costly due to the ill-conditioning caused by the separation of scales, *i.e.* these problems are numerically *stiff*. On the other hand, the observation of these systems suggests that their phenomenology is essentially two-dimensional. It is then reasonable to look for suitable reduced two-dimensional models that be able to capture the fundamental properties of the real three-dimensional system. Elastic problems in thin film systems are a typical instance of *singular perturbation problems*, where setting to zero the small parameters would provide meaningless equations. The techniques of the asymptotic study of boundary value problems, stated under a variational form, as their natural "small parameters" tend to zero are dealt extensively in [Lio73] and have allowed for the rigorous justification of the linear and nonlinear reduced dimension theories for bars, rods and strings [MM06]; plates and shells [Cia97], among other fruitful applications.

In fracture mechanics of brittle thin film systems, the asymptotic study of a variational singular perturbation problem couples naturally with the study of its irreversible quasi-static variational evolution laws. Such rich mathematical structure has indeed kindled the attention of the applied mathematics community. Variational convergence studies for fractures in single-layer thin films has been studied in [BF01], [BFL02], [Bab06] whereas interfacial debonding has been investigated in [BFF02], [KMR05], [RSZ09].

This work. We propose to investigate the brittle elastic system and characterize the phenomena related to both multiple fissuration and debonding as a irreversible, quasi-

static evolution of singular perturbation problem, following a variational principle of energy minimization.

We shall, to this end, make extensive use of the techniques of the Calculus of Variations and the notions of variational convergence. Their interest, in this setting, goes beyond the original use of exotic mathematical tools and provides a key to investigate the essential mechanisms by unveiling their *asymptotic* and *necessary* properties.

We present here, within a unitary framework, rigorous mathematical results on their mechanical ground, for they both contribute shedding light on the behavior of brittle thin film systems. The work is organized as follows.

In Chapter 1, after a brief sketch of some essential elements in the variational approach to fracture mechanics, we introduce the mechanical system of our concerns: the three-dimensional brittle elastic multilayer. We specify the *thought experiment* we will perform, fix notations and give the definitions that will be used in the sequel of the work.

In Chapter 2 we illustrate the capabilities of the proposed formulation in a most simplified setting of dimension one. Upon the assumption of a reduced model to describe the system, only phenomenological so far, we proceed to a thorough investigation of the solutions of both static and evolutionary brittle fracture problems, on the basis of a global energy minimization principle.

In Chapter 3 we *derive* the reduced model used in the preceding chapter, as the result of an asymptotic study. The limit model is constructed gradually. We start by studying the possible families of limit models arising from a three-dimensional elastic multilayer, once a general scaling law is assumed for thicknesses and stiffnesses. We extend the asymptotic study of one of the limit regimes, namely that of membranes over elastic foundation, performing the dimension reduction in the setting of three-dimensional vector elasticity. Subsequently, we allow for cracking and study the asymptotic behavior of a brittle elastic multilayer. The chapter terminates with the statement of the limit static and evolution problems in the case of vector two-dimensional elasticity.

In Chapter 4 we present numerical experiments based on the approximation of the brittle fracture problem by a regularized, nonlocal, gradient damage model. We introduce its numerical implementation and we perform several numerical experiments which, other than showing the strengths of our approach, allow us to recover and interpret various regimes observed in reality.

Finally, we draw some conclusions in light of a critic re-reading of the results obtained and issues raised, proposing a few threads of future investigation.

ALB
Paris, November 2013

Figure 1: A cracked vinyl sticker at École Polytechnique, Palaiseau, France. Crack pattern are robust, fractures nucleate even away from singularities and debonding starts from the boundaries.

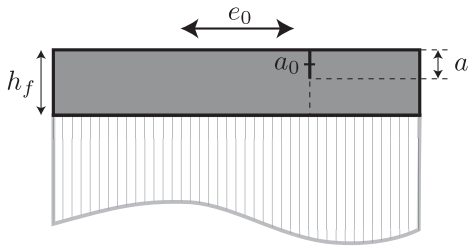

(a) A cross section of a brittle multilayer. To identify conditions for the extension of an "initial flaw" of length a_0, the energy release rate is computed for $0 < a_0 < a < h_f$ along a given segment, see [Beu92].

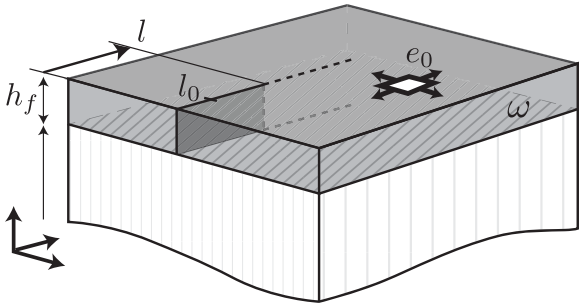

(b) For a fully developed, macroscopic crack approaching to a boundary, the energy release rate is computed as a function of $0 < l_0 < l$. The idea of "steady state cracking" is formulated in [HS91] as the condition for which the energy release rate reaches an asymptotic value, typically for l larger than few film thicknesses.

Figure 2: Scenarios for the computation of energy release rates. In Figure 2(a) for the condition of propagation along a vertical segment of an initial crack, in Figure 2(b) for the extension of a existent macroscopic crack.

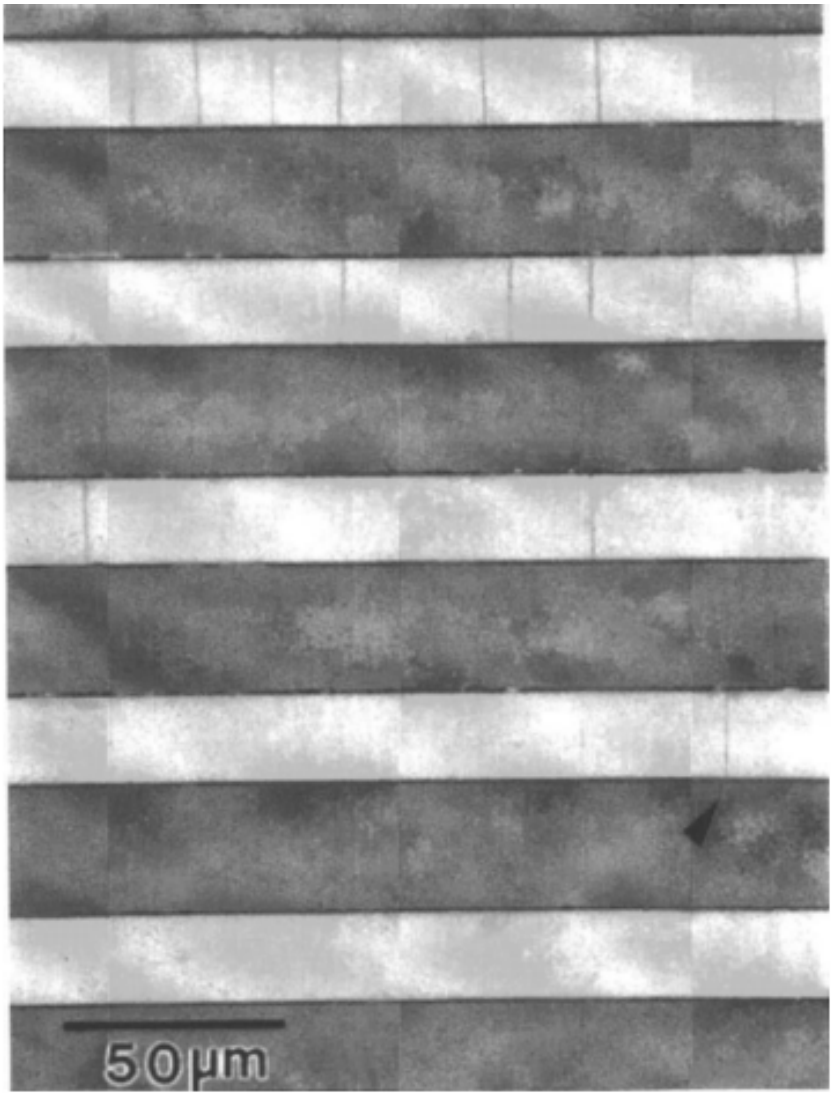

Figure 3: Multiple periodic cracks appearing in thin, macroscopically homogeneous, sound, strips of Si films. A bending moment is applied, orthogonal to the plane. The uni-axial strain applied to each strip increases linearly (from bottom to top) with the distance from the neutral plane. Image adapted from [LHE95].

(a) A pattern of hexagonal cracks appears during cooling of lava flows, due to the propagation of a tensile front.

(b) A two dimansional quasi-periodic crack pattern in a glazed vase.

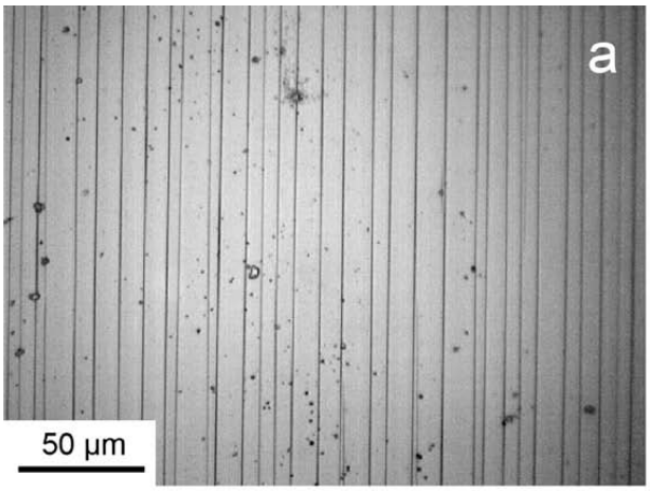

(c) Periodic fragmentation in a thin film MEMS device under uni-axial tension, [Let+10].

Figure 4: Three examples of quasi-periodic multifissuration, for systems with different constitutive laws and evolving at different scales. An characteristic length scale is associated to the period in the network.

Notation

A few words about the adopted notation. We use Einstein's summation convention throughout the paper, unless specified otherwise. Roman and greek subscripts denote components of tensors of rank $1, 2$ or 3, respectively spanning the sets $\{1, 2, 3\}$ and $\{1, 2\}$. We deal with "thin" domains in nD ($n = 2, 3$), *i.e.* with domains for which one characteristic dimension is much smaller than the remaining $n - 1$. We denote by Ω the reference configuration of a three-dimensional brittle elastic (possibly non-homogeneous) cylinder whose basis is $\omega \subset \mathbb{R}^2$. The associated energy density function is denoted by $W : \mathbb{R}^{m\times n} \to \mathbb{R}$, where $\mathbb{R}^{m\times n}$ stands for the set of real $m \times n$ tensors. In the sequel we deal with 3D elasticity ($m = n = 3$), 2D plane elasticity ($m = n = 2$) and scalar elasticity ($m = 3,\ n = 1$). Accordingly, the linearized gradient of the deformation is $e(u) := \frac{1}{2}(\nabla u + \nabla^\top u) = \frac{1}{2}(\partial_j u_i + \partial_i u_j)$ in 3D elasticity, $e(u) := \frac{1}{2}(\nabla' u + \nabla'^\top u) := \frac{1}{2}(\partial_\alpha u_\beta + \partial_\beta u_\alpha)$ in 2D elasticity – the prime sign indicating derivatives with respect to the in-plane coordinates – and reduces to the gradient $e(u) = \nabla u$ in scalar elasticity. We denote by a dot the scalar (inner) product. We shall use the usual notations for function spaces: $H^1(\Omega;\mathbb{R}^n), L^2(\Omega;\mathbb{R}^n), L^\infty(\Omega;\mathbb{R}^n)$ and $SBV(\Omega;\mathbb{R}^n)$ are respectively the space of square integrable functions with squared integrable derivatives, the Lebesgue space of square integrable functions, the space of functions with finite sup-norm and the space of special functions of bounded variations, defined on the set Ω and with values in $\mathbb{R}^n$. Whenever $n = 1$, for simplicity, we will use the abbreviated notations $H^1(\Omega), L^2(\Omega), L^\infty(\Omega)$ and $SBV(\Omega)$. Whenever we need to distinguish between dimensional and non-dimensional (resp. unscaled and scaled) quantities, *i.e.* for the non-dimensionalization (resp. rescaling) of the energy functionals, we mark with a superposed tilde *dimensional* (resp. unscaled) functions, domains and operators. We shall distinguish between the strong and the weak problem of brittle films. The strong problem will always be defined for admissible displacements in a suitable subspace of the usual Sobolev space $H^1(\cdot)$. For the weak problem, we denote by a calligraphic capital letter, *e.g.* $\mathcal{C}(\cdot)$, the subset of special functions of bounded variations $SBV(\cdot)$ of admissible displacements. In favor of legibility, we commit an abuse of notation allowing us to label *different* functions with the *same* symbol, provided that they have a different number of arguments, so that *e.g.* no ambiguity shall arise between the two different functions $P(u, \Gamma)$ and $P(u)$. Generic real constants are denoted by C and may differ from line to line. Also, we denote by

$$E(u)'(v) := \frac{d}{dh} E(u + hv)\bigg|_{h=0}$$

the directional derivative (Gâteaux derivative) of a functional E with respect to the function u in the direction v.

We have tried to keep the number of symbols to a reasonable minimum. This means that we will reuse symbols whenever the context is clear enough to avoid ambiguities.

This page intentionally left blank.

Chapter 1

Introduction to variational fracture mechanics of thin film systems

We introduce the variational framework of variational mechanics. Starting from the open issues of classical Griffith's theory, the latter is revisited under the variational light of an energy minimization principle. The energy to be minimized is composed by the bulk elastic energy and a surface term associated to cracks. The three-pronged associated variational principle allows us to embrace in the analysis all phases of fracture: nucleation, propagation and selection of the crack path. In addition, it enables us to consider non-regular evolutions in space and time. We then decline this variational framework for the study of fracture of thin film systems.
The introductory material presented in Section 1.1 is proffered in the paper [Leó+13a], submitted for review.

Contents

1.1 Elements of variational fracture mechanics 15
1.2 Variational fracture mechanics of thin films 21
1.2.1 The general setting: three-dimensional brittle system 21
1.2.2 The scalar case 24
1.2.3 Static fracture problem 24
1.2.4 Quasi-static evolution problem 25

1.1 Elements of variational fracture mechanics

We sketch here a few elements, in an intentionally simplified setting, of the variational theory of fracture originally proposed in [FM98] and extensively developed in [BFM08]. We start by pointing out some of the motivations that led to its formulation.

A first consistent theory for the study of the propagation of cracks in brittle bodies dates to the early 1920's with the work of Griffith [Gri21]. Its fundamental contribution is twofold: introduces the notion of an "energy" associated to cracks, and a global energetic criterion for their propagation. The former, in analogy with the surface tension in fluids, is associated to the "work [that] must be done against the cohesive forces of the molecules on either sides of the crack". This has allowed to interpret and define usable, fail-safe design criteria against rupture in brittle materials, considered beforehand of almost unpredictable nature. The "theoretical criterion of rupture" [Gri21] hence stipulates that an infinitesimal crack advance is possible only if the rate at which the elastic potential energy is released by the advancing crack equals the rate of expense of surface energy associated to that infinitesimal advance. In the simplest setting the latter reduces to a material constant, the toughness G_c. No crack extension is possible, on the other hand, if the released energy is less than the rate of surface energy expense. Further works of Rice [Ric68b], [Ric68a] and Irwin [Irw58] have allowed to solve problems of brittle structures with valuable results from an engineering standpoint, in cases where a reasonable a priori knowledge of the crack path can be exploited to obtain fail-safe criteria for crack extension. However, from a more fundamental point of view, the classical theory of Griffith leaves open three major issues. First, an initial macroscopic crack has to be present in the brittle body. In other words, it is unable to deal with *initiation* but only with *propagation* of cracks. This has been already briefly discussed for the case of thin films, in which the problem of nucleation is apparently avoided pushing it to the small scales, *i.e.* that of initial flaws. Second, it implicitly assumes a smooth propagation in time and space. That is, both brutal propagation and geometrically non-smooth crack paths (less regular than a C^1 curve) cannot be accounted for. Last, the crack path along which the crack tip will propagate has to be known in advance. In fact, already in Griffith's natural setting of dimension two, the one scalar equation of the proposed criterion is not sufficient to determine the path followed by the advancing crack tip. The latter is determined by two functions of time (or load), *e.g.* the parametrized position of the crack tip $(x_1(t), x_2(t))$. Griffith's criterion, however, only provides one scalar equation; it proves to be insufficient for the selection of the crack path. Additional criteria have hence been proposed to provide an additional scalar equation. However, although they have found useful application from a practical point of view, their *ad hoc* nature and their misconsistencies [CFM09], [CFM10] do not allow them to ascend to a general theory of fracture.

A departure from the classical theory is able to palliate these issues, as is first shown in [FM98]. The availability of modern analytical tools of the direct method in the calculus of variations [Dac92] and functional analysis [Bre83], has allowed to revisit classical Griffith's theory under the new light of variational mechanics. In this new framework, the problem of brittle fracture can be stated as follows. Let us place ourselves in dimension two and consider a brittle elastic body whose reference domain is $\omega \subset \mathbb{R}^2$. It is subject to imposed displacement w on a part of its boundary $\partial_D\omega$ and free along its complement to $\partial\omega$. An admissible crack, denoted by Γ, is any set of finite 1-dimensional Hausdorff

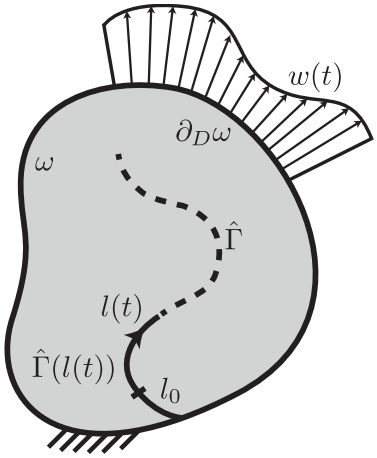

(a) An energy stationarity principle allows to determine the propagation of the crack tip $\hat{\Gamma}(l(t))$ along a prescribed smooth curve $\hat{\Gamma}$ starting from a non-vanishing initial crack, *i.e.* $l_0 > 0$.

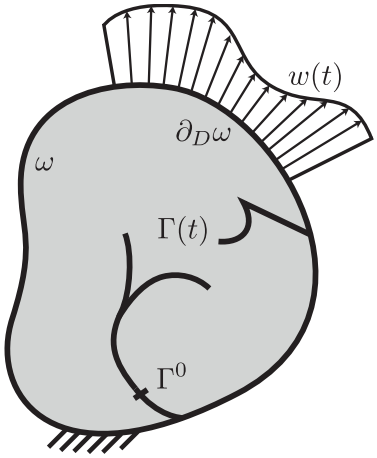

(b) The minimality principle is exploited to study nucleation, path selection and propagation of irreversible evolving cracks $\Gamma(t)$. Also non-smooth paths can be accounted for to include branching, intersection, kinking ...

Figure 1.1: Brittle elastic, two-dimensional problem based on energy stationarity and given crack path $\hat{\Gamma}$ (left); based on energy minimality with free crack path. Note that Γ^0 can be the empty set.

measure to which we associate the surface energy

$$S(\Gamma) := \int_\Gamma G_c(x;\nu)\,\mathrm{d}\,\mathcal{H}^1. \tag{1.1}$$

In the case of an homogeneous and isotropic body, the toughness $G_c(x;\nu)$, in principle depending upon the position $x \in \omega$ and the local normal ν to the crack Γ, reduces to a constant. Hence, the energy $S(\Gamma)$ has the same interpretation as that proposed by Griffith, *i.e.* the surface energy associated to a crack Γ is proportional to its length via a material constant. The quantity defined by (1.1) is called Griffith surface energy.

Admissible displacements are sufficiently regular fields v defined on the sound domain $\omega \setminus \Gamma$, satisfying the kinematic conditions $v = w$ on $\partial_D\omega$, *i.e.* laying in the set $\{\hat{v} \in H^1(\omega \setminus \Gamma), \hat{v} = w(t) \text{ a.e. on } \partial_D\omega\}$, where $w(t)$ is the time-dependent Dirichlet boundary condition. To such admissible displacements we associate a bulk energy defined:

$$P(v,\Gamma) := \int_{\omega\setminus\Gamma} W(e(v))dx,$$

where $W(\cdot)$ is the energy density function of the elastic body and $e((v))$ is the elastic strain associated to the displacement v. We define the total energy of the brittle body as the sum of bulk and surface energies. In the simplified setting adopted, it reads:

$$\begin{aligned} E(v,\Gamma) :=& P(v,\Gamma) + S(\Gamma) \\ =& \int_{\omega\setminus\Gamma} W(e(v))dx + G_c\mathcal{H}^1(\Gamma) \end{aligned}$$

Assuming that the crack path $\hat{\Gamma}$ be known, the state of the system is identified once the equilibrium displacement and the position of the crack tip are known. The latter can be parametrized by a scalar function $l(t)$, the arclength coordinate along $\hat{\Gamma}$, see Figure 1.1. It is hence shown in [BFM08] that the evolution of displacement v and crack tip $\hat{\Gamma}(l(t))$ can be sought as a solution of an evolution problem ruled by a law consisting in i) an irreversibility constraint on crack growth, ii) a unilateral stationarity principle and iii) a weak form of energy balance. The evolution law reads as follows:

Definition 1.1 (Strong variational evolution, energy stationarity, prescribed path)**.** *The mapping pair $t \mapsto (u(t), l(t))$ is a quasi-static evolution for the displacement field and the crack tip along a prescribed curve $\hat{\Gamma}$ if, given the initial state l^0 and the loading history $t \mapsto w(t)$, it satisfies the initial condition $l(0) = l^0$ and verifies the following conditions for $t \in (0, T]$:*

(irr): $\dot{l}(t) \geq 0$

(ust): $(u(t), l(t))$ *is a stationary point of:*

$$\hat{E}(v,l) := E(v,\Gamma(l)) := \int_{\omega\setminus\Gamma(l)} W(e(v))dx + G_c\, l$$

among all $l \geq l(t)$, $\forall v \in H^1(\omega \setminus \Gamma(l))$ such that $v = w(t)$ on $\partial_D\omega \setminus \Gamma(l)$.

(eb): *The total energy:*

$$\mathcal{E}(t) := \int_{\omega\setminus\Gamma(l(t))} W(e(v(t)))dx + G_c l(t)$$

is absolutely continuous on $[0, T]$ and satisfies the energy balance:

$$\frac{d\mathcal{E}(t)}{dt} = \int_{\partial_D\omega\setminus\Gamma(l(t))} \nabla W(e(v(t))) \cdot \dot{w}(t)dx$$

This law is shown to be equivalent to Griffith's classical formulation for sufficiently smooth cracks when the function $\mathcal{P} : l \mapsto \inf_v \{E(v, \Gamma(l)\}$ (the inf taken among admissible v's) is strictly convex [BFM08]. Here, $\mathcal{P}(l)$ is the elastic energy of the body at equilibrium with the crack of length l. The well-posedness of this infimum problem, pertains to the coerciveness and strict convexity properties of the energy density $W(\cdot)$ and to the regularity of the data (geometry and loads).

In the case of strict convexity of the potential energy $\mathcal{P}(l)$, the unilateral *stationarity* becomes a unilateral *minimality* principle and opens the way for the adoption of a

minimality principle to cope with crack path selection. In other words, the variational minimality principle can be exploited to choose the crack path itself, so that the hypothesis of *a priori* knowledge of the crack path can be removed. Consequently, an evolution law based on global minimality is formulated as follows:

Definition 1.2 (Strong variational evolution, global energy minimality)**.** *The mapping pair $t \mapsto (u(t), \Gamma(t))$ is a quasi-static evolution for the displacement field and crack set if, given the initial crack state Γ^0 and the loading history $t \mapsto w(t)$, it satisfies the initial condition $\Gamma(0) = \Gamma^0$ and verifies the following conditions for $t \in (0, T]$:*

(irr): $\Gamma(t)) \nearrow t$

(ugm): $(u(t), \Gamma(t))$ *is a global minimizer of:*

$$E(v, \Gamma) := \int_{\omega \setminus \Gamma} W(e(v))dx + G_c \mathcal{H}^1(\Gamma)$$

among all $\Gamma \supset \Gamma(t)$, $v \in H^1(\omega \setminus \Gamma)$ analyzed $v = w(t)$ on $\partial_D \omega \setminus \Gamma$.

(eb): *The total energy:*

$$E(t) := \int_{\omega \setminus \Gamma(t)} W(e(v(t)))dx + G_c \mathcal{H}^1(\Gamma(t))$$

is absolutely continuous on $[0, T]$ and satisfies the energy balance:

$$\frac{dE(t)}{dt} = \int_{\partial_D \omega \setminus \Gamma(t)} \nabla W(e(v(t))) \cdot \dot{w}(t)dx$$

Under restrictive hypotheses upon the topology of the cracks, an existence theory for the problem above has been established by [DT02a] in the setting of scalar elasticity and by [Cha03] in the case of two-dimensional linearized elasticity. The reason for demanding the introduction of the topological restrictive hypothesis (namely cracks are connected curves) is related to the lack of lower semicontinuity of the surface energy, *i.e.* of the Hausdorff metric. A proper variational setting, in which is proved the existence of solutions of the above problem, is introduced in [FL03] exploiting the analogies with the Mumford-Shah problem [MS89] arising in image segmentation. The existence theory for the latter problem has been developed in [GCL89]. The evolution problem finds in [FL03] a well-posed weak variational formulation in the space BV (and its variants), of functions of Bounded Variation [Amb89].

The evolution law written in Definition 1.2 rests on global minimization. The need for such setting is essentially related to the issue of initiation with Griffith-type surface energies, see [BFM08, Chap. 4]. With global minimization, it is shown that initiation always occurs in a finite time [BFM08], nonetheless this setting rules out the possibility of considering body loads and implicitly assumes that the transition between different (cracked) states is always possible, regardless of how "far" the states are in the

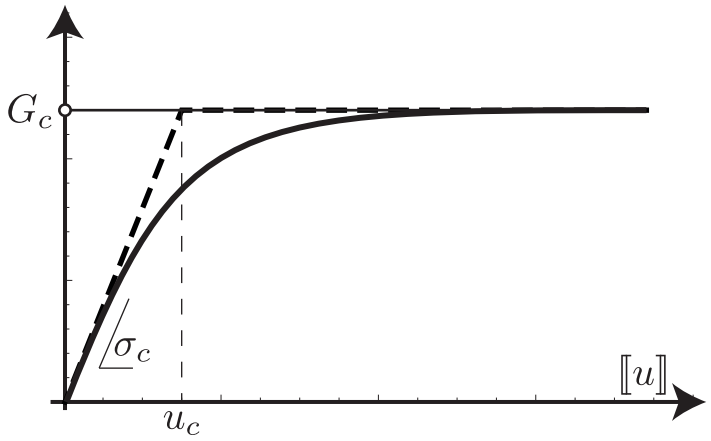

Figure 1.2: Griffith (thin), Dugdale (dashed) and Barenblatt (thick) surface energy densities. Griffith energy density is constant (G_c) as soon as the crack opening $[\![u]\!]$ is positive. Dugdale energy density is piecewise constant, linear up to G_c below the critical opening threshold u_c. Barenblatt is smooth and concave. For the two latter, the derivative at 0 is associated to the critical stress σ_c.

configuration space. This may be unphysical and demands a finer study in cases *e.g.* of brutal fracture. On the other hand, renouncing to the global minimization setting while sticking with Griffith surface energies, renders impossible the nucleation of cracks in a body without strong singularities (*e.g.* an initial crack or a discontinuity in boundary conditions). Indeed the sound, elastic, solution branch is always a locally stable minimum of the total energy.

The reason for the impossibility of crack nucleation, with Griffith-type surface energies, is due to allowing for unbounded stresses in the body (still of finite energy). This can be palliated by introducing a concept of critical stress, via *e.g.* more refined surface energies of cohesive type (like Barenblatt's [Bar62] or Dugdale's [Dug60]), or nonlocal gradient damage models. In the former case, Barenblatt and Dugdale energies (sketched in Figure 1.2) introduce an additional length scale associated to the slope of the surface energy at the origin, providing the critical stress threshold. Nucleation is then produced once stresses reach their critical finite value. Consequently, with energies of such kind, the global minimality requirement can be relaxed to local minimality statement, in a reasonable topology. The properties of cohesive models in the setting of local minimization have been analyzed in [Cha+00] and their link with Griffith's model is unveiled in [BDG99], [MT04]. It is shown, indeed, that Griffith's model is reached by a suitable asymptotic process as the internal length scale induced by the cohesive energy goes to zero. Whenever one resorts to a local minimality statement, the choice (not univocal) of the norm defining the neighborhoods of states, *i.e.* the adopted topology, has important mechanical consequences.

From a different point of view, a more detailed account of the nucleation phase than that of the revisited Griffith setting, is possible by introducing nonlocal gradient damage

models with softening [PM10a], [PM10b]. These models rely on a continuous damage variable and an additional material length scale associated to damage localization. This translates into the existence of a critical stress, attained which, damage is produced. Because of the softening behavior, the stress drops in the damaged region which localizes into narrow bands, whose width controlled by the internal damage length. When damage reaches its peak value, a newly created crack is obtained at the expense its dissipated energy [Pha+10]. The process of nucleation described above is driven by the loss of stability and subsequent bifurcation of equilibrium states.

Also for these models, the revisited Griffith setting can be recovered by an asymptotic procedure as the damage internal length scale goes to zero. This asymptotic result has been shown, from the global minimization standpoint. in [Gia05], [Cha04] by Γ-convergence, and, relying on first order unilateral stability conditions, in [SM12] by asymptotic expansions.

From a specular perspective, cohesive fracture models can be recovered when coupling between plasticity (*i.e.* irrecoverable deformations) and damage (possibly leading to localization) takes place, as it has been recently studied in [AMV]. The interplay between these two physically different and independent phenomena may couple to produce cohesive responses culminating in irreversible fracture. On the same spirit and with different analytic techniques, the asymptotic properties of energies in which a coupling between damage, plasticity and fracture appears, are investigated in [FI13], [MI13].

After this brief and non-comprehensive sketch of some elements of the variational framework of fracture, we tackle the problem of fracture and debonding of thin film systems. In the following section, we specialize the definitions illustrated above for a three-dimensional thin film system within the global minimization setting.

1.2 Variational fracture mechanics of thin films

We start the study by focusing on the three-dimensional system. We identify of a suitable *thought experiment* under which we expect to be able to reveal the mechanisms of multiple fissuration and debonding in thin film systems. We define the composite multilayer system of our concern: the geometry, the applied loads, the material behavior and its energy. This allows us to further formally state the static and evolution laws for the brittle fracture problem.

1.2.1 The general setting: three-dimensional brittle system

The geometric configuration

Let us consider the three-dimensional reference system sketched in Figure 1.3. It is composed by a thin film occupying the set $\overline{\Omega}_f = \overline{\omega} \times [0, h_f]$ is bonded to a rigid substrate $\overline{\Omega}_s = \overline{\omega} \times [-h_s, -h_b]$ by the means of a bonding layer $\overline{\Omega}_b = \overline{\omega} \times (-h_b, 0)$. Here $\omega \subset \mathbb{R}^2$ is the basis of the cylinder $\Omega = \Omega_s \cup \Omega_b \cup \Omega_f$. In all that follows, the subscript b indicates quantities relative to the bonding layer and f to the film. The interface between the

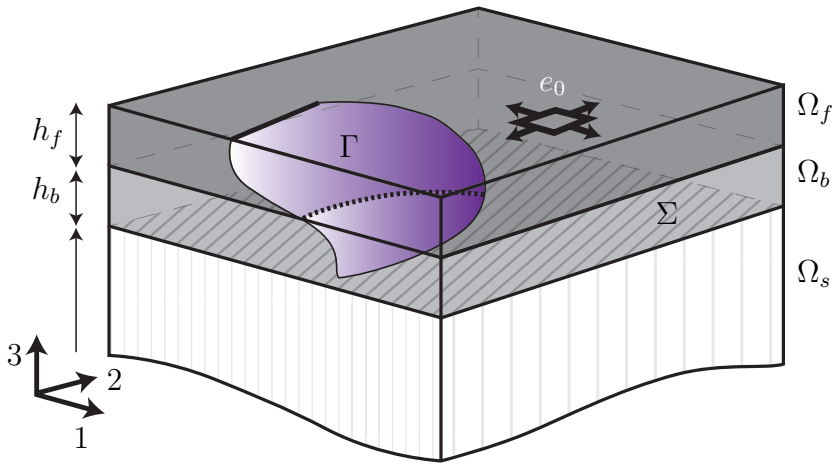

Figure 1.3: The three-dimensional model of the brittle system: a thin film Ω_f is bonded to a rigid substrate Ω_s via a bonding layer Ω_b. Crack surfaces are noted Γ.

latter and the substrate is denoted by $\omega_- = \omega \times \{-h_b\}$ whereas the interface between the two layers is denoted by $\omega_0 = \omega \times \{-0\}$.

The loads

We consider two types of loading modes. The first is due to the structure subject to the structural loads. Considering the substrate infinitely rigid with respect to the film and bonding layer, the displacement at the interface $w = (w)_i : \omega_- \mapsto \mathbb{R}^3$ can be identified as the displacement that the structure would undergo under structural loads, neglecting the presence of the surface coating layers. Hence, the interface ω_- is a Dirichlet boundary for the layer system and w is the datum. Since we do not model the structural response of the substrate, it is considered as a given.

The second type of loads is an inelastic strain acting inside the film. Physically, it may rise due to thermal loadings, humidity or drying processes, just to note some of the possible multi-physical couplings that may take place. The inelastic strain $e_0 = (e_0)_{ij} : \Omega \mapsto \mathbb{R}^{3\times3}$ is interpreted as the strain that the film and the bonding layer would accommodate if they were free from compatibility constraints. We focus here on shrinking loads and choose not to account for all the multi-physical phenomena that may induce the loads and their coupling, hence we model both loads as independent assigned parameters.

The behavior of the bulk

We assume the two layers are isotropic and linearly elastic, the elasticity tensor being characterized by two material constants, *e.g.* the Lamé parameters (λ_f, μ_f) and (λ_b, μ_b) respectively of the coating film and bonding layer. Hence the energy density W :

$\mathbb{R}^{3\times3}_{\rm sym} \times \Omega_f \cup \Omega_b \mapsto \mathbb{R}$ associated to the elastic strain is

$$W(e,x) = \frac{1}{2}\left\{\lambda(x)\mathrm{tr}(e)^2 + 2\mu(x)e\cdot e\right\}$$

where $\lambda(x)$ and $\mu(x)$ are the piecewise constant elasticity parameters of the non-homogenous body, namely:

$$(\lambda,\mu)(x) := \begin{cases}(\lambda_f,\mu_f) & \text{if } x\in\Omega_f\\ (\lambda_b,\mu_b) & \text{if } x\in\Omega_b\end{cases}.$$

The energies

Without an a priori geometric characterization, we allow cracks, denoted by Γ, to appear anywhere inside the two layers. Cracks may be any set $\Gamma\subset\Omega$ of finite 2-dimensional Hausdorff measure. In correspondence of a crack Γ the displacement field may exhibit a jump and we model cracks as traction-free surfaces. In Figure 1.3 a general crack Γ is sketched. For clarity, the ones inside the film are noted $\Gamma_f := \Gamma\cap\Omega_f$ whereas those inside the bonding layer are $\Gamma_b := \Gamma\cap\Omega_b$. Note that instead of resorting a formulation in a space that admits arbitrary jumps of the displacement field (*i.e.* the space BD and its variants) we shall stick to subspaces of Sobolev spaces accordingly defined on the *sound* part of the body $\Omega\setminus\Gamma$. For the formal definitions below, we hence provide the so called *strong* formulation of the brittle fracture problem.

Cracks are created at the expense of a surface energy of the Griffith-type, *i.e.* proportional to the measure of the crack surface by a material constant, the toughness G_c. We define the surface energy as follows:

$$\mathcal{S}(\Gamma_f,\Gamma_b) := \int_{\Gamma_f\cup\Gamma_b} G_c(x)\,d\mathcal{H}^2, \qquad \text{with} \quad G_c(x) := \begin{cases}G_f, & \text{if } x\in\Omega_f\\ G_b, & \text{if } x\in\Omega_b\end{cases},$$

where $d\mathcal{H}^2$ is the Hausdorff surface measure.

In the framework of three-dimensional linear elasticity, the space of admissible displacements is that of the square integrable vector fields with square integrable derivatives, defined on the sound part of the body $\Omega\setminus\Gamma$ and satisfying the boundary condition on the extended domain Ω_s, namely:

$$H^1_w(\Omega\setminus\Gamma;\mathbb{R}^3) := \left\{v\in H^1(\Omega\setminus\Gamma;\mathbb{R}^3), v = w \text{ on } \Omega_s\right\}.$$

In the framework of three-dimensional brittle elasticity we associate to any admissible displacement field u the elastic energy defined as:

$$\begin{aligned}\mathcal{P}(u,\Gamma_f,\Gamma_b) &:= \int_{\Omega\setminus(\Gamma_f\cup\Gamma_b)} W(e(u(x))-e_0(x),x)\,dx\\ &= \frac{1}{2}\int_{\Omega\setminus(\Gamma_f\cup\Gamma_b)}\left\{\lambda(x)\mathrm{tr}(e(u)-e_0)^2 + 2\mu(x)(e(u)-e_0)\cdot(e(u)-e_0)\right\}dx.\end{aligned}$$

The total energy of the thin film system is the sum of the elastic potential energy and the surface energy, namely:

$$\mathcal{E}(u, \Gamma_f, \Gamma_b) := \mathcal{P}(u, \Gamma_f, \Gamma_b) + \mathcal{S}(\Gamma_f, \Gamma_b)$$

1.2.2 The scalar case

Let us introduce the setting of scalar elasticity, *i.e.* where the displacement is considered to be a scalar function $u : \Omega \in \mathbb{R}^3 \mapsto \mathbb{R}$. This setting proves to be fruitful for establishing many of the rigorous results. Although the case of scalar elasticity has an evident physical meaning only in the case of two-dimensional domains (anti-plane elasticity), we consider the $3D$ case where $\Omega \subset \mathbb{R}^3$. This allows us to obtain, without any further mathematical difficulty, a clearer analogy to the full vectorial problem. Referring to the sketch in Figure 1.3, admissible scalar displacements are in the space $\mathcal{C}_w(\Omega \setminus \hat{\Gamma}) := \{v \in H^1(\Omega \setminus \Gamma) : v = w \text{ in } \Omega_s\}$, the symmetrized gradient of displacement reduces to the scalar gradient ∇u and the elastic energy density $W : \mathbb{R}^3 \times \Omega \mapsto \mathbb{R}$ is given by $W(\nabla u, x) = \mu(x)|\nabla u|^2$. Accordingly, the total energy is brittle scalar elasticity reads:

$$\begin{aligned}\mathcal{E}(u, \Gamma_f, \Gamma_b) :=& \frac{1}{2} \int_{\Omega \setminus (\Gamma_f \cup \Gamma_b)} W(\nabla u(x) - e_0(x))\, dx + \mathcal{S}(\Gamma_f, \Gamma_b) \\ =& \int_{\Omega \setminus (\Gamma_f \cup \Gamma_b)} \mu(x)|\nabla u - e_0|^2 + \int_{\Gamma_f \cup \Gamma_b} G_c(x)\, d\mathcal{H}^2\end{aligned}$$

where here $e_0 = (e_{0i}) : \Omega \mapsto \mathbb{R}^3$ and analogously to the vectorial case:

$$\mu(x) := \begin{cases} \mu_f & \text{if } x \in \Omega_f \\ \mu_b & \text{if } x \in \Omega_b \end{cases}.$$

1.2.3 Static fracture problem

We introduce the following definition of *static* fracture problem. The label *static* emphasizes that the solution is sought for a fixed load intensity, and crack irreversibility does not play any role.

Problem 1.1 (Static, three-dimensional, brittle problem)**.** *The static three-dimensional problem of brittle thin film systems consists in finding, for a given load intensity* (e_0, w)*, crack sets* Γ *and (possibly) discontinuous displacement fields* $u \in H^1_w(\Omega \setminus \Gamma; \mathbb{R}^3)$ *solving the following minimization problem*

$$\inf\{\mathcal{E}(u, \Gamma) : \quad \Gamma \subset \Omega,\ u \in H^1_w(\Omega \setminus \Gamma; \mathbb{R}^3)\},$$

i.e. *that satisfy the following global minimality condition:*

$$\textit{(GM)}: \qquad \mathcal{E}(u, \Gamma) \leq \mathcal{E}(\hat{u}, \hat{\Gamma}), \quad \forall \hat{\Gamma} \subset \Omega,\ \forall \hat{u} \in H^1_w(\Omega \setminus \hat{\Gamma}; \mathbb{R}^3).$$

1.2.4 Quasi-static evolution problem

Unlike in the static case, irreversibility plays a fundamental role in evolution problems. Upon prescribing a load history, parametrized by a load parameter t, the three-dimensional evolution problem for brittle thin film systems consists in finding the displacement field and the crack set verifying a variational statement under the irreversibility constraint which forbids self-healing of cracks during the loading process. In the framework of variational fracture mechanics, the energetic formulation of evolution problem falls into the class of rate-independent processes as studied in [Mie05]. The rate-independence implies that solutions to the evolution problem are stable under a reparametrization of the loading parameter, *i.e.* solutions are the same regardless of the velocity of the applied load. These systems are the limit regime for "slow" loads, where the system is supposed to be in static equilibrium at each load level. In this context we allow ourselves to interpret the arbitrarily increasing loading parameter t as a "time" variable. We focus here on the time-discrete formulation of the problem.

Problem 1.2 (Time-discrete, three-dimensional evolution problem)**.** *Let be* $0 = t_0 \leq t_1 \leq \ldots \leq t_N = T$ *the discretization of the time interval* $[0, T]$ *into* N *time steps. A time-discrete quasi-static evolution for the displacement field and crack set of the three-dimensional system is a mapping* $t_i \mapsto (u^i, \Gamma^i)$ *that, given the initial crack state* Γ^0 *and the loading history* (e_0^i, w^i)*, verifies the following global unilateral minimality conditions* $\forall i \in 1, \ldots, N$*:*

$$\Gamma^i \supseteq \Gamma^{i-1}, \tag{1.2a}$$

$$\mathcal{E}(u^i, \Gamma^i) \leq \mathcal{E}(u, \Gamma) \qquad \forall \Gamma \text{ with } \Gamma^{i-1} \subseteq \Gamma \subset \Omega, \quad \forall u \in H^1_{w^i}(\Omega \setminus \Gamma; \mathbb{R}^3), \text{ with } e_0 = e_0^i. \tag{1.2b}$$

These conditions are equivalent to require that (u^i, Γ^i) *be a solution of the minimization problem*

$$\inf \left\{ \mathcal{E}(u, \Gamma) : \quad \Gamma^{i-1} \subseteq \Gamma \subset \Omega,\ u \in H^1_{w^i}(\Omega \setminus \Gamma; \mathbb{R}^3) \right\}.$$

In the problem above, the condition (1.2a) ensures the irreversibility of the fracture process and prevents crack self-healing, whilst condition (1.2b) requires the constrained energy minimality of the solution at a given time step among all the admissible competitors. The weak regularity assumption on the crack set (finiteness of the two-dimensional Hausdorff measure) will allow the crack to take complex spatial shapes and including branching, intersections and coalescences.

The time incremental formulation presented above is exploited from a numerical standpoint to construct piecewise linear interpolations in time of the evolutions by solving the variational inequalities associated to the *static* minimization problems (1.2b) under the irreversibility constraint.

When computations can be carried in closed form, we need a time-continuous version of Problem 1.2.

A formal substitution of the discrete variable t_i with a continuous time t leads to a 2-pronged formulation based on irreversibility and global stability. It is shown in [FM98] that such formulation is ill-posed. Crack paths are over-determined and an additional criterion for their selection is proposed. A first formulation of selection criterion is given in [FM98], based on necessary conditions for global energy minimality, assuming a brittle linearly elastic body under monotonically increasing loads. Subsequently, considering more applied loads, in [DT02b] existence is proved for the continuous evolution. The result is based on the study of the asymptotic limit problem associated to the discrete-in-time Problem 1.2, for a fixed time horizon T, as the timestep $1/N \to 0$. This additional crack path selection criterion emerging in the time-continuous limit amounts to energy balance. The result is generalized by dropping the restrictive hypotheses upon the topology of the crack sets in [FL03]. The irreversible, quasi-static, time-continuous formulations of the brittle fracture problem finds a variational formulation fitting within the broader class of *rate-independent* processes whose abstract framework is studied in [Mie05].

In this spirit, we formally introduce the time-continuous, quasi-static, evolution problem of the brittle, three-dimensional multilayer as follows:

Problem 1.3 (Time-continuous, three-dimensional evolution problem)**.** *Given a loading path (e_{0t}, w_t) for $t \in [0,T]$, a function $t \mapsto (u_t \in H^1_{w_t}(\Omega \setminus \Gamma_t),\ \Gamma_t \subset \Omega)$ is a quasi-static evolution if it satisfies the following items:*

(IR) Irreversibility of the crack evolution: *The function Γ_t must be non-decreasing with t:*

$$\Gamma_t \supseteq \Gamma_s, \quad \forall\, 0 \le s \le t.$$

(GST) Unilateral global stability: *At every time t the state $(u_t \in H^1_{w_t}(\Omega \setminus \Gamma_t), \Gamma_t)$ is the* global *minimizer of the total energy among all admissible states:*

$$E(u_t, \Gamma_t) \le E(u, \Gamma), \quad \forall u \in H^1_{w_t}(\Gamma), \quad \forall \Gamma \supseteq \Gamma_t.$$

(EB) Energy balance: *The function $\mathscr{E}(t) := E(u_t, \Gamma_t)$ is absolutely continuous in t and satisfies:*

$$\mathscr{E}(t) - \mathscr{E}(0) = -\int_0^t \left\{ \int_{\Omega\setminus\Gamma} \sigma_t \cdot \dot{e}_{0t} dx + \int_{\omega_-} u_t \cdot \dot{w}_t dx' \right\} dt,$$

where we denote by a dot the time-derivative ($\dot{f}(t) := \frac{df}{dt}$) and by $\sigma_t := \left.\frac{\partial W(e)}{\partial e}\right|_{e(u_t)-e_{0t}}$ the Cauchy stress at equilibrium.

With the general framework just sketched, we outline an illustrative example in the simple setting of the one-dimensional limit case for a thin film system. The general definitions of the problems above are used in this simplified setting allowing to obtain remarkably rich solutions to the fracture problem of a thin film system.

Chapter 2

The one-dimensional film

We study analytically the static and evolution problems of transverse fracture and debonding of a narrow thin film under bi-axial load. The system is approximated by a one-dimensional membrane over elastic foundation model. On the basis of the energy minimization principle, we recover the key qualitative properties highlighted by experimental evidence: sequential cracking, periodicity of transverse cracks, peripheral debonding. The evolution of the system is computed in closed form and phase diagrams, based on material properties and sample's geometry, synthesize possible evolutions.
The results presented in this chapter constitute the bulk of the material published in [Leó+13d].

Contents

2.1 A simplified one-dimensional model 30
2.1.1 Dimensional analysis 32
2.2 The static problem: energy minimizers at fixed load 33
2.2.1 The sound elastic film 33
2.2.2 The debonding problem 35
2.2.3 The transverse fracture problem 40
2.2.4 Coupled transverse fracture and debonding 42
2.3 The quasi-static evolution problem 48
2.3.1 Evolution of transverse cracks 48
2.3.2 Evolution of debonding 49
2.3.3 Film subject to coupled transverse cracks and debonding . . 50
2.3.4 Comments and extensions 51
2.4 Conclusions of the chapter 56
2.A Properties of the minimizers 57

The framework sketched in the preceding section is valid in general in three-dimensions. Here, upon assuming a phenomenological one-dimensional model for the energy of the system, we outline in the simplest setting the features of the variational approach, in

circumstances where the classical techniques are unable to yield satisfactory results. A robust feature of crack patterns in situations where the response of the system is essentially one-dimensional, is the appearance of a periodic array of cracks, in a sequential, cascade evolution. In Figures 2.1 two different experiments, by [NE93] and [Ber+02] show an equally-spaced array of transverse cracks. Different crack spacing is obtained for different load levels (Figure 2.1(a)) and thicknesses (Figure 2.1(b)). An homogeneous load is produced within the thin coating film by applying a bending moment along the direction orthogonal to the plane of the narrow film.

Phenomenological one-dimensional models have been widely proposed to study segmentation and debonding of thin films. In these studies, the geometry of both transverse and debonding cracks is introduced as a necessary, a priori, assumption. In [BM06], upon prescribing the distribution of the cracks and the location of debonded zones, a maximal stress criterion is used to determine the critical loads, the number of film cracks is discussed for several constitutive laws assumed for the interface. In [BM07] an energetic argument is compared to the maximal stress criterion for the prediction of the number of cracks and debonding critical loads, introducing frictional, cohesive and plastic effects. A shear lag model for the interface is introduced in [YTN98] and the number of cracks as a function of the imposed strain is computed assuming that cracks are equally spaced and new cracks form in the middle of each segment. Debonding is proscribed. In [Han02] similar results are discussed considering a general nonlinear shear lag law for the interface. The scaling and statistical properties of crack spacing are computed numerically assuming a probabilistic distribution of the maximal allowed stress.

Instead of postulating the geometric properties of fractures, their distribution and location, we shall derive them as consequence of the variational statement. On a different mechanical ground, many inelastic phenomena have been studied in depth in the simple one-dimensional setting with a variational approach. In [DT01], [PT98] distributed (diffused) and localized fracture are investigated as the locally stable states of a system whose total energy is the sum of a bulk and a surface energy. By varying the convexity properties of the latter, the authors show that convex-concave surface energies enlarge the space of local minimizers, allowing for diffused fractures, associated to damage which does not alter the stiffness of the structure, and localized fracture. Two regimes are further discriminated depending upon the irreversibility assumptions: the completely "elastic case", for reversible cracks, and the "inelastic case", for strictly irreversible cohesive cracks. In [MT04] the issue of nucleation is investigated for the fiber pullout test, which reduces to a scalar case due to symmetry and the assumed slenderness. The natural strain localization provides a setting to compare the initiation criteria for Griffith, Dugdale and Baremblatt energies in the setting of local minimization.

We now investigate and provide a complete study in closed form of the implications of the energy minimality in the static and quasi-static evolution of a slender thin film system that allows for a one-dimensional representation. In dimension one computations can be carried analytically. Along the study, we reveal and establish analytically in $1D$ some properties that characterize the interplay between the elasticity and the two failure modes. Their validity will prove to be ampler than the one-dimensional setting.

In addition, even in the simple setting of dimension one, most of the difficulties of more complex problems arise. They regard the mathematical formulation, the analytic techniques and the physical interpretation.

In order to keep the analysis simple and to focus on the main concerns, we start off by assuming two crucial working hypotheses. In particular, we postulate i) the form of the limit elastic energy representing the three-dimensional system and ii) the geometry of cracks, both in the film and the bonding layer. This geometric characterization, in turn, determines the form of the associated surface energies.

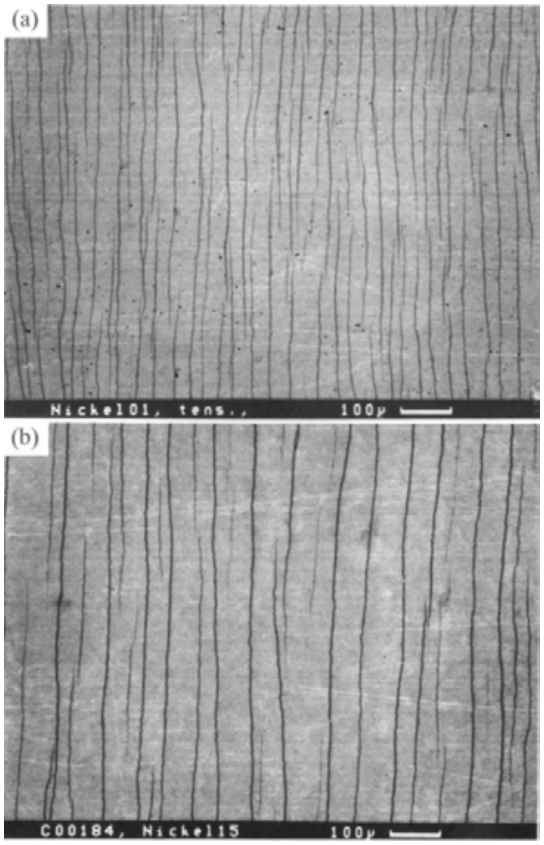

(a) Micrograph of the cracked surface of a thin NiO oxide film for different loads. The load intensity ratio (bottom to top) is 3. Adapted from [Nag+93].

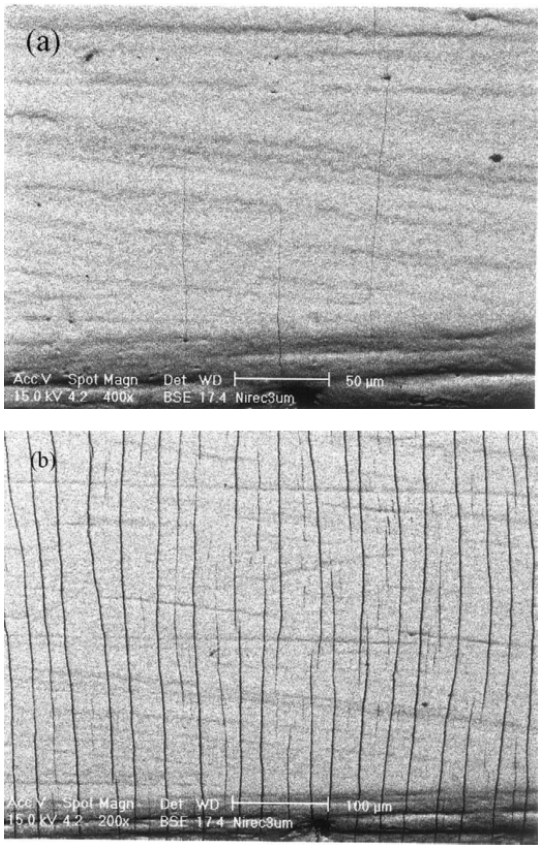

(b) Micrograph of the cracked surface of a thin NiO oxide film for different thicknesses of the film. The thickness ration (bottom to top) is 2.5. Adapted from [Ber+02].

Figure 2.1: Thin films under uni-axial homogeneous loading conditions show the appearance of periodically distributed cracks, following a sequential cascade of successive bisections.

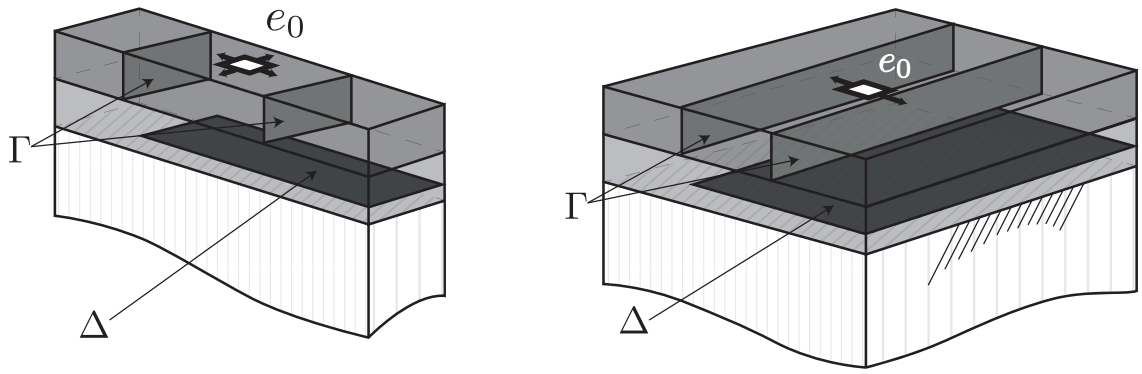

(a) A narrow thin film system under an equi-bi-axial load.

(b) A wide thin film system under a uni-axial load.

Figure 2.2: Three dimensional systems that can be approximated by the one-dimensional model. The load is denoted by e_0, transverse cracks by Γ and debonding cracks by Δ.

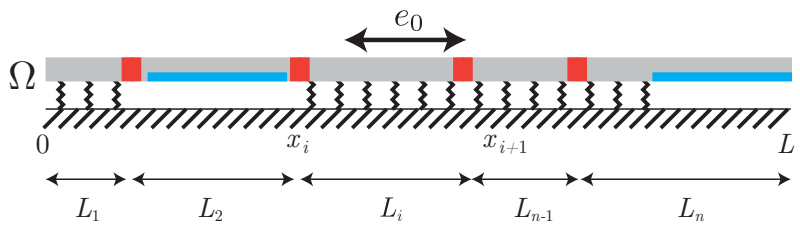

Figure 2.3: The one-dimensional phenomenological model a bar subject to the inelastic strain e_0 over a linear elastic foundation of stiffness k. Cracks cut the entire film at points x_n, debonded regions are segments along which no stress is transferred between the film and the rigid substrate

2.1 A simplified one-dimensional model

We adopt a phenomenological one-dimensional model for the brittle film system, extending [XH00] in order to account for arbitrary cracks in the film, possible debonding and imposed displacement load at the interface with the substrate. Such one-dimensional model approximates the response of either a narrow thin film under equi-biaxial loads (Figure 2.2(a)) and a wide thin film under uni-axial load (Figure 2.2(b)). The domain of the thin film system is the interval $\mathcal{A} = [-L/2, L/2]$, see Figure 2.3. We assume that cracks may develop within the film and can the film layer can debond from the substrate. The former cracks are denoted by Γ whereas the latter by Δ in Figures 2.2. Consequently, cracks in the film are traction-free boundaries and no elastic interaction between the film and the underlying substrate is present in debonded regions, see Figure 2.3. We hence

assume the following expression for the elastic energy of the system:

$$P(u,\Gamma,\Delta) := \frac{1}{2}\int_{\mathcal{A}\setminus\Gamma} \mu h_f (u' - e_0)^2 dx + \frac{1}{2}\int_{\mathcal{A}\setminus\Delta} k(u-w)^2 dx,$$

which is defined for admissible displacements in the space $H^1(\mathcal{A}\setminus\Gamma)$, that is for square integrable displacements with square integrable derivatives, defined on the crack-free domain $\mathcal{A}\setminus\Gamma$.

The first term in elastic energy is the energy of a pre-stressed linear bar of one-dimensional equivalent stiffness μh_f, the pre-stress is given by the inelastic strain e_0. The term $u' - e_0$ is the local *elastic* strain, difference between the *geometric* and the *inelastic* strains. The second term models the elastic contribution of the bonding layer as an elastic foundation of stiffness k, paying for the mismatch between the film displacement u and that imposed by the substrate w. This term is extended to the bonded domain $\mathcal{A}\setminus\Delta$, considering that in debonded regions the film can freely accommodate the inelastic strain without any elastic coupling with the substrate. It is noted that, in this one-dimensional model, debonding cracks do not induce displacement discontinuities. At sound points, the energy density associated to (2.1) is quadratic with respect to both the elastic strain $(u' - e_0)$ and the mismatch displacement $(u - w)$. This model of bilateral, linear, elastic, foundation is known to the engineering community as a foundation *à la Winkler* [Win67].

The surface energy associated to the two families of cracks is, under the adopted Griffith assumption, proportional to their topological measure. In this simple one-dimensional model, cracks in the film, denoted by Γ, are sets of dimension 0, *i.e.* are the discrete set of points at which the displacement can jump. Their measure reduces to the counting measure $\#(\Gamma)$. On the other hand, the crack set associated to debonding cracks Δ is of dimension 1, their associated energy is proportional to the one-dimensional Lebesgue measure (length) $\mathcal{L}(\Delta)$.

Hence, the surface energy per unit depth is given by:

$$S(\Gamma,\Delta) := G_f h_f \,\#(\Gamma) + G_b\,\mathcal{L}(\Delta),$$

where G_f and G_b are the three-dimensional toughnesses of the film and bonding layer, their dimensions being that of an energy per unit length.

Finally, the total energy the brittle system, sum of the elastic and surface energies, reads:

$$\begin{aligned} E(u,\Gamma,\Delta) :=& P(u,\Gamma,\Delta) + S(\Gamma,\Delta) \\ =& \frac{1}{2}\int_{\mathcal{A}\setminus\Gamma} \mu h_f (u' - e_0)^2 dx + \frac{1}{2}\int_{\mathcal{A}\setminus\Delta} k(u-w)^2 dx \\ &+ G_f h_f \,\#(\Gamma) + G_b\,\mathcal{L}(\Delta). \end{aligned} \tag{2.1}$$

Remark 2.1. *The one-dimensional assumption is reasonable for slender three-dimensional systems,* i.e. *for thin strips, under bi-axial loads or for very deep strips under uni-axial loads, away from the boundaries, where the fields are invariant with respect to the direction orthogonal to the load, see Figures 2.2.*

More delicate are the assumptions underlying the form of the limit energy (2.1)*, regarding the elastic energy and the geometric characterization of the crack surfaces. Both have profound influence on the analysis that follows. They imply that the bonding layer essentially undergoes shear deformations, whereas the film is a linear shear-free membrane; and on the other hand, that cracks in the film are vertical and cut the entire film, whereas cracks in the bonding layer are planes parallel to the surface. The justification of these two assumptions as asymptotic properties of a three-dimensional system satisfying specific scaling laws is the main concern of Chapter 3.*

2.1.1 Dimensional analysis

We recast the energy of Equation (2.1) into a non-dimensional form to isolate the meaningful parameters, introducing the length scales x_0, u_0 and the non-dimensional spatial variable $\tilde{x}$ and displacement $\tilde{u}$ defined by:

$$\tilde{x} := x/x_0 \quad \text{and} \quad \tilde{u} := \frac{u-w}{u_0},$$

Note the rescaling of the displacement field which allows us to incorporate the effect of the imposed displacement w into the inelastic strain. Thus the latter is indeed the most general form of load. In fact, although we can always absorb w into e_0 by a simple change of variables, the converse is always true only in dimension one. In higher dimensions in fact, this possibility holds only if e_0 satisfies additional compatibility conditions (*i.e.* for the solvability of a system of linear PDEs).

We choose length scales x_0 and u_0 such that the equivalent stiffness of the elastic foundation and the film's toughness are unit, that is:

$$x_0 = \sqrt{\mu h_f/k}, \qquad \frac{u-w}{\sqrt{G_f x_0/\mu}}.$$

Consequently, denoting by $\tilde{\mathcal{A}}$, $\tilde{\Gamma} \equiv \Gamma$ and $\tilde{\Delta}$ the rescaled axis and crack sets, the total energy (2.1) is rewritten:

$$\tilde{E}(\tilde{u}, \tilde{\Gamma}, \tilde{\Delta}) = \frac{1}{2}\int_{\tilde{\mathcal{A}}\setminus\tilde{\Gamma}} (\tilde{u}'(\tilde{x}) - \tilde{e}_0)^2 \, d\tilde{x} + \frac{1}{2}\int_{\tilde{\mathcal{A}}\setminus\tilde{\Delta}} \tilde{u}(x)^2 \, d\tilde{x} + \#(\tilde{\Gamma}) + \gamma\mathcal{L}(\tilde{\Delta}).$$

where:

$$\tilde{e}_0 = e_0\sqrt[4]{\frac{(\mu h_f)^3}{G_f^2 k}}, \qquad \gamma = \sqrt{\frac{\mu h_f}{k}}\frac{G_b}{G_f} = \frac{G_b}{G_f}x_0, \qquad \tilde{E} := E/(x_0 G_f).$$

Finally, dropping the tilde for sake of conciseness, the total energy reduces to:

$$E(u, \Gamma, \Delta) := \int_{\mathcal{A}\setminus\Gamma} \frac{1}{2}\left(u'(x) - e_0\right)^2 dx + \int_{\mathcal{A}\setminus\Delta} \frac{1}{2}u(x)^2 dx + \#(\Gamma) + \gamma\mathcal{L}(\Delta). \tag{2.2}$$

Three non-dimensional parameters determine uniquely the energy function (2.2): the non-dimensional length of the film L (in x_0-units), the relative bonding toughness γ, and the loading intensity e_0.

Remark 2.2. *The choice of the scaling parameters x_0 and u_0 is free. The present choice is dictated by convenience: it allows to obtain a simpler expression of the strong equilibrium equations. However, no matter what the choice of the scaling parameters is, the important feature of this system is that an* intrinsic length scale *exists, given by the competition between the strain energy of the bar (non-dimensional) and the energy of the elastic foundation (homogeneous to the square of a length). Another possible choice is to set x_0 so to rescale the physical domain to a fixed* unit *domain. In this case, the equivalent stiffness of the elastic foundation is $\kappa = \frac{kL^2}{\mu h_f}$ and we can isolate a non-dimensional characteristic length scale $\ell_e = \kappa^{-1/2}$.*

2.2 The static problem: energy minimizers at fixed load

We address now the question of finding energy minimizers for a given load intensity, without involving any notion of history or irreversibility. We characterize, for any given load, the energy minimizers and establish their qualitative properties. With the modeling assumptions illustrated above, the static problem of brittle fracture of Section 1.2.3, reduces to the one-dimensional problem reformulated as follows.

Problem 2.1 (Strong formulation of the static problem in one-dimension)**.** *The static one-dimensional problem of the reduced brittle thin film system consists in finding, for a given load intensity e_0, the crack set Γ, debonded set Δ and the displacement field $u \in H^1(\mathcal{A} \setminus \Gamma)$ that solve the following minimization problem*

$$\inf\{E(u,\Gamma,\Delta): \quad \Gamma \subset \mathcal{A}, \Delta \subset \mathcal{A},\ u \in H^1(\mathcal{A}\setminus\Gamma),$$

i.e. *that satisfy the following global minimality condition:*

$$(gm): \quad E(u,\Gamma,\Delta) \le E(\hat{u},\hat{\Gamma},\hat{\Delta}), \quad \forall \hat{\Gamma} \subset \mathcal{A},\ \forall \hat{\Delta} \subset \mathcal{A},\ \forall \hat{u} \in H^1(\mathcal{A}\setminus\hat{\Gamma};\mathbb{R}). \tag{2.3}$$

By selecting appropriate test functions, the variational inequality (2.3) allows us to retrieve necessary properties that characterize minimizers. In particular, choosing $\Gamma = \Delta = \emptyset$ we investigate the sound elastic response of the body and by choosing $\Delta = \emptyset$ (resp. $\Gamma = \emptyset$) we characterize the fully bonded system subject to transverse cracks only (resp. the sound film subject to debonding only). Finally, combining the necessary properties of such states we study the fully coupled problem, highlighting the interplay between the two failure modes and the elastic response. We consider homogeneous inelastic strain loads which, in the one-dimensional setting, are represented by a scalar constant. We henceforth denote the inelastic strain by t, the analogies with the notion of "time" that this notation evokes, are discussed further in Section 2.3.

2.2.1 The sound elastic film

We look for the elastic solution for a sound film, *i.e.* the displacement field that verifies Equation (2.3) for $\Delta = \Gamma = \emptyset$. The solution is unique because of the strict convexity

and coercivity of the elastic energy density. The equilibrium displacement satisfies the following first order local minimality condition:

$$D_u E(u,\emptyset,\emptyset)(v) = \int_{\mathcal{A}} \left\{ \left(u(x)' - e_0\right) v(x)' + u(x)v(x) \right\} dx = 0, \qquad \forall v \in H^1(\mathcal{A}), \quad (2.4)$$

where $D_u E(u,\cdot,\cdot)(v)$ denotes the Gateaux derivative of the functional $E(u,\cdot,\cdot)$ with respect to u along the direction v. After integration by parts and applying standard arguments of the Calculus of Variations, one writes the Euler-Lagrange equations associated to the first order necessary conditions for energy minimality. From (2.4) we obtain:

$$\begin{aligned} \text{(equilibrium)} \qquad & -u''(x) + u(x) = 0 \quad \text{a.e. } x \in (-L/2, L/2) \\ \text{(boundary conditions)} \qquad & u'(-L/2) = u'(L/2) = e_0 \end{aligned}$$

which are the strong formulation of the equilibrium equations and the associated natural boundary conditions. They are integrated to get the expression of the equilibrium displacement field under the load t which reads:

$$u_t(x) := e_0 \, \frac{\sinh(x)}{\cosh(L)}. \quad (2.5)$$

The associated non-dimensional equilibrium stress is:

$$\sigma_t(x) = u_t'(x) - e_0 = e_0 \left(\cosh(x)\,\mathrm{sech}(L/2) - 1\right). \quad (2.6)$$

The elastic displacement field is plotted in Figure 2.4. The total energy corresponding to this solution is:

$$E_t(L) := \mathcal{E}(u_t,\emptyset,\emptyset) = {e_0}^2 F(L), \qquad \text{with} \qquad F(L) = \left(\frac{L}{2} - \tanh\left(\frac{L}{2}\right)\right). \quad (2.7)$$

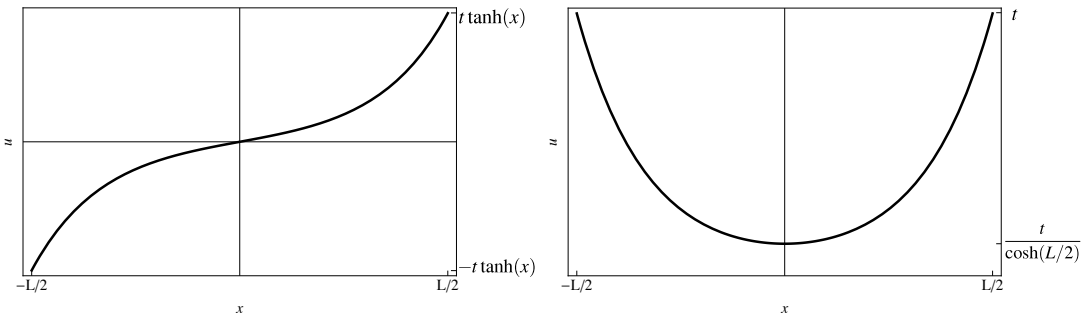

Figure 2.4: Elastic displacement (left) and strain (right) for a sound film of dimensionless length $L = 6$

2.2.2 The debonding problem

The sound elastic solution is fully characterized and we now focus on the problem of debonding alone of an initially sound film. Physically, this is the case when the transverse fracture toughness is much higher than the debonding toughness, *i.e.* $\gamma \ll 1$ and transverse cracking is not an energetically viable mechanism to reduce the stored energy. However, note that the properties of the debonded solutions established below hold independently of the fracture toughness ratio and spring from necessary properties of energy minimizers.

Fixing $\Gamma = \emptyset$, the global minimality (gm) requirement of Equation (2.3) reads:

$$E(u, \emptyset, \Delta) \leq E(\hat{v}, \emptyset, \hat{\Delta}), \quad \forall \hat{v} \in H^1(\mathcal{A}), \quad \forall \hat{\Delta} \subseteq \mathcal{A}.$$

Introducing the characteristic function χ_Δ of the debonded region Δ, defined as:

$$\chi_\Delta : \mathcal{A} \mapsto [0,1], \qquad \chi_\Delta(x) = \begin{cases} 1, & \text{if } x \in \Delta \\ 0, & \text{otherwise} \end{cases}$$

the total energy (2.2) is rewritten as follows:

$$E(u, \emptyset, \chi_\Delta) \;:=\; \int_{\mathcal{A}} \left\{ \frac{1}{2} \left(u'(x) - e_0\right)^2 + \frac{1}{2} u(x)^2 (1 - \chi_\Delta) + \gamma\, \chi_\Delta \right\} dx.$$

Characterization of the debonded domain

The energy density of the last equation, at a given point $x \in \mathcal{A}$ is a linear functional with respect to χ_Δ. The minimality principle with respect to χ_Δ in (2.3) reduces to the box-constrained minimization of a linear functional. Moreover, the functional $\chi_\Delta \mapsto E(\cdot, \cdot, \chi_\Delta)$ is local (derivative-free). By a localization argument, the order one optimality condition with respect to χ_Δ yields a local debonding condition. At a point x, debonding is energetically favorable if $|u(x)| < \sqrt{2\gamma} := u_d$ and the debonded domain is explicitly computed:

$$\chi_\Delta(x) = \begin{cases} 1, & \text{if } |u(x)| < u_d \\ 0, & \text{if } |u(x)| \geq u_d \end{cases}, \tag{2.9}$$

where $u_d = \sqrt{2\gamma}$ is the critical displacement threshold for debonding. This yields the first property of debonded states.

Property 2.1. *The debonding condition is a local criterion based on the absolute value of the displacement, to be compared to a critical debonding threshold $u_d = \sqrt{2\gamma}$ function of the material parameters of the system.*

The elimination of χ_Δ according to (2.9) allows us to rewrite the energy in terms of u and Γ alone as follows:

$$\mathcal{E}(u, \Gamma) := \frac{1}{2} \int_{\mathcal{A}} \left(u'(x) - e_0\right)^2 dx + \int_{\mathcal{A}} f(|u(x)|)\, dx,$$

where we introduced the non-smooth, non-convex energy density

$$f(\delta) = \begin{cases} \frac{\delta^2}{2}, & \text{if } \delta < u_d \\ \gamma, & \text{if } \delta \geq u_d \end{cases},$$

accounting for both the elastic contribution of the bonding layer at bonded points, and the surface energy related to debonding in debonded regions. The energy density in (2.2.2) is non-convex with respect to u and not differentiable in u at the critical threshold u_d.

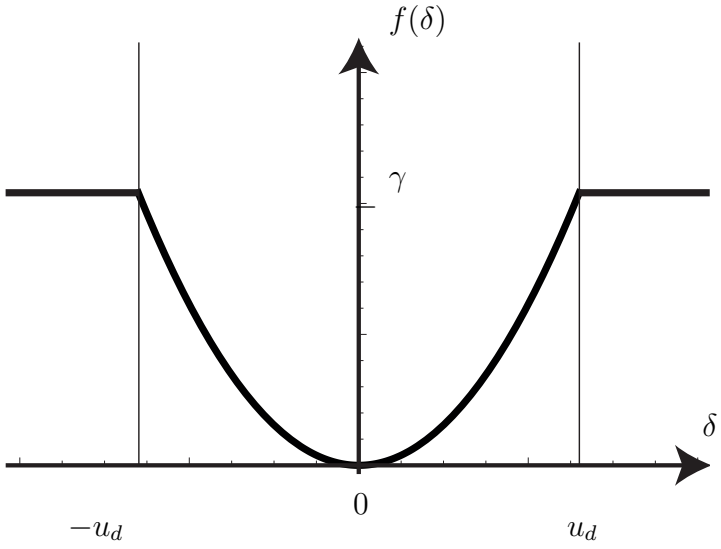

Figure 2.5: The non-convex, non-smooth energy density $f(\delta)$ accounting for both the elastic and debonding energy. Such energy density is quadratic in the elastic phase (for $\delta \leq u_d$) and constantly equal to γ after debonding.

According to the global minimality principle (gm), the problem of finding the solution with debonding and without transverse fractures (i.e. $\Gamma = \emptyset$) is formulated as follows:

$$\min_{u \in H^1(\mathcal{A})} \mathcal{E}(u, \emptyset).$$

Here, unlike in the purely elastic case (Section 2.2.1), the solution for the displacement cannot be derived using the classical Euler-Lagrange equations associated to the first order local minimality conditions for $\mathcal{E}(u, \emptyset)$. This is due to the non-differentiability of the energy density at $u = u_d$. However, a characterization of local minimizers of $\mathcal{E}(u, \emptyset)$ is provided by the following fundamental properties, the proofs being given in Appendix 2.A. Note that the present problem and the results below are very similar to those presented in [MT04].

Lemma 2.1. *If a field $u \in H^1(\mathcal{A})$ is a local minimizer of $\mathcal{E}(u, \emptyset)$, then u is a monotonic function of x.*

Lemma 2.2. *Let $f : \mathbb{R} \mapsto \mathbb{R}$ be a continuous function. If a field $u \in H^1(\mathcal{A})$ is a local minimizer of $\mathcal{E}(u, \emptyset)$ then it satisfies the following first integral and boundary conditions:*

$$\begin{aligned} \exists C \in \mathbb{R}: \qquad & u'(x)^2 - {e_0}^2 - f(|u(x)|) = C, && \forall x \in [0, L], \\ & u'(-L/2) = u'(L/2) = e_0. \end{aligned}$$

The monotonicity of the solution (Lemma 2.1) implies that the maximal values of $|u|$ are attained at the free boundaries of the domain. Hence, in view of the debonding condition (2.9), we have the following property characterizing the bonded domain.

Property 2.2. *If debonding takes place, the bonded region of the film is an interval, and the debonded domain is of the form:*

$$\begin{aligned} \Delta &= [-L/2, -L/2 + D_1] \cup [L/2 - D_2, L/2], \\ \textit{with} \quad & 0 \le D_1, D_2 \in \mathbb{R}, \quad \textit{and } D := D_1 + D_2 \le L. \end{aligned} \tag{2.11}$$

The monotonicity of the displacement field rules out the possibility of a relaxation phenomenon associated to the coexistence of fine mixtures of debonded and bonded phases. The property of monotonicity is due to the convexity (although not strict) of the energy $\mathcal{E}(u, \cdot)$. The lack of strict convexity, in turn, results into a lack of uniqueness of the displacement solution, as analyzed in the sequel.

Using Equations (2.10) one computes explicitly the solution with debonding which is in the form (see Figure 2.6(a)):

$$u(x) = \begin{cases} e_0(x + L/2 - D_1 + u(-L/2 + D_1), & -L/2 \le x < -L/2 + D_1 \\ e_0 \dfrac{\sinh(x - \xi_0)}{\cosh((L - D)/2)}, & -L/2 + D_1 \le x \le L/2 - D_2, \\ e_0(x - L/2 + D_2 + u(L/2 - D_2)), & -L/2 - D_2 < x \le L/2 \end{cases} \tag{2.12}$$

where $\xi_0 = (D_1 - D_2)/2$ is the coordinate of the center of the bonded domain. In particular, the debonded regions are stress free and the elastic energy vanishes therein. Hence, denoting by D the total debonded length and $B := L - D$ the length of the bonded interval, the total energy of the system is a function of B alone and reads as

$$\bar{E}_t(B) := E_t(B) + \gamma(L - B) = e_0^2 F(B) + \gamma(L - B),$$

where $E_t(\cdot)$ is given by (2.7). The dependence of $\bar{E}_t$ only upon the length of the bonded interval B implies that to all equilibrium states satisfying (2.10) corresponds the same value of energy, regardless of the distribution of the debonded domains, *i.e.* independently of D_1, D_2 provided that the size of the bonded domain $B = L - D_1 - D_2$ is the same.

Size of the debonded domain for a given load

To close the static problem of debonding, it remains to determine the optimal size of the debonded region for a given load t which by (gm) solves the following problem:

$$\min_{0 \le B \le L} \bar{E}_t(B).$$

This is the minimization of a strictly convex function of B with inequality constraints and admits a *unique* solution for the optimal bonded length $0 \leq B^* \leq L$. This solution has to satisfy the following first order local minimality condition:

$$\bar{E}_t'(B^*)(B - B^*) \geq 0, \quad \forall\, 0 \leq B \leq L, \quad \text{with } \bar{E}_t'(B) = t^2 \tanh^2(B/2)/2 - \gamma.$$

By the properties of convex functions, the unique minimum is attained in $B^* = 0$ if $E'(0) \geq 0$, in $B^* = L$ if $E'(L) \leq 0$, and in $0 < B^* < L$ such that $\bar{E}_t'(B^*) = 0$ otherwise.

The first case $B^* = 0$, *i.e.* a completely debonded film, is impossible because $\bar{E}_t'(0) = -\gamma < 0$.

The second case $B^* = L$ corresponds to a solution without debonding. It is obtained only if $t \leq \sqrt{2\gamma}$ or $L \leq 2\,\mathrm{arctanh}\sqrt{2\gamma/t^2}$.

Finally, for $t > \sqrt{2\gamma}$ and $L > 2\,\mathrm{arctanh}\sqrt{2\gamma/t^2}$, the solution is such that $\bar{E}_t'(B^*) = 0$, that is $B^* = 2\,\mathrm{arctanh}\sqrt{2\gamma/t^2}$. This latter case corresponds to solutions with debonding.

We resume the results of the debonding of a film of length L without transverse fracture in the following Proposition:

Proposition 2.1. *For a fixed load t, the solution of Problem* (2.1) *with debonding and without transverse fractures (*i.e. $\Gamma = \emptyset$*) is in the form* (2.12)*. The displacement field u is a monotonic function of x, the bonded domain is an interval and debonding, if present, takes place at the free ends of the domain. The debonded domain Δ has the form* (2.11)*. The total debonded length D is uniquely determined, but the lengths D_1 and D_2 are arbitrary. The optimal length of the bonded interval is*

$$B_t(L) = \begin{cases} L & \text{for} \quad L \leq L_d(t,\gamma) \\ L_d(t,\gamma) & \text{for} \quad L > L_d(t,\gamma) \end{cases}, \tag{2.13}$$

where

$$L_d(t,\gamma) := \begin{cases} \infty & \text{for} \quad t \leq t_d = \sqrt{2\gamma} \\ 2\,\mathrm{arctanh}\sqrt{2\gamma/t^2}, & \text{for} \quad t > t_d \end{cases}, \tag{2.14}$$

In particular, for $t \leq t_d = \sqrt{2\gamma}$ there is no debonding, independently of the film length. For $t > t_d$ the film debonds if and only if it is suffciently long ($L > L_d(t,\gamma)$) or, equivalently, the load is sufficient high, i.e. *$t > t_b(L,\gamma)$, with*

$$t_b(L,\gamma) := \sqrt{2\gamma}\,\coth\frac{L}{2}. \tag{2.15}$$

The energy of the optimal solution is:

$$\begin{aligned} \hat{E}_t(L) &:= \bar{E}_t(B_t(L)) \\ &= \begin{cases} t^2\,(L/2 - \tanh\,(L/2)) & \text{for } L \leq L_d(t,\gamma) \\ \gamma L + 2t^2\left((1 - 2\gamma/t^2)\,\mathrm{arctanh}\sqrt{2\gamma/t^2} - \sqrt{2\gamma/t^2}\right) & \text{for } L > L_d(t,\gamma) \end{cases}. \end{aligned} \tag{2.16}$$

The main results are graphically illustrated in Figure 2.6 which shows a phase diagram for the bonded length B as a function of (L,t), and a snapshot of the displacement field for a partially bonded film.

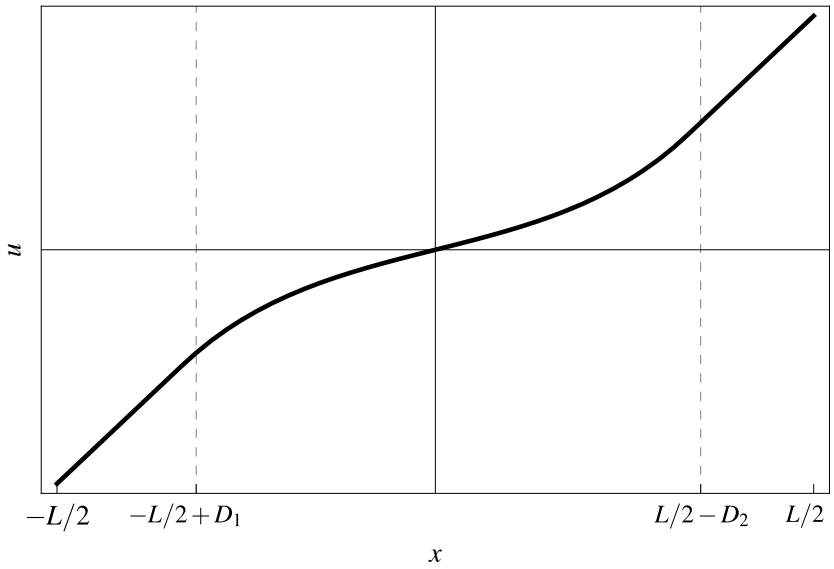

(a) Phase diagram of the optimal size of the bonded domain, as function of the film length and load intensity, where $L_d(t,\gamma)$ is given in Equation (2.14).

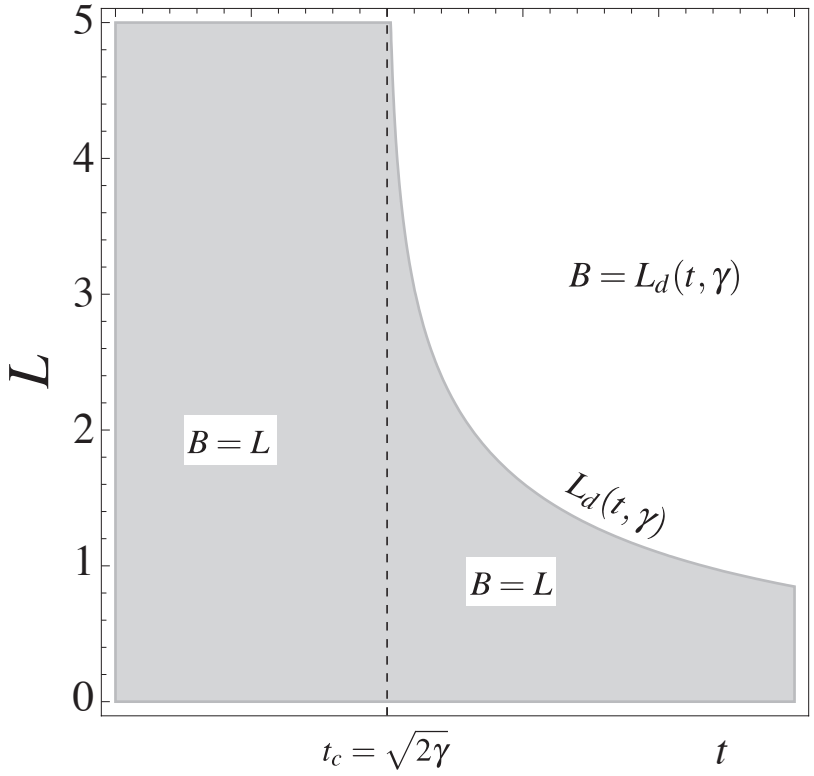

(b) Displacement field for the partially bonded film, see Equation (2.12).

Figure 2.6: Solution of (GM) for a film with debonding and without transverse fracture.

2.2.3 The transverse fracture problem

We now focus the attention on the problem of transverse fracture alone. Physically, transverse cracks are the only energetically efficient way of reducing the stored energy in the limit regime where the film toughness is small compared to the debonding toughness, *i.e.* when $\gamma \ll 1$. However, as in the preceding case, the properties established below are general properties of energy minimizers and hold regardless of the value of the toughness ratio.

The topology of the cracks in the one-dimensional setting is simple. As introduced above, in the reduced model they amount to a set of points. A general state with $n-1$ cracks is sketched in Figure 2.7. The domain $\mathcal{A}$ is split into n segments, the crack set is the set of $n-1$ points $\Gamma^{(n)} = \{x_i : -L/2 < x_i < L/2\}_{i=1}^{n-1}$.

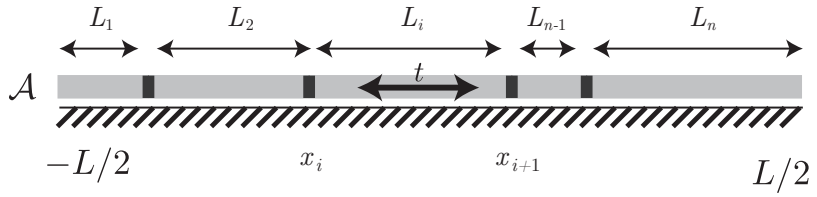

Figure 2.7: A $1D$ film split into n segments with $n-1$ transverse cracks.

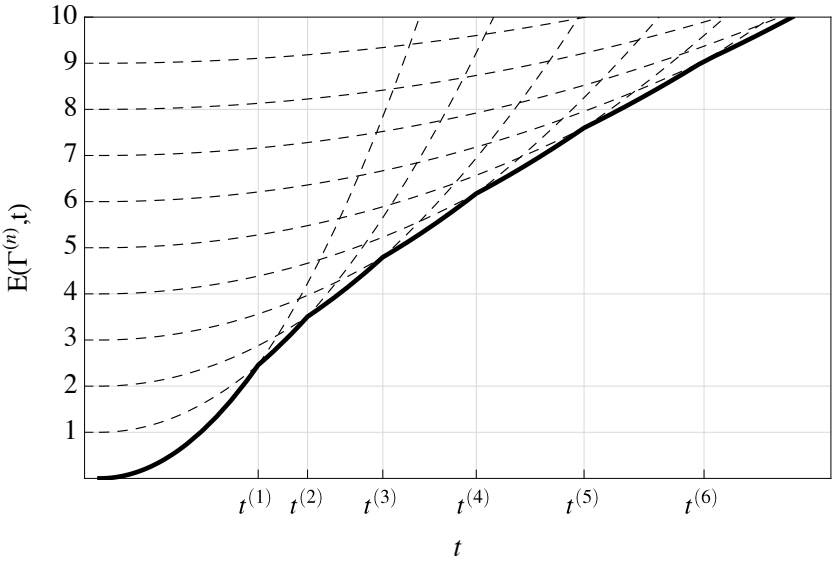

Figure 2.8: Total energy for transverse fracture without debonding for different number of cracks. The cracks are equally spaced. The optimal crack number for a given loading is that of the curve attaining the lowest energy level, this last indicated by the continuous stroke.

Each segment can be seen as a sound domain of non-dimensional length $L_i = x_i - x_{i-1}$, where $x_0 = -L/2$ and $x_n = L/2$. Hence, using the results of Section 2.2.1 and the expression of the equilibrium energy (see Equation (2.7)), the total energy of the system

is written as the following function of the number of segments n and their lengths L_i:

$$E_t(n; L_1, \dots, L_n) = t^2 \sum_i^n F(L_i) + (n-1),$$

where $F(L)$ is defined in Equation (2.7).

Characterization of transverse cracks

For a fixed number of cracks n, the problem of finding the optimal segment lengths $L_1, \dots, L_n$ according to (gm) consists in solving the following minimization problem:

$$\min_{L_1,\dots,L_n} E_t(n; L_1, \dots, L_n), \quad \text{with} \quad \sum_{i=1}^n L_i = L, \quad L_i > 0, \tag{2.17}$$

which is an optimization problem for a function of n scalar variables with linear constraints. Observing that $\partial^2 E_t / \partial L_i \partial L_j = \delta_{ij} t^2 F''(L_i)$, where $\delta_{ij} = 1$ for $i = j$ and $\delta_{ij} = 0$ for $i \neq j$, and being

$$F''(L_i) = 4 \sinh(L_i/2)^4 / \cosh(L_i)^3 > 0, \qquad \forall L_i > 0,$$

we conclude that the energy is a strictly convex function of L_i. Consequently the minimization problem (2.17) admits one and only one solution given by

$$L_i = \frac{L}{n}, \qquad \forall i = 1, \dots, n.$$

Hence, for any given number of cracks $n-1$, energy minimizers enjoy the following property.

Property 2.3 (Distribution of cracks)**.** *A crack set minimizing the energy 2.2.3 consists in equally spaced array of transverse cracks.*

The optimal crack arrangement is that of an equally distributed array of cracks throughout the film, recovering experimental evidence of periodicity of the cracks highlighted in [Nag+93], [Fuk+99], [Ber+02], [Let+04], [Let+10].

The total energy of a system with $n-1$ equally spaced transverse fractures is:

$$E_t^{(n)} = t^2 \sum_i^n F\left(L/n\right) + (n-1). \tag{2.18}$$

The energy in the last expression is a family of parabolæ. In Figure 2.8, we plot $E_t^{(n)}$ as a function of t for different values of n.

Number of cracks for a given load

By (gm), the optimal number of cracks for a given load is associated to the energy curve attaining the lowest value. The corresponding critical loads $t^{(n)}$ in Figure 2.8 are found analytically by looking for the intersections between $E_t^{(n)}$ and $E_t^{(n+1)}$. We conclude with the following result.

Proposition 2.2. *The solution of the Problem* (2.1) *without debonding is that of an equally spaced array of cracks partitioning the film into n regular segments of length* $L_i = L/n$. *The displacement in each regular segment is of the form* (2.5) *with* $L = L_i$ *and the total energy of the system is given by Equation* (2.18). *Let* $1 \leq n \in \mathbb{N}$, *then the solution with* $n-1$ *cracks is optimal for:*

$$t^{(n-1)} < t < t^{(n)}, \quad \textit{with} \quad \begin{array}{l} t^{(n)} = \dfrac{1}{\sqrt{(1+n)\tanh\dfrac{L}{2(1+n)} - n\tanh\dfrac{L}{2n}}}, \\ t^{(0)} := 0. \end{array} \tag{2.19}$$

2.2.4 Coupled transverse fracture and debonding

We now consider the case in which transverse fracture and debonding may take place at the same time in a film of length L. Suppose that the film is subdivided by $n-1$ transverse fractures in n segments of lengths $\{L_1, \ldots, L_n\}$. Given the segment length L_i, the solution for the displacement in the i-th segment is that of a film with possible debonding and without transverse fracture, as described in Proposition 2.1. Hence, the total energy of the system may be written as follows:

$$\hat{E}_t(n; L_1, \ldots, L_n) := \sum_i^n \hat{E}_t(L_i) + (n-1),$$

where $\hat{E}_t(L_i)$, defined in equation (2.16), is the sum of the elastic and the debonding energy of the i-th segment. As in Section 2.2.3, for a fixed number of transverse cracks, the problem of finding the optimal segment lengths L_i's may be formulated as the following constrained optimization problem:

$$\min_{L_1,\ldots,L_n} \hat{E}_t(n; L_1, \ldots, L_n), \quad \text{with} \quad \sum_{i=1}^n L_i = L, \quad L_i > 0. \tag{2.20}$$

For $t < t_c$ the energy is strictly convex with respect to the L_i's. As in Section 2.2.3, the solution is in the form of periodic transverse cracks without delamination, with $L_i = L/n$ and the displacement field in each segment is as in equation (2.5) and Figure 2.4 (with $L = L_i$).

For $t > t_c$ the energy is not convex anymore with respect to the L_i's. Introducing the Lagrange multiplier λ associated to the equality constraint $\sum_{i=1}^n L_i = L$, the first order optimality conditions for (2.20) read:

$$\hat{E}_t'(L_i) = \lambda \quad \text{for} \quad i = 1 \ldots n \quad \text{and} \quad \sum_{i=1}^n L_i = L. \tag{2.21}$$

The derivative of the energy of a single segment, $\hat{E}_t'(L_i)$, is strictly monotonic, it increases from 0 to γ, for $0 \leq L_i < L_b(t, \gamma)$ and is constantly equal to γ for $L_i > L_b(t, \gamma)$. Hence, we classify the solution of (2.21) in two types, depending upon the optimal value of λ:

(i) $\lambda < \gamma$ *(solutions without debonding).* In this case $\hat{E}'_t(L_i) = \lambda$ admits a unique solution for each L_i. All the segments' lengths L_i are the equal and, from $\sum_{i=1}^n L_i = L$, we obtain $L_i = L/n$. This is the case of periodic cracking without debonding, as in Section 2.2.3. This solution is admissible only if $L_i = L/n \leq L_b(t, \gamma)$, i.e. for $t < t_b(L/n, \gamma)$, where $t_b(L, \gamma)$ is the critical load for debonding a film of length L given by Equation (2.15).

(ii) $\lambda = \gamma$ *(Solutions with debonding).* In this case the problem (2.21) admits infinitely many solutions with $L_i \geq L_b(t)$. Even if the L_i's are not uniquely determined, being $L_i \geq L_b(t)$ debonding is necessarily present in each segment. The length of the bonded interval in each domain is $B = L_b(t, \gamma)$ and the displacement field in each segment is in the form (2.12) (see Proposition 2.1). Being $L = \sum_{i=1}^n L_i \geq n\, L_b(t, \gamma)$, this solution is possible only for $t > t_b(L/n, \gamma)$. Note that only the length of the bonded interval of each segment is uniquely determined. The lengths L_i are not uniquely determined because, for each segment, all the solutions obtained transferring debonded regions from one end of the segment to the other, without changing the bonded length, are energetically equivalent.

Hence we may conclude with the following proposition which gives the static solution with $n-1$ transverse fractures and with free debonding as a function of t.

Proposition 2.3. *The solution of the problem* (gm) *for a film of initial length L and relative fracture toughness γ with possible debonding and with $n-1$ transverse cracks is as follows:*

(i) For $t < t_d^{(n)} := t_b(L/n, \gamma)$ there is no debonding and the cracks are equally spaced with $L_i = L/n$.

(ii) For $t \geq t_d^{(n)}$, there is debonding. The solution for the displacement field in each segment of the film is in the form (2.12) *with $L = L_i$, $D_1 = D_{1,i}$ and $D_2 = D_{2,i}$. The length of the bonded interval is $L_b(t, \gamma)$ in each segment. The total debonded length is $D := \sum_{i=1}^n D_{1,i} + D_{2,i} = L - n\, L_b(t, \gamma)$. However, the lengths of the debonded intervals in each segment are not uniquely determined, because all the solutions obtained by varying $D_{i,1}, D_{i,2}$ and keeping constant the total debonded length D have the same energy.*

The total energy of the solution is

$$\hat{E}_t^{(n)} := \begin{cases} t^2\,(L/2n - \tanh\,(L/2n)) + (n-1) & \text{for} \quad t \leq t_d^{(n)} \\ (\gamma\, L - 1) + n(\,1 - t^2 \varphi(\sqrt{2\gamma}/t)) & \text{for} \quad t > t_d^{(n)} \end{cases}, \tag{2.22}$$

where $\varphi(x) = x + (x^2 - 1)\mathrm{arctanh}(x)$.

In order to close the problem, we must minimize $\hat{E}_t^{(n)}$ for a given load t. We are not able to provide a complete analytical solution of the latter, however we illustrate

a typical scenario for specific values of the numerical parameters with the help of the energy plot. In Figure 2.9 we show the total energy *vs* t for different values of n, for the coupled transverse fracture–debonding problem for $\gamma = 2.2$ and $L = 6$. The right figure is a zoom on the gray shaded region. The value of n corresponding to each of the curves is identified noticing that, for a vanishing load, the energy reduces to the number of cracks $n-1$. The dashed lines in the figure distinguish the states in which debonding has been triggered. We reconstruct the optimal state of the system by comparing the energy levels in Figure 2.9. For $t < t_d^{(4)}$ the optimal solution is with transverse fracture without debonding. The critical loads $t^{(n)}$, defining the range of optimality for a solution with $n-1$ cracks, are those defined by Equation (2.19). Moreover, there exists a critical load t^* beyond which the optimal solution is always a single debonded segment of length $L_b(t,\gamma)$ see Equation (2.14) for the expression of the debonded length. Indeed, for $t > t^*$ the lowest energy is always attained with $n = 1$. Such critical load is the (unique) solution of the equation: $1 - t^2\varphi(\sqrt{2\gamma}/t) = 0$, where $\varphi(x)$ is defined in Proposition 2.3. The range of the loading parameter for which there is a true coupling between debonding and transverse fracture is $t^{(4)} \le t \le t^*$. To better illustrate the solution, we report in Figure 2.10 the optimal displacement field for the following three representative loadings:

- $t = 3.00$, Figure 2.10(a): the minimum energy is attained on the energy curve relative to $n = 4$, at point A in Figure 2.9. The load is below the debonding threshold $t_d^{(4)} = 3.22$ associated to $n = 4$. The film is in the periodic multifissuration regime, with three transverse fractures.

- $t = 3.30$, Figure 2.10(b): the minimum energy is attained at point B of Figure 2.9 on the energy branch for which debonding is active. The energy curve is associated to $n = 4$, and the value of the bonded domain size, for each of the four segments into which the film is split, is $B_t = 1.16$.

- $t = 4.51$, Figure 2.10(c): the global energy minimizer is the state without transverse fractures denoted by point C in Figure 2.9. The film is bonded on a domain of size $B_t = 1.08$.

This result may be extended to generic values of L and γ as follows.

Proposition 2.4. *For a film of length L and relative debonding toughness γ, let $\bar{n}$ be the smallest (positive integer) value of n for which $t_d^{(n)} < t^{(n+1)}$ and let t^* be the (unique) root of $1 - t^2\varphi(\sqrt{2\gamma}/t) = 0$. Then the solution of the static Problem (2.1) with free transverse fracture and debonding is in the following form:*

- *For $t < t_d^{(\bar{n})}$, it is with transverse fractures only, with $n-1$ equally spaced cracks in each loading interval $t^{(n-1)} < t < t^{(n)}$ with $n \le \bar{n}$, as in Proposition 2.2.*

- *For $t > t^*$ it is with debonding only, as in Proposition 2.1.*

The number $\bar{n}$ is the minimum number of segments in which a film is split by transverse fractures when there is debonding. The dependence of $\bar{n}$ and t^* on the two dimensionless parameters L and γ is illustrated numerically in Figure 2.11. The critical load t^* is independent of L.

For loadings in the interval $t_d^{(\bar{n})} < t < t^*$, there is a nontrivial coupling between transverse fracture and debonding and we are not able to derive a general and simple result for generic values of γ and L.

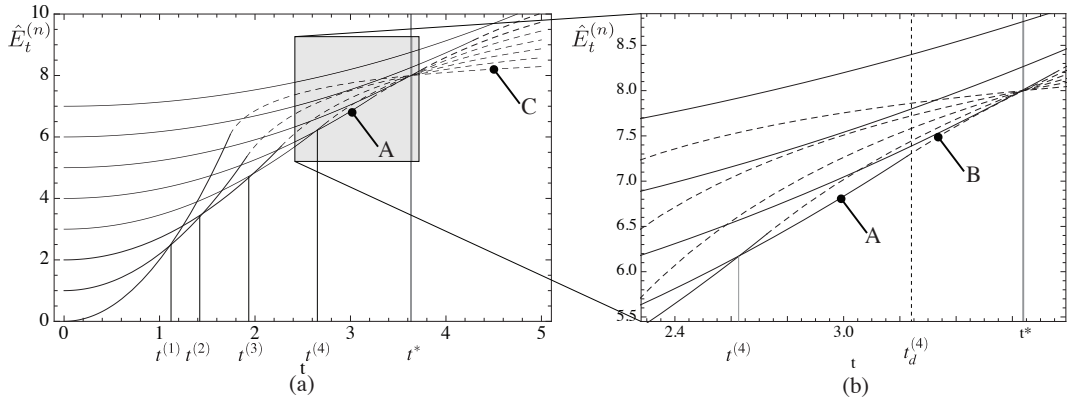

Figure 2.9: Energy curves $\hat{E}_t^{(n)}$ with possible debonding and transverse fracture for $\gamma = 2.2, L = 6$. Each curve is for a specific number $n-1$ of transverse fractures, corresponding to the value at the intersection with the axis $t = 0$. The solid continuous lines indicate the energy is obtained for a state without debonding, the dashed line for a state with debonding. The critical time t^* is indicated with a solid vertical line.

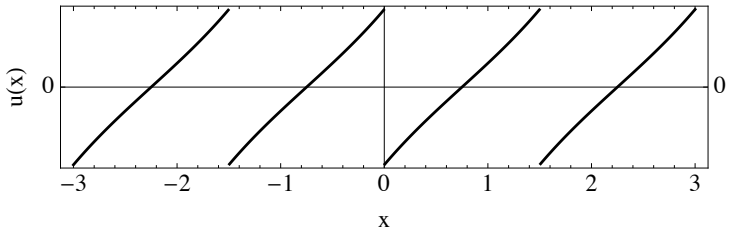

(a) Displacement field for the film split into four segments without debonding. This state corresponds to point A in Figure 2.9

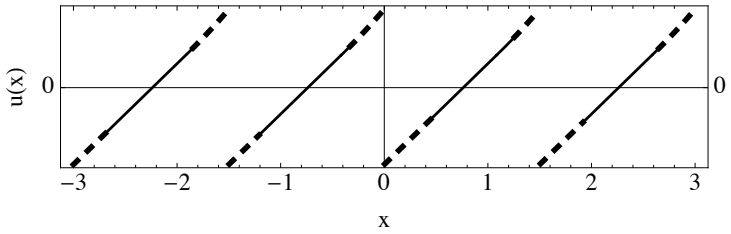

(b) Four debonded segments, point B in Figure 2.9. The size of the bonded segment is unique, the distribution of the debonded regions at the free boundaries is not.

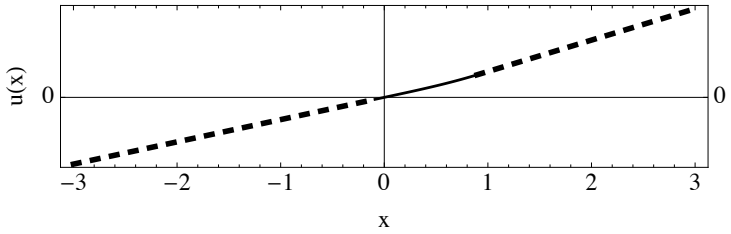

(c) The optimal solution above the critical load threshold t^* is a single debonded segment. See Figure 2.9, point C

Figure 2.10: The optimal displacement fields for the states A, B, C of Figure 2.9. Debonded regions are indicated with a dashed line.

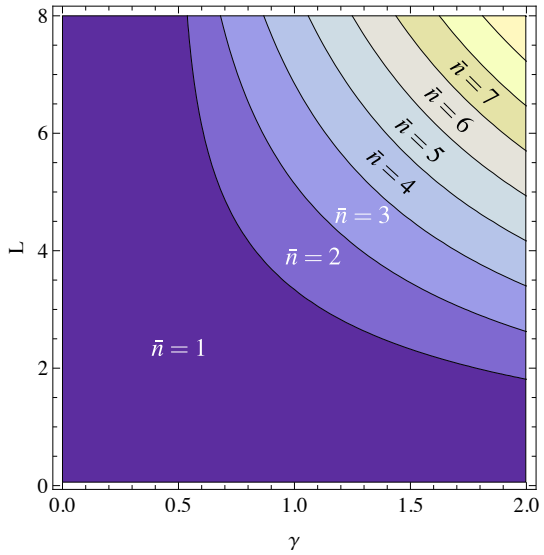

(a) Plot of $\bar{n}$ as a function of L and γ, $\bar{n}$ being the minimum number of pieces into which the film is split by transverse fractures when debonding appear

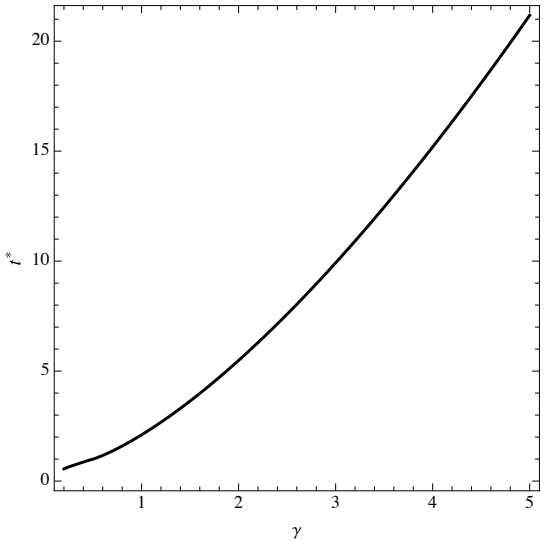

(b) Plot of t^* as a function of the relative debonding toughness γ, t^* being the critical load beyond which the optimal solution is that of a debonded film without transverse fractures (t^* is independent of the non-dimensional length L of the film), see also Figure 2.9.

Figure 2.11: Key properties of the solution of the static problem of a film of non-dimensional length L and relative debonding toughness γ (see Proposition 2.4). (b)

2.3 The quasi-static evolution problem

The analysis presented above characterizes static minimizers. We now turn the attention to the irreversible evolution of the system under an increasing load starting from an initially sound and unloaded state, *i.e.* $(u = 0, \Gamma = \emptyset, \Delta = \emptyset)$ at $t = 0$.

In the simplified case under study, Problem 1.3 reads as follows:

Problem 2.2 (Time-continuous, one-dimensional, evolution problem)**.** *Given a loading path $(e_0(t), w(t))$ for $t \in [0, T]$, the mapping $t \mapsto (u_t \in H^1(\mathcal{A} \setminus \Gamma_t),\ \Gamma_t \in \mathcal{A}, \Delta_t \subset \mathcal{A})$ is a quasi-static evolution if it satisfies the following items:*

(ir) Irreversibility:

$$\Gamma_t \supseteq \Gamma_s, \Delta_t \supseteq \Delta_s \quad \forall\, 0 \leq s \leq t.$$

(gst) Global stability:

$$E(u_t, \Gamma_t, \Delta_t) \leq E(u, \Gamma, \Delta), \quad \forall u \in H^1(\mathcal{A} \setminus \Gamma),\ \forall \Gamma \supseteq \Gamma_t, \forall \Delta \supseteq \Delta_t. \tag{2.23}$$

(eb) Energy balance:

$$\mathscr{E}(t) - \mathscr{E}(0) = -\int_0^t \left\{ \int_{\mathcal{A}\setminus\Gamma} \sigma_t \cdot \dot{e_0}(t) dx \right\} dt,$$

where here $\sigma_t := \left.\frac{\partial W(e)}{\partial e}\right|_{e(u_t)-e_0(t)} = \mu(e(u_t) - e_0(t))$.

The evolutions satisfying items (ir), (gst) and (eb) are constructed on the basis of the results of the static analysis of the previous section.

Remark 2.3. *The condition (gm) given in Problem* (2.1) *is stronger that the condition (gst) given in Equation* (2.23)*. In (gst), the admissible transverse cracks and debonded sets must satisfy the additional irreversibility conditions* $\hat{\Gamma} \supseteq \Gamma$, $\hat{\Delta} \supseteq \Delta$.

Indeed, all the static solutions *a fortiori* verify the (gst) condition. The (eb) condition is met by imposing the continuity of the total energy with respect to the load t, a requirement which is verified also by the static solutions reported in Figures 2.8, 2.16, and 2.9. A major novelty is the introduction of the irreversibility condition (ir) of Equation 2.2.

2.3.1 Evolution of transverse cracks

In the case without debonding ($\Delta = \emptyset$), the static analysis of Section 2.2.3 (Proposition 2.2) concludes that the state with $n - 1$ cracks partioning the domain in n regions of length L/n is optimal in the sense of global stability (gst) for loads t in the interval $(t^{(n-1)}, t^{(n)})$, given by Equation (2.19). The critical loads of Equation (2.19) are a strictly increasing sequence with respect to n, thus for an initially sound film, the first critical

load is $t^{(2)}$ corresponding to the first crack in the middle of the film. After the first crack, the irreversibility condition (ir) imposes a restriction on the admissible crack sets.

In summary, the admissible crack are the sets of $n_j - 1$ equally spaced cracks splitting the film in n_j segments of length L/n_j, with $n_j := 2^j$, and $j \in \mathbb{N}$, *i.e.* the number segments of is a power of two. Hence, the quasi-static evolution of the crack set of an initially sound film is determined specializing to this case the results of Proposition 2.2. In particular, the solution of the evolution problem is with $n_j - 1$ equally spaced cracks for loadings in the interval $t^{(n_j-1)} < t < t^{(n_j)}$ with $t^{(n_j)} = t_f\,(L/n_j)$, $t^{(0)} = 0$, where

$$t_f(L) = \frac{1}{\sqrt{2\tanh\frac{L}{4} - \tanh\frac{L}{2}}}, \tag{2.24}$$

is the critical load at which a sound film of length L splits in two segments of equal length with a transverse crack in the middle. The total energy of the solution obtained in this way and the number or segment n versus the load t are plotted in Figures 2.12(a) and 2.12(b), respectively.

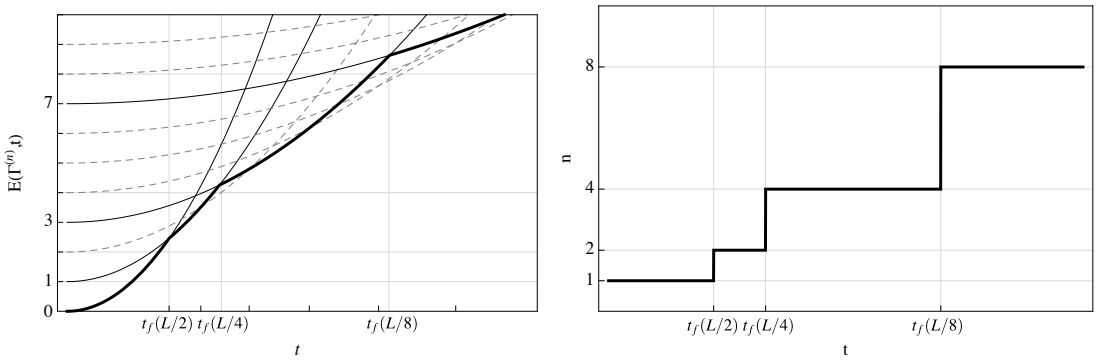

(a) (b)

Figure 2.12: Quasi-static evolution without debonding: (a) Energy curves $E(\Gamma^{(n)}, t)$ vs t for different n, the thick solid line denotes the global minimum corresponding to the solution of the evolution problem; (b) Number of parts n_j of length L/n_j vs t formed by the $n_j - 1$ equally spaced cracks, with $n_j = 2^j$.

2.3.2 Evolution of debonding

After the static solution of the debonding problem without cracks is known, its quasi-static counterpart is trivial. Essentially, we have to enforce irreversibility (ir) and restrict the energy competition to the admissible Δ's in (gm), *i.e.* to those that at time t verify the inclusion $\Delta_t \supseteq \Delta_s \quad \forall\, 0 \le s \le t$. The irreversibility condition is a two-fold requirement: the size of the debonded domain must be non decreasing and a *pointwise* irreversibility must be ensured.

The first requirement is satisfied by the static solution given in Proposition 2.1. Indeed the bonded length B_t given in Equation (2.13) is strictly decreasing with t. The

second condition is fulfilled provided that the lengths of the debonded intervals D_1 and D_2, in Equation (2.11), are *non-decreasing* functions of t. Hence, the result synthesized in Proposition 2.1 holds for the quasistatic evolution of irreversible debonding when instead of constants D_1 and D_2 we consider non–increasing functions $D_1(t)$ and $D_2(t)$. In the case of an irreversible quasistatic debonding evolution, a film of non–dimensional length L and relative toughness γ does not debond for $t < t_b(L, \gamma)$. At $t = t_b(L, \gamma)$ it starts debonding, and the length of the bonded interval is $L_b(t, \gamma)$.

2.3.3 Film subject to coupled transverse cracks and debonding

The analysis of the static problem in the coupled case concludes with the Propositions 2.2 and 2.3 which are the starting point for constructing solutions of the corresponding quasi-static problem.

Irreversibility imposes that the number of transverse cracks be of the form $n_j = 2^j - 1$, with $j \in \mathbb{N}$ and non-decreasing with t, and that the debonded domain be non-decreasing with t. For a given number $n - 1$ of transverse cracks, the static solution given in Proposition 2.1 may be directly extended to the quasi-static setting. At the critical load $t_b(L/n, \gamma)$ given by Equation (2.15), debonding starts simultaneously in each segment from –one or both– free boundaries. The energy of the solution is given by $\hat{E}_t^{(n)}$ of Equation (2.22). The length of the bonded part in each segment is L/n for $t < t_b(L/n, \gamma)$ and $L_b(t, \gamma)/n$ for $t > t_b(L/n, \gamma)$, with $L_b(t, \gamma)$ given by Equation (2.14). This solution respects irreversibility because of the monotonicity of $L_b(t, \gamma)$ with respect to t. Of course, the lengths of the debonded domains in each segment, $D_{1,i}$ and $D_{2,i}$, must be non-decreasing functions of t.

The determination of the evolution of the optimal number of transverse cracks is not an easy problem in the general case. We illustrate here a typical quasi-static evolution for specific values of the parameters L and γ, starting with a sound film at $t = 0$. We trace for each admissible value of n in the form $n_j = 2^j$ the corresponding total energy as a function of the loading t, according to Equation (2.22) (gray lines in Figure 2.13(a)). The evolution of the film satisfying the (gst) and (ir) conditions is the one corresponding to the lowest value of the energy and marked with a thick black stroke in Figure 2.13(a). This evolution satisfies also the energy balance (eb) because of the continuity of the energy and is therefore a well-defined solution of the quasi-static evolution problem. The corresponding displacement fields is illustrated in Figure 2.14. Figure 2.13(b) reports the evolution of bonded length in each segment. At $t = 0$, it is equal to the total length of the sound bar. At point A, corresponding to the intersection of the energy branch with the curve $t_f(B)$, given by Equation (2.24), the film breaks in $n = 2$ parts without debonding. Then, the bonded length in each segment is $B = L/2$, until the next intersection with the curve $t_f(B)$ at point C where each part further splits in two totally bonded segments of length $B = L/4$. At point D the load reaches the critical debonding load $t_b(B, \gamma)$ of Equation (2.15). Here, the film splits into $n = 4$ segments and then debonding starts. No further transverse cracks appear for higher loading.

More in general, the quasi-static evolution reduces to a cascade of $\bar{j}$ transverse cracks followed by debonding. An interesting property of the solution is the number $n_{\bar{j}}$, which

is the maximum number of segments (of equal length) in which the film splits before debonding. As done in the static problem, this number is obtained by looking for the smallest integer value of j for which $t_b(L/n_j, \gamma) < t_f(L/n_j)$. Figure 2.15 reports a phase diagram giving the n_j obtained as a function of the relevant parameters L and γ.

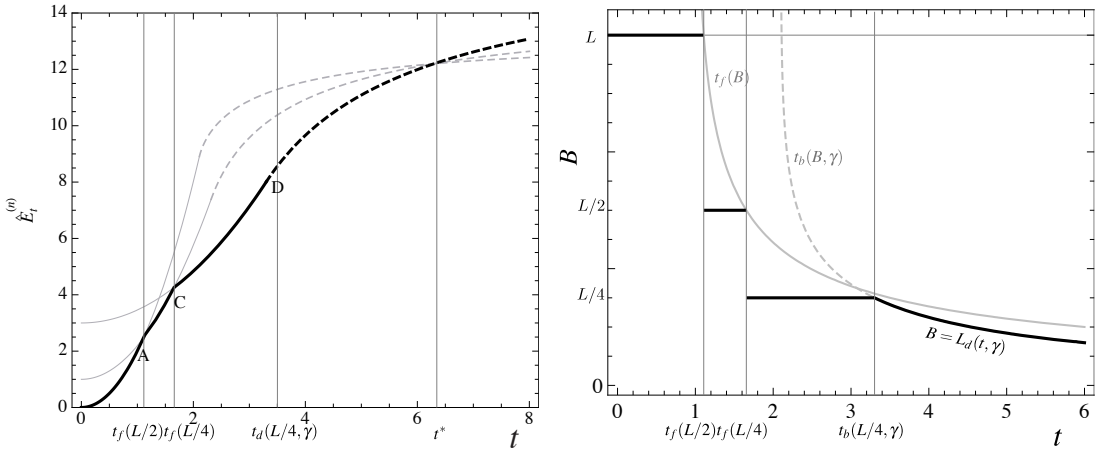

(a) (b)

Figure 2.13: Quasi-static evolution of an initially sound thin film of length $L = 6$, with $\gamma = 2.2$. (a) In gray, total energies calculated according to Equation (2.22) as a function of the load t for different number segments, the bonded states are marked by a dashed stroke. In black, the energy of the quasi-static evolution respecting (GST), (IR) and (EB). (b) In black, the length B of the bonded interval in each of the film's segments as a function of the load t. The continuous and dashed gray lines are the critical loads for transverse cracking and debonding of a sound film of length B given by $t_f(B)$ and $t_b(B, \gamma)$, respectively.

2.3.4 Comments and extensions

A limit model for long films. When the film is very long it may be consistent to describe the system in terms of a "fracture density" rather than by the absolute number of fractures. In such setting, fracture density may be thought of as a macroscopic characterization of a damaging process. A limit model for long films is deduced from the total energy of Equation (2.18) replacing the discrete variable n with the continuous density of fractures defined by $\alpha := n/L$. Minimizing the energy (2.18), seen as a function of α for $\alpha > 0$, we recover the concave envelope of the family of energies $E_t^{(n)}$, for $n \in \mathbb{N}$. The total energy for the limit model is displayed in Figure 2.16(a), enveloping the family of energies $\bar{E}_t^{(n)}$. In Figure 2.16(b) we compare the discrete number n_t of cracks with the crack density α_t, in the long film regime. Both figures relate to a film of non-dimensional length $L = 20$. Note that long films with transverse cracks can be regarded as an example

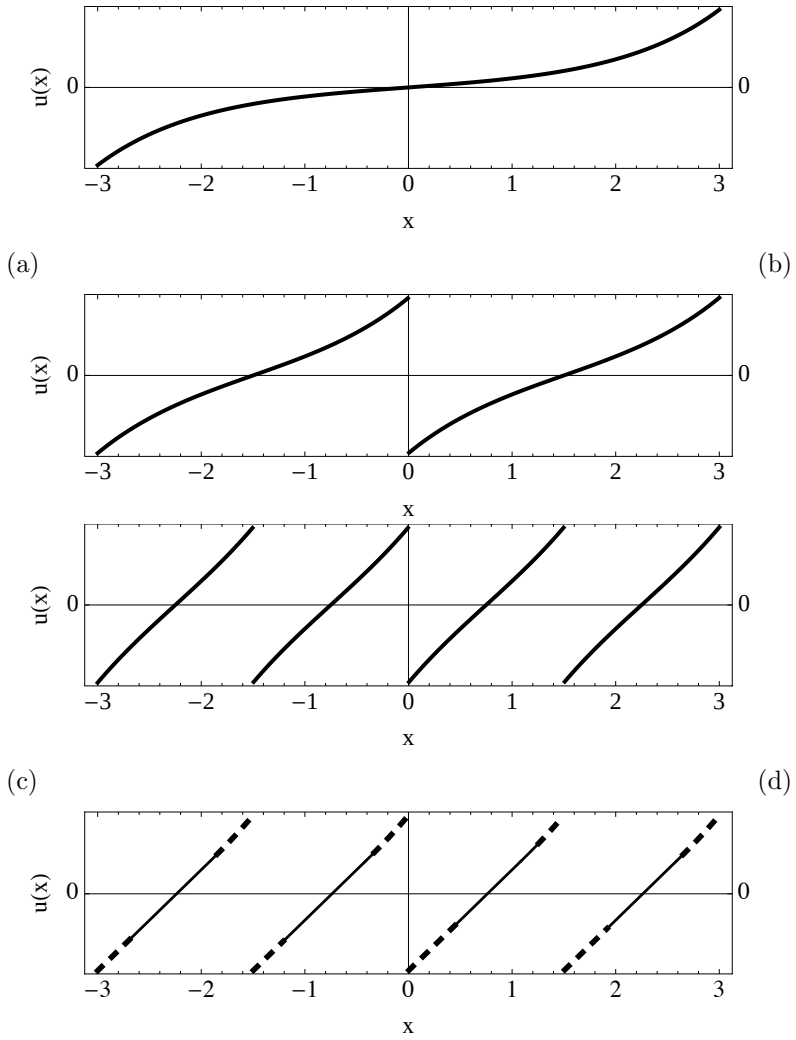

Figure 2.14: Snapshots of the displacement field for states O, A, C, D of Figure 2.13(a). The debonded region is indicated with a thicker dashed line.

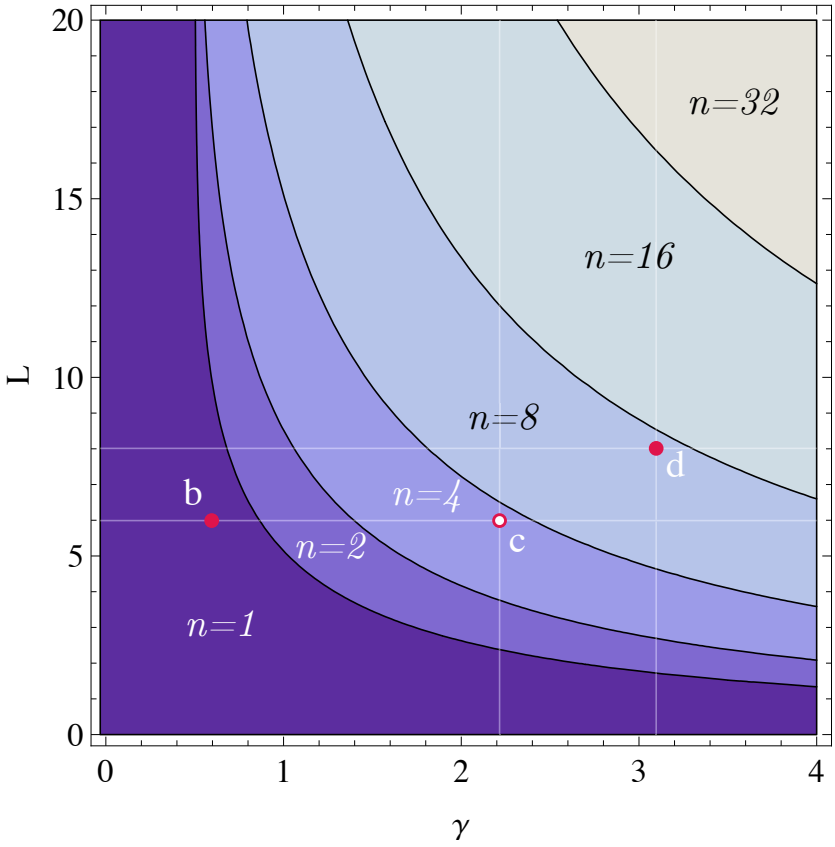

Figure 2.15: Phase diagram for the coupled transverse cracking and debonding problem. For a quasi-static evolution, to each couple of parameters (L, γ) the phase diagram associates the (maximum) number of parts n into which the film is split before debonding takes place. We point out with a white dot the couple of parameters of the evolution illustrated in Section 2.3.3, with a red dot the couples of parameters referring to the numeric experiments detailed in Section 4.3.1.

of continua with structured deformations and modeled within the framework developed in [DO04].

The reduced model and the one dimensional assumption. The two crucial assumptions that allow the analysis of the remarkable richness of the reduced one-dimensional model are i) the form of the elastic energy density and ii) the geometry of cracks. Although such model has been extensively used in the literature in the field of fracture mechanics of thin film systems, no attempt has been made, at least to the knowledge of the author, to establish a rigorous derivation starting from the three-dimensional equations. The reduced model has been studied as a model *per se*, without assessing its origin or its validity. In the sequel of the work, we shall relax such assumptions instead *obtain* them as *asymptotic* properties of a class of three-dimensional systems.

The size effect. The fundamental ingredient in the reduced model of Equation 2.1.1 is the existence of an internal length scale. The size effect associated to such length scale is evident in the expression of the elastic equilibrium displacement (Equation (2.5)) and is outlined in Figure 2.4. The presence of the intrinsic length-scale, provided by the non-trivial coupling of the membrane energy of the bar and the equivalent elastic foundation, is then *revealed* by the fracture phenomena. In fact, due once again to the non-homogeneity of the surface terms, the internal length scale reappears in the relative determination of the two surface energy components, one related to transverse cracks, the other to debonded regions. All the properties established for the energy minimizers (equilibrium states) can be reinterpreted under the light of the size effect, the *global* feature that determines the emergence of the complex (even in 1D) interplay of the two failure modes. Among all the possible arrangements of transverse cracks and debonded regions, the size effect sharply discriminates between a regime of multiple cracking and that of extensive debonding. This is the essential content of Propositions 2.3, 2.4. In this sense, as a consequence of the energy minimality statement, in the simple one-dimensional case the coupling between transverse fracture and debonding is only *weak*, in the sense that the two failure modes do not intervene simultaneously.

However, in dimension two, the size effect allows a novel phenomenology to emerge, resulting in a stronger coupling between the two failure modes. It determines a new regime in which, the simultaneous propagation of transverse cracks and debonding is the only way to release the stored elastic energy and the internal characteristic length plays a key role.

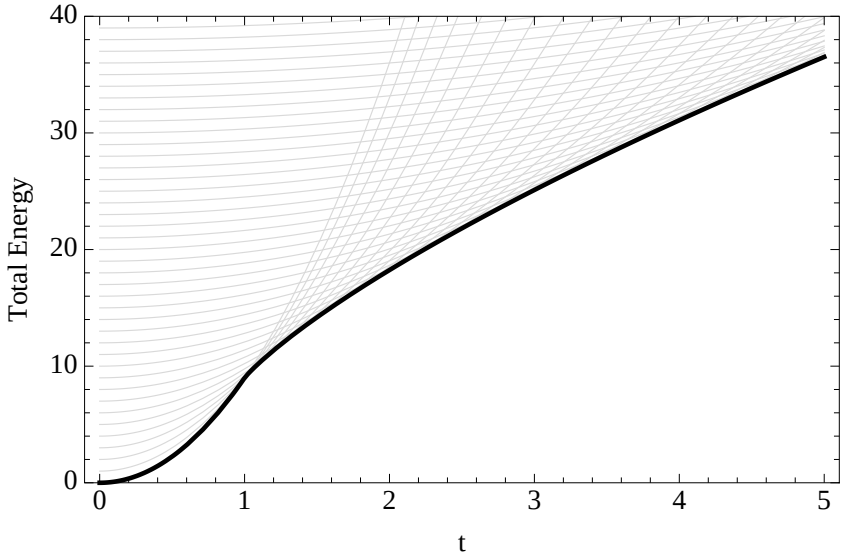

(a)

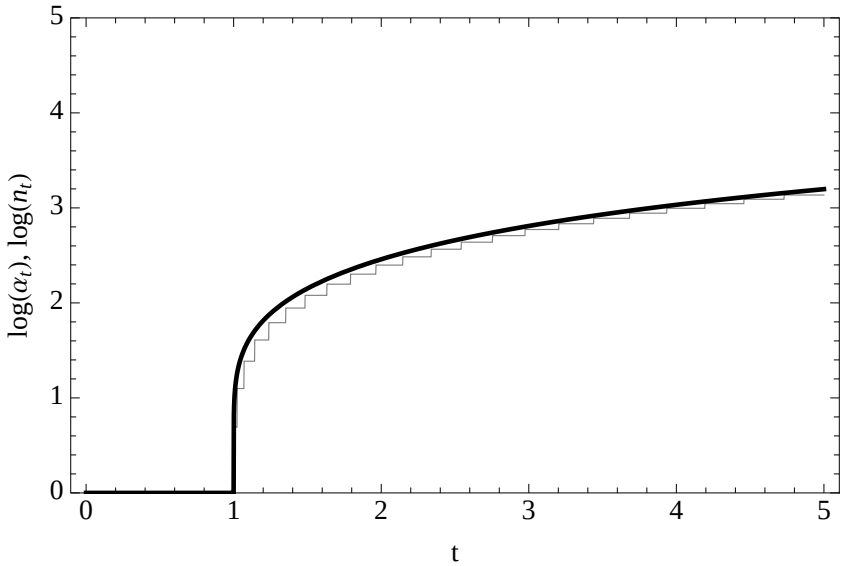

(b)

Figure 2.16: Energy and fracture density curves in the "long film" regime. Thick lines show the results of the limit model, they are compared with the discrete family of energies (2.18). The limit model can macroscopically characterize high fracture density regimes with a damage-like parameter.

2.4 Conclusions of the chapter

In this chapter, we have applied the variational approach to fracture mechanics of a thin film system represented by a phenomenological one-dimensional model, where the film appears as a linear membrane and the role of the bonding layer is played by an equivalent elastic foundation. In the reduced model, transverse and debonding cracks appears with a different geometric nature. Whereas the former are of geometrical co-dimension 1 (a set of points), the latter are of co-dimension 0 (segments in 1D). Considering the two failure modes associated to film cracking and debonding, we have analyzed the properties of the solutions to the fracture problem. This difference entails a distinct analytic treatment and solutions with disparate qualitative properties. This point has been emphasized by presenting separately the solutions of the transverse fracture and debonding problems, before tackling the more complex coupled case. First, we have studied the static problem, *i.e.* the equilibrium configurations under a given load. This allows for establishing the qualitative properties of the energy minimizers. For debonding without transverse cracks, the main result is that the bonded part of the domain is a single connected segment, which is uniquely determined as a function of the loading. Equivalently, debonding may appear only at the free boundaries of the domain. Moreover, this property is true for all local minima of the energy. The modeling of transverse cracks requires us to formulate problem in terms of global minimization, as customary in the variational approach to fracture mechanics with a Griffith–type surface energy. We showed that transverse cracks are equally spaced and lead to periodic solutions. This behavior was only postulated in previous studies and is a robust experimentally observed feature. We have then studied the quasi-static irreversible evolution under increasing load. The coupling of transverse fracture and debonding produces an interesting and rich behavior even in the 1D setting. Through analytical results and phase diagrams, we unveiled the dependence of the key qualitative properties of the solutions on the two non-dimensional parameters of the model. The main result is that the evolution of the system necessarily consists in a sequential cascade of n bisections of the segments (hence 2^{n-1} cracks) and then simultaneous debonding of all the segments, starting from the free boundaries. The critical load for debonding which depends upon the internal length scale of the system, discriminates two distinct phases of evolution: that of periodic sequential fissuration of the film and that of extensive debonding. The analysis will now be turned to the *derivation* of the limit model whose solutions have been presented, as the outcome of an asymptotic process. This is the aim of the next chapter.

2.A Properties of the minimizers

Proof 2.1 (of Lemma 2.1)*:* We consider a sound bar $\Gamma = \emptyset$ and let u be a local minimizer of $\tilde{\mathcal{E}}_t(u, \emptyset)$.

Let us first prove that there exists $x \in [-L/2, L/2]$ such that $|u(x)| < u_c$, by contradiction. Let us consider the following family of admissible displacement fields $v_h = u + hv$ with $h > 0$ and $v \in H^1(\mathcal{A})$. Since v_h converges to u as $h \to 0$, we must have for h sufficiently small

$$0 \geq \tilde{\mathcal{E}}_t(u, \emptyset) - \tilde{\mathcal{E}}_t(v_h, \emptyset) = \int_{-L/2}^{L/2} \left(2h(u' - t)v' + h^2 v'^2 + f(|u(x)|) - f(|v_h(x)|)\right) dx. \quad (2.25)$$

Since $f(|u(x)|) = \gamma \geq f(|v_h(x)|)$, one gets:

$$0 \geq \int_{-L/2}^{L/2} \left(2h(u' - t)v' + h^2 v'^2\right) dx.$$

Dividing by h and passing to the limit as $h \to 0$, one obtains $\int_{-L/2}^{L/2}(u' - t)v'dx = 0$, equality which must hold for every $v \in H^1(\mathcal{A})$. It is possible only if $u' = t$. Inserting this relation into (2.25) leads to a contradiction. Therefore there exists $x \in [-L/2, L/2]$ such that $|u(x)| < u_c$.

Then, let us prove that u has (at least) a zero in $[-L/2, L/2]$, still by contradiction. Suppose that u has the same sign on $[-L/2, L/2]$, say $t = \pm 1$. For $h \in (0, \min|u|)$, let us consider the following family of admissible displacement fields v_h:

$$v_h(x) = u(x) - th.$$

Since v_h converges to u as $h \to 0$, we must have for h sufficiently small

$$0 \geq \tilde{\mathcal{E}}_t(u, \emptyset) - \tilde{\mathcal{E}}_t(v_h, \emptyset) = \int_{[0,L]} f(|u(x)|) - f(|v_h(x)|)$$

But since $|v_h(x)| < |u(x)|$ and since f is strictly increasing in the interval $[0, u_c]$, the above inequality can be satisfied only if $|u(x)| \geq u_c$ for all x which we have proved before that is impossible. Therefore u has at least a zero.

We are now in a position to prove that u is monotonic, by contradiction. If $u(x)$ is not monotonic, then it has a positive local maximum or a negative local minimum in $(-L/2, L/2)$ and we can find $U \in \mathbb{R}$ such that there exist constants $a, b \in \mathbb{R}$ such that $-L/2 \leq a < b \leq L/2$ verifying:

$$u(a) = u(b) = U \qquad \text{and} \qquad |u(x)| > |U|\,, \quad \forall x \in (a, b)$$

For $h \in (0, 1)$, let us consider the following family of admissible displacement fields v_h:

$$v_h := \begin{cases} u(x), & \text{if } x \notin (a, b) \\ (1 - h)u(x) + hU & \text{if } x \in [a, b] \end{cases} \quad (2.26)$$

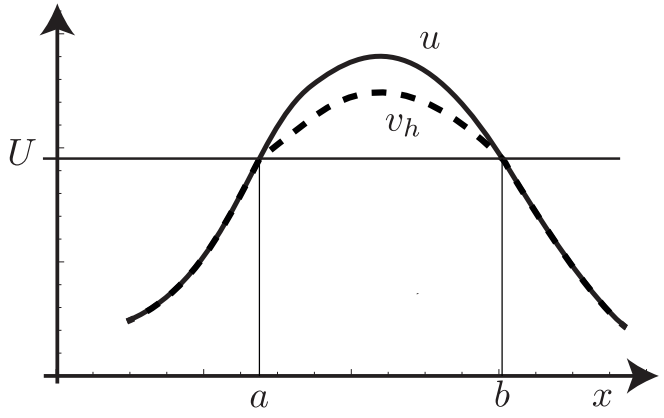

Figure 2.17: The construction of the test field of Equation (2.26) used to show the monotonicity of minimizers in the Proof 2.1. The energy of a non-monotonic function u can always be reduced.

Since v_h converges to u as $h \to 0$, we must have for h sufficiently small

$$\begin{aligned}
0 &\geq \tilde{\mathcal{E}}_t(u, \emptyset) - \tilde{\mathcal{E}}_t(v_h, \emptyset) \\
&= \int_{[a,b]} \left\{ (u'(x) - t)^2 + f(|u(x)|) \right\} dx \\
&\qquad - \int_{[a,b]} \left\{ (u'(x)(1-h) - t)^2 - f(|v_h(x)|) \right\} dx \\
&= \int_{[a,b]} u'^2(x)(1 - (1-h)^2) dx - 2h \int_{[a,b]} t u'(x) dx \\
&\qquad + \int_{[a,b]} \{ f(|u(x)|) - f(|v_h(x)|) \} dx \\
&= \int_{[a,b]} u'^2(x)(1 - (1-h)^2) dx + \int_{[a,b]} f(|u(x)|) - f(|v_h(x)|) dx.
\end{aligned}$$

Since both the integrands are non negative, for the inequation to be satisfied both the integrands must vanish. This leads to $u'(x) = 0$ in (a, b) and since $u(x) = U$ for $x = a, b$ and u must be continuous, one should have $u(x) = U$ in (a, b) which contradicts $|u(x)| > |U|$ in (a, b). Then $u(x)$ is monotonic. □

Proof 2.2 (of Lemma 2.2)*:* Let $v \in C_0^\infty([-L/2, L/2])$ and $h \in \mathbb{R}$. When $|h|$ is sufficiently small, then $\varphi_h(x) := x + hv(x)$ is a C^∞-diffeomorphism on $[-L/2, L/2]$. Let $u \in H^1([-L/2, L/2])$, and define $u_h := u \circ \varphi_h^{-1}$. One has $\lim_{h\to 0} u_h(x) = u(x)$ pointwise. If u is a local minimizer then $I(u) \leq I(u_h)$ for some sufficiently small h. We compute

$$I(u_h) = \int_0^L \left(\left(\frac{u'(y)}{\varphi_h'(y)} - t \right)^2 + f(|u(y)|) \right) \varphi_h'(y)\, dy$$

The last quantity is differentiable with respect to h, attaining its minimum value for $h = 0$, u being a minimizer. We therefore require that the first derivative with respect to h vanishes for $h = 0$

$$0 = \left.\frac{dI(u_h)}{dh}\right|_{h=0} = \int_0^L \left(-(u'^2(x) - t^2) + f(|u(x)|)\right) v'(x)dx, \qquad \forall v \in C_0^\infty([-L/2, L/2])$$

We easily infer the prime integral: $u'(x)^2 - t^2 - f(|u(x)|) = C$, $\forall x \in [-L/2, L/2]$. Let us compute the boundary conditions. Define $x_h = L/2(1-h)$ for $h \in (0,1)$ and $\forall \vartheta \in \mathbb{R}$ construct a test field v_h as follows:

$$v_h(x) := \begin{cases} u(x), & \text{if } x \in [-L/2, x_h] \\ u(x) + \vartheta(x - x_h) & \text{if } x \in [x_h, L/2] \end{cases}$$

Such a test field is admissible and $v_h \to u$ pointwise for $h \to 0$. Let u be a minimizer, then we can write the following inequality:

$$\begin{aligned} 0 &\leq \tilde{\mathcal{E}}_t(v_h(x), \emptyset) - \tilde{\mathcal{E}}_t(u, \emptyset) \\ &= \int_{[x_h, L]} (u'(x) - t)^2 + f(|u(x)|)dx - \int_{[x_h, L]} (u'(x) + \vartheta - t)^2 - f(|v_h(x)|)dx \\ &= \int_{[x_h, L]} \vartheta^2 + 2\vartheta u'(x) - 2\vartheta t + (f(|v_h(x)|) - f(|u(x)|))\, dx \end{aligned}$$

dividing the last equation by h and passing to the limit for $h \to 0$, the term in parentheses vanishes grace to the pointwise convergence $v_h \to u$. The inequality

$$0 \leq \vartheta^2 + 2\vartheta(u'(L) - t)$$

has to be verified $\forall \vartheta \in \mathbb{R}$. This leads to the desired boundary condition: $u'(L/2) = t$. Symmetrically we can construct test fields to retrieve the boundary condition on $x = 0$ as follows

$$v_h(x) := \begin{cases} u(x) + \vartheta(x - x_h) & \text{if } x \in [-L/2, x_h] \\ u(x), & \text{if } x \in [x_h, L/2] \end{cases}$$

where now $x_h = h$. We have the same pointwise convergence as above and we derive the boundary condition $u'(-L/2) = t$. □

This page intentionally left blank.

Chapter 3

Derivation of the limit models

We explore the asymptotic behavior of a three-dimensional bilayer system bonded on a rigid substrate. In scalar elasticity, by rigorous asymptotic analysis of the weak formulation of the elastic problem, a general scaling law for thicknesses and elastic moduli of the layers allows us to hierarchically determine limit regimes depending on their relative ratio. Among them, we identify: linear bars under shear, linear membranes over three-dimensional elastic substrates, higher order linear beams, membranes over elastic foundation. This latter regime entails the asymptotic emergence of an internal length scale; it is further discussed in vectorial elasticity to establish a reduced dimension, plate-like, theory of elastic multilayers. We then allow for fracture and deduce, via Γ*-convergence, a two-dimensional limit model consisting of a brittle membrane on a brittle elastic foundation. By the energy minimality principle, fracture sets are naturally discriminated between transverse cracks in the film (curves in* $2D$*) and debonded surfaces (two-dimensional planar regions). We finally formulate the reduced-dimension, rate-independent, irreversible, evolution law for transverse fracture and debonding of thin film systems.*
The material presented in Sections 3.1 and 3.2 is still unpublished. The results shown in Sections 3.3, 3.4 constitute the bulk of the paper [Leó+13a], submitted for review.

Contents

3.1 A parametric asymptotic study in scalar elasticity 65
3.1.1 Rescaling of the problem 68
3.1.2 The open half space $\delta > 0$. 71
3.1.3 The closed half space $\delta \leq 0$. 71
3.1.4 The open half space $\delta < 0$. 72
3.1.5 The straight line $\delta = 0$. 75
3.1.6 The energy of the two-dimensional limit model 83
3.2 A reduced dimension theory for thin films in vector elasticity 85
3.2.1 Identification of the cascade problems 89
3.2.2 Comments and extensions 94
3.3 Brittle thin films in scalar elasticity 97
3.3.1 Constitutive assumptions 97
3.3.2 Variational formulation in SBV 98
3.4 Brittle thin films, application in two-dimensional vectorial elasticity 107
3.4.1 The reduced limit energy in two-dimensional vectorial elasticity 107
3.4.2 Nondimensionalization and free parameters 109
3.4.3 Formulation of the reduced problem 109
3.5 Conclusions of the chapter 111
3.A Proof of the dimensional reduction for scalar elasticity . . . 113
3.B Spaces of functions with measure derivatives 120

In the previous section, we have analyzed the phenomenology of multiple cracking and debonding in a simplified setting relying on two strong assumptions: the expression of the elastic energy (Equation 2.1.1) modeling the system as a linear membrane over a linear elastic foundation and the geometry of cracks (transverse in the film and planar in the bonding layer). In this section we remove these two *assumptions* and instead *derive* them as the outcome of an asymptotic analysis. In the simple one-dimensional example, the properties characterizing the equilibrium configurations and the quasi-static evolution of crack patterns are essentially linked to the decoupling of fracture modes and the existence of a *scale effect* due to the presence of an intrinsic characteristic length scale. As already remarked, the internal length scale arises from the coupling of the membrane and the elastic foundation terms in the elastic energy density. Hence, it is clearly of *elastic* origin only. The presence of that length scale also determines the fundamental properties outlined in the previous section: the equi-distribution of cracks, the debonding criterion and its peripheral onset; the separation between a sequential multifissuration regime and the extensive debonding phase.

Now we dedicate a more detailed study to the problem of derivation of the reduced dimension theory underlying the modeling assumptions of the previous section. To this end, we shall exploit the techniques of asymptotic analysis [Lio73], [SS92]. Asymptotic

techniques have been fruitfully employed to tackle problems in solid and fluid mechanics where small parameters, historically denoted by ε, determine a problem in which the coefficients have different orders of magnitude (with respect to ε), or in which its *differential type* is different for $\varepsilon > 0$ and for $\varepsilon = 0$. This is, for instance the case when periodic, small scale, micro-structure exists and influences the macroscopic response; or when the behavior of the system can be conveniently approximated by an asymptotic reduced dimension theory. The domains of applications of asymptotic techniques is rather wide, it includes problems of fluid flow around fixed obstacles [San82], [All91a], [All91b], flows in reactive porous media [AR07], effective static behavior of periodic interfaces [AM00], [DMP12], thin elastic junctions [CB89], structures comprising substructures of different dimensions [Cia90], reduced dimension theories for nonlinear bars, rods and strings [MM06]; linear and nonlinear plates and shells [CLM96], [Cia97], [FJM06], and dynamic problems in periodic media [Sán80].

We focus here on the static (and quasi-static) problems in linear elasticity and linear brittle elasticity, where the separation of scales derives from one dimension (the thickness) being much smaller than the other two. Linear theories are, themselves, the limit of genuinely nonlinear systems and are determined by the order of magnitude of loads, discriminating the hierarchy of limit models among which linear theories emerge, see[MHC01], [MM06], [FJM06].

The asymptotic justification of the linear theory of clamped (or partially clamped) Kirchhoff-Love plates is obtained in [Cia97] under scaling assumptions of the elastic coefficients [Mia94]; that of membrane and flexural equations for shells are carried in [CLM96] and [CL96].

Static fractures in single-layer thin films have been investigated by means of a Γ-convergence analysis that allows the identification of an effective reduced 2D model [BF01], [BFL02]. The quasi-static evolution of cracks in thin films is studied in [Bab06] proving the convergence of the full three-dimensional evolution to the reduced two-dimensional one. These analyses are obtained considering a single-layer system and the resulting cracks that are asymptotically invariant in the thin direction. The dimension reduction of a bilayer thin film allowing for debonding at the interface has been investigated by [BFF02]. The debonding is penalized by a phenomenological interfacial energy paying for the jump of the deformation at the interface. The limiting models are discussed according to the weight of interfacial energy. Rigorous derivations of decohesion-type energies have been given in [ABZ07], [Ans04] by means of a homogenization procedure. In these works the interfacial energy appears as the limit of a Neumann sieve, debonding being regarded as the effect of the interaction of two thin films through a suitably periodically distributed contact zone.

We want to extend the investigation to thin film systems susceptible to cracking both in the film and in the bonding layer.

In the first part of the Chapter (Section 3.1), we study the purely elastic systems consisting in a stack of two superposed layers bonded to a rigid substrate, whose elastic and geometric dimensions may vary significantly.

In the setting of scalar elasticity, in Section 3.1 we provide parametric study of the *limit* models approximating three-dimensional film systems. Providing a general scaling law for the geometric and elastic quantities as a function of a natural small parameter ε destined to tend to zero, we study parametrically the hierarchy of limit models reached in the limit $\varepsilon \to 0$, depending on the thickness and stiffness ratios of the two layers. We hence identify a number of qualitatively different limit regimes. Among these, a class of systems appears that expresses, as an asymptotic property, an intrinsic characteristic length scale.

In the second part of the Chapter (Section 3.2) we tackle the more physically relevant case of three-dimensional vectorial elasticity. This richer setting, still reflecting the properties outlined in the scalar case, shows a novel phenomenology: the possibility of undergoing rotations, *i.e.* bending deformations are admissible deformation modes. We derive an asymptotic, linear, reduced dimension, model for a stiff film over a compliant bonding layer. The outcome of the analysis is the justification of the kinematics, the identification of the limit energy and the associated variational problem of equilibrium. The asymptotic analysis turns to be necessary to establish the correspondence between the three-dimensional physical parameters and their associated two-dimensional reduced quantities.

In the third part of the Chapter (Section 3.3) we study the brittle case allowing for cracks to appear anywhere within the system. This changes drastically the analytical treatment, requiring to state the problem in a larger space of functions that allow for arbitrary jumps of the displacement. We identify a regime in which a non-trivial coupling of the energies provides a competition between the elastic terms and the surface energies associated to cracks in both layers. Once a suitable reduced model is established, as the outcome of the asymptotic study, we propose a quasi-static formulation of the evolution problem under increasing loads, analogous to Problem 1.2 introduced in Section 1.2.4. Finally, these results are applied to the more realistic case of two-dimensional vectorial elasticity, which serves as a basis for the numerical experiments performed in the next chapter.

3.1 A parametric asymptotic study in scalar elasticity

Let us study a three-dimensional elastic system, with the goal of identifying the asymptotic limit regimes arising when the small parameters appearing in the system approach their natural limit.

We perform the study in the setting of three-dimensional scalar elasticity as introduced in Section 1.2.2, *i.e.* when displacement field can be identified with a scalar function. The model system, sketched in Figure 3.1, consists in two superposed linear, homogeneous, isotropic, elastic, layers bonded to a rigid substrate. Let ω be a bounded domain in $\mathbb{R}^2$ of characteristic diameter $L = \mathrm{diam}(\omega)$ and let H be the characteristic thickness of the system. We consider that the film system is "thin": one characteristic dimension, the thickness, is much smaller than the other two. Consequently, the ratio thickness to diameter naturally appears as a small parameter. The domain of the film is the set $\overline{\Omega_f} = \overline{\omega} \times [0, h_f]$, that of the middle layer is $\overline{\Omega_b} = \overline{\omega} \times [-h_b, 0)$. We assume that the set $\overline{\Omega} = \overline{\Omega_f \cup \Omega_b}$ is the reference configuration of the elastic system in absence of applied loads, *i.e.* Ω is a natural state.

We consider here a rather wide class of conservative volume loads within the film layer, their density is $f : \Omega_f \mapsto \mathbb{R}$. The rigid substrate imposes a boundary condition of place in correspondence to the interface $\omega_- := \omega \times \{-h_b\}$ between the middle layer and the substrate. The rest of the boundary, *i.e.* the lateral boundary $\partial\omega \times (-h_b, h_f)$ and the upper surface $\omega \times \{h_f\}$, is left free.

Assumptions on the data

We intend to investigate the asymptotic regimes of the system when the thickness of the layers and the elastic constants of the layers may exhibit significant variations. To this end, we prescribe a general scaling law for the ratios of the shear moduli and thicknesses as powers of the natural small parameter, denoted henceforth by ε. More precisely, we state this choice as follows.

Hypothesis 1 (Scaling law of thicknesses and elastic moduli)**.** *For*

$$\varepsilon := \frac{h_f}{L} \ll 1,$$

and given two constants $\alpha, \beta \in \mathbb{R}$, we assume that the ratio between the (non-dimensional) thickness of the film h_f and that of the bonding layer h_b scales as ε^α, and that the ratio between the shear modulus of the bonding layer and that of the film scales as ε^β, viz. *:*

$$\frac{h_b}{h_f} = \varrho_h \varepsilon^\alpha, \qquad \frac{\mu_b}{\mu_f} = \varrho_\mu \varepsilon^\beta \tag{3.1}$$

where ϱ_h and ϱ_μ are non–dimensional coefficients independent of ε.

The non-dimensional ε-dependent domain occupied by the film is $\Omega_f^\varepsilon = \omega \times (0, \varepsilon L/H)$, the domain occupied by the middle layer is $\Omega_b^\varepsilon = \omega \times (-\varrho_h \varepsilon^{\alpha+1} L, 0]$. In terms of orders

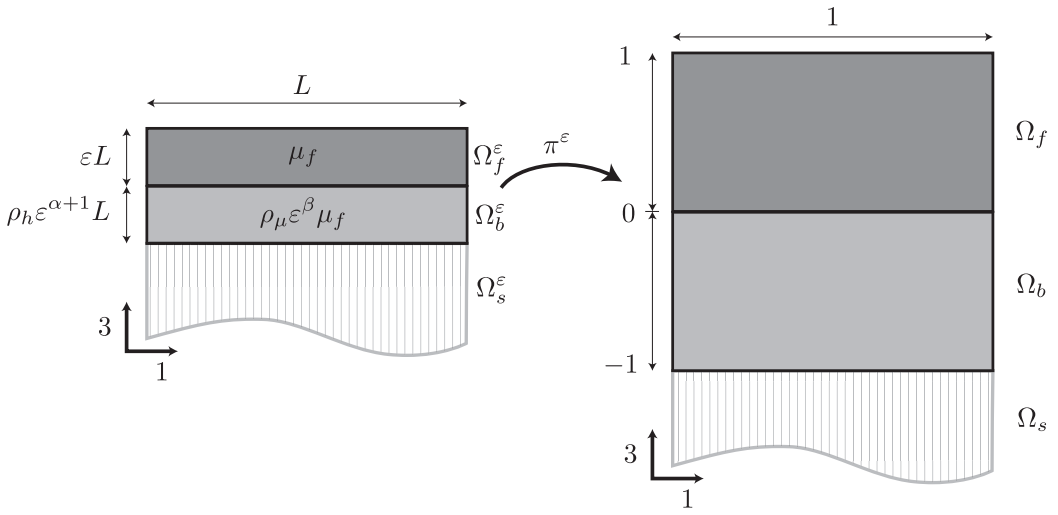

Figure 3.1: The three-dimensional system in scalar elasticity: a thin film Ω_f is bonded to a rigid substrate Ω_s via an intermediate layer Ω_b.

of magnitude, depending upon the values of α we identify three-dimensional systems for which the middle layer is thicker (for $\alpha < 0$), thinner (for $\alpha > 0$) or as thick as the film (for $\alpha = 0$). Analogously, depending upon β, the middle layer is more compliant (for $\beta > 0$), stiffer (for $\beta < 0$) or as stiff as the film (for $\beta = 0$).

The functional setting and the elastic energy. The space of kinematically admissible displacements is that of the square integrable scalar functions with squared integrable derivatives, defined on the ε-dependent domain $\Omega^\varepsilon := \Omega_f^\varepsilon \cup \Omega_b^\varepsilon$ and satisfying the boundary condition of place on $\omega \times \{-h_b\}$, namely:

$$\mathcal{C}_w^\varepsilon(\Omega^\varepsilon) := \left\{ v \in H^1(\Omega^\varepsilon),\ v = w(x') \text{ a.e. on } \omega \times \{-h_b\} \right\}.$$

The vector space associated to $\mathcal{C}_w^\varepsilon(\Omega^\varepsilon)$ is

$$\mathcal{C}_0^\varepsilon(\Omega^\varepsilon) := \left\{ v \in H^1(\Omega^\varepsilon),\ v = 0 \text{ a.e. on } \omega \times \{-h_b\} \right\}.$$

For ease of computation, we perform a change of variable in order to recover a homogeneous boundary condition for the unknown displacement field. Extending constantly the imposed displacement $w \in L^2(\omega)$, defined on the lower boundary $\omega \times \{-h_b\}$, to the entire domain Ω^ε, the new unknown is

$$\hat{v} = v - \hat{w}, \tag{3.2}$$

where $\hat{v} \in \mathcal{C}_0^\varepsilon(\Omega^\varepsilon)$, $v \in \mathcal{C}_w^\varepsilon(\Omega^\varepsilon)$ and $\hat{w}$ is the constant extension of w to Ω. In the case of scalar elasticity, the elastic energy density reduces to $\mu|\nabla v|^2$, where μ is the (piecewise constant) shear modulus of the elastic body. To admissible displacements $v \in \mathcal{C}_0^\varepsilon(\Omega^\varepsilon)$ is

associated the a family of energy functionals indexed by ε reading as follows:

$$E_\varepsilon(v) := \frac{1}{2}\int_{\Omega_f^\varepsilon} \mu_f |\nabla v|^2 dx + \frac{1}{2}\int_{\Omega_b^\varepsilon} \mu_b |\nabla v|^2 dx - \mathcal{L}^\varepsilon(v). \tag{3.3}$$

Here, $\mathcal{L}^\varepsilon(v)$ is the ε-dependent linear form associated to the potential of loads applied in the film, of density f^ε:

$$\mathcal{L}^\varepsilon(v) = \int_{\Omega_f^\varepsilon} f^\varepsilon(x) v dx.$$

In the general case of genuinely nonlinear elasticity, the order of magnitude of the applied loads with respect to the volume of the body, *i.e.* with respect to ε, plays a crucial role in establishing the limit asymptotic models. This role is although hidden in the present limit case of linearized elasticity. This point is further developed in the sequel. We keep track of the order of magnitude of the density of applied loads by the superscripted ε.

Remark 3.1. *Instead of applied body loads we may consider inelastic strain loads within the film layer. In such case the linear form associated to the external work reads:*

$$\mathcal{L}^\varepsilon(\nabla v) = \int_{\Omega_f^\varepsilon} e_0^\varepsilon(x) \cdot \nabla v dx.$$

where $e_0^\varepsilon(x) \in L^2(\Omega_f^\varepsilon)$ is an imposed inelastic strain.

The problem of finding the equilibrium displacement in the three-dimensional elastic body reads:

Problem 3.1 (Unscaled three-dimensional elastic problem)**.**

$$\mathcal{P}(\Omega^\varepsilon): \quad \textit{Find } u^\varepsilon \in \mathcal{C}_0(\Omega^\varepsilon) \textit{ minimizing } E_\varepsilon(v) \textit{ among } v \in \mathcal{C}_w^\varepsilon(\Omega^\varepsilon)$$

We want to perform an asymptotic study of the problem $\mathcal{P}(\Omega^\varepsilon)$ as $\varepsilon \to 0$. More precisely we study the limit (if the limit exists) of the sequences of displacements $(u^\varepsilon)_{\varepsilon>0}$, solving Problem (3.1), *i.e.* the admissible minimizers of the energy (3.3) for $\varepsilon \to 0$. We denote them by u^ε for conciseness. We obtain, depending upon the values of α and β, a hierarchy of asymptotic limit regimes.

We use the techniques of rigorous asymptotic analysis of variational problems depending upon a small parameter as extensively studied in [Lio73]. These techniques have been applied for the derivation and justification of lower dimensional theories in linear and genuinely nonlinear elasticity for bars, rods and strings in [MM06] and plates, membranes and shells in [Cia97]. As is customary, we start by performing an anisotropic rescaling of the domains in order to state the problem on fixed domains independent of ε. Then we look for and establish uniform bounds for sequences of (scaled) displacements and strains, allowing us to state their convergence properties. Finally we identify the weak variational equations verified the limit displacements, *i.e.* the limit equilibrium equations associated to the various asymptotic regimes.

3.1.1 Rescaling of the problem

Denoting by $x' = (x_1, x_2) \in \omega$ and by $\tilde{x}' = (\tilde{x}_1, \tilde{x}_2)$ (here the tilde denotes rescaled, non-dimensional quantities), the following anisotropic scalings:

$$\begin{aligned} \pi^\varepsilon : x = (x', x_3) \in \overline{\Omega_f^\varepsilon} \mapsto (\tilde{x}', \varepsilon \tilde{x}_3) \in \overline{\Omega_f} \\ \pi^\varepsilon : x = (x', x_3) \in \overline{\Omega_b^\varepsilon} \mapsto (\tilde{x}', \varrho_h \varepsilon^{\alpha+1} \tilde{x}_3) \in \overline{\Omega_b} \end{aligned} \tag{3.4}$$

map the domains Ω_f^ε and Ω_b^ε into the fixed *unit* domains $\Omega_f = \omega \times [0, 1)$ and $\Omega_b = \omega \times (-1, 0)$. They also define the scaled differential operators as follows:

$$\nabla^\varepsilon \mapsto \tilde{\nabla}^\varepsilon = \left(\frac{\partial}{\partial \tilde{x}'} \middle| \frac{1}{\varepsilon} \frac{\partial}{\partial \tilde{x}_3} \right) := \left(\tilde{\nabla}' \middle| \frac{1}{\varepsilon} \tilde{\partial}_3 \right) \qquad \text{in } \Omega_f^\varepsilon$$

and

$$\nabla^\varepsilon \mapsto \tilde{\nabla}^\varepsilon = \left(\frac{\partial}{\partial \tilde{x}'} \middle| \frac{1}{\varrho_h \varepsilon^{\alpha+1}} \frac{\partial}{\partial \tilde{x}_3} \right) := \left(\tilde{\nabla}' \middle| \frac{1}{\varrho_h \varepsilon^{\alpha+1}} \tilde{\partial}_3 \right) \qquad \text{in } \Omega_b^\varepsilon.$$

Performing the change of variables in the energy of Equation (3.3), the rescaled non-dimensional energy reads:

$$\begin{aligned} \tilde{E}_\varepsilon(v) = \frac{E_\varepsilon(v)}{\varepsilon L \mu_f} := \frac{1}{2} \int_{\Omega_f} \left\{ |\tilde{\nabla}' v|^2 + \frac{1}{\varepsilon^2} |\tilde{\partial}_3 v|^2 \right\} dx \\ + \frac{1}{2} \varrho_\mu \varrho_h \varepsilon^\alpha \varepsilon^\beta \int_{\Omega_b} \left\{ |\tilde{\nabla}' v|^2 + \frac{1}{\varrho_h^2 \varepsilon^{2\alpha+2}} |\tilde{\partial}_3 v|^2 \right\} dx - \tilde{\mathcal{L}}^\varepsilon(v), \end{aligned} \tag{3.5}$$

where $\tilde{\mathcal{L}}^\varepsilon(v) = \dfrac{\mathcal{L}^\varepsilon(v)}{\varepsilon L \mu_f}$. We drop the overset tilde for the sake of conciseness and henceforth consider the non-dimensional expression of the energy functional. Using the change of variables, the rescaled, fixed, space of kinematically admissible displacements reads:

$$\mathcal{C}_w(\Omega) := \left\{ v \in H^1(\Omega),\ v = w(x') \text{ a.e. on } \omega \times \{-1\} \right\},$$

and its associated vector space is:

$$\mathcal{C}_0(\Omega) := \left\{ v \in H^1(\Omega),\ v = 0 \text{ a.e. on } \omega \times \{-1\} \right\}.$$

The dependence of the energy upon ε is now explicit and the minimization problem (or equivalently the variational formulation of the equilibrium equations) can be posed on fixed domains independent of ε. It is clear by the expression of the rescaled energy (3.5) that the meaningful parameters are only two, namely $\gamma, \delta \in \mathbb{R}$ defined by the relations:

$$\gamma = \alpha + \beta \quad \text{and} \quad \delta = \beta - \alpha - 2. \tag{3.6}$$

The former is the order of magnitude of the ratio between the "membrane" strain energy of the middle layer and that of the film, the latter is the order of magnitude of the ratio between the "shear" energy of the middle layer and the membrane energy of the film.

Remark 3.2. *We commit here a slight abuse of notation in labeling by "membrane" (resp. "shear") the strain terms just identified since we are dealing here with a "thermal plate". Problem 3.1 is indeed that of stationary thermal diffusion [DL72]. The analogy, and hence the justification, of these labels will be clear in the study of the general vectorial problem tackled in Section 3.2.*

We refer to the terms:

$$\frac{1}{\varepsilon^2}|\partial_3 u^\varepsilon| \qquad \text{and} \qquad \frac{1}{\varepsilon^{2\alpha+2}}|\partial_3 u^\varepsilon|^2$$

as the *scaled* transverse strains, within the film and the middle layer respectively. The boundedness of these terms turns crucial for establishing the asymptotic properties of the elastic multilayer. Owing to the linearity of the problem, up to a rescaling of displacements, we can always set:

$$\mathcal{L}^\varepsilon(v) = \mathcal{L}^0(v), \tag{3.7}$$

i.e. we can fix the order of magnitude of the work of external loads at the order of magnitude of the membrane energy of the film. Consequently, we expect the loads to work on membrane deformations.

Remark 3.3. *Note that this freedom of the arbitrary rescaling of the loads only holds in the setting of linearized elasticity. In the more general setting of genuine nonlinear elasticity, it is indeed the order of magnitude of the applied loads that hierarchically determines the limit regimes, see* e.g. *[MM06], [FJM06]. In the current setting, this is hidden by the linearity which renders equivalent (up to a rescaling) all the asymptotic problems, regardless of the order of magnitude of the applied loads.*

In the scaled non-dimensional energy, indeed, the membrane energy of the film is of order zero with respect to ε, whereas the energy related to transverse strains within the film is singular, of order $\mathcal{O}(\varepsilon^{-2})$. In the bonding layer, the in-plane and transverse components of the energy are singular or regular depending on the values of the exponents α and β.

For the sake of conciseness and without any restriction, we set to one all coefficients independent of ε. Recalling the definitions of γ and δ, the scaled energy reads:

$$E_\varepsilon(v) = \frac{1}{2}\int_{\Omega_f}\left\{|\nabla' v|^2 + \frac{1}{\varepsilon^2}|\partial_3 v|^2\right\}dx + \frac{1}{2}\varepsilon^\gamma\int_{\Omega_b}|\nabla' v|^2 dx + \frac{1}{2}\varepsilon^\delta\int_{\Omega_b}|\partial_3 v|^2 dx - \mathcal{L}^0(v).$$

The elasticity problem in the unit, rescaled, ε-independent, domain is:

Problem 3.2 (Rescaled minimization problem on the unit domain in scalar elasticity)**.**

$$\mathcal{P}(\varepsilon,\Omega): \quad \textit{Find } u^\varepsilon \in \mathcal{C}_0(\Omega) \textit{ minimizing } E_\varepsilon(v) \textit{ among } v \in \mathcal{C}_0(\Omega)$$

Two parameters identify the single three-dimensional multilayer, we perform the parametric study of the families three-dimensional system in a two-parameter phase space: (α,β) or equivalently (δ,γ). We divide the parametric study in several steps.

First we discuss the systems belonging to open half space $\delta > 0$, which leads us to the study of the degenerate case of a material without transverse coherence. Then we study the open half plane $\delta < 0$. It has, at first order, a trivial homogeneous limit solution to the elasticity problem. In this case in fact, the boundary condition of place on the lower interface determines a uniform and homogeneous solution. We sketch the analysis of the first non-trivial higher order term, whose order of magnitude depends upon the stiffness ratio. Lastly, we study the straight line $\delta = 0$ along which we further identify three limit regimes: the slender bars under shear, the membranes over a three-dimensional elastic substrate and finally the membranes over an elastic foundation. This last regime provides an rich asymptotic limit and lays the basis of the sequel of the work.

The Problem $\mathcal{P}(\varepsilon,\Omega)$ can be put into the equivalent variational form, see [Cia88]:

Problem 3.3 (Rescaled variational problem on the unit domain)**.**

$$\mathcal{P}(\varepsilon,\Omega): \quad \textit{Find } u^\varepsilon \in \mathcal{C}_0(\Omega) \textit{ such that} E'_\varepsilon(u^\varepsilon)(v) = 0, \quad \forall v \in \mathcal{C}_0(\Omega)$$

Problem 3.3 represents the first order necessary optimality conditions for minimality and amounts to the weak formulation of the equilibrium equations. It reads explicitly:

Find u^ε such that :

$$\int_{\Omega_f} \left\{ \nabla' u^\varepsilon \nabla' v + \frac{1}{\varepsilon^2} \partial_3 u^\varepsilon \partial_3 v \right\} dx + \varepsilon^\gamma \int_{\Omega_b} \nabla' u^\varepsilon \nabla' v dx + \varepsilon^\delta \int_{\Omega_b} \partial_3 u^\varepsilon \partial_3 v dx = \mathcal{L}^0(v), \qquad \forall v \in \mathcal{C}_0(\Omega) \quad (3.8)$$

First, we have a useful general result which holds independently of the values of γ and δ.

Lemma 3.1 (Poincaré inequality in the rescaled system)**.** *For any admissible $u^\varepsilon \in \mathcal{C}_w(\Omega)$ the following inequality holds:*

$$|u^\varepsilon|_\Omega \leq C \left(|\partial_3 u^\varepsilon|_{\Omega_f} + |\partial_3 u^\varepsilon|_{\Omega_b} \right)$$

Proof. The proof is trivial, it suffices to use Cauchy-Schwartz's inequality to estimate displacements on a vertical segment, use Hölder inequality and then integrate along the in-plane coordinate. □

This inequality provides a means to control (the L^2-norm of) displacements once the transverse gradients are controlled, *i.e.* $|u^\varepsilon|_\Omega$ and $|\partial_3 u^\varepsilon|_\Omega$ are equivalent norms over $\mathcal{C}_0(\Omega)$.

3.1.2 The open half space $\delta > 0$.

When $\delta > 0$, the energy of transverse strains within the middle layer is small compared to that of in-plane deformations in the film and the work of external loads. The rescaled transverse strains in the middle layer are unbounded and can be arbitrarily large. Considering displacements delivering a uniformly bounded energy, they can be as large as $\varepsilon^{-\delta/2}$. Hence, loosely speaking, the middle layer can undergo unbounded transverse deformations without any energy expense. This corresponds to a material without a transverse coherence, *i.e.* a material behaving as a stack of superposed planes at each $x_3 \in (-1, 0]$. Despite an elastic energy is associated to in-plane deformations, the stress is not transferred along the vertical direction and the middle layer is unloaded, *i.e.* no elastic energy is stored. This limit case is not interesting for our purposes and is skipped.

3.1.3 The closed half space $\delta \leq 0$.

If $\delta \leq 0$, on the contrary, the boundedness of the energy provides a bound on the scaled transverse strains throughout the whole domain. Taking $v = u^\varepsilon$ in the variational formulation of the equilibrium, we can write the following bounds:

$$\begin{aligned}
&\varepsilon^{-2} \left|\partial_3 u^\varepsilon\right|^2_{\Omega_f} + \varepsilon^\delta \left|\partial_3 u^\varepsilon\right|^2_{\Omega_b} \\
&\qquad \leq \left|\nabla' u^\varepsilon\right|^2_{\Omega_f} + \varepsilon^{-2} \left|\partial_3 u^\varepsilon\right|^2_{\Omega_f} + \varepsilon^\gamma \left|\nabla' v\right|^2_{\Omega_b} + \varepsilon^\delta \left|\partial_3 u^\varepsilon\right|^2_{\Omega_b} \leq \|\mathcal{L}\|_{\mathscr{L}^0(H^1(\Omega);\mathbb{R})} \left|u^\varepsilon\right|_\Omega \\
&\qquad\qquad \leq C \left(\left|\partial_3 u^\varepsilon\right|_{\Omega_f} + \left|\partial_3 u^\varepsilon\right|_{\Omega_b}\right) \\
&\qquad\qquad\qquad \leq C \left(\varepsilon^{-2} \left|\partial_3 u^\varepsilon\right|_{\Omega_f} + \left|\partial_3 u^\varepsilon\right|_{\Omega_b}\right) \qquad (3.9)
\end{aligned}$$

from which we can derive that:

$$\varepsilon^{-2} \left|\partial_3 u^\varepsilon\right|_{\Omega_f} + \varepsilon^\delta \left|\partial_3 u^\varepsilon\right|_{\Omega_b} \leq C, \qquad \text{if } \delta \leq 0. \tag{3.10}$$

This estimate allows us to refine (3.9) as follows:

$$\left|\nabla' u^\varepsilon\right|^2_{\Omega_f} + \varepsilon^{-2} \left|\partial_3 u^\varepsilon\right|^2_{\Omega_f} + \varepsilon^\gamma \left|\nabla' u^\varepsilon\right|^2_{\Omega_b} + \varepsilon^\delta \left|\partial_3 u^\varepsilon\right|^2_{\Omega_b} \leq C. \tag{3.11}$$

We can establish the following property.

Property 3.1 (Convergence of the rescaled displacements in $L^2(\Omega)$)**.** *For $\delta \leq 0$ there exists a function $u \in L^2(\Omega)$ such that:*

$$u^\varepsilon \rightharpoonup u \quad \textit{weakly in } L^2(\Omega)$$

and in particular

$$u^\varepsilon \to u \quad \textit{strongly in } L^2(\Omega_f).$$

Proof. Using again the Poincaré inequality we infer that $\left|u^\varepsilon\right|_\Omega \leq C$. In addition, strong convergence within the film follows from the boundedness of the scaled gradient of u^ε as a consequence of Rellich-Kondrachov theorem [Dac04]. □

It is hence meaningful to study the asymptotic properties of the order zero weak limit displacement u, depending upon the values of γ and $\delta \leq 0$.

Within the film and for any $\delta \leq 0$, the weak limit displacement u enjoys the following property:

Property 3.2 (Transverse invariance within the film)**.** *For any γ, and $\delta \leq 0$ the weak limit u is such that, within the film:*

$$\partial_3 u = 0, \qquad \text{in } \Omega_f$$

or equivalently, we can identify the weak limit $u \in H^1(\Omega_f)$ to a function $u \in H^1(\omega)$

$$u = u(x'), \qquad \text{in } \Omega_f$$

Proof. For any γ and $\delta \leq 0$, the energy estimate (3.9) yields:

$$|\nabla' u^\varepsilon|_{\Omega_f} \leq C, \qquad |\partial_3 u^\varepsilon|_{\Omega_f} \leq C\varepsilon^2 \to 0 \text{ as } \varepsilon \to 0,$$

hence there exists a function $u \in H^1(\Omega_f)$ such that $u^\varepsilon \rightharpoonup u$ in $H^1(\Omega_f)$. In addition the weak limit displacement u is such that $\partial_3 u = 0$ in Ω_f, *i.e.* the limit displacement in the film is a function of the in-plane coordinates alone $u = u(x')$ in Ω_f; equivalently, it can be identified to a function $u \in H^1(\omega)$ defined on the middle surface ω. □

The invariance with respect to the transverse direction is a consequence of the "thinness" of the film, *i.e.* that its thickness scales as ε (or, in general, as a positive power of ε) with respect to the diameter L. As a consequence, the unscaled transverse strains are singular and the rescaled transverse strain vanishes, implying the transverse invariance of displacements in the film.

3.1.4 The open half space $\delta < 0$.

This regime physically corresponds to very stiff systems along the vertical direction. For $\delta < 0$ from the bound (3.10) and the Poincaré inequality (Lemma (3.1)) we deduce that:

$$|u^\varepsilon|_\Omega \leq |\partial_3 u^\varepsilon|_{\Omega_f} + |\partial_3 u^\varepsilon|_{\Omega_b} \leq C\varepsilon^{\min(2,|\delta|)} \to 0 \text{ as } \varepsilon \to 0, \qquad \text{in } L^2(\Omega).$$

Hence the first order limit displacement u is the trivial homogeneous solution. The system is so stiff that, at order 0 in ε, the displacement vanishes as a consequence of the transverse strains converging to zero. We are driven to look for higher order terms. To this end, we refine the estimate used to establish (3.11) which was not optimal. Indeed, from (3.9), by solving asymptotically the inequality:

$$\frac{1}{\varepsilon^2} |\partial_3 u^\varepsilon|^2_{\Omega_f} + \varepsilon^\delta |\partial_3 u^\varepsilon|^2_{\Omega_b} \leq C \left(|\partial_3 u^\varepsilon|_{\Omega_f} + |\partial_3 u^\varepsilon|_{\Omega_b} \right), \qquad \delta < 0$$

we identify three regimes and derive the associated energy estimates which depend upon the relative transverse stiffness between the film and the middle layer. The three regimes

correspond to: $-2 < \delta < 0$, $\delta = -2$ and $\delta < -2$. These regimes are associated to systems in which the middle layer is more compliant, as stiff as, and stiffer than the film, respectively.

We sketch some elements of analysis of the first case, namely for $-2 < \delta < 0$. This regime is identified on the phase diagram of Figure 3.2 with the gray-shaded region. We expect the first order non-trivial displacement to be driven by the middle layer (and hence its order of magnitude by the exponent δ of the stiffness), since the latter is more compliant relatively to the film. Here, transverse strains in the film are more singular than those in the middle layer and the order of magnitude of the first non-trivial displacements is that which allows to balance the applied load. Hence, we look for displacements of order ε^δ, we rescale $\tilde{u}^\varepsilon = \varepsilon^\delta u^\varepsilon$, so that the associated variational formulation of the equilibrium equations reads:

$$\int_{\Omega_f} \left\{ \varepsilon^{-\delta} \nabla' u^\varepsilon \nabla' v + \varepsilon^{-\delta-2} \partial_3 u^\varepsilon \partial_3 v \right\} dx + \int_{\Omega_b} \varepsilon^{\gamma-\delta} \nabla' u^\varepsilon \nabla' v dx + \int_{\Omega_b} \partial_3 u^\varepsilon \partial_3 v dx = \mathcal{L}^0(v), \qquad \forall v \in \mathcal{C}_0(\Omega).$$

Remark 3.4. *Note that we would have obtained the same variational formulation if, instead of* (3.7)*, we had considered loads whose potential is of order* $\mathcal{O}(\varepsilon^{1-\delta})$*. In this sense, fixing the order of the applied loads is strictly equivalent to a suitable rescaling of the unknown displacements.*

Taking $v = \tilde{u}^\varepsilon$ in the variational formulation of the equilibrium (at order ε^δ) and dropping the tilde we obtain the estimate:

$$\varepsilon^{-\delta} \left|\nabla' u^\varepsilon\right|^2_{\Omega_f} + \varepsilon^{-\delta-2} \left|\partial_3 u^\varepsilon\right|^2_{\Omega_f} + \varepsilon^{\gamma-\delta} \left|\nabla' u^\varepsilon\right|^2_{\Omega_b} dx + \left|\partial_3 u^\varepsilon\right|^2_{\Omega_b} = \mathcal{L}^0(u^\varepsilon) \leq \|\mathcal{L}^0\|_{\mathscr{L}(H^1(\Omega);\mathbb{R})} \left|u^\varepsilon\right|_\Omega .$$

Since displacements are controlled by the transverse strains, we need to establish their boundedness. Again, by solving asymptotically the inequality

$$\varepsilon^{-\delta-2} \left|\partial_3 u^\varepsilon\right|^2_{\Omega_f} + \left|\partial_3 u^\varepsilon\right|^2_{\Omega_b} \leq C \left(\left|\partial_3 u^\varepsilon\right|_{\Omega_f} + \left|\partial_3 u^\varepsilon\right|_{\Omega_b} \right), \qquad \delta < 0,$$

for $\varepsilon \to 0$ we have:

$$\left|\partial_3 u^\varepsilon\right|_{\Omega_f} \leq C\varepsilon^{\frac{-\delta-2}{2}} \to 0 \text{ as } \varepsilon \to 0,$$
$$\left|\partial_3 u^\varepsilon\right|_{\Omega_b} \leq C.$$

Hence, from the Poincaré inequality, it derives that $\left|u^\varepsilon\right|_\Omega \leq C$, hence there exists a function $u \in L^2(\Omega)$ such that (possibly passing to a subsequence) $u^\varepsilon \rightharpoonup u$ in $L^2(\Omega)$. Moreover, the weak limit u in the film is such that $\partial_3 u = 0$, hence $u = u(x')$, *i.e.* displacements are constant with respect to the thickness in the film and can be identified to a function $u \in H^1(\omega)$ defined on the middle surface ω.

The boundedness of the displacements allows to further refine the estimate on the in-plane gradients:

$$\begin{aligned} \varepsilon^{\delta/2} \left|\nabla' u^\varepsilon\right|_{\Omega_f} &\leq C, \\ \varepsilon^{(\gamma-\delta)/2} \left|\nabla' u^\varepsilon\right|_{\Omega_b} &\leq C. \end{aligned} \tag{3.12}$$

We can rewrite the variational formulation as follows:

$$\begin{aligned} \varepsilon^{-\delta/2} \int_{\Omega_f} \varepsilon^{-\delta/2} \nabla' u^\varepsilon \nabla' v dx + \varepsilon^{(-\delta-2)/2} \int_{\Omega_f} \varepsilon^{(-\delta-2)/2} \partial_3 u^\varepsilon \partial_3 v dx \\ + \varepsilon^{(\gamma-\delta)/2} \int_{\Omega_b} \varepsilon^{(\gamma-\delta)/2} \nabla' u^\varepsilon \nabla' v dx + \int_{\Omega_b} \partial_3 u^\varepsilon \partial_3 v dx \\ = \mathcal{L}^0(v), \qquad \forall v \in \mathcal{C}_0(\Omega). \end{aligned} \tag{3.13}$$

Since all the integrands are now bounded, we can pass to the limit.

i) If $\gamma - \delta < 0$, by (3.12) we have that $\left|\nabla' u^\varepsilon\right|_{\Omega_b} \to 0$ as $\varepsilon \to 0$, hence the weak limit u is a function of x_3 alone, *i.e.* $u = u(x_3)$ in Ω_b. It is now possible to test the variational formulation of the equilibrium equations (3.13) for all test functions v that are independent of x_3 within Ω_b, constantly extended in Ω_f. Passing to the limit we obtain:

$$\int_{\Omega_b} u'v' = \bar{f} v(0), \qquad \forall v \in \left\{ H^1([-1,0]), \varphi(0) = 0 \right\},$$

where $\bar{f} = \int_{\Omega_f} f(x) dx$ is the averaged load within the film. To the last variational equation is associated the following strong equilibrium equation and natural boundary conditions:

$$u''(x_3) = 0, \quad x_3 \in [-1,0], \qquad u'(0) = \bar{f}.$$

ii) If $\gamma - \delta > 0$ the in-plane gradient of displacement in the middle layer is not uniformly bounded and is allowed to be as large as $\varepsilon^{(\gamma-\delta)/2}$ as $\varepsilon \to 0$. Taking in (3.13) test functions $v \in H^1([-1,0])$ constantly extended in $(0,1]$ we obtain:

$$\int_{\Omega_b} \partial_3 u v' = \int_\omega f(x', x_3) v(0) dx', \qquad \forall v \in \left\{ H^1([-1,0]), \varphi(0) = 0 \right\}.$$

It follows an equilibrium equation where x_1 has the role of a parameter. Hence, for almost every $x_1 \in \omega$ the limit displacement $u(x', x_3)$ satisfies the following strong equilibrium equation and natural boundary condition:

$$\partial_{33} u(x', x_3) = 0, \quad x_3 \in [-1,0], \qquad u'(x', 0) = \int_0^1 f(x) dx_3.$$

iii) If $\gamma - \delta = 0$, membrane and shear strains in the middle layer are of the same order of magnitude and, along with the imposed load, the only regular terms in (3.13). In this case, a coupling between in-plane and transverse strains occurs in the middle

layer and the equilibrium displacement is determined as a function of the imposed load, averaged within the entire film layer. Indeed, it suffices to pass to the limit in (3.13) taking test functions $v \in H^1(\Omega_b), v = 0 \,\text{on}\, \omega \times \{-1\}$, constantly extended in Ω_f, to obtain the weak, limit, equilibrium equations in Ω_b, namely:

$$\int_{\Omega_b} \nabla u \nabla v dx = \int_{\omega} \hat{f}(x') v dx', \quad \forall v \in \left\{ H^1([-1,0]), \varphi(0) = 0 \right\},$$

where $\hat{f}(x')$ denotes, as usual, the applied load averaged along the thickness of the film.

Higher order models for $\delta \leq -2$ can be derived systematically with the same spirit. However, a pedissequous investigation of higher order regimes would not be of much help for the sequel of the work, since the most interesting regimes arise at order 0, for $\delta = 0$. This regime is identified by a straight segment in the phase diagram $(\gamma - \delta)$, see Figure 3.2.

3.1.5 The straight line $\delta = 0$.

Three-dimensional systems laying on the straight $\delta = 0$, are such that the energy of the transverse strains of the middle layer is of the same order of magnitude as the membrane energy of the film, a coupling is hence expected. The energy reduces to:

$$\frac{1}{2}\int_{\Omega_f} |\nabla' v|^2 dx + \frac{1}{2}\int_{\Omega_f} \frac{1}{\varepsilon^2} |\partial_3 u^\varepsilon| dx \\ + \frac{1}{2}\varepsilon^\gamma \int_{\Omega_b} |\nabla' v|^2 dx + \frac{1}{2}\int_{\Omega_b} |\partial_3 u^\varepsilon|^2 dx - \mathcal{L}^0(u^\varepsilon)$$

and the associated weak formulation of the equilibrium equations reads:

$$\int_{\Omega_f} \nabla' u^\varepsilon \nabla' v dx + \int_{\Omega_f} \frac{1}{\varepsilon^2} \partial_3 u^\varepsilon \partial_3 v dx + \varepsilon^\gamma \int_{\Omega_b} \nabla' u^\varepsilon \nabla' v dx \\ + \int_{\Omega_b} \partial_3 u^\varepsilon \partial_3 v dx = \mathcal{L}^0(v), \qquad \forall v \in \mathcal{C}_0(\Omega)$$

From $\delta = 0$ follows that $\gamma = 2\alpha + 2$ and $\beta = \alpha + 2$. Physically, the desired scaling of energies (given by $\delta = 0$) can be obtained either with a very thick and stiff or with a very thin and compliant middle layer. We furthermore discriminate three limit regimes depending upon the value of γ, determining the thickness of the middle layer.

"Pointed bars". For $\gamma < 0$, the boundedness of rescaled transverse strains (3.10) and the energy estimate (3.9) imply:

$$|\nabla' u^\varepsilon|_{\Omega_b} \leq C\varepsilon^{-\gamma/2}.$$

This, combined with the uniform bound on the rescaled transverse strains within the middle layer, yields the existence of a function $u \in H^1(\Omega_b)$ such that $u^\varepsilon \rightharpoonup u \in H^1(\Omega_b)$. As a first consequence, along the whole straight line $\delta = 0$ in the phase diagram, Property 3.1 can be refined. Owing to the weak convergence of the gradient, the convergence of displacement is strong in $L^2(\Omega)$.

Moreover, the weak limit u in Ω_b is such that $\nabla u = 0$, hence

$$u \to u(x_3), \qquad \text{in } L^2(\Omega_b).$$

Loosely speaking, the limit system only allows for displacements with zero in-plane gradient in the middle layer, that is functions that depend only upon the transverse coordinate x_3. Within the film, on the other hand, limit displacements are invariant by transverse translation (Property 3.2), *i.e.* they depend only upon the in-plane coordinate. Displacement must be continuous at the interface: these two properties are compatible if and only if the displacement at the interface is a constant. Hence, at $\omega \times \{0\}$ the following must hold:

$$u(x')|_{\omega\times\{0\}} = u(x_3)|_{\omega\times\{0\}} = U \in \mathbb{R},$$

where U is an unknown constant determined by the loads and boundary conditions.

Taking test functions $v = 0$ in the film and $v = \hat{v}(x_3)$ in the middle layer, with $\hat{v} \in H^1_0([-1,0])$, the variational formulation of the equilibrium reads:

$$\int_{\Omega_b} \partial_3 u^\varepsilon \hat{v}' dx = 0, \qquad \forall \hat{v} \in H^1_0([-1,0]).$$

We can now pass to the limit and get:

$$\int_{\Omega_b} \partial_3 u \hat{v}' dx = 0, \qquad \forall \hat{v} \in H^1_0([-1,0]).$$

Localizing along the vertical segment $[-1,0]$, integrating by parts, solving and imposing boundary conditions one obtains:

$$u(x_3) = U(x_3 + 1), \qquad x_3 \in (-1,0].$$

The equilibrium displacement belongs, along each vertical segment, to the one-parameter family of the affine continuous functions indexed by U. They belong to a space parametrized by a real constant which we denote by $C^1_U((-1,1))$ and write as follows:

$$C^1_U((-1,1)) := \big\{ v \in H^1(\Omega) : v = U, \text{for } x_3 \in (0,1), v = U(x_3+1), \\ \text{for } x_3 \in (-1,0], U \in \mathbb{R} \big\}.$$

We need to determine the constant U delivering the minimal energy. The problem reduces to the minimization of an energy with respect to a real constant. Taking in the variational formulation of the equilibrium $v = \hat{v} \in C^1_V((-1,1))$, we have:

$$\int_{\Omega_b} \partial_3 u^\varepsilon \partial_3 \hat{v} dx = \mathcal{L}^0(\hat{v}), \qquad \forall \hat{v} \in C^1_V((-1,1))$$

by the convergences established above we can pass to the limit $\varepsilon \to 0$ and obtain:

$$U\left(\int_{\Omega_b} dx\right) V = \left(\int_{\Omega_f} f dx\right) V, \qquad \forall V \in \mathbb{R}$$

which we integrate to determine the optimal value U^*:

$$U^* = \frac{1}{|\omega|}\int_\omega \hat{f}(x')dx'. \tag{3.14}$$

Here we denote by $|\omega| := \int_\omega dx$ the area of the middle surface ω and by $\hat{f}(x') = \int_0^1 f(x', x_3)dx_3$ the applied load in the film, averaged along the thickness. The constant U^* just identified delivers the optimal (minimum) energy and solves the equilibrium problem.

In the case under study, the displacement is the same along each segment $x'\times \in (-1, 1)$, for $x' \in \omega$: it reduces essentially to a one-dimensional problem. We are indeed tackling the case of a (trivial) theory of thermal bars undergoing only shear deformations. In fact, with $\delta = 0$, then γ is negative only when $\alpha < -1$. Recalling the form of the scaling in (3.1), this identifies the unscaled three-dimensional systems consisting of a film whose thickness goes to zero with ε and a middle layer whose thickness goes to infinity with $\varepsilon^{-|\alpha|+1}$, as $\varepsilon \to 0$. Hence, the system is more and more slender in the transverse direction as $\varepsilon \to 0$, its limit is that of a bar (undergoing only shear) with a superficial added stiffness due to the film supporting the loads. It is clear that a symmetrical distribution of the applied load $\hat{f}(x')$ results into an elastic response with zero displacement.

A three-dimensional middle layer. For $\gamma = \delta = 0$, all derivatives of displacements are bounded and the convergence of displacements (Property 3.1) can be refined. Indeed, there exists $u \in H^1(\Omega)$ such that $u^\varepsilon \rightharpoonup u$ in $H^1(\Omega)$. Taking test functions $\hat{v} \in H^1(\omega)$ in Ω_f and $v = \hat{v} \in \left\{H^1(\Omega_b) : v|_{\omega\times\{-1\}} = 0\right\}$ in Ω_b, for all such functions the following must hold:

$$\int_{\Omega_f} \nabla' u^\varepsilon \nabla' v dx + \int_{\Omega_b} \nabla u^\varepsilon \nabla v dx + = \mathcal{L}^0(v).$$

by the convergences established above, we can pass to the limit and get, for the same test functions:

$$\int_\omega \nabla' u \nabla' v dx' + \int_{\Omega_b} \nabla u \nabla v dx = \hat{\mathcal{L}}^0(v),$$

where $\hat{\mathcal{L}}^0(v) := \int_\omega \hat{f}(x')v dx_3$ and the averaged load along the thickness is defined as in (3.14). Although in the film, owing to the invariance with respect to the transverse direction (Property 3.2), we can integrate along x_3 and obtain in the limit an integral defined on the middle surface ω, *i.e.* a reduced dimension theory for the film, the same is not true for the middle layer. The variational formulation of the equilibrium equations satisfied by the weak limit is hence three-dimensional, because of the middle layer Ω_b. Recalling the scalings (3.1), $\gamma = \delta = 0$ imply that $\alpha = -1$ and $\beta = 1$. The unscaled

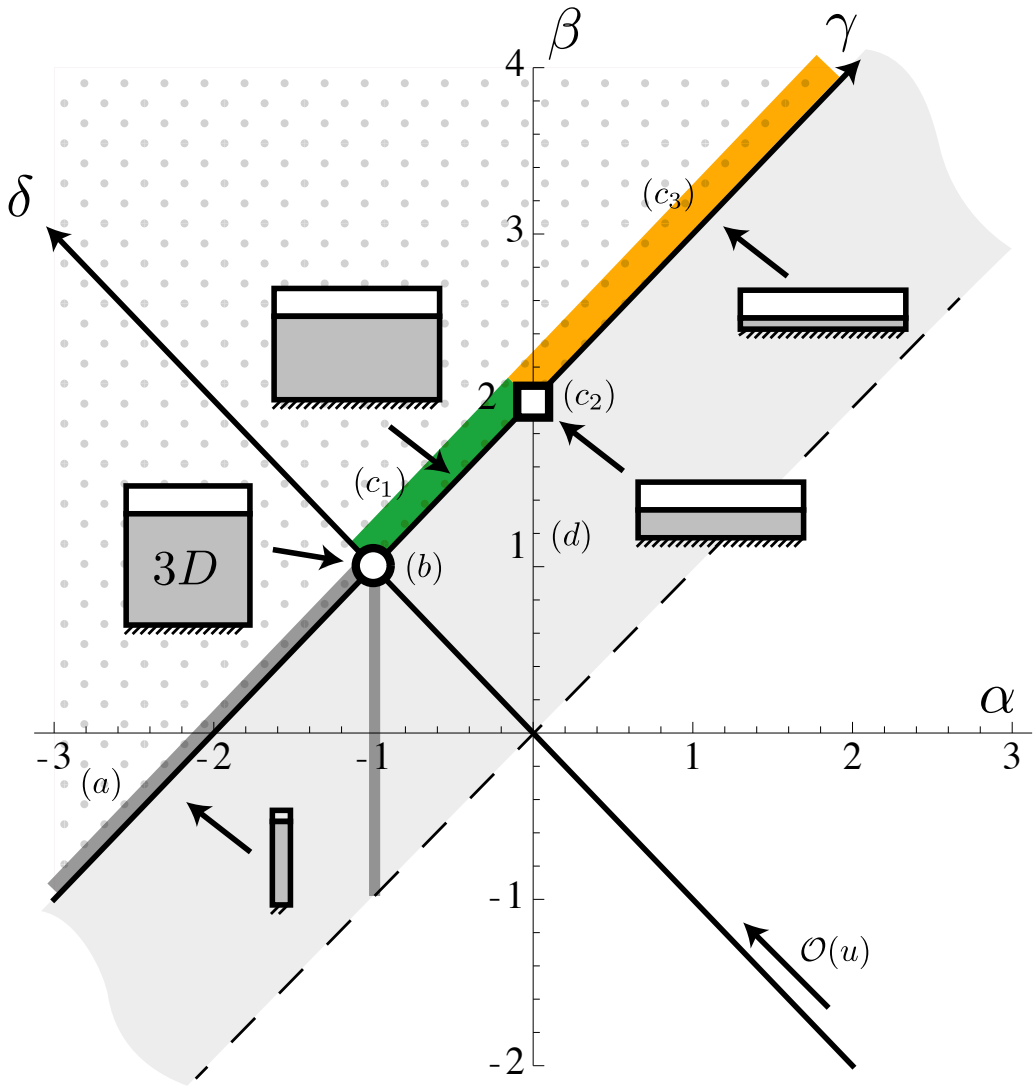

Figure 3.2: The phase diagram of three-dimensional film systems. The order of magnitude of the first non-trivial limit displacements decreases with δ. The dotted region corresponds to possibly unbounded displacements, see Section 3.1.2. Along the straight line $\delta = 0$ displacements are of order one, see Section 3.1.5. For $\gamma < 0$ we identify the regime of slender bars under shear, (a) in the figure. For $\gamma = 0$ we have a thin film over a three-dimensional substrate, (b). For $\gamma > 0$ we find the interesting limit regime of membranes over an elastic foundation (c). Along this open straight line we further individuate different (unscaled) three-dimensional systems: thin films over a thick substrate (c_1), stiff films over a compliant bonding layer (c_2) and stiff films over a thin bonding layer (c_3). In the region $-2 < d < 0$ (shaded in light gray), the first order non-trivial displacement is of order ε^δ. We identify an interesting regime of "thermal beams" (d), see Section 3.1.4.

(a) The "pointed bar" is asymptotically a one dimensional bar under shear with an added stiffness which carries the load.

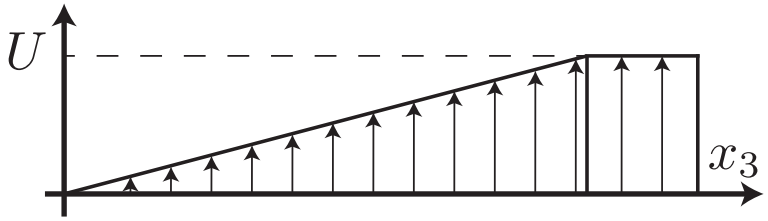

(b) The displacement field is piecewise linear and identified univocally by the real constant U to be determined, as a consequence of equilibrium, by (3.14).

Figure 3.3: The three dimensional domain and displacement field in the "pointed bar" regime.

three-dimensional domain is a film of thickness of order ε upon a layer of finite thickness whose stiffness is of order ε. In this case, the elasticity couples both the shear and in-plane strains of the middle layer to the membrane strains of the film and to the work of external loads (all are of order zero with respect to ε). The limit model is that of a three-dimensional body with a linear membrane on the upper surface undergoing in-plane displacements and acting as an added stiffness, see Figure 3.3. Differently from the case 3.1.4.iii), here, the membrane strains of the topmost film are coupled to the three-dimensional elasticity problem of the middle layer and appear explicitly in the equilibrium equations. These three-dimensional systems are identified in the phase diagram γ-δ by the intersection denoted by A in Figure 3.2 and the associated energy functional is:

$$E_2(u) = \frac{1}{2}\int_\omega |\nabla' u|^2 dx' + \frac{1}{2}\int_{\Omega_b} |\nabla u|^2 dx - \hat{\mathcal{L}}^0(u).$$

A reduced theory with an internal length. The last case is $\gamma > 0$ and corresponds to systems for which the in-plane deformations within the middle layer are allowed to be large. Such systems lay on the open half line ($\delta = 0, \gamma > 0$).

Let us focus on the rescaled transverse strains. First, note that the energy of in-plane deformations within the middle layer vanishes in the limit. Indeed, the energy estimate (3.9) and Poincaré inequality (3.1) provide the following bound on the in-plane strains within the middle layer:

$$\varepsilon^{\gamma/2} \left|\nabla' u^\varepsilon\right|_{\Omega_b} \leq C.$$

By the bound (3.10) we obtain that:

$$|\partial_3 u^\varepsilon|_{\Omega_b} \leq C,$$

hence there exists a function $\xi \in L^2(\Omega_b)$ such that (up to a subsequence, not relabeled) $\partial_3 u^\varepsilon \rightharpoonup \xi$ in $L^2(\Omega_b)$.

We now show that the weak limit ξ of the rescaled transverse strain is constant with respect to x_3. Localizing the variational formulation of Equation (3.8) in the middle layer, *i.e.* choosing test functions $v = 0$ in Ω_f, and $v \in H^1_0(\Omega_b)$ in the middle layer, the rescaled equilibrium equations (3.8) reduce to:

$$\varepsilon^{\gamma/2} \int_{\Omega_b} \varepsilon^{\gamma/2} \nabla' u^\varepsilon \nabla' \hat{v} dx + \int_{\Omega_b} \partial_3 u^\varepsilon \partial_3 \hat{v} dx = \mathcal{L}^0(\hat{v}), \qquad \forall \hat{v} \in H^1_0(\Omega_b).$$

By the convergences established above, the first term converges to 0 as $\varepsilon \to 0$, we can pass to the limit in the last equation and obtain:

$$\int_{\Omega_b} \xi \partial_3 \hat{v} dx = 0, \qquad \forall \hat{v} \in H^1_0(\Omega_b)$$

We write $\hat{v} = g(x_\alpha)h(x_3)$ where $g \in C^\infty_0(\omega)$ and $h \in L^2_0((-1,1))$ and for all such functions:

$$\int_\omega \left(\int_0^1 \xi h' dx_3 \right) g dx' = 0.$$

This allows to derive an equation, for each $x' \in \omega$, along the vertical segment $(-1, 0)$ in the middle layer. After integration by parts we obtain:

$$\partial_3 \xi = 0, \qquad \text{a.e. } x' \in \omega,\ x_3 \in (-1, 0)$$

from which follows that $\xi = \xi(x')$, *i.e.* ξ is a constant with respect to x_3.

The value of this constant is fixed imposing the continuity of displacements across the interface $\omega \times \{0\}$ and the boundary condition of place on ω_-. Since we also have that $\xi = \partial_3 u$ (the derivative taken in the sense of distributions), we compute the value of the displacement on the interface. From below:

$$u|_{\omega \times \{0^-\}} = u(x', -1) + \int_{-1}^0 \xi(x') dx_3 = \xi(x'),$$

where we have used the boundary condition $u(x', -1) = 0$. From above:

$$u|_{\omega \times \{0^+\}} = u(x'),$$

since in the film displacements are constant through the thickness. Finally, the continuity $[\![u]\!]_{\omega \times \{0\}} = 0$ fixes:

$$\xi(x') = u(x').$$

Consequently, for $\delta = 0$ and $\gamma > 0$, the rescaled transverse strains within the middle layer equal the mismatch between the film displacement and the imposed substrate' displacement.

Property 3.3. *For $\delta = 0$ and $\gamma > 0$, transverse strains of a sequence of minimizers u^ε converge, in the middle layer, to a constant function with respect to the thickness which equals the value of the displacement mismatch between the film and imposed boundary condition at $\omega \times \{0\}$*

$$u^\varepsilon \text{ such that } \partial_3 u^\varepsilon \rightharpoonup \xi(x') = u(x')$$

where $u \in H^1(\omega)$ is the displacement of the film, defined on the middle surface ω.

Note that the weak convergence of the scaled transverse strains in the bonding layer is sufficient to determine the elastic response of the system. Indeed, since in-plane gradients of displacements can be large, the sequences of displacements in the bonding layer do not in principle converge to a limit. Displacements in the bonding layer may exhibit large variations in the in-plane directions since no in-plane stress is transfered within the bonding layer. In this sense, each segment $x' \times (-1, 0)$ is independent from the others, analogously to what was observed in the case of Section 3.1.2 along the orthogonal direction. However, displacements are controlled by the boundary condition of place at $\omega \times \{-1\}$ and the continuity at $\omega \times \{0\}$ with the displacement of the film. Since the former is not affected by the rescaling, the control of the displacements within the whole domain reduces to the control of the displacements of the film.

At this point the optimal transverse profile of the weak limit displacement is known both in the film and within the middle layer: it is constant and linear with respect to the transverse coordinate respectively. Choosing, in the variational formulation (3.8), test functions with the same profile as the optimal limit displacement, *i.e.*

$$v(x) = \begin{cases} \hat{v}(x')(x_3 + 1), & \text{if } (x', x_3) \in \Omega_b \\ \hat{v}(x'), & \text{if } (x', x_3) \in \Omega_f \end{cases}, \qquad \hat{v} \in H^1(\omega)$$

we obtain:

$$\int_{\Omega_f} \nabla' u^\varepsilon \nabla \hat{v} dx + \varepsilon^{\gamma/2} \int_{\Omega_b} \varepsilon^{\gamma/2} \nabla' u^\varepsilon \nabla \hat{v} dx + \int_{\Omega_b} \partial_3 u^\varepsilon \hat{v} dx = \mathcal{L}^0(\hat{v}), \qquad \forall v \in H^1(\omega).$$

By the bounds established above all the integrals are bounded, we can pass to the limit $\varepsilon \to 0$, integrate through the thickness, and obtain:

$$\int_\omega \{\nabla' u \nabla' \hat{v} + u\hat{v}\} \, dx' = \hat{\mathcal{L}}^0(\hat{v}), \qquad \forall \hat{v} \in H^1(\omega). \tag{3.15}$$

The limit equations (3.15) are the weak two-dimensional limit equilibrium equations satisfied by the weak limit u under the averaged load and correspond to the first order necessary conditions for minimality of the following limit energy:

$$E_{2D}(u) := \frac{1}{2} \int_\omega \left\{ |\nabla' u|^2 + u^2 \right\} dx' - \hat{\mathcal{L}}^0(u). \tag{3.16}$$

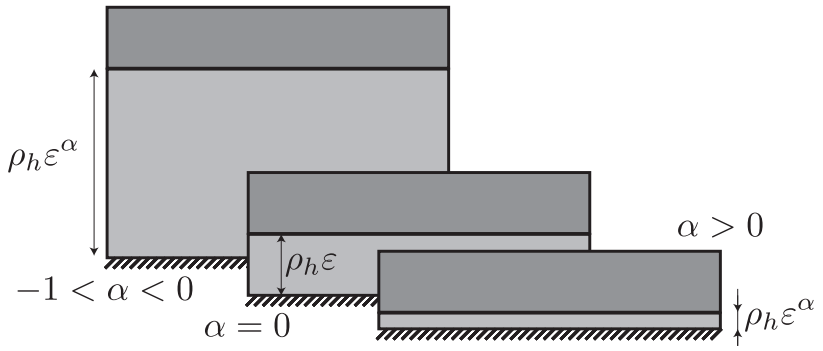

Figure 3.4: Different three-dimensional systems afferent to the same asymptotic regime of thin films over elastic foundation. From left to right: a thin film over a thick substrate; a film over a bonding layer, their thickness of the same order of magnitude; and a thin film over a much thinner compliant interface.

defined for displacement fields $u \in H^1(\omega)$. The relations $\delta = 0$ and $\gamma > 0$ identify a *class* of three-dimensional systems admitting the same two-dimensional limit energy. The equilibrium configuration of these systems is determined solving Equation (3.15). In the limit equilibrium equations a new term appears with respect to the three-dimensional equations, namely $\int_\omega u^2 dx'$, estimating the limit shear energy of the bonding layer. It is interpreted as a *linear elastic foundation*. This model has been known to the engineering community since the late 1860's under the name of (bilateral) "Winkler foundation" [Win67] and widely applied, other than in thin film systems, especially to soil engineering, railroad systems, highway slabs, floating structures, floor systems etc. Although this model is commonly introduced by phenomenological intuition, it indeed has the rigorous asymptotic derivation just shown.

We can further discriminate among these systems. which are equivalently identified by the relations: $\alpha > -1$ and $\beta = \alpha + 2$ (recall the definitions of γ and δ in (3.6)).

For $\alpha > 0$ the corresponding unscaled three-dimensional systems are composed of a middle layer whose thickness goes to zero faster than that of the film. That is, at fixed ε the middle layer is much thinner than the film. For $\alpha = 0$ the thickness of both the film and bonding layer is of the same order of magnitude. Finally, for $-1 < \alpha < 0$ the unscaled three-dimensional system (at fixed ε) is constituted by a film much thinner than the middle layer. Equivalently, for these systems the thickness of the film goes to zero faster than that of the middle layer. These three scenarios are illustrated in Figure 3.4 and offer a key to interpret the vast and fruitful application of this simple linear model to a plethora of problems, some of which recalled above.

We synthesize the main results of this section in the following theorem.

Theorem 3.1 (Zoological characterization of the asymptotic regimes)**.** *Let u^ε be the solution of the problem $\mathcal{P}(\varepsilon, \Omega)$. Then, if $\delta \leq 0$, the family of scaled displacements $(u^\varepsilon)_{\varepsilon>0}$*

admits a weak limit u, as $\varepsilon \to 0$, in the space $L^2(\Omega)$. Depending upon the values of γ, δ we identify the following asymptotic regimes:

a) If $\delta < 0$, the first order weak limit u is zero. The order of the first non-trivial limit displacement field depends upon δ. For $-2 < \delta < 0$ the first non-trivial limit displacement is of order δ. We distinguish three sub-regimes depending upon the relative membrane-to-shear order of magnitude in the middle layer: the one-dimensional bar (for $\gamma - \delta < 0$, see Section 3.1.4.i), a three-dimensional layer under surface loads (for $\gamma - \delta = 0$, see Section 3.1.4.ii), a system of mutually independent, vertical, linear bars (for $\gamma - \delta > 0$, see Section 3.1.4.iii)

b) If $\delta = 0$ and $\gamma = 0$, the weak limit u is the (unique) solution of the following scaled three-dimensional problem:

$\mathcal{P}_{3D}(\Omega)$: Find $u \in \mathcal{C}_w(\Omega)$ such that :

$$\int_\omega \nabla' u \nabla' \hat{v} dx' + \int_{\Omega_b} \nabla u \nabla \hat{v} dx = \hat{\mathcal{L}}^0(v), \qquad \forall \hat{v} \in \mathcal{C}_0(\Omega).$$

This is the asymptotic regime of membranes over a three-dimensional elastic body*.*

c) If $\delta = 0$ and $\gamma > 0$ the weak limit u is the (unique) solution of the following scaled two-dimensional problem:

$\mathcal{P}_{2D}(\Omega)$: Find $u \in H^1(\omega)$ such that

$$\int_\omega \{\nabla' u \nabla' \hat{v} + u\hat{v}\} \, dx' = \hat{\mathcal{L}}^0(\hat{v}), \qquad \forall \hat{v} \in H^1(\omega).$$

This is the asymptotic regime of membranes over elastic foundation*.*

d) If $\delta = 0$ and $\gamma < 0$ the weak limit u reduces to the one-parameter family of displacements, parametrized by the constant U and constructed as follows:

$$u(x_3) = \begin{cases} U^*, & \text{in } \Omega_f \\ U^* x_3, & \text{in } \Omega_b \end{cases}, \qquad \text{with } U^* = \frac{1}{|\omega|} \int_\omega \hat{f}(x') dx'.$$

This is the asymptotic regime of one-dimensional bars undergoing shear deformations*.*

3.1.6 The energy of the two-dimensional limit model

The only interesting asymptotic regime for the sequel of the study is that of linear membranes over elastic foundation, case *c)* of Theorem 3.1. The additional term (quadratic with respect to u) arises from the coupling of the shear deformation of the middle layer and the in-plane strains of the film. Although in-plane strains are not controlled by the energy bound within the middle layer, the boundary condition on the interface with the substrate and the continuity of displacements at the interface with the film control the displacements of the middle layer. Note that the boundary condition

plays a crucial role delivering affine displacements in the intermediate layer which in turn determine the contribution to the limit energy as an elastic foundation.

It is useful at this point to reintroduce the geometric and material parameters to highlight their mechanical role. The energy of Equation (3.16) is issued from the limit analysis of the energies defined on the rescaled *unit* domains. In order to let the material and geometric quantities appear in the limit energy we map the non-dimensional unit domains Ω_f and Ω_b to the non-dimensional domains $\omega \times \{0, h_f\}$ and $\omega \times \{-h_b, 0\}$, respectively. Reintroducing the tilde notation for non-dimensional quantities, a scale for displacements u_0 and a scale for lengths x_0 we define the dimensional displacements and lengths as follows:

$$u = u_0 \tilde{u}, \qquad x' = x_0 \tilde{x}'.$$

We perform a change of variable, inverse to that of Equation (3.2), in order to explicitly recover the imposed boundary displacement. After some calculations we obtain:

$$u_0 \tilde{E}(v) = \frac{\mu_f \varepsilon L}{2} \int_\omega \left\{ |\nabla u|^2 + \frac{\varrho_\mu x_0^2}{\varrho_h h_f^2} (u - w)^2 \right\} dx' - \varepsilon L \hat{\mathcal{L}}^0(v)$$

Taking the as length scale the diameter of the domain ω, since the membrane and elastic foundation terms are not homogeneous, the intrinsic length scale

$$\ell_e^2 := \frac{\varrho_\mu L^2}{\varrho_h h_f^2} = \frac{\mu_f L^2}{\mu_b h_f h_b},$$

emerges from the competition between the membrane and the elastic foundation energy densities, determined by the geometric and material parameters. This length scale, issued from the asymptotic process and to be compared to the size of the structure, emerges as a new feature springing from the original three-dimensional system where no characteristic scale is involved. This length scale, as it has been seen in the simple one-dimensional fracture problem in Chapter 2 case, is responsible of the richness of phenomenology revealed by fracture processes and essentially characterizes a *class* of different three-dimensional systems allowing for the *same* limit representation.

3.2 A reduced dimension theory for thin films in vector elasticity

The asymptotic study in the framework of scalar elasticity of the previous section provides a qualitative picture of the elastic couplings that arise, and has allowed for the identification of a class of thin film systems whose fundamental asymptotic characteristic is to express an intrinsic length scale in the limit.

The study performed in the preceding section is confined to the case of scalar elasticity. With a slight abuse of language, we have associated the in-plane deformations, *i.e.* the in-plane gradient of the scalar displacement u, to *membrane strains* and the transverse variations of displacement to *shear strains*. The scalar assumption is restrictive but sufficient to highlight the qualitative key couplings between the components of the energy. We now extend the study to the more physically relevant case of vectorial three-dimensional elasticity, establishing the link between the "thermal plates" of the preceding section and the "elastic plates". In this setting, the fundamentally new phenomenology, inexistent in scalar elasticity, is the possibility to undergo *rotations* still associated to infinitesimal strains. It is indeed from such rotations that plate (or beam) theories with bending emerge, see [Cia97].

The present study focuses on the derivation of an asymptotic plate-like theory for the elastic multilayer, allowing both in-plane and transverse deformations.

We use the techniques of asymptotic analysis by formal asymptotic expansions and look for the solution of the elasticity problem under the form of a power series of the small parameter ε. Besides the initial ansatz providing the power expansion, the procedure is rigorous and deductive. The model system is sketched in Figure 3.5. Allowing ourselves to redefine symbols already introduced, the notation is kept consistent with that of Section 3.1. The energy density associated to the elastic strains e reads:

$$W(e) = \lambda(x)\,\mathrm{tr}(e)^2 + 2\mu(x)e \cdot e. \tag{3.17}$$

where $(\lambda, \mu)(x)$ are the non-homogeneous piecewise constant Lamé parameters of the elastic body.

Assumptions on the data. We perform an asymptotic study of one instance of the class identified in Section 3.1, *i.e.* the class of systems for which the shear energy of the middle layer is of the same order of magnitude of the membrane energy of the film.

We choose to specialize to systems whose layers' thickness is of the same order of magnitude, that is we specialize our scaling law to a system analogous to that labeled c_2 in Figure 3.2. In addition, we assume a uniform scaling with respect to ε of the two elastic parameters (λ, μ) in (3.17), *i.e.* we do not introduce strong material anisotropies. The associated scaling law hence reads as follows:

Hypothesis 2 (A stiff film over a compliant bonding layer)**.** *Setting*

$$\varepsilon := \frac{h_f}{L} \ll 1,$$

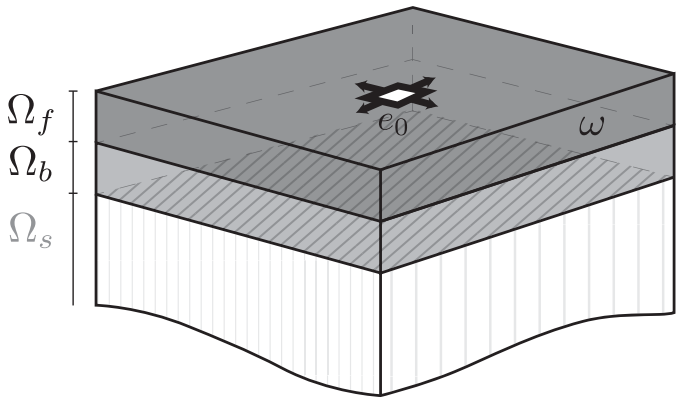

Figure 3.5: The three-dimensional elastic multilayer in vectorial elasticity.

we assume that both the thickness of the film h_f and that of the bonding layer h_b scale with ε with respect to L. Also, we assume that the ratio between the elastic constants of the bonding layer and that of the film scales as ε^2:

$$\frac{h_b}{h_f} = \varrho_h, \qquad \left(\frac{\lambda_b}{\lambda_f}, \frac{\mu_b}{\mu_f}\right) = \varepsilon^2 \left(\varrho_\lambda, \varrho_\mu\right)$$

where $\varrho_h, \varrho_\lambda$ and ϱ_μ are non-dimensional coefficients independent of ε.

The film and the bonding layer occupy the domains $\overline{\Omega_f^\varepsilon} = \overline{\omega} \times (0, \varepsilon L]$ and $\overline{\Omega_b^\varepsilon} = \overline{\omega} \times [-\varrho_h \varepsilon L, 0]$.

Denoting by $\Omega^\varepsilon = \Omega_f^\varepsilon \cup \Omega_b^\varepsilon$ the reference configuration of the two layers, the space of admissible displacements is:

$$\mathcal{C}_w^\varepsilon(\Omega^\varepsilon) := \left\{ v \in H^1(\Omega^\varepsilon), v = w \text{ a.e. on } \omega \times \{-\varrho_h \varepsilon L\} \right\},$$

and its associated vector space is:

$$\mathcal{C}_0^\varepsilon(\Omega^\varepsilon) := \left\{ v \in H^1(\Omega^\varepsilon), v = 0 \text{ a.e. on } \omega \times \{-\varrho_h \varepsilon L\} \right\},$$

to each of such displacements we associate the family of three-dimensional elastic energies indexed by ε:

$$E_\varepsilon(v) = \frac{1}{2} \int_{\Omega^\varepsilon} \left\{ \lambda(x) \operatorname{tr}(e(v))^2 + 2\mu(x) e(v) \cdot e(v) \right\} dx - \mathcal{L}^\varepsilon(v),$$

where

$$(\lambda, \mu)(x) = \begin{cases} (\lambda_f, \mu_f), & \text{if } x \in \Omega_f^\varepsilon \\ (\lambda_b, \mu_b), & \text{if } x \in \Omega_b^\varepsilon \end{cases}$$

and $\mathcal{L}^\varepsilon(v) = \int_{\Omega_f^\varepsilon} f^\varepsilon v dx$ is the potential of the loads in the film, whose order of magnitude can be expressed as a function of ε. Equilibrium displacements $\tilde{u}^\varepsilon \in \mathcal{C}_w^\varepsilon(\Omega^\varepsilon)$ are then

sought as the energy minimizers. The equilibrium problem for $\tilde{u}^\varepsilon$ is posed on the ε-dependent domain Ω^ε.

The usual anisotropic scaling of the space coordinates (3.4) maps $\Omega^\varepsilon = \Omega_f^\varepsilon \cup \Omega_b^\varepsilon$ into $\Omega = \Omega_f \cup \Omega_b = \omega \times (0,1) \cup \omega \times [-1,0]$. We also scale the components of the unknown displacement field as follows:

$$u_\alpha^\varepsilon = \tilde{u}_\alpha^\varepsilon, \qquad u_3^\varepsilon = \tilde{u}_3^\varepsilon/\varepsilon \tag{3.18}$$

Using the above scalings, the components of the scaled strain tensor are related to those of the strain tensor by the following relations:

$$e_{33}^\varepsilon(u^\varepsilon) = \frac{1}{\varepsilon^2} e_{33}(u^\varepsilon), \qquad e_{\alpha 3}^\varepsilon(u^\varepsilon) = e_{\alpha 3}(u^\varepsilon), \qquad e_{\alpha\beta}^\varepsilon(u^\varepsilon) = \varepsilon^2 e_{\alpha\beta}(u^\varepsilon),$$

The first term is the transverse strain associated to variations of the vertical displacement through the thickness, the second is the shear strain and the third the in-plane strain. Plugging the above expressions into the energy and collecting the terms of the same power in ε, the scaled elastic energy reads as:

$$\begin{aligned}
\frac{E_\varepsilon(u^\varepsilon)}{\varepsilon} = \frac{1}{2\varepsilon^4} \int_{\Omega_f} (\lambda_f + 2\mu_f) e_{33}(u^\varepsilon)^2 dx \\
+ \frac{1}{2\varepsilon^2} \int_{\Omega_f} \left\{ \lambda_f (e_{\alpha\alpha}(u^\varepsilon) e_{33}(u^\varepsilon)) + 2\mu_f e_{\alpha 3}(u^\varepsilon)^2 \right\} dx \\
+ \frac{1}{2} \int_{\Omega_f} \left\{ (\lambda_f + 2\mu_f)(e_{\alpha\alpha}(u^\varepsilon) e_{\beta\beta}(u^\varepsilon)) + 2\mu_f e_{\alpha\beta}(u^\varepsilon) e_{\alpha\beta}(u^\varepsilon) \right\} dx \\
+ \frac{1}{2\varepsilon^2} \int_{\Omega_b} (\varrho_f \lambda_f + 2\varrho_\mu \mu_f) e_{33}(u^\varepsilon)^2 \\
+ \int_{\Omega_b} \varrho_f \lambda_f (e_{\alpha\alpha}(u^\varepsilon) e_{33}(u^\varepsilon)) + 2\varrho_\mu \mu_f e_{\alpha 3}(u^\varepsilon)^2 \\
+ \frac{1}{2}\varepsilon^2 \int_{\Omega_b} \left\{ (\varrho_f \lambda_f + 2\varrho_\mu \mu_f)(e_{\alpha\alpha}(u^\varepsilon) e_{\beta\beta}(u^\varepsilon)) + 2\varrho_\mu \mu_f e_{\alpha\beta}(u^\varepsilon) e_{\alpha\beta}(u^\varepsilon) \right\} dx \\
- \frac{\mathcal{L}^\varepsilon(u^\varepsilon)}{\varepsilon}.
\end{aligned}$$

As in Section 3.1, we extend constantly the boundary displacement to Ω and perform the change of variable to recover homogeneous boundary conditions for the unknown displacements.

The associated minimization problem on the fixed domain Ω reads:

Problem 3.4 (Rescaled minimization problem on the unit domain in vector elasticity)**.**

$$\mathcal{P}(\varepsilon, \Omega): \quad \textit{Find } u^\varepsilon \in \mathcal{C}_w(\Omega) \textit{ minimizing } E(u^\varepsilon) \textit{ in } \mathcal{C}_0(\Omega)$$

The above manipulations allow us to let the explicit dependence upon ε of the terms of the energy appear, and thus to reveal the order of magnitude of the different elastic contributions in the regime determined by the geometric and constitutive assumptions of Hypothesis 2.

In the present analysis, we want to model loads inducing in-plane deformations of the film. It is therefore reasonable to consider the external work $\mathcal{L}^\varepsilon$ to be of the same order of magnitude as the energy of in-plane deformations within the film. We hence fix: $\mathcal{L}^0 := \mathcal{L}^\varepsilon/\varepsilon$. The same remarks raised after the rescalings in Section 3.1 apply here. The legitimacy of the arbitrariness in the rescalings of $\mathcal{L}^\varepsilon$ and of the displacements (3.18) is a byproduct of the linear setting. Indeed, it is only from a genuinely nonlinear asymptotic theory that one can derive the proper scaling of loads yielding the linear limit and its regime of validity. The scalings (3.18) suggest that the regime of validity of the limit linear theory is limited to transverse displacements of the order of the thickness of the plate, which in turn implies that the first non-trivial term in the expansion of the in-plane displacements is of order ε^2.

The inspection of the above energy provides some useful insight on the problem and on the expected behavior as $\varepsilon \searrow 0$. The most singular term (of order $\mathcal{O}(\varepsilon^{-4})$) is the energy of scaled transverse strains in the film. Requiring a bounded energy at the order of the external work implies that such term must vanish. The same applies at order $\mathcal{O}(\varepsilon^{-2})$ for shear the strain within the film and the transverse strain in the bonding layer. We shall see that, it is the vanishing of all these terms in the limit, that contributes to the limit energy and the kinematic characterization of limit displacements. The leading term of the energy in bonding layer is that related to transverse strains. Up to $\mathcal{O}(\varepsilon^{-2})$ the elasticity of the film is uncoupled from that of the bonding layer. At $\mathcal{O}(\varepsilon^0)$ the in-plane problem of the film and the shear terms of the bonding layer are coupled, under the action of the external loads.

We tackle the problem using the techniques of formal asymptotic expansions. Supposing that the displacement field can be expanded as a power series of the parameter ε we plug such expression in the variational formulation of the equilibrium equations. We then identify and solve the cascade of variational problems verified by subsequent orders of the expansion until we are able to compute the leading term. The expansion of displacements is given by the following Ansatz.

Ansatz 3.1. *Displacements u^ε can be written as an integer power series of ε. The problem being linear, we shall let the series start at order* 0*.*

$$u^*(\varepsilon) = u^0 + \varepsilon^2 u^1 + \varepsilon^4 u^2 + \cdots + \varepsilon^{2i} u^i. \tag{3.19}$$

where $u^0 \neq 0$. Each component of u^i for $i \geq 0$ belongs to $H^1(\Omega)$. We require that the first order u^0 satisfy the boundary condition of place on ω_-.

Note that it is sufficient to consider only *even* terms of the expansion since only even terms are present in the expression of the energy. The same arguments (and equations) would then hold *verbatim* for the odd terms. Note also that this method is only *formal*, in the sense that convergence of $u^*(\varepsilon)$ to a limit u is not guaranteed. However, apart

the assumption that the displacement can be expanded as powers of ε, the method is rigorous and deductive. A stronger convergence result is the object of Theorem 3.2.

The first order optimality conditions (the variational formulation of the equilibrium), obtained by plugging Ansatz (3.19) into Problem 3.4, read:

Problem 3.5.

$$\begin{aligned}\mathcal{P}(\varepsilon,\Omega): \quad & \textit{Find } u_i^0 \in \mathcal{C}_0(\Omega), u_i^n \in H^1(\Omega) \textit{ for } n = 1, 2\ldots, \\ & i \in \{1,2,3\} \textit{ such that}: \\ & \\ & \varepsilon^{-4}\mathscr{A}_f(u^*(\varepsilon),v) + \varepsilon^{-2}\mathscr{B}_f(u^*(\varepsilon),v) + \mathscr{C}_f(u^*(\varepsilon),v) \\ & + \varepsilon^{-2}\mathscr{A}_b(u^*(\varepsilon),v) + \mathscr{B}_b(u^*(\varepsilon),v) \\ & + \varepsilon^{-4}\mathscr{C}_b(u^*(\varepsilon),v) = \mathcal{L}^0(v), \qquad \forall v \in \mathcal{C}_0(\Omega)\end{aligned}$$

In the last expression, we let:

$$\begin{aligned}&\mathscr{A}_f(u,v) = \mathscr{A}(u,v,\Omega_f), \qquad \mathscr{B}_f(u,v) = \mathscr{B}(u,v,\Omega_f), \mathscr{C}_f(u,v) = \mathscr{C}(u,v,\Omega_f),\\ &\mathscr{A}_b(u,v) = \mathscr{A}(u,v,\Omega_b), \qquad \mathscr{B}_b(u,v) = \mathscr{B}(u,v,\Omega_b), \mathscr{C}_b(u,v) = \mathscr{C}(u,v,\Omega_b),\end{aligned}$$

where

$$\begin{aligned}\mathscr{A}(u,v;\Omega) &= \int_\Omega (\lambda+2\mu)e_{33}(u)e_{33}(v)\\ \mathscr{B}(u,v;\Omega) &= \int_\Omega \lambda(e_{\alpha\alpha}(u)e_{33}(v) + e_{33}(u)e_{\alpha\alpha}(v)) + 4\mu e_{\alpha 3}(u)e_{\alpha 3}(v)\\ \mathscr{C}(u,v;\Omega) &= \int_\Omega (\lambda+2\mu)(e_{\alpha\alpha}(u)e_{\beta\beta}(v)) + 2\mu e_{\alpha\beta}(u)e_{\alpha\beta}(v).\end{aligned}$$

The first bilinear form ($\mathscr{A}(u,v;\cdot)$) defined above is associated to the work of transverse strains, the second ($\mathscr{B}(u,v;\cdot)$)to the work of shear strains and that due to the Poisson effect, the last ($\mathscr{C}(u,v;\cdot)$) to the work of in-plane strains. For $\varepsilon \ll 1$ the equality in Problem 3.5 must hold separately in cascade for all the terms factoring the powers of ε. We are lead to identify four variational problems, starting from the most singular term at order $\mathcal{O}(\varepsilon^{-4})$.

3.2.1 Identification of the cascade problems

Problem at $\mathcal{O}(\varepsilon^{-4})$

The identification of the coefficient of ε^{-4} in the equilibrium equations leads to find $u_i^0 \in \mathcal{C}_0(\Omega)$ such that

$$\mathscr{A}_f(u^0,v) = 0, \qquad \forall v \in H^1(\Omega_f),$$

that is:

$$\int_{\Omega_f} (\lambda_f+2\mu_f)e_{33}(u^0)e_{33}(v) = 0, \qquad \forall v \in H^1(\Omega_f).$$

We deduce that transverse strains are constant and vanish due to the free condition at the upper boundary,

$$e_{33}(u^0) = 0, \quad \text{in } \Omega_f \tag{3.20}$$

This implies:

$$u_3^0 = \zeta_3(x'), \quad \zeta_3 \in H^1(\omega)$$

i.e. transverse displacements at order zero are constant with respect to the thickness in the film. This is essentially the same result as Property 3.2, although here we do not track the rate of convergence.

Problem at $\mathcal{O}(\varepsilon^{-2})$

The problem at order $\mathcal{O}(\varepsilon^{-2})$ is to find $u_\alpha^0, u_3^1 \in H^1(\Omega_f), u_i^0 \in \mathcal{C}_0(\Omega)$ such that:

$$\mathscr{A}_f(u^1, v) + \mathscr{B}_f(u^0, v) + \mathscr{A}_f(u^0, v) = 0, \qquad \forall v \in \mathcal{C}_0(\Omega_f)$$

which reads explicitly:

$$\begin{aligned}\int_{\Omega_f} (\lambda_f + 2\mu_f) e_{33}(u^1) e_{33}(v) \\ + \int_{\Omega_f} \lambda_f (e_{\alpha\alpha}(u^0) e_{33}(v)) + 2\mu_f e_{\alpha 3}(u^0)(\partial_\alpha v_3 + \partial_3 v_\alpha) \\ + \int_{\Omega_b} (\varrho_\lambda \lambda_f + 2\varrho_\mu \mu_f) e_{33}(u^0) e_{33}(v) = 0, \quad \forall v_i \in H^1(\Omega).\end{aligned}$$

Here we have used the fact that $e_{33}(u^0) = 0$ in Ω_f. From the variational formulation we can always derive two sets of variational equations (coupled in principle) associated to the *in-plane* (resp. *transverse*) equilibrium problem, taking test functions whose in-plane components (resp. vertical) are the only non zero terms.

Kinematics in the film

Choosing test functions $v = (\hat{v}_\alpha, 0)$ with $\hat{v}_\alpha \in H^1_{\omega\times\{0\}}(\Omega_f)$ and $\hat{v}_\alpha = 0$ on $\omega \times \{0\}$ in Ω_f and $v_i = 0$ in Ω_b, equilibrium implies:

$$\int_{\Omega_f} 2\mu_f e_{\alpha 3}(u^0) \partial_3 \hat{v}_\alpha = 0, \qquad \forall \hat{v} \in H^1_{\omega\times\{0\}}(\Omega_f)$$

from which we deduce that necessarily $e_{\alpha 3}(u^0) = 0$ in Ω_f. Combined with (3.20) yields:

$$e_{i3}(u^0) = 0, \quad i = 1, 2, 3 \quad \text{in } \Omega_f.$$

The last relation characterizes the subspace of $H^1(\Omega_f)$ of Kirchhoff-Love displacements $V_{KL}(\Omega_f) := \{v \in H^1(\Omega_f), e_{i3}(v) = 0 \text{ in } \Omega_f\}$.

Lemma 3.2. *In addition, the identification of this space allows to identify the kinematics of displacements. A function v belonging to $V_{KL}(\Omega)$ is necessarily of the form:*

$$\begin{cases} v_\alpha(x', x_3) = \eta_\alpha(x') - x_3 \partial_\alpha \eta_3(x') \\ v_3(x_3) = \eta_3(x') \end{cases}, \quad \text{with } \eta_\alpha \in H^1(\omega), \eta_3 \in H^2(\omega)$$

Proof. It suffices to integrate the equations $\varepsilon_{i3} = 0$ with respect to the vertical direction. □

Note that the vanishing of shear strains implies a higher regularity ($H^2(\omega)$) on transverse displacements. We summarize the characterization of the kinematics in the film with the following property.

Property 3.4 (Kinematics in the film)**.** *The first order displacement u^0 belongs to the space $V_{KL}(\Omega_f)$, equivalently it is of the form:*

$$\begin{cases} u^0_\alpha(x', x_3) = \zeta_\alpha(x') - x_3 \partial_\alpha \zeta_3(x') \\ u^0_3(x_3) = \zeta_3(x') \end{cases}, \quad \text{with } \zeta_\alpha \in H^1(\omega), \zeta_3 \in H^2(\omega). \tag{3.21}$$

Now, choosing test functions $v = (\hat{v}_\alpha, 0)$ in Ω_f with $\hat{v} \in H^1(\Omega_f)$, $\hat{v} = 0$ on $\omega \times \{0\}$, $v = 0$ in Ω_b and integrating by parts the equilibrium equations, one determines the optimal second order transverse strain as a function of the first order in-plane strain:

$$e_{33}(u^1) = -\frac{\lambda_f}{\lambda_f + 2\mu_f} e_{\alpha\alpha}(u^0), \quad \text{in } \Omega_f. \tag{3.22}$$

Transverse displacements in the bonding layer

Localizing the problem at order ε^{-2} in the bonding layer, *i.e.* choosing test functions $v = \hat{v}_3 \in H^1(\Omega_b)$, $\hat{v}_3 = 0$ on $\omega \times \{-1\}$ leads to:

$$\int_{\Omega_b} (\varrho_\lambda \lambda_f + 2\varrho_\mu \mu_f) e_{33}(u^0) e_{33}(\hat{v}) = 0, \qquad \forall \hat{v}_3 \in H^1(\Omega_b)$$

from which we infer that:

$$e_{33}(u^0) = 0, \quad \text{in } \Omega_b, \tag{3.23}$$

i.e. the first order transverse strain vanishes and first order transverse strains depend only upon the in-plane coordinate, *i.e.* is a constant with respect to the thickness: $u^0_3(x', x_3) = \zeta_3(x')$ in Ω_b with $\zeta_3 \in H^1(\omega)$. Consequently, the transverse displacement is determined by the boundary condition at the interface $\omega_- := \omega \times \{-1\}$ between the bonding layer and the substrate, *i.e.*

$$\zeta_3(x') = w_3(x'), \text{ in } \Omega_b. \tag{3.24}$$

Problem at $\mathcal{O}(\varepsilon^0)$

The problem at order ε^0 is to find u^0, u^1, u^2 such that:

$$\mathscr{A}_f(u^2, v) + \mathscr{B}_f(u^1, v) + \mathscr{C}_f(u^0, v) + \mathscr{A}_b(u^1, v) + \mathscr{B}_b(u^0, v) = \mathcal{L}(v), \qquad \forall v \in H^1(\Omega_f \cup \Omega_b).$$

The last variational equation reads explicitly:

$$\begin{aligned}\int_{\Omega_f} \left((\lambda_f + 2\mu_f) e_{33}(u^2) + \lambda_f e_{\alpha\alpha}(u^1)\right) e_{33}(v) + \int_{\Omega_f} 4\mu_f e_{\alpha 3}(u^1) e_{\alpha 3}(v) \\ + \int_{\Omega_f} \frac{\mu_f \lambda_f}{\lambda_f + 2\mu_f} e_{\alpha\alpha}(u^0) e_{\beta\beta}(v) + 2\mu_f e_{\alpha\beta}(u^0) e_{\alpha\beta}(v) \\ + \int_{\Omega_b} (\varrho_\lambda \lambda_b + 2\varrho_\mu \mu_f) e_{33}(u^1) e_{33}(v) \\ + \int_{\Omega_b} \varrho_\lambda \lambda_b e_{\alpha\alpha}(u^0) e_{33}(v) + 4\varrho_\mu \mu_f e_{\alpha 3}(u^0) e_{\alpha 3}(v) = \mathcal{L}(v), \quad \forall v_i \in H^1(\Omega_f \cup \Omega_b),\end{aligned}$$

where we used (3.20), (3.22), (3.23) and the fact that $e_{33}(u^0) = 0$ in the bonding layer.

Shear in the bonding layer

Localizing the equilibrium equations in bonding layer, *i.e.* testing the equilibrium for all $v = 0$ in Ω_f and $\hat{v} \in H^1_{\omega_0 \cup \omega_-}(\Omega_b)$ we write:

$$\begin{aligned}\int_{\Omega_b} (\varrho_\lambda \lambda_b + 2\varrho_\mu \mu_f) e_{33}(u^1) e_{33}(\hat{v}) \\ + \int_{\Omega_b} \varrho_\lambda \lambda_b e_{\alpha\alpha}(u^0) e_{33}(\hat{v}) + 4\varrho_\mu \mu_f e_{\alpha 3}(u^0) e_{\alpha 3}(\hat{v}) = 0, \qquad \forall \hat{v}_i \in H^1_{\omega_0 \cup \omega_-}(\Omega_b)\end{aligned}$$

from which, restricting to the in-plane equation, we obtain:

$$\int_{\Omega_b} e_{\alpha 3}(u^0) \partial_3 v_\alpha = 0, \quad \forall \hat{v}_\alpha \in H^1_{\omega_0 \cup \omega_-}(\Omega_b).$$

After integration by parts we derive that the shear within the bonding layer is a constant with respect to the thickness: $e_{\alpha 3}(u^0) = c(x')$. Unlike within the film, the constant $c(x')$ is fixed by the essential boundary conditions on ω_- and the continuity on ω_0. Localizing and integrating by parts the last equation we get:

$$\partial_{33} u^0_\alpha = 0, \qquad \text{in } \Omega_b,$$

where we have used $u^0_3 = w_3(x')$. Integrating twice with respect to the transverse variable we obtain:

$$u^0_\alpha = c(x')(x_3 + 1) + w_\alpha.$$

Imposing the boundary condition on ω_- and the continuity on ω_- we determine the first order in-plane (membrane) displacement as:

$$u^0_\alpha = (u^0_\alpha(x',0) - w_\alpha)(x_3+1) + w_\alpha,$$

where, by what we saw above:

$$u^0_\alpha(x',0) = \zeta_\alpha(x')$$

Note that the constant shear in the bonding layer is given by the mismatch displacement between the film and that imposed by the substrate:

$$e_{\alpha 3}(u^0) = (\zeta_\alpha - w_\alpha)(x'). \tag{3.25}$$

This result is the analogous of Property 3.3 obtained in the scalar case. Now, however, we have the correct mechanical interpretation of the shear strains. Finally, recalling (3.24), the first order displacement within the bonding layer is completely determined as a function of the first order in-plane displacement $\zeta_\alpha(x')$ of the film and boundary conditions:

$$\begin{cases} u^0_\alpha(x',x_3) = (\zeta_\alpha - w_\alpha)(x')(x_3+1) + w_\alpha(x') \\ u^0_3(x') = w_3(x') \end{cases}, \quad \text{in } \Omega_b. \tag{3.26}$$

The limit model

Equations (3.21) and (3.26) determine the order one displacements in Ω as a function of ζ_α. The vertical problem is trivially solved imposing the continuity of displacements at ω_0 and gives a constant vertical displacement within both layers, fixed by the boundary condition, namely:

$$u^0_3(x',x_3) = w_3(x'), \qquad \text{in } \Omega.$$

The elastic equilibrium reduces to an in-plane problem. Indeed, taking test fields $\hat{v} = (\eta_\alpha, 0)$ in Ω_f and $\hat{v} = (\eta_\alpha(x_3+1), 0)$ where $\eta_\alpha \in H^1(\omega)$ one is led to solve the following variational problem:

Problem 3.6 (Reduced limit in-plane problem)**.**

$\mathcal{P}(\omega)$: *Find* $\zeta_\alpha \in H^1(\omega)$ *such that* :

$$\int_\omega \left\{ \frac{\mu_f \lambda_f}{\lambda_f + 2\mu_f} \partial_\alpha \zeta_\alpha \partial_\beta \zeta_\beta + 2\mu_f \partial_\alpha \zeta_\beta \partial_\alpha \zeta_\beta \right\} dx'$$
$$+ \int_\omega \varrho_\mu \mu_f \left(\zeta_\alpha - w_\alpha\right) \eta_\alpha dx' = \hat{\mathcal{L}}(\eta) + \hat{\mathcal{L}}'(\nabla\eta),$$
$$\forall \eta_\alpha \in H^1(\omega), \alpha = 1,2.$$

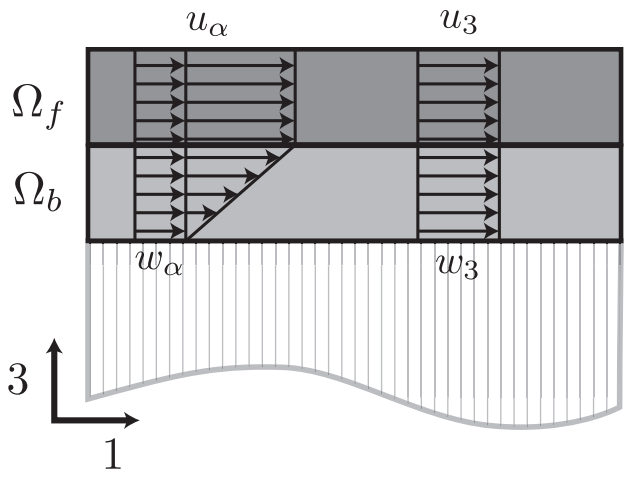

Figure 3.6: Profile of order zero optimal displacements. In-plane displacements (left) are affine in the bonding layer, varying linearly between the boundary condition w_α and the constant film displacement. Transverse displacements (right) are constant within the entire domain and equal the boundary condition $u_3 = w_3$.

In the last expression:

$$\hat{\mathcal{L}}(\eta) = \int_\omega \hat{f}(x')v dx', \qquad \text{with } \hat{f}(x') := \int_0^1 f(x', x_3) dx_3 \text{ and}$$
$$\hat{\mathcal{L}}'(\nabla\eta) = \int_\omega \left\{ \frac{\mu_f \lambda_f}{\lambda_f + 2\mu_f} \partial_{\alpha\alpha} w_3 \partial_\beta \eta_\beta + 2\mu_f \partial_{\alpha\beta} w_3 \partial_\alpha \eta_\beta \right\} dx'.$$

The profile of optimal (first order) displacements is shown in Figure 3.6.

3.2.2 Comments and extensions

The major novelty in vector elasticity (with respect to scalar elasticity) is the possibility to undergo rotations, this is seen in the characterization of the Kirchhoff-Love subspace V_{KL} of admissible displacements.

The starting three-dimensional problem breaks down, along the asymptotic process, into an in-plane and a vertical problem. Unlike in classical theory of (possibly partially) clamped plates (see [Cia97]), the latter is trivial and the solution is fixed by the boundary condition of place at the lower boundary. Despite such boundary condition renders the vertical problem trivial, it allows for non-vanishing shear deformations and enlarges (with respect to classical plate theories) the space of admissible functions within the bonding layer. In classical linear plates, bending arises as a way to deliver shear-free deformations. Since here the shear is prescribed, see Equation (3.25), the bonding layer does not undergo rotations, *i.e.* there is no bending. On one hand, the boundary condition on ω_- is crucial to obtain the shear term which, in turn, yields the elastic foundation and the existence of an intrinsic length scale. On the other hand, it rules out any bending

and vertical displacements are constant. This constant vertical displacement, however, appears as an additional loading term (the linear form $\hat{\mathcal{L}}'(\nabla\eta)$) for the membrane and the in-plane and vertical displacements are necessarily *coupled*. In this case indeed, we cannot exploit symmetry to decouple the in-plane displacements from the vertical displacements, as it may the case for standard partially clamped plates [Cia97].

The increased richness of the two-dimensional model with respect to the original three-dimensional one (associated to the emergence of an intrinsic length scale) is only apparent. It is indeed present but not explicit in the three-dimensional equations. The asymptotic analysis allows to highlight how the assumptions on the data determine the limit model, through the influence of the associated singular terms. We stress that the singular terms (*e.g.* in the variational Problem 3.5) do indeed contribute to the limit energy. They provide the elastic foundation term and determine the two-dimensional membrane elasticity operator a whose components are:

$$a_{\alpha\beta\sigma\tau} = \frac{4\lambda\mu}{\lambda+2\mu}\delta_{\alpha\beta}\delta_{\sigma\tau} + 2\mu(\delta_{\alpha\sigma}\delta_{\beta\tau} + \delta_{\alpha\tau}\delta_{\beta\sigma}) \in \mathbb{R}.$$

This operator associates the stresses to elastic strains $\sigma = a : e$. It cannot be seen *stricto sensu* as a *constitutive equation* since it crucially depends upon the assumption on the data and imposed loads.

The deductive asymptotic analysis sketched above provides a valuable insight on the asymptotics of the bilayer system, it can be refined to establish a stronger result, in the spirit of Γ-convergence which we state as follows:

Theorem 3.2. *Define* $E_\varepsilon : L^2(\Omega\cup\Omega';\mathbb{R}^3) \to [0,+\infty]$ *by*

$$E_\varepsilon(u) := \begin{cases} J_\varepsilon(u) & \text{if } \begin{cases} u \in H^1(\Omega\cup\Omega'), \\ u(\cdot,-1) = 0, \end{cases} \\ +\infty & \text{otherwise,} \end{cases}$$

and let $E_0 : L^2(\Omega;\mathbb{R}^3) \to [0,+\infty]$ *be given by*

$$E_0(u) := \begin{cases} \dfrac{1}{2}\displaystyle\int_\omega \left\{ \frac{2\lambda_f\mu_f}{\lambda_f+2\mu_f} e_{\alpha\alpha}(u)e_{\beta\beta}(u) + 2\mu_f e_{\alpha\beta}(u)e_{\alpha\beta}(u) \right\} dx' \\ \qquad +\varrho_f\mu_f \displaystyle\int_\omega u_\alpha u_\alpha \, dx', \qquad \text{if } \begin{cases} u_\alpha \in H^1(\omega), \\ u_3 = 0, \end{cases} \\ +\infty \quad \text{otherwise.} \end{cases}$$

- **Lower bound.** *For every* $u \in L^2(\Omega;\mathbb{R}^3)$ *and every sequence* $(u_\varepsilon) \subset L^2(\Omega\cup\Omega';\mathbb{R}^3)$ *such that* $u_\varepsilon \to u$ *strongly in* $L^2(\Omega;\mathbb{R}^3)$*, then*

$$E_0(u) \le \liminf_{\varepsilon\to 0} E_\varepsilon(u_\varepsilon);$$

- **Upper bound** *For every* $u \in L^2(\Omega;\mathbb{R}^3)$*, there exists sequence* $(\overline{u}_\varepsilon) \subset L^2(\Omega\cup\Omega';\mathbb{R}^3)$ *and such that* $\overline{u}_\varepsilon \to u$ *strongly in* $L^2(\Omega;\mathbb{R}^3)$ *and*

$$E_0(u) \ge \limsup_{\varepsilon\to 0} E_\varepsilon(\overline{u}_\varepsilon).$$

Remark 3.5. If u is smooth enough (*e.g.* $u_\alpha \in H^2(\omega)$) then the optimal sequence reaching the upper bound in Theorem 3.2 is given by

$$\overline{u}_\varepsilon(x', x_3) := \begin{cases} u(x') - \frac{\lambda\varepsilon^2 x_3}{\lambda+2\mu} \begin{pmatrix} 0 \\ 0 \\ e_{\alpha\alpha}(u)(x') \end{pmatrix} & \text{if} \quad x \in \Omega, \\ (x_3+1)u(x') & \text{if} \quad x \in \Omega'. \end{cases}$$

3.3 Brittle thin films in scalar elasticity

We have studied the asymptotic properties of the *purely elastic* systems and the interplay of the elastic energy components, whose separation of scales is induced by the geometric and the material behavior. We now introduce the surface energies and the possibility to develop arbitrary cracks within the layers. The object of the study is, to *obtain* the geometric characterization of crack surfaces as the outcome of a crack path selection. Here, the cracks Γ are a genuine unknown of the problem, whose properties we determine exploiting the minimality principle used as a selection criterion for crack paths.

3.3.1 Constitutive assumptions

We study a thin film whose thickness is of the same order of magnitude of the thickness of the bonding layer. As in the asymptotic study in vectorial elasticity, we specialize the asymptotic study to one instance of the class providing the limit model of a membrane over elastic foundation. Referring to the notation introduced in Section 3.1, we choose $\alpha = 0$ in (3.1); hence the ratio between the shear modulus of the film with respect to that of the bonding layer is fixed, in order for the shear and membrane energies of the bonding layer and film to be of the same order of magnitude. We summarize the elastic and geometric assumptions as follows:

Hypothesis 3 (A stiff film on a compliant bonding layer in scalar elasticity)**.** *Setting*

$$\varepsilon := \frac{h_f}{L} \ll 1,$$

we assume that both the non-dimensional thicknesss of the film h_f and of the bonding layer h_b scale as εL, whereas that the ratio between the elastic constant of the bonding layer and that of the film scales as ε^2:

$$\frac{h_b}{h_f} = \varrho_h, \qquad \frac{\mu_b}{\mu_f} = \varrho_\mu \varepsilon^2 \tag{3.27}$$

where ϱ_h and ϱ_μ are non-dimensional coefficients independent of ε.

The sketch in Figure 3.7 represents the reference system with the usual notation with the addition of the jump set J_u (of a displacement field u) and its unit normal oriented vector ν_u.

In order to highlight the coupled interplay between cracks in the film and in the bonding layer, simple dimensional considerations allow us to identify a regime where coupling between transverse fractures and debonding cracks is expected. Indeed, the elastic energy stored in the bonding layer and that stored in the film are of the same order of magnitude, to exhibit an interplay between transverse and debonding cracks, their associated surface energy must be of the same order of magnitude. Hence, being G_f and G_b the toughnesses of the film and bonding layer respectively, the following must hold:

$$G_f h_f L \sim G_b L^2.$$

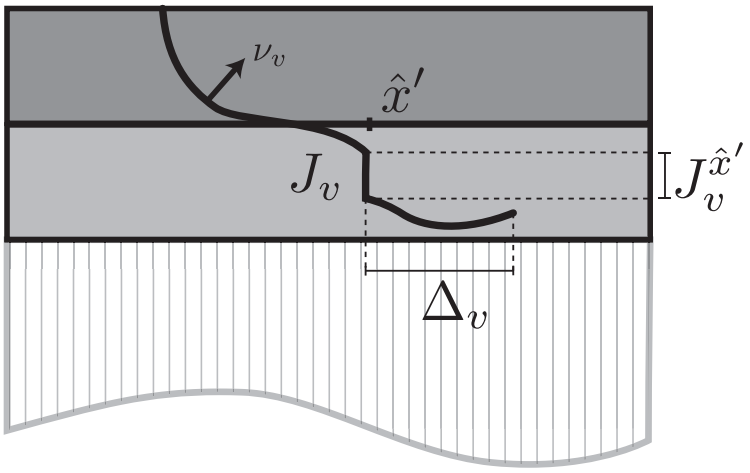

Figure 3.7: The brittle elastic thin film system. The jump set of a function $v \in SBV(\Omega)$ is displayed along with its normal vector ν_v. The transverse

For thin layers, this regime corresponds to a system where the film is much tougher (by a factor $1/\varepsilon$) than the bonding layer. By this dimensional argument we assume the following scaling law for the material toughnesses:

Hypothesis 4 (Scaling law of toughnesses)**.** *Being $\varepsilon = h_f/L$, the fracture toughnesses of the film G_f and of the bonding layer G_b are such that:*

$$\frac{G_b}{G_f} = \varepsilon\, \varrho_G,$$

where ϱ_G is a non-dimensional constant independent of ε.

3.3.2 Variational formulation in SBV

We formulate the problem on an extended domain $\Omega = \Omega_f \cup \Omega_b \cup \Omega_s$ including a portion of the substrate, say $\Omega_s := \tilde{\omega} \times [-2h_b, -h_b)$. This allows to consider possible cracks at the interface ω_- identified as the set of points for which the one-sided traces on ω_- differ.

As is customary in free-discontinuity problems, in order to state the problem in a suitable mathematical framework, we interpret the crack set Γ as the set of discontinuity points of the displacement u. The proper functional setting is that of the space of special functions with bounded variations SBV, which allows introduce a notion of jump set J_u of the function u and an approximate gradient, *i.e.* the regular part of the differential. We shall denote the latter by ∇u in analogy to the usual gradient for smooth functions.

The space of all admissible displacements is given by:

$$\mathcal{C}_w(\tilde{\Omega}) := \{\tilde{u} \in SBV(\Omega) : \tilde{u} = w \text{ a.e. in } \Omega_s, \text{ and } \|\tilde{u}\|_{L^\infty(\Omega_f)} \leq M\}.$$

Note that the Dirichlet datum w is only defined at the interface $\tilde{\Sigma}$ between the substrate and the bonding layer. We implicitly extend it constantly to the whole domain $\tilde{\Omega}$ so that, from now on, w is identified to a function on $\tilde{\Omega}$ independent of the out of plane variable. Therefore, the boundary condition $\tilde{u} = w$ on $\tilde{\Sigma} = \omega \times \{-h_b\}$ is expressed on the whole set of finite volume Ω_s. We further assume that every deformation takes place in a container K which is a compact subset of $\mathbb{R}^3$, *i.e.* $\|\tilde{u}\|_{L^\infty(\Omega)} \leq M$ for some fixed constant $M > 0$, and $\|w\|_{L^\infty(\Omega_s)} \leq M$. The last hypothesis and can be removed at the expense of some additional technicalities (see [MFT05]).

To state the variational problem in a framework suitable for the mathematical analysis, the energy functional is rewritten in the following form. For any displacement $\tilde{u} \in \mathcal{C}_w(\tilde{\Omega})$, let

$$\tilde{\mathcal{E}}_\varepsilon(\tilde{u}) = \frac{\mu_f}{2}\int_{\Omega_f} |\nabla \tilde{u} - e_0|^2 \,\mathrm{d}\,\tilde{x} + \frac{\mu_b}{2}\int_{\Omega_b} |\nabla \tilde{u} - e_0|^2 \,\mathrm{d}\,\tilde{x} + G_f \mathcal{H}^2(J_{\tilde{u}} \cap \Omega_f) + G_b \mathcal{H}^2(J_{\tilde{u}} \cap \Omega_b).$$

As already familiar and with the usual notation, we apply the anisotropic scaling of Equation (3.4) of the spatial coordinates in order to reveal explicitly the dependence upon ε and state the variational problem in domains independent of ε. In the present case, denoting by $\tilde{x}' = (\tilde{x}_1, \tilde{x}_2) \in \Omega_f^\varepsilon$ and by $x' = (x_1, x_2)$, the anisotropic scalings read as follows:

$$\pi^\varepsilon : x = (\tilde{x}', \tilde{x}_3) \in \overline{\Omega^\varepsilon} \mapsto (x', \varepsilon x_3) \in \overline{\Omega}.$$

The anisotropic rescaling of the coordinates intervenes in the surface energy via the rescaling of the unit normal $\nu_{\tilde{u}}$ to the jump set $J_{\tilde{u}}$. Thinking of the jump set as a regular curve given by an implicit relation $J_{\tilde{u}} : f(\tilde{x}', \tilde{x}_3) = 0$, its unit normal $\nu_{\tilde{u}}$ is given by:

$$\nu_{\tilde{u}} = \frac{\left(\nabla' f(\tilde{x}', \tilde{x}_3), \dfrac{\partial f(\tilde{x}', \tilde{x}_3)}{\partial \tilde{x}_3}\right)}{\sqrt{\nabla' f(\tilde{x}', \tilde{x}_3)^2 + \dfrac{\partial f(\tilde{x}', \tilde{x}_3)}{\partial \tilde{x}_3}^2}},$$

where we denote the in-plane components of the unit normal by $\nu'_{\tilde{u}} = ((\nu_{\tilde{u}})_1, (\nu_{\tilde{u}})_2)$. Consequently, denoting respectively by $\nu_{\tilde{u}}$ and ν_u the unit normal to the jump sets $J_{\tilde{u}}$ and J_u before and after rescaling (see Figure 3.8), the scaled unit normal reads:

$$\nu_u = (\nu'_u, (\nu_u)_3) = \frac{\left(\nabla' f(x', x_3), \dfrac{\partial f(x', x_3)}{\partial x_3}\right)}{\sqrt{\nabla' f(x', x_3)^2 + \dfrac{\partial f(x', x_3)}{\partial x_3}^2}} = \left(\nu'_{\tilde{u}}, \frac{1}{\varepsilon}(\nu_{\tilde{u}})_3\right)$$

Finally, the surface measure of $J_{\tilde{u}}$ rescales as follows:

$$\mathcal{H}^2(J_u) = \int_{J_u} |\nu_u| \, d\mathcal{H}^2 = \int_{J_u} \left|\left(\nu'_{\tilde{u}}, \frac{(\nu_{\tilde{u}})_3}{\varepsilon}\right)\right| \, d\mathcal{H}^2.$$

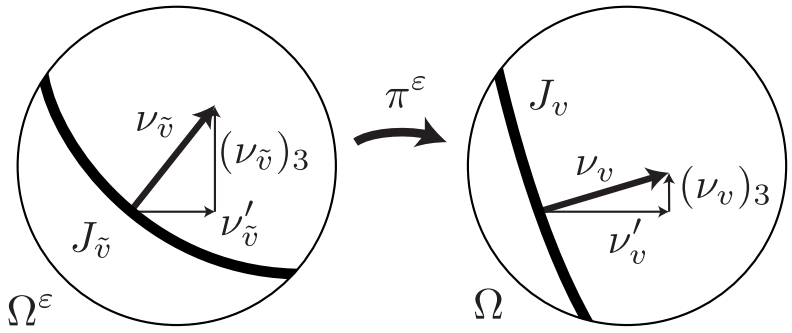

Figure 3.8: Rescaling of the unit normal to the jump set by the mapping π^ε. of Equation 3.3.2. The unscaled (left) and the scaled (right) unit normal vectors to the jump set are related by Equation 3.3.2. Note that only the vertical component is affected by the anisotropic rescaling.

The total scaled energy of the brittle system (up to a multiplicative constant $1/\varepsilon$) reads as:

$$\begin{aligned}\mathcal{E}_\varepsilon(u) := \frac{\tilde{\mathcal{E}}_\varepsilon(\tilde{u})}{\varepsilon} = \frac{\mu_f}{2}\int_{\Omega_f}\left(|\nabla' u - e'_0|^2 + \frac{1}{\varepsilon^2}(\partial_3 u - (e_0)_{33})^2\right)dx \\ + \frac{\mu_f \varrho_\mu}{2}\int_{\Omega_b}\left(\varepsilon^2|\nabla' u|^2 + (\partial_3 u)^2\right)dx \\ + G_f\int_{J_u\cap\Omega_f}\left|\left(\nu'_u, \frac{(\nu_u)_3}{\varepsilon}\right)\right|\,\mathrm{d}\,\mathcal{H}^2 + G_f\varrho_G\int_{J_u\cap\Omega_b}|(\varepsilon\,\nu'_u, (\nu_u)_3)|\,\mathrm{d}\,\mathcal{H}^2. \quad (3.28)\end{aligned}$$

In the previous expression we have supposed for simplicity that the inelastic strain is of the form $e_0 = (e'_0, 0)$, with $e'_0 \in L^2(\Omega;\mathbb{R}^2)$, *i.e.* there is no transverse imposed strain. Note that since w is independent of the out of plane variable, it is not affected by the change of variable. Identifying w with a function defined only on the plane, we henceforth assume that $w \in H^1(\omega)\cap L^\infty(\omega)$. Consequently, the rescaled space of all admissible displacements is

$$\mathcal{C}_w(\Omega) := \{v \in SBV(\Omega) : v = w \text{ a.e. in } \Omega_s, \text{ and } \|v\|_{L^\infty(\Omega_f)} \le M\}$$

and is independent of ε.

In this setting, the static fracture mechanics problem is formulated as follows.

Problem 3.7 (Static problem for scalar elasticity. Weak formulation)**.** *For a given load intensity (e_0, w), find $u \in \mathcal{C}_w(\Omega)$ that satisfy the following global minimality condition:*

$$\mathcal{E}_\varepsilon(u) \le \mathcal{E}_\varepsilon(v), \qquad \forall v \in \mathcal{C}_w(\Omega)$$

Standard arguments ensure that this problem is well posed for fixed ε, in the sense that there exists at least a solution and its energy is finite. The result is formalized by the following proposition. Note that, in general, uniqueness cannot be expected in fracture mechanics.

Proposition 3.1. *(Existence of minimizers at fixed ε) For each $\varepsilon > 0$, $w \in L^2(\Omega_f)$ and $w \in H^1(\omega) \cap L^\infty(\omega)$, there exist a minimizer:*

$$u_\varepsilon \in \operatorname*{arg\,min}_{u \in \mathcal{C}_w(\Omega)} \mathcal{E}_\varepsilon(u).$$

For the proof, the reader can refer to [AFP00]. The inspection of the energy of Equation (3.28) provides some useful insight on the expected asymptotic behavior of the system.

- Looking in (3.28) at the terms proportional to ε^{-2} and ε^{-1}, one may expect that the solution of the limit problem for $\varepsilon \to 0$ has transverse strains $\partial_3 u$ in the film equal to the transverse component of the inelastic strain $(e_0)_{33}$ and that the cracks in the film should be purely transverse (*i.e.* with $(\nu_u)_3 = 0$).

- The scaling hypotheses of Section 3.3.1 imply that the energy contributions associated to in-plane deformations in the film, through-the-thickness shear in the bonding layer, transverse cracks in the film, and in-plane cracks in the bonding layer are of the same order in ε in (3.28). This entails the emergence of an interesting coupled problem involving all these phenomena. This will be captured by the forthcoming limit energy of Equation (3.29).

- In the energy (3.28) the elastic energy density associated to the in-plane gradient of the displacement inside the bonding layer Ω_b is proportional to ε^2, and thus vanishing for $\varepsilon \to 0$. This fact implies that in the limit $\varepsilon \to 0$ these gradients may possibly diverge. From a mathematical point of view, it translates into a lack of compactness inside the bonding layer. This issue is bypassed by the fact that the displacement on the bottom surface of the bonding layer is imposed by the Dirichlet boundary condition on the substrate, and the displacement on the top surface of the bonding layer is given by the displacement in the film. In debonded regions no compatibility between the substrate and the film is enforced, hence the film is free to accommodate the inelastic strain.

The main result of this section is summarized in the following theorem:

Theorem 3.3. *For any $u \in \mathcal{C}(\omega)$ let us define:*

$$\mathcal{E}_0(u) := \frac{L\mu_f}{2} \int_\omega |\nabla' u - e_0'|^2 \, dx' + \frac{L\mu_b}{2h_f h_b} \int_{\omega \setminus \Delta_u} |u - w|^2 \, dx' + LG_f \mathcal{H}^1(J_u') + \frac{LG_b}{h_f} \mathcal{H}^2(\Delta_u), \quad (3.29)$$

where

$$\Delta_u := \left\{ x' \in \omega : |u(x') - w(x')| > u_d := \sqrt{\frac{2G_b h_b}{\mu_b}} \right\} \tag{3.30}$$

is the delamination set. Then the energy $\mathcal{E}_0$ *admits at least one minimizer over* $\mathcal{C}(\omega)$ *and*

$$\min_{u \in \mathcal{C}(\omega)} \mathcal{E}_0(u) = \lim_{\varepsilon \to 0} \min_{u \in \mathcal{C}_w(\Omega)} \tilde{\mathcal{E}}_\varepsilon(u).$$

In addition, if u_ε *is a minimizer of* $\tilde{\mathcal{E}}_\varepsilon$ *over* $\mathcal{C}_w(\Omega)$*, and* $u_\varepsilon \to u_0$ *strongly in* $L^2(\Omega_f)$ *for some* $u_0 \in \mathcal{C}(\omega)$*, then* u_0 *is a minimizer of* $\mathcal{E}_0$ *over* $\mathcal{C}(\omega)$*.*

Up to the debonding term, the elastic part of the limit energy $\mathcal{E}_0(u)$ of Equation (3.29) is analogous to that encountered in the preliminary study in Section 3.1. The elastic energy density comprises a contribution $\frac{L\mu_f}{2}|\nabla' u - e_0'|^2$ given by the membrane energy, estimating the elastic energy in the film, and a term $\frac{L\mu_b}{2}|u - w|^2/(h_f h_b)$ due to the interaction with the substrate, estimating the elastic energy of the bonding layer. This latter is present only in bonded regions. The novel result regards the crack sets. The limit system naturally discriminates between transverse cracks J_u' and debonded regions Δ_u. The former are of codimension 1 whereas the latter are of codimension 0 in the two-dimensional limit domain ω. A sketch of the limit two-dimensional body is given in Figure 3.9. Debonded regions are explicitly determined by the local threshold criterion (3.30) on the absolute value of the mismatch between the membrane displacement u and the imposed displacement w by the substrate. We shall show this with an argument similar that in Section 2.2.2.

The proof of Theorem 3.3 is based on a Γ-convergence approach, its structure is rather classical and rests on three lemmas:

i) *Compactness*: If (u_ε) is a sequence with uniformly bounded energy $\mathcal{E}_\varepsilon$, then (up to a subsequence) it converges strongly in $L^2(\Omega_f)$ to some $u \in \mathcal{C}(\omega)$;

ii) *Lower bound*: For any $u \in \mathcal{C}_w(\omega)$ and for any sequence $(u_\varepsilon) \subset \mathcal{C}_w(\Omega)$ such that $u_\varepsilon \to u$ strongly in $L^2(\Omega_f)$, then

$$\mathcal{E}_0(u) \leq \liminf_{\varepsilon \to 0} \mathcal{E}_\varepsilon(u_\varepsilon);$$

iii) *Upper bound* (existence of a recovery sequence): For any $u \in \mathcal{C}(\omega)$, there exists a sequence $(\overline{u}_\varepsilon) \subset \mathcal{C}_w(\Omega)$ such that $\overline{u}_\varepsilon \to u$ strongly in $L^2(\Omega_f)$ and

$$\mathcal{E}_0(u) \geq \limsup_{\varepsilon \to 0} \mathcal{E}_\varepsilon(\overline{u}_\varepsilon).$$

The three previous properties ensure the convergence of minimizers as well as the convergence of the minimal value of the energy. Indeed, the compactness property implies

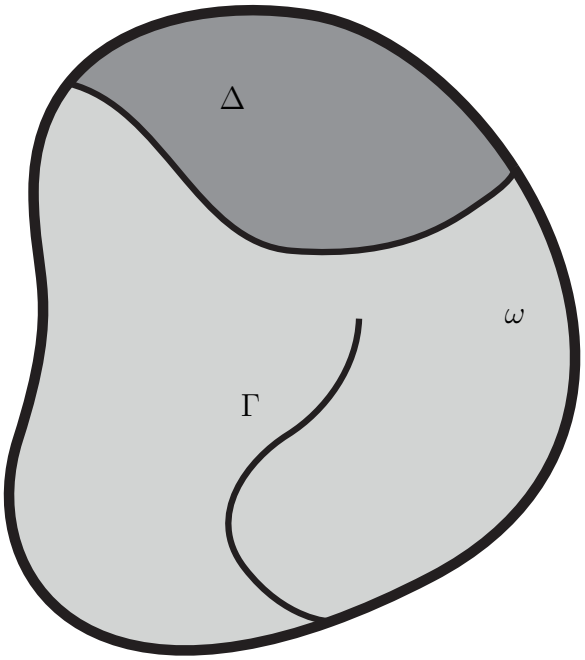

Figure 3.9: In the limit two-dimensional body ω, transverse cracks Γ and debonded regions Δ are naturally discriminated. Their nucleation and evolution under imposed loads is ruled by the variational principle.

that, if u_ε is a minimizer of $\mathcal{E}_\varepsilon$ over $\mathcal{C}_w(\Omega)$, then a suitable subsequence converges strongly in $L^2(\Omega_f)$ to some $u_0 \in \mathcal{C}(\omega)$, and the lower bound gives

$$\mathcal{E}_0(u_0) \leq \liminf_{\varepsilon\to 0} \mathcal{E}_\varepsilon(u_\varepsilon).$$

On the other hand, if $v \in \mathcal{C}(\omega)$ is a competitor for the reduced two-dimensional problem, the upper bound gives in turn the existence of some recovery sequence $(\overline{v}_\varepsilon) \subset \mathcal{C}_w(\Omega)$ converging strongly in $L^2(\Omega_f)$ to v, and such that

$$\mathcal{E}_0(v) \geq \limsup_{\varepsilon\to 0} \mathcal{E}_\varepsilon(\overline{v}_\varepsilon).$$

According to the minimality property of u_ε at fixed ε, we infer that

$$\mathcal{E}_0(u_0) \leq \liminf_{\varepsilon\to 0} \mathcal{E}_\varepsilon(u_\varepsilon) \leq \limsup_{\varepsilon\to 0} \mathcal{E}_\varepsilon(u_\varepsilon) \leq \limsup_{\varepsilon\to 0} \mathcal{E}_\varepsilon(\overline{v}_\varepsilon) \leq \mathcal{E}_0(v),$$

where the second inequality follows trivially from the definition of lim sup. This ensures that u_0 is a minimizer of $\mathcal{E}_0$ over $\mathcal{C}(\omega)$. Taking in particular $v = u_0$ in the previous chain of inequalities yields

$$\min_{u\in\mathcal{C}_w(\Omega)} \mathcal{E}_\varepsilon(u) = \mathcal{E}_\varepsilon(u_\varepsilon) \to \mathcal{E}_0(u_0) = \min_{u\in\mathcal{C}(\omega)} \mathcal{E}_0(u)$$

which gives the convergence of the minimal value.

The limit energy $\mathcal{E}_0$ is therefore a "good" variational approximation of the sequence of functionals $\mathcal{E}_\varepsilon$ as $\varepsilon \searrow 0$. Although the structure of the proof by Lemmas *i)–iii)* is classical, the mechanical interpretation of the lemmas, besides the expression of the limit energy itself, is original for it sheds light upon the asymptotic behavior of the system. In particular we obtain the geometric characterization of cracks within the film and within the bonding layer, the general representation of the energy of the bonding layer and the profile of optimal displacements through the thickness.

We outline below the essential mechanical implications springing from the mathematical analysis, postponing to Section 3.A the detailed proof of Lemmas i)–iii).

Cracks within the film

First, a classical result for bounded sequences in SBV spaces ensures compactness of sequences of displacements (u_n) of finite energy in the film. Hence, there exists a function $u \in SBV(\Omega_f)$ such that u_n converges (possibly up to a subsequence) in SBV to u. Furthermore, we obtain a characterization of (the regular part of) displacements and the geometry of the associated cracks. In fact, the weak limit u satisfies:

$$\int_\Omega |\partial_3 u|^2 dx + \int_{\Omega \cap J_u} |(\nu_u)_3| d\mathcal{H}^2 = 0$$

Hence, in the limit $\varepsilon_n \searrow 0$ for $n \to \infty$, any sequence of displacements u_n of uniformly bounded energy in the film converges to a limit displacement u such that, in the film, *i)* cracks are transverse to the mean membrane, *i.e.* the crack set J_u is (in the scaled unit domain) necessarily of the form $J_u = J'_u \times (0, L)$ where J'_u is a curve belonging to ω, and *ii)* vertical strains vanish. As a consequence, in the film, the limit displacement is independent of the thickness, *i.e.* it can be identified to a function $u \in SBV(\omega)$ defined on the middle surface ω.

Cracks within the bonding layer

We now turn the attention to the bonding layer. Analogously to the pure elastic case tackled in Section 3.1 we cannot conclude a compactness result for sequences of displacements of bounded energy within the bonding layer which allows for unbounded in-plane strains. This is due to the presence of the factor ε^2 in front of the in-plane gradient term in the expression of the energy (3.28). However, limit displacements u are controlled by those of the film and those imposed by the substrate. Unlike in the coating film, the contribution to the surface energy associated to cracks within the bonding layer arises from the in-plane component of the jump set. In the expression of the surface energy in the film, see Equation (3.28), the energy of transverse cracks within the bonding layer vanishes in the limit as $\varepsilon \searrow 0$. Hence the transverse component of cracks in the bonding layer $J_u \cap \Omega_b$ is negligible and cracks are essentially planes, their contribution to the energy derives from their projection on the middle surface ω. The orthogonal projection of the jump set J_u (of a function u) is denoted by Δ and shown in Figure 3.7.

The limit energy of the bonding layer the onset of debonding

Given a minimizing sequence u_n and denoting by Δ_n the projection of its crack set on the mean membrane, we show that the characteristic function of Δ_n converges in $L^\infty(\omega;[0,1])$ to a function ϑ taking values on $[0,1]$. It is a convergence in an "averaged sense" and ϑ can be thought of as a point-wise "debonding density". The projection of the crack set of an admissible displacement v is shown in Figure 3.7 and denoted by Δ. Using ϑ we write the general integral representation of the energy of the bonding layer defined on the middle surface ω. It reads:

$$(u,\vartheta) : H^1(\omega) \times L^\infty(\omega) \mapsto \frac{1}{2}\int_\omega \frac{\mu_b}{h_b}(1-\vartheta)(u-w)^2 dx' + \int_\omega G_b \vartheta dx'$$

The first term is the elastic energy. Its density takes all values in the interval $[0, \frac{\mu_b}{h_b}(u-w)^2]$, the extrema attained respectively at points where the debonding density ϑ is 1 and 0. By optimizing (*i.e.* minimizing the bonding layer's energy with respect to) ϑ we determine, as an explicit function of the displacement mismatch $(u-w)$, the limit crack set within the bonding layer. The minimization of this energy with respect to the characteristic function of the debonded domain is a trivial box-constrained minimization of a local linear functional, and reduces to checking the sign of the slope of the linear problem. The local first order optimality condition reads:

$$G_b - \frac{\mu_b}{h_b}(u-w)^2 \geq 0;$$

hence a minimizer is:

$$\eta^*(x') = \chi_{\left\{|u-w|>\sqrt{\frac{2G_b h_b}{\mu_b}}\right\}}(x').$$

The minimization of the energy of the bonding layer yields a point-wise criterion for the onset of debonding based on the absolute value of the mismatch between the film's displacement u and the imposed boundary displacement w. Since the boundary datum is a given, optimal limit cracks within the boundary layer are necessarily planes parallel to the medium surface and determined explicitly

$$\Delta_u = \chi_{\left\{|u-w|>\sqrt{\frac{2G_b h_b}{\mu_b}}\right\}}.$$

Lastly, a regularity consideration. No relaxation effect is present at the boundaries of the debonded set Δ_u and no microstructure of arbitrary fine length scale develops. The boundary of the debonded domain is necessarily "smooth" and its perimeter finite.

Profile of displacements

The construction of a recovery sequence allows to conclude that the lower bound is indeed an *optimal* bound, *i.e.* that there exists a particular sequence (the recovery sequence) such that the lower bound is attained in the limit. The asymptotic study tackled in Section 3.1 provides the intuition for the construction of such optimal displacement.

In analogy to the purely elastic case, in order not to let the bulk energy associated to transverse strain (of order $1/\varepsilon^2$) blow up in the film, we expect that the displacements be constant through the thickness. In addition, to ensure that the term of order $1/\varepsilon$ in the surface energy remains finite, we expect the jump set to be purely transversal. Concerning the bonding layer, as already intuited and made clear in the proof of the lower bound inequality, we expect no contribution from the in-plane strain and the out-of-plane cracks since these terms vanish as the thickness tends to zero. In the purely elastic case, we had shown that optimal displacements were affine, matching the boundary condition $w(x')$ at the interface with substrate and the displacement of the film $u(x')$ at the interface with the film. The same applies in the present case at bonded points $x' \in \omega \setminus \Delta$. On the other hand, if x' is a debonded point, then the displacement of the film is free to accommodate the imposed inelastic strain and no compatibility conditions are enforced. The optimal profile of displacements is sketched in Figure 3.10 for bonded and debonded points. Defining the critical displacement threshold $u_d := \sqrt{\frac{2G_b h_b}{\mu_b}}$, optimal displacements $\bar{v}$ are hence constructed as follows:

$$\bar{v}(x', x_3) := \begin{cases} u(x'), & \text{if } (x', x_3) \in \Omega_f, \\ (x_3+1)u(x') - x_3 w(x'), & \text{if } (x', x_3) \in \Omega_b \\ & \quad \text{and } |u(x') - w(x')| \leq u_d \in \Omega_f, \\ w(x'), & \text{if } (x', x_3) \in \Omega_s \text{ or } (x', x_3) \in \Omega_b \\ & \quad \text{and } |u(x') - w(x')| > u_d \end{cases}$$

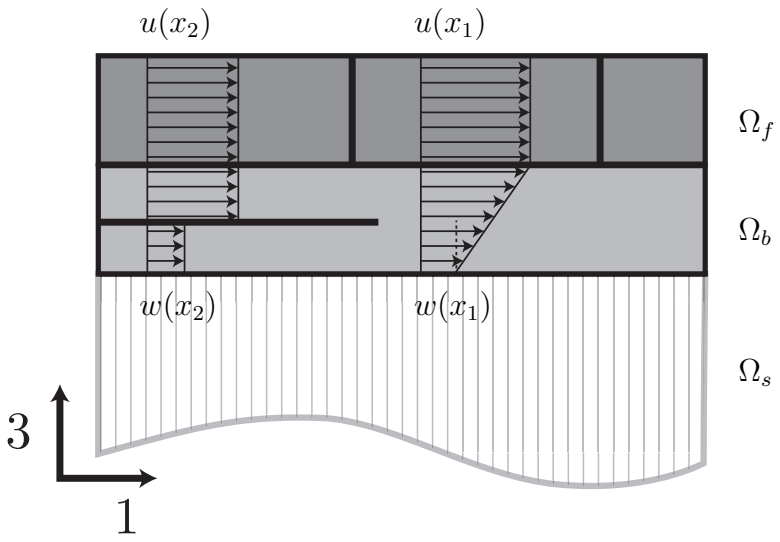

Figure 3.10: Crack surfaces are geometrically characterized based on the variational principle. Cracks are transverse within the film and parallel to the mid-surface within the bonding layer. The displacement profile is displayed at a bonded (x_1) and debonded (x_2) points.

3.4 Brittle thin films, application in two-dimensional vectorial elasticity

This section concludes the chapter which focuses on the derivation of reduced dimension theories for brittle thin films.

The results shown so far are in the setting of scalar elasticity for what regards the identification of the class of three-dimensional systems and in vectorial three-dimensional elasticity the asymptotic analysis of one instance of the class brittle multi layers.

The gap between the latter and the application we are going to present is due to major technical mathematical difficulties arising in the non-trivial extension from scalar to vectorial free-discontinuity problems in linearized elasticity. However, we believe that the preliminary studies have given a sufficient insight into the problem to allow us to inductively apply the results to the vectorial case. Here we choose to proceed by induction and simply transpose (without proof) the results of the preceding Section in the vectorial setting. In particular, we retain the form of the limit elastic energy, as the sum of the membrane energy of the film and the elastic foundation estimating the energy of the bonding layer, and of the surface energy, as the sum of the contributions due to transverse fracture and debonding, with the corresponding geometric characterization of the crack surfaces. Currently, we are able to provide a full proof (not reported here) of this limit model only in the purely elastic case without fractures. The two dimensional reduced model for thin brittle films is constructed as follows.

3.4.1 The reduced limit energy in two-dimensional vectorial elasticity

We consider a two-dimensional brittle elastic membrane occupying the domain $\omega \in \mathbb{R}^2$. In analogy to the scalar case, we discriminate between transverse cracks Γ and debonded regions Δ_u. In two dimensions, the former are sets of codimension 1 whereas the latter are sets of codimension 0. We assume that the membrane undergoes only in-plane displacements $u = (u_1, u_2) \in H^1(\omega; \mathbb{R}^2)$ and that the displacement field is regular on the crack-free domain $\omega \setminus \Gamma$. The space of admissible displacement is:

$$H^1((\omega \setminus \Gamma); \mathbb{R}^2).$$

In analogy to the reduced elastic energy in the scalar case (Equation (3.29)), given the loading as an inelastic isotropic strain $e_0 \in L^2(\omega; \mathbb{R}^{2\times 2})$ and an imposed displacement of the substrate $w \in H^1(\omega; \mathbb{R}^2) \cap L^\infty(\omega; \mathbb{R}^2)$, in the case of vectorial elasticity the strong limit two-dimensional elastic energy is taken as follows:

$$P(u, \Gamma) = \frac{1}{2} \int_{\omega \setminus \Gamma} A(e(u) - e_0) \cdot (e(u) - e_0)\, dx + \frac{1}{2} \int_{\omega \setminus \Delta_u} \frac{\mu_b}{h_b} (u - w) \cdot (u - w)\, dx, \quad (3.31)$$

where A is the forth-order tensor representing the isotropic stress-strain relation for the film as a two-dimensional membrane in plane-strain. It is defined by

$$A\, e = h_f \frac{\lambda_f \mu_f}{\lambda_f + 2\mu_f} (\operatorname{tr} e) I_2 + 2\mu_f h_f\, e$$

where I_2 is the two-dimensional identity tensor. The second integral in the elastic energy (3.31) accounts for the presence of the bonding layer as an elastic foundation. The surface energy is assumed to be the sum of the contribution given by the transverse cracks Γ and the debonded regions Δ_u:

$$S(u,\Gamma) = h_f G_f \mathcal{H}^1(\Gamma) + G_b \mathcal{H}^2(\Delta_u),$$

Δ_u being given explicitly as function of the displacement u by the following threshold criterion as in (3.30):

$$\Delta_u := \left\{ x \in \omega : |u(x) - w(x)| > u_d := \sqrt{\frac{2G_b h_b}{\mu_b}} \right\}.$$

Hence, the total energy of the two dimensional model is:

$$\begin{aligned} E(u,\Gamma) &:= P(u,\Gamma) + S(u,\Gamma) \\ &= \frac{1}{2}\int_{\omega\setminus\Gamma} A(e(u)-e_0)\cdot(e(u)-e_0)\,dx + \int_\omega f(u-w)\,dx \\ &\quad + h_f G_f \mathcal{H}^1(\Gamma), \end{aligned} \tag{3.32}$$

where the total energy of the bonding player is rewritten in terms of the nonlinear energy density:

$$f(u) = \begin{cases} \frac{1}{2}\frac{\mu_b}{h_b}\, u\cdot u, & \text{if } |u| \le u_d \\ G_b, & \text{otherwise} \end{cases}.$$

A non-dimensional form of such energy density is plotted in Figure 3.11.

Remark 3.6. *Equation* (3.31) *is the energy of a linear elastic prestressed plate undergoing purely in-plane displacements plus the energy of a linear elastic foundation in the bonded regions. In the purely elastic (*i.e. *when* $\Gamma = \Delta_u = \emptyset$*), for the scaling hypotheses* (3.27) *and the assumed in-plane loading, the elastic energy* (3.31) *is be obtained as an asymptotic limit for* $\varepsilon \searrow 0$ *of the elastic energy of the three dimensional system in Theorem 3.2. The problem is much more difficult in the brittle case because of the technicalities arising when dealing with vectorial fields in free discontinuity problems.*

Remark 3.7. *The energy density of the film is a quadratic function of the the mismatch between the geometric strains* $e(u)$ *and inelastic strains* e_0*. On the other hand the energy density of the bonding layer,* f*, is quadratic before debonding,* i.e. *where* $|u-w| \le u_d$*, and constant after debonding. Its dependence on* u *is sketched in figure 3.11. Hence, even in the case without transverse cracks, the total elastic energy* $E(u,\emptyset)$ *is non-linear, non-smooth and non-convex with respect to* u*. As a consequence of the lack of convexity, we expect lack of uniqueness of the displacement solution as soon as debonding is triggered, recall Section 2.2.2.*

3.4.2 Nondimensionalization and free parameters

Introducing the non-dimensional space variable and displacement field defined by

$$\tilde{x} = x/x_0, \qquad \tilde{u} = \frac{u - w}{\sqrt{G_f x_0/\mu_f}},$$

the total energy (3.32) may be rewritten in the following non-dimensional form:

$$\tilde{E}(\tilde{u}, \tilde{\Gamma}, \tilde{\Delta}) = \frac{1}{2}\int_{\tilde{\omega}\setminus\tilde{\Gamma}} \tilde{A}(\tilde{e}(\tilde{u}) - \tilde{e}_0)\cdot(\tilde{e}(\tilde{u}) - \tilde{e_0})\,\tilde{dx} + \frac{1}{2}\int_{\tilde{\omega}\setminus\tilde{\Delta}} \kappa|\tilde{u}|^2\,\tilde{dx} + \mathcal{H}^1(\tilde{\Gamma}) + \gamma\,\mathcal{H}^2(\tilde{\Delta}), \quad (3.33)$$

where

$$\tilde{E} = \frac{E}{h_f G_f x_0}, \quad \tilde{A} = \frac{A}{\mu_f h_f}, \quad \tilde{e} = \sqrt{\frac{\mu_f x_0}{G_f}}e, \quad \tilde{e}_0 = \sqrt{\frac{\mu_f x_0}{G_f}}\,(e_0 - e(w))$$

and

$$\kappa = \frac{\mu_b}{\mu_f}\frac{x_0^2}{h_f h_b}, \qquad \gamma = \frac{G_b}{G_f}\frac{x_0}{h_f} \quad (3.34)$$

Henceforth we consider the total energy in this form dropping the overset tilde for sake of conciseness. We conclude from this dimensional analysis that the non-dimensional parameters that fully characterize the energy are:

- The loading parameter e_0, which may be used to model both the effect of inelastic strain in the film and the imposed displacement of the substrate;
- The relative stiffness of the bonding layer and the film κ;
- The debonding to transverse cracking relative fracture toughness γ;
- The Poisson ratio in the film.

Note that one can always choose the scaling length $x_0 = \sqrt{h_f h_b \mu_f/\mu_b}$ in order to have $\kappa = 1$. However in that case the dimension of the domain (in x_0-units) will be an additional parameter. In the following we will adopt the opposite point of view, setting x_0 such that the diameter of the domain $\tilde{\omega}$ is of order 1 and keeping κ as a free parameter.

3.4.3 Formulation of the reduced problem

We formulate below the static problem and the discrete-in-time evolution problem for the reduced model by extending those of Sections 1.2.3-1.2.4 to include the presence of the two fracture modes given by transverse cracks and debonding cracks.

Problem 3.8 (Static solution of the reduced model)**.** *Given a loading e_0, find $u \in H^1(\omega \setminus \Gamma; \mathbb{R}^2)$, $\Gamma \subset \omega$, $\Delta \subseteq \omega$ such that*

$$E(u, \Gamma, \Delta) \leq E(v, \hat{\Gamma}, \hat{\Delta}), \quad \forall \hat{\Gamma} \subset \omega,\ \forall \hat{\Delta} \subseteq \omega,\ \forall v \in H^1(\omega \setminus \hat{\Gamma}; \mathbb{R}^2).$$

This condition is equivalent to require that (u, Γ, Δ) solve the following minimization problem

$$\inf\{E(u, \Gamma, \Delta) : \quad \Gamma \subset \omega,\ \Delta \subseteq \omega,\ u \in H^1(\omega \setminus \hat{\Gamma}; \mathbb{R}^2)\}.$$

Remark 3.8. *As done in the case of scalar elasticity, for any admissible u, one can find explicitly the optimal debonded set by solving a linear optimization problem for the characteristic function χ_Δ of the domain Δ, see Theorem 3.3, which gives:*

$$\Delta_u := \left\{ x \in \omega : |u(x)| > u_d := \sqrt{\frac{2\gamma}{\kappa}} \right\}. \tag{3.35}$$

Hence the static problem may be alternatively reformulated as the minimization of the energy

$$E(u, \Gamma) := \int_{\omega \setminus \Gamma} \frac{1}{2} A(e(u(x)) - e_0) \cdot (e(u) - e_0)\, dx + \mathcal{H}^1(\Gamma) + \int_{\omega \setminus \Delta_u} \frac{\kappa}{2} |u|^2\, dx + \int_{\Delta_u} \gamma\, dx \tag{3.36}$$

In Equation (3.36), the energy density due to the film is a quadratic function of the mismatch between the geometric strains $e(u)$ and inelastic strains e_0. On the other hand the energy density due to the bonding layer, say f, is quadratic in u ($f(u) = \kappa\, u \cdot u/2$) before debonding ($|u| \leq u_d$) and constant ($f(u) = \gamma$) after debonding. Its dependence on u is sketched in Figure 3.11. Hence, even in the case without transverse cracks, the total elastic energy $E(u, \emptyset)$ is non-linear, non-smooth and non-convex with respect to u. As a consequence of the lack of convexity, we expect lack of uniqueness of the displacement solution as soon as debonding is triggered, even without considering transverse cracks. This kind of problem has been studied is detail in the one-dimensional case in [Leó+13d].

Problem 3.9 (Time-discrete evolution of the reduced model)**.** *Let be $0 = t_0 \leq t_1 \leq \ldots \leq t_N = T$ the discretization of the time interval $[0, T]$ into N time steps. A time-discrete quasi-static evolution for the displacement field and crack set of the reduced two-dimensional model is a mapping $t_i \mapsto (u^i, \Gamma^i, \Delta^i)$ that, given the initial crack state Γ^0, Δ^0 and the loading history e_0^i, verifies the following global unilateral minimality conditions $\forall i \in 1, \ldots, N$:*

$$\Gamma^i \supseteq \Gamma^{i-1}, \quad \Delta^i \supseteq \Delta^{i-1},$$

$$E(u^i, \Gamma^i, \Delta^i) \leq E(\hat{u}, \hat{\Gamma}, \hat{\Delta}), \quad \forall \hat{\Gamma} \text{ with } \Gamma^{i-1} \subseteq \hat{\Gamma} \subset \omega, \quad \forall \hat{\Delta} \text{ with } \Delta^{i-1} \subseteq \hat{\Delta} \subseteq \omega,\ \forall \hat{u} \in H^1(\omega \setminus \hat{\Gamma}; \mathbb{R}^2). \tag{3.37a}$$

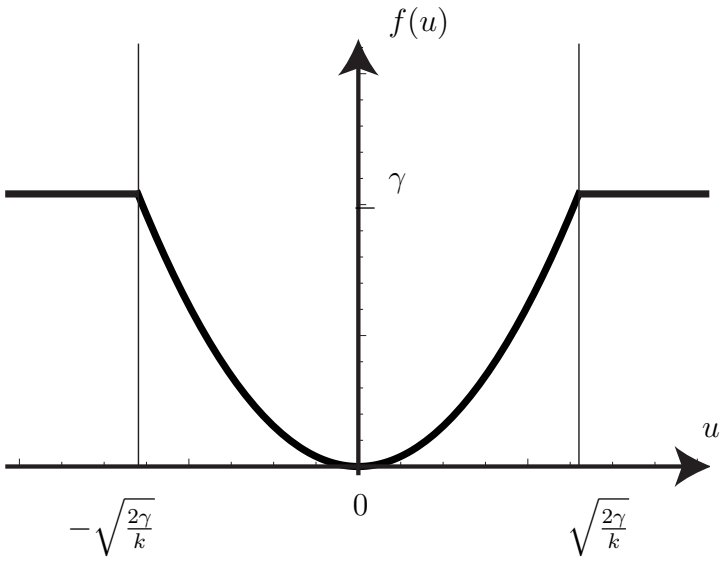

Figure 3.11: Qualitative properties of the energy density of the reduced model. The total energy density in the film is quadratic with respect to u in the elastic phase and constant after debonding, see Equation (3.36).

These conditions are equivalent to require $(u^i, \Gamma^i, \Delta^i)$ *to be a solution of the minimization problem*

$$\inf\{E(u,\Gamma,\Delta): \quad \Gamma^{i-1} \subseteq \Gamma \subset \omega,\ \Delta^{i-1} \subseteq \Delta \subseteq \omega,\ u \in H^1(\omega \setminus \Gamma; \mathbb{R}^2)\}.$$

3.5 Conclusions of the chapter

In this chapter we have progressively constructed a reduced two-dimensional model to take account of the competition between the elasticity and fracture in film systems. It seemed necessary to study the purely elastic system at first, its simplicity in the scalar case allows to rapidly investigate the three dimensional systems possibly showing severe mismatches in stiffness and thickness. These two are indeed the only parameters to take account of in linear elasticity. Performing a complete parametric asymptotic study we have observed that, among all three dimensional systems, there exists a particular class of systems which, in the limit, are represented by the same equivalent system: a linear membrane over an elastic foundation. These systems naturally manifest the existence of an intrinsic length scale determined by the elastic and geometric quantities, and plays its role by measuring the relative weight of the film and elastic foundation energies. The limit energy is the same as the one proposed by [XH00] and assumed in Chapter 2 for the study of the one-dimensional response. We then chose to further investigate one instance of the identified class: a thin film bonded to the substrate through a soft brittle bonding layer.

Allowing for cracks, on the other hand, is more challenging. The difficulties are essentially related to the characterization and representation of the arbitrary free surfaces. Fractures may appear both in the membrane and in the bonding layer. The asymptotic analysis characterizes their respective nature. In the limit two-dimensional model, transverse cracks in the membrane are curves where the displacement may jump, whilst debonding cracks are two-dimensional surfaces which are explicitly identified. Indeed, the debonding condition reduces to a simple threshold criterion on the norm of the displacement. The extension of the dimension reduction result to the case of full vectiorial elasticity is not straightforward. We hence inductively propose a reasonable application to two-dimensional elasticity which will serve as a basis for the numerical exploration, the topic of the next Chapter.

The model presented here is based on several strong hypotheses, which may be difficult to reproduce in experimental conditions. Perhaps the strongest among them is to assume a perfectly linear-elastic brittle behavior of the bonding layer, while in real materials plastic effects may play an important role.

From the mathematical point of view, the present dimensional reduction results should be extended to fully justify the limit model in the framework of vectorial elasticity. Another investigation thread is to consider the effect of bending and its interplay with stretching, in circumstances where it is not inhibited by boundary conditions, and derive a complete plate model (membrane and flexural equations) under general scaling hypotheses on the material and geometric properties of the three-dimensional system.

3.A Proof of the dimensional reduction for scalar elasticity

This section is devoted to give a rigorous proof of Theorem 3.3. As explained in Section 3.3.2, it will be obtained in three steps: we first show that sequences with uniformly bounded energy admit converging subsequences. Then we prove a lower bound for the limit energy. Eventually, we show that this lower bound is optimal through the construction of a recovery sequence which gives an upper bound.

Compactness in the film

Lemma 3.3. *Let $(\varepsilon_n) \searrow 0^+$ and $(u_n) \subset \mathcal{C}_w(\Omega)$ be sequences satisfying*

$$\sup_{n\in\mathbb{N}} \mathcal{E}_{\varepsilon_n}(u_n) < \infty. \tag{3.38}$$

Then there exists a subsequence (not relabeled) and $u \in SBV(\Omega_f)$ such that

$$\begin{cases} u_n \to u \text{ strongly in } L^2(\Omega_f), \\ u_n \rightharpoonup u \text{ weakly* in } L^\infty(\Omega_f), \\ \nabla u_n \rightharpoonup \nabla u \text{ weakly in } L^2(\Omega_f;\mathbb{R}^3). \end{cases}$$

Moreover, $\partial_3 u = 0$ a.e. in Ω_f, and $(\nu_u)_3 = 0$ $\mathcal{H}^2$-a.e. on $J_u \cap \Omega_f$. Hence, the limit displacement field u (can be identified to a function that) belongs to $SBV(\omega)$, it satisfies $\|u\|_{L^\infty(\omega)} \le M$, and

$$\begin{cases} L\displaystyle\int_\omega |\nabla' u - e_0'|^2\, dx' \le \liminf_{n\to\infty} \int_{\Omega_f} \left(|\nabla' u_n - e_0'|^2 + \frac{1}{\varepsilon_n^2} |\partial_3 u_n|^2 \right) dx, \\ L\mathcal{H}^1(J_u') \le \displaystyle\liminf_{n\to\infty} \int_{\Omega_f \cap J_{u_n}} \left| \left((\nu_{u_n})', \frac{1}{\varepsilon_n} (\nu_{u_n})_3 \right) \right| d\mathcal{H}^2. \end{cases}$$

Proof. According to (3.38), the definition of the energy $\mathcal{E}_{\varepsilon_n}$ and of that of the space of kinematically admissible displacements $\mathcal{C}_w(\Omega)$, we have the following bounds

$$\|u_n\|_{L^\infty(\Omega_f)} + \|\nabla u_n\|_{L^2(\Omega_f;\mathbb{R}^3)} + \mathcal{H}^2(J_{u_n} \cap \Omega_f) \le C$$

for some constant $C > 0$ independent of n. According to Ambrosio's compactness Theorem in SBV (see [AFP00, Thms 4.7 and 4.8]), we deduce the existence of a subsequence $(u_{n_k}) \subset (u_n)$ and a function $u \in SBV(\Omega_f)$ such that $u_{n_k} \to u$ strongly in $L^2(\Omega_f)$, $u_{n_k} \rightharpoonup u$ weakly* in $L^\infty(\Omega_f)$, $\nabla u_{n_k} \rightharpoonup \nabla u$ weakly in $L^2(\Omega_f;\mathbb{R}^3)$, and

$$\mathcal{H}^2(J_u \cap \Omega_f) \le \liminf_{k\to+\infty} \mathcal{H}^2(J_{u_{n_k}} \cap \Omega_f).$$

Let us prove that u is actually independent of x_3. Using the expression of the energy in the film, we deduce that

$$\int_{\Omega_f} |\partial_3 u_{n_k}|^2\, dx + \int_{\Omega_f \cap J_{u_{n_k}}} |(\nu_{u_{n_k}})_3|\, d\mathcal{H}^2 \le C\varepsilon_{n_k} \to 0.$$

Since the left hand side of the previous inequality is lower semicontinuous with respect to the convergences established for (u_{n_k}) (see *e.g.* [Bab06], [BF01], [BFL02]), we conclude that $\partial_3 u = 0$ a.e. in Ω_f, and $(\nu_u)_3 = 0$ $\mathcal{H}^2$-a.e. on $J_u \cap \Omega_f$. This implies that the distributional derivative $D_3 u = 0$ in $\mathcal{D}'(\Omega_f)$, and thus the limit displacement field u (can be identified to a function that) belongs to $SBV(\omega)$.

By definition of $\mathcal{C}_w(\Omega)$, we have that $\|u_n\|_{L^\infty(\Omega_f)} \leq M$. Therefore, we deduce by lower semicontinuity of the norm with respect to weak* convergence in $L^\infty(\Omega_f)$ that $\|u\|_{L^\infty(\omega)} \leq M$.

Since u is independent of x_3, the approximate gradient is given by $\nabla u = (\nabla' u, 0)$ and the jump set can be written as $J_u = J'_u \times (0, L)$ for some 1-rectifiable set $J'_u \subset \omega$. Finally, since $\varepsilon_{n_k} \leq 1$, we infer that

$$L \int_\omega |\nabla' u - e'_0|^2 \, dx' \leq \liminf_{k\to\infty} \int_{\Omega_f} |\nabla u_{n_k} - (e'_0, 0)|^2 \, dx \\ \leq \liminf_{k\to\infty} \int_{\Omega_f} \left(|\nabla' u_{n_k} - e'_0|^2 + \frac{1}{\varepsilon_{n_k}^2} |\partial_3 u_{n_k}|^2 \right) dx,$$

and

$$L\mathcal{H}^1(J'_u) = \mathcal{H}^2(J_u \cap \Omega_f) \leq \liminf_{k\to\infty} \mathcal{H}^2(J_{u_{n_k}} \cap \Omega_f) \\ \leq \liminf_{k\to\infty} \int_{\Omega_f \cap J_{u_{n_k}}} \left| \left((\nu_{u_{n_k}})', \frac{1}{\varepsilon_{n_k}} (\nu_{u_{n_k}})_3 \right) \right| d\mathcal{H}^2,$$

which completes the proof of the lemma. □

Lower bound

Proposition 3.2. *For any $u \in \mathcal{C}(\omega)$, and any sequences $(\varepsilon_n) \searrow 0^+$ and $(u_n) \subset \mathcal{C}_w(\Omega)$ such that $u_n \to u$ strongly in $L^2(\Omega_f)$, then*

$$\mathcal{E}_0(u) \leq \liminf_{n\to\infty} \mathcal{E}_{\varepsilon_n}(u_n).$$

Proof. Let us extract a subsequence (not relabeled) such that the previous lim inf is actually a limit. Then for n large enough, one has

$$\mathcal{E}_{\varepsilon_n}(u_n) \leq C, \tag{3.39}$$

for some constant $C > 0$. According to Proposition 3.3, $u_n \to u$ strongly in $L^2(\Omega_f)$, $u_n \rightharpoonup u$ weakly* in $L^\infty(\Omega_f)$, $\nabla u_n \rightharpoonup \nabla u$ weakly in $L^2(\Omega_f; \mathbb{R}^3)$, and

$$\begin{cases} \mu_f L \displaystyle\int_\omega |\nabla' u - e'_0|^2 \, dx' \leq \liminf_{n\to\infty} \mu_f \int_{\Omega_f} \left(|\nabla' u_n - e'_0|^2 + \frac{1}{\varepsilon_n^2} |\partial_3 u_n|^2 \right) dx, \\ G_f L\mathcal{H}^1(J'_u) \leq \displaystyle\liminf_{n\to\infty} G_f \int_{\Omega_f \cap J_{u_n}} \left| \left((\nu_{u_n})', \frac{1}{\varepsilon_n} (\nu_{u_n})_3 \right) \right| d\mathcal{H}^2. \end{cases}$$

Consequently, it is enough to consider the energy in the bonding layer Ω_b, and to check that

$$\frac{L\mu_b}{h_f h_b}\int_{\omega\setminus\Delta_u}|u-w|^2\,dx' + \frac{LG_b}{h_f}\mathcal{H}^2(\Delta_u) \\ \leq \liminf_{n\to\infty}\left(\mu_f\varrho_\mu\int_{\Omega_b}\left(\varepsilon_n^2|\nabla' u_n|^2+|\partial_3 u_n|^2\right)dx \right. \\ \left. +G_f\varrho_G\int_{\Omega_b\cap J_{u_n}}|(\varepsilon_n(\nu_{u_n})',(\nu_{u_n})_3)|\,d\mathcal{H}^2\right). \quad (3.40)$$

The rest of the proof is devoted to show (3.40). The main difficulty consists in defining the debonding set. This is performed as follows: let $x'\in\omega$, we define the transverse section of the jump set of u_n by $J_n^{x'}:=\{x_3\in(-2L\varrho_h,L):(x',x_3)\in J_{u_n}\}$ and

$$\Delta_n:=\{x'\in\omega : J_n^{x'}\neq\emptyset\}.$$

The set Δ_n is made of all points in the plane from which the vertical section intersects the jump set J_{u_n} or, in other words, Δ_n is the orthogonal projection of J_{u_n} on ω. It can be interpreted as an approximation of the debonding zone. Unfortunately, it is not clear how to show that it converges to some (debonding) set because we only control the $L^\infty(\omega)$ norm of its characteristic function. Therefore, possibly for a subsequence (not relabeled), one can find some $\vartheta\in L^\infty(\omega;[0,1])$ such that $\chi_{\Delta_n}\rightharpoonup\vartheta$ weakly* in $L^\infty(\omega;[0,1])$.

Step 1. We first obtain that, outside the debonding set Δ_n, the trace $u_n(\cdot,0)$ of u_n at the interface $\omega\times\{0\}$ between the film and the bonding layer converges strongly in $L^2(\omega)$ to the limit displacement u (which is independent of x_3). In absence of debonding, this property is standard as a consequence of the compactness of the trace operator from $H^1(\Omega_f)$ to $L^2(\omega)$. However, in the presence of debonding, since u_n is a $SBV(\Omega_f)$ function, this property does not hold anymore. What makes the argument work in our case is that the function $x_3\mapsto u_n(x',x_3)$ is Sobolev whenever x' lives outside the debonding set Δ_n. To be more precise, let us show that

$$\int_{\omega\setminus\Delta_n}|u(x')-u_n(x',0)|^2\,dx'\to 0. \quad (3.41)$$

For each $x'\in\omega$, let us define $u_n^{x'}(x_3):=u_n(x',x_3)$. According to slicing properties of SBV functions (see [AFP00, Thms 3.107 and 3.108]), we have $u_n^{x'}\in SBV(-2L\varrho_h,L)$, and $J_{u_n^{x'}}=J_n^{x'}$ for a.e. $x'\in\omega$. Hence by definition of Δ_n, we deduce that $u_n^{x'}\in H^1(-2L\varrho_h,L)$ for a.e. $x'\in\omega\setminus\Delta_n$. In addition, for a.e. $x_3\in(0,L)$, we have $(u_n^{x'})'(x_3)=\partial_3 u_n(x',x_3)$ (by [AFP00, Prop. 4.35]), and

$$|u_n(x',x_3)-u_n(x',0)|=|u_n^{x'}(x_3)-u_n(x',0)|\leq\int_0^{x_3}|(u_n^{x'})'(s)|\,ds \\ \leq\int_0^L|\partial_3 u_n(x',s)|\,ds.$$

Integrating with respect to $x_3 \in (0, L)$ and $x' \in \omega \setminus \Delta_n$, the Cauchy-Schwarz inequality and (3.39) yield

$$\int_{\omega\setminus\Delta_n} \int_0^L |u_n(x', x_3) - u_n(x', 0)|^2 \, dx_3 \, dx' \\ \leq L^2 \int_{\omega\setminus\Delta_n} \int_0^L |\partial_3 u_n(x', x_3)|^2 \, dx_3 \, dx' \leq L^2 \int_{\Omega_f} |\partial_3 u_n(x)|^2 \, dx \leq C\varepsilon_n^2.$$

In addition, since $u_n \to u$ strongly in $L^2(\Omega_f)$, and u is independent of x_3, we finally obtain (3.41).

Step 2. We next show lower bounds in terms of the density ϑ of debonding for the volume and surface energies in the bonding layer:

$$\frac{L\mu_b}{h_f h_b} \int_\omega (1-\vartheta)(u-w)^2 \, dx' \leq \liminf_{n\to\infty} \mu_f \varrho_\mu \int_{\Omega_b} \left(\varepsilon_n^2 |\nabla' u_n - e_0'|^2 + |\partial_3 u_n|^2\right) \, dx \tag{3.42}$$

and

$$\frac{LG_b}{h_f} \int_\omega \vartheta \, dx' \leq \liminf_{n\to\infty} G_f \varrho_G \int_{\Omega_b \cap J_{u_n}} |(\varepsilon_n (\nu_{u_n})', (\nu_{u_n})_3)| \, d\mathcal{H}^2. \tag{3.43}$$

Intuitively the term of order ε_n^2 in (3.42) and the term of order ε_n in (3.43) can be neglected so that we only focus on terms of order 1. Let us start by proving (3.42). Using the Cauchy-Schwarz inequality and the fact that $\chi_{\Delta_n} \rightharpoonup \vartheta$ weakly* in $L^\infty(\omega; [0,1])$, we infer that

$$\begin{aligned} \liminf_{n\to\infty} \int_{\Omega_b} \left(\varepsilon_n^2 |\nabla' u_n - e_0'|^2 + |\partial_3 u_n|^2\right) \, dx \\ &\geq \liminf_{n\to\infty} \int_{\omega\setminus\Delta_n} \int_{-L\varrho_h}^0 |\partial_3 u_n|^2 \, dx_3 \, dx' \\ &\geq \liminf_{n\to\infty} \frac{1}{L\varrho_h} \int_{\omega\setminus\Delta_n} \left(\int_{-L\varrho_h}^0 \partial_3 u_n \, dx_3\right)^2 dx' \\ &\geq \frac{1}{L\varrho_h} \int_\omega (1-\vartheta)(u-w)^2 \, dx' \\ &\quad + \liminf_{n\to\infty} \frac{1}{L\varrho_h} \int_{\omega\setminus\Delta_n} \left[\left(\int_{-L\varrho_h}^0 \partial_3 u_n \, dx_3\right)^2 - (u-w)^2\right] dx'. \end{aligned} \tag{3.44}$$

Since $u_n(x', \cdot) \in H^1(-2L\varrho_h, L)$ for a.e. $x \in \omega \setminus \Delta_n$, then the trace $u_n(\cdot, -2L\varrho_h)$ of u_n at the interface $\{x_3 = -2L\varrho_h\}$ between the bonding layer and the substrate satisfies $u_n(x', -2L\varrho_h) = w(x')$, and thus

$$\int_{\omega\setminus\Delta_n} \left[\left(\int_{-L\varrho_h}^0 \partial_3 u_n \, dx_3\right)^2 - (u-w)^2\right] dx' \\ = \int_{\omega\setminus\Delta_n} \left[(u_n(x', 0) - w(x'))^2 - (u(x') - w(x'))^2\right] dx'.$$

Using now (3.41), the fact that u_n (and hence its trace $u_n(\cdot,0)$) is uniformly bounded by M, and the Cauchy-Schwarz inequality we deduce that

$$\int_{\omega\setminus\Delta_n}\left[(u_n(x',0)-w(x'))^2-(u(x')-w(x'))^2\right]dx'\to 0.$$

Thus (3.42) follows from (3.44).

We next prove (3.43). Let us denote by $\pi:\mathbb{R}^3\to\mathbb{R}^2\times\{0\}$ the orthogonal projection onto the hyperplane $\{x_3=0\}$. Then

$$\begin{aligned}\liminf_{n\to\infty}\int_{\Omega_b\cap J_{u_n}}|(\varepsilon_n(\nu_{u_n})',(\nu_{u_n})_3)|\,d\mathcal{H}^2&\geq\liminf_{n\to\infty}\int_{\Omega_b\cap J_{u_n}}|(\nu_{u_n})_3|\,d\mathcal{H}^2\\&=\liminf_{n\to\infty}\mathcal{H}^2(\pi(J_{u_n}\cap\Omega_b))\geq\liminf_{n\to\infty}\mathcal{H}^2(\pi(J_{u_n}))-\limsup_{n\to\infty}\mathcal{H}^2(\pi(J_{u_n}\cap\Omega_f)).\end{aligned}$$

But since $\pi(J_{u_n})=\Delta_n$, and, in view of (3.39)

$$\mathcal{H}^2(\pi(J_{u_n}\cap\Omega_f))=\int_{\Omega_f\cap J_{u_n}}|(\nu_{u_n})_3|\,d\mathcal{H}^2\leq C\varepsilon_n\to 0,$$

we obtain that

$$\liminf_{n\to\infty}\int_{\Omega_b\cap J_{u_n}}|(\varepsilon_n(\nu_{u_n})',(\nu_{u_n})_3)|\,d\mathcal{H}^2\geq\liminf_{n\to\infty}\mathcal{H}^2(\Delta_n)=\int_\omega\vartheta\,dx',$$

which completes the proof of (3.43).

Step 3. Let us prove that

$$\begin{aligned}\frac{L\mu_b}{2h_fh_b}\int_\omega(1-\vartheta)(u-w)^2\,dx'+\frac{LG_b}{h_f}\int_\omega\vartheta\,dx'&\\\geq\frac{L\mu_b}{2h_fh_b}\int_{\omega\setminus\Delta_u}|u-w|^2\,dx'+\frac{LG_b}{h_f}\mathcal{H}^2(\Delta_u),&\quad(3.45)\end{aligned}$$

where Δ_u is the debonding set defined by (3.30). Clearly, one has

$$\begin{aligned}\frac{L\mu_b}{2h_fh_b}\int_\omega(1-\vartheta)(u-w)^2\,dx'+\frac{LG_b}{h_f}\int_\omega\vartheta\,dx'&\\\geq\frac{L}{h_f}\int_\omega\inf_{\eta\in[0,1]}\left[\eta\left(G_b-\frac{\mu_b}{2h_b}(u-w)^2\right)+\frac{\mu_b}{2h_b}(u-w)^2\right]dx'.&\end{aligned}$$

It is easy to check that a minimizer η^* in $[0,1]$ of

$$\eta\mapsto\eta\left(G_b-\frac{\mu_b}{2h_b}(u-w)^2\right)+\frac{\mu_b}{2h_b}(u-w)^2$$

is given by

$$\eta^*=\chi_{\left\{|u-w|>\sqrt{\frac{2G_bh_b}{\mu_b}}\right\}}(x')$$

and (3.45) follows from the definition (3.30) of the debonding set. □

Upper bound and existence of a recovery sequence

Proposition 3.3. *For any $u \in \mathcal{C}(\omega)$ and any sequence $(\varepsilon_n) \searrow 0^+$, there exists $(\overline{u}_n) \subset \mathcal{C}_w(\Omega)$ such that $\overline{u}_n \to u$ strongly in $L^2(\Omega)$ and*

$$\mathcal{E}_0(u) \geq \limsup_{n\to\infty} \mathcal{E}_{\varepsilon_n}(\overline{u}_n).$$

Proof. In order to get an intuition of the form of the recovery sequence, let us analyze what would make optimal the lower bound established in Proposition 3.2. Concerning the part in the film, we expect a displacement independent of the transverse variable x_3 in order to ensure that the term of order $1/\varepsilon_n^2$ in the bulk energy, and that of order $1/\varepsilon_n$ in the surface energy, do not blow up. Concerning the bonding layer, as already observed in the proof of the lower bound, we expect no contributions from the in-plane strain and of in-plane cracks since these terms vanish as the thickness tends to zero. On the other hand, according to estimate (3.44), we used the Cauchy-Schwarz inequality for the function $x_3 \mapsto \partial_3 u(x', x_3)$ when x' lives outside the debonding set. It is known that such inequality is an equality whenever the function is constant. Therefore, when x' does not belong to the debonding set, we expect that the function $x_3 \mapsto u(x', x_3)$ is affine, joining continuously the prescribed displacement $w(x')$ on the substrate and the displacement $u(x')$ of the film. Finally, if x' is a debonded point, then the displacement of the film does not match that of the substrate.

Let us make this observation rigorous. By the coarea formula in BV ([AFP00, Theorem 3.40]), there exists a sequence $(t_k) \searrow u_d$ such that the sets $\{|u - w| \leq t_k\}$ have finite perimeter for each $k \in \mathbb{N}$. Let us define

$$u^k(x', x_3) := \begin{cases} u(x') & \text{if } (x', x_3) \in \Omega_f, \\ \left(\dfrac{x_3}{L\varrho_h} + 1\right) u(x') - \dfrac{x_3}{L\varrho_h} w(x') & \text{if } \begin{cases} (x', x_3) \in \Omega_b, \\ |u(x') - w(x')| \leq t_k, \end{cases} \\ w(x') & \text{if } (x', x_3) \in \Omega_s \\ & \quad \text{or } \begin{cases} (x', x_3) \in \Omega_b, \\ |u(x') - w(x')| > t_k. \end{cases} \end{cases}$$

Clearly, $u^k \in SBV(\Omega)$, $u^k = w$ a.e. in Ω_s and $\|u^k\|_{L^\infty(\Omega)} \leq M$ so that $u^k \in \mathcal{C}_w(\Omega)$ is admissible. Then for each $k \in \mathbb{N}$,

$$\int_{\Omega_f} \left(|\nabla' u^k - e_0'|^2 + \frac{1}{\varepsilon_n^2} |\partial_3 u^k|^2 \right) dx = L \int_\omega |\nabla' u - e_0'|^2 \, dx', \tag{3.46}$$

$$\int_{\Omega_f \cap J_{u^k}} \left| \left((\nu_{u^k})', \frac{1}{\varepsilon_n} (\nu_{u^k})_3 \right) \right| d\mathcal{H}^2 = L\mathcal{H}^1(J_u'), \tag{3.47}$$

and

$$\int_{\Omega_b} \left(\varepsilon_n^2|\nabla' u - e_0'|^2 + |\partial_3 u|^2\right)\, dx$$
$$= \frac{1}{L\varrho_h}\int_{\{|u-w|\le t_k\}} (u-w)^2\, dx' + L\varrho_h\varepsilon_n^2 \int_{\{|u-w|>t_k\}} |\nabla' w - e_0'|^2\, dx'$$
$$+ \varepsilon_n^2 \int_{\{|u-w|\le t_k\}\times(-L\varrho_h,0)} \left| \left(\frac{x_3}{L\varrho_h}+1\right)\nabla' u - \frac{x_3}{L\varrho_h}\nabla' w - e_0' \right|^2 dx$$
$$\xrightarrow[n\to\infty]{} \frac{1}{L\varrho_h}\int_{\{|u-w|\le t_k\}} (u-w)^2 dx'. \quad (3.48)$$

It remains to compute the surface energy in the bonding layer. To this end, we observe that

$$J_{u^k} \cap \Omega_b \subset \Big[J_u' \times [-L\varrho_h, 0]\Big] \cup \Big[\{|u-w| > t_k\} \times \{0\}\Big]$$
$$\cup \Big[\partial^*\{|u-w| \le t_k\} \times [-L\varrho_h, 0]\Big],$$

where $\partial^* E$ stands for the reduced boundary of the set of finite perimeter E (see [AFP00, Definition 3.54]). Then, for each $k \in \mathbb{N}$,

$$\int_{\Omega_b \cap J_{u^k}} |(\varepsilon_n(\nu_{u^k})', (\nu_{u^k})_3)|\, d\mathcal{H}^2$$
$$\le L\varrho_h\varepsilon_n \mathcal{H}^1(J_u') + \mathcal{H}^2(\{|u-w| > t_k\}) + L\varrho_h\varepsilon_n \mathcal{H}^1(\partial^*\{|u-w| \le t_k\})$$
$$\xrightarrow[n\to\infty]{} \mathcal{H}^2(\{|u-w| > t_k\}). \quad (3.49)$$

Gathering (3.46), (3.47), (3.48), (3.49) yields, for each $k \in \mathbb{N}$,

$$\limsup_{n\to\infty} \mathcal{E}_{\varepsilon_n}(u^k) \le L\mu_f \int_\omega |\nabla' u|^2\, dx' + \frac{L\mu_b}{h_f h_b}\int_{\{|u-w|\le t_k\}} (u-w)^2\, dx'$$
$$+ LG_f \mathcal{H}^1(J_u') + \frac{LG_b}{h_f}\mathcal{H}^2(\{|u-w| > t_k\}).$$

Letting $k \to +\infty$ and using the monotone convergence theorem leads to

$$\limsup_{k\to+\infty}\limsup_{n\to+\infty} \mathcal{E}_{\varepsilon_n}(u^k) \le L\mu_f \int_\omega |\nabla' u|^2\, dx' + \frac{L\mu_b}{h_f h_b}\int_{\{|u-w|\le u_d\}} (u-w)^2\, dx'$$
$$+ LG_f \mathcal{H}^1(J_u') + \frac{LG_b}{h_f}\mathcal{H}^2(\{|u-w| > u_d\}).$$

Finally, thanks to a diagonalization procedure, it is possible to find a sequence $k_n \nearrow +\infty$ such that

$$\limsup_{n\to+\infty} \mathcal{E}_{\varepsilon_n}(\overline{u}_n) \le \mathcal{E}_0(u)$$

with $\overline{u}_n := u^{k_n}$, which completes the proof of the proposition. □

3.B Spaces of functions with measure derivatives

The object of this section is to recall some notations about spaces of functions with measure derivatives that are used throughout the paper. Let U be a bounded open subset of $\mathbb{R}^n$. The Lebesgue measure is denoted by $\mathcal{L}^n$ while $\mathcal{H}^{n-1}$ stands for the $(n-1)$-dimensional Hausdorff measure.

Special functions of bounded variation

The space $SBV(U)$ of *special functions of bounded variation* is made of all (scalar) functions $u \in L^1(U)$ such that the distributional derivative Du is a bounded Radon measure which can be written as In the previous formula:

- $\nabla u \in L^1(U;\mathbb{R}^n)$ denotes the approximate gradient, *i.e.* the density of Du with respect to the Lebesgue measure $\mathcal{L}^n$;
- J_u is the jump set of u. It is a rectifiable set whose unit normal is denoted ν_u;
- $u^{\pm}$ are the one-sided traces of u on J_u.

We refer to [AFP00] for systematic study of that space.

Special functions of bounded deformation

The space $SBD(U)$ of *special functions of bounded deformation* is made of all vector valued functions $u \in L^1(U;\mathbb{R}^n)$ such that the symmetric part of the distributional derivative, *i.e.* $Eu := (Du + Du^T)/2$, is a bounded Radon measure which can be written as In the previous formula:

- $e(u) \in L^1(U;\mathbb{R}^{n\times n})$ denotes the density of Eu with respect to the Lebesgue measure $\mathcal{L}^n$;
- J_u is the jump set of u. It is a rectifiable set whose unit normal is denoted ν_u;
- $u^{\pm}$ are the one sided traces of u on J_u.

We refer to [ACM97], [BCD98] for more informations about that space.

Chapter 4

Exploring crack patterns: numerical experiments

We propose an irreversible, rate-independent approximation of the fracture problem 1.3 based on a gradient damage model with local minimization. The latter provides a "smeared" representation of crack surfaces and converges to the brittle fracture model in the sense of Γ*-convergence. Its numerical implementation allows us to perform several numerical experiments where, without any a priori assumption on the crack geometry, we capture complex evolving crack patterns in different regimes. We explore parallel, sequential, periodic cracking and possible debonding in a uniaxial traction test; appearance of polygonal crack patterns in a two-dimensional wafer under equi-biaxial load; and cracking in a geometrically complex domain. Finally, we present a novel experiment in which the crack pattern characterized by a strong coupling between fracture and debonding.*
The numerical experiments shown in Subsections 4.3.1–4.3.3 are presented in the paper [Leó+13a], submitted for review. The experiment introduced in Subsection 4.3.4 is still unpublished.

Contents

4.1 The regularized energy 124

4.2 The regularized formulation 127

4.2.1 Mechanical interpretation of the regularized model with local minimization 130

4.3 Numerical experiments 131

4.3.1 Multiple cracking and debonding of a slender strip 131

4.3.2 Multiple cracking and debonding of a thin disk 139

4.3.3 Vinyl lettering on a metal substrate 144

4.3.4 *Ouverture*: a strongly coupled two-dimensional pattern . . . 148

4.4 Conclusions of the chapter 150

We now turn the attention to the numerical experimentation of evolving crack patterns that follow the evolution law stated in Problem 3.9 to explore to what extent it can capture the rather wide range of observed phenomenology.

We propose to investigate the regimes of sequential periodic cracking in one and two dimensions under uniform equi-biaxial loads; highlight hierarchical domain subdivision; as well as crack-to-crack interactions and their interplay with debonding. Crack patterns commonly observed include isolated star-shaped cracks, independent channeling cracks, partially connected network of intersecting cracks and fully connected polygonal patterns. Classically, a non-dimensional "cracking number", depending on the thickness of the film, the stiffness mismatch of the multilayer and on the toughnesses of the layers, is related to the observed crack pattern as proposed in [EDH88], see also [HS91]. A typical scenario of multiple cracking of a thin film on rigid substrate is shown in Figures 4.1. The upper row of images (4.1(a))) refers to a layer of drying cornstarch [LN00], the lower row (4.1(b))) to consolidating colloidal particles by dessiccation on a rigid substrate [LP11]. In both cases, the images are related to different thicknesses of the film layer, increasing from left to right. In thicker films (right), the initial stages of cracking are dominated by isolated running cracks starting from the boundaries. They can be identified in Figure 4.1(a) since are those associated to wider aperture of the crack lips. Successive cracks (*e.g.* the two horizontal cracks approximately in the middle of the domain in Figure 4.1(a)) intersect at right angles. Further cracking produces a finer segmentation and although the size of all cells is of the same order of magnitude, they do not show a preferred shape. In a thinner film (center), a clear distinction between two cracking regimes, the first with isolated cracks and a second characterized by successive segmentation, is not evident. In the thinnest specimens in Figure 4.1(a)(left), a single characteristic length scale related to the size of the cells is manifest. A similar trend appears in Figure 4.1(b)(b). A closer inspection shows that $2\pi/3$-junctions between cracks are more prominent than right intersections and that nucleation of cracks is more likely to appear in the interior than at the boundaries. In Figure 4.1(b)(a), triangular star-shaped nucleating cracks are present in the bulk of the body. These features are robust and reported in many experimental works, see [GK94], [LP11], [TA06].

The numerical simulation of such complex evolving pattern has been undertaken by many authors since the pioneering work of [Mea87] where a two-dimensional elastic thin film is represented by a discrete lattice of springs and the bond with the underlying rigid substrate is obtained by a second series of elastic springs: the discrete analogous of the asymptotic elastic foundation term. The same approach is used in [CdR93], [HSB96], [LN00]. In [Mea87], crack nucleation and propagation, under tensile stresses, is obtained by randomly breaking the elastic bonds based upon a probability that depends on the local stress at each node. The same type of inhomogeneity is introduced in [HSB96] whereas in [CMP09] localization of stresses is introduced by adding spatial randomness to the applied loads. In [Kit99] in addition to film cracking, possible slipping (*i.e.* debonding) of the film is considered and both mechanisms are assumed to respond to a threshold criterion based on the elastic strain energy density. Cracking and debonding

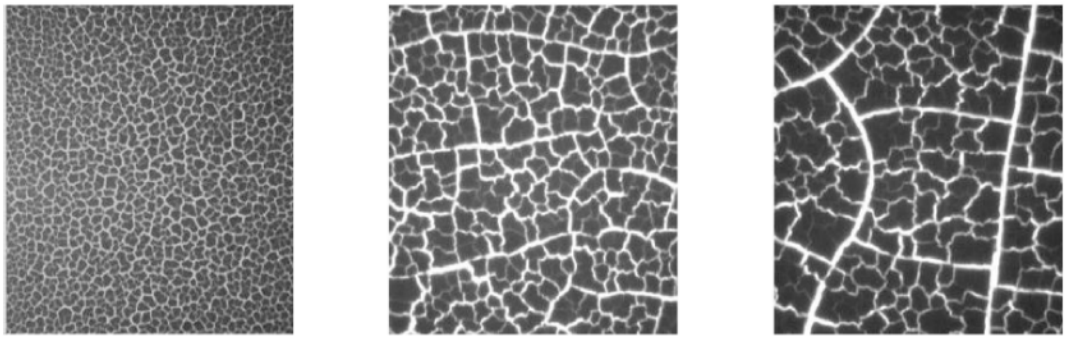

(a) Crack patterns observed in a drying thin film of corn starch, adapted from [LN00].

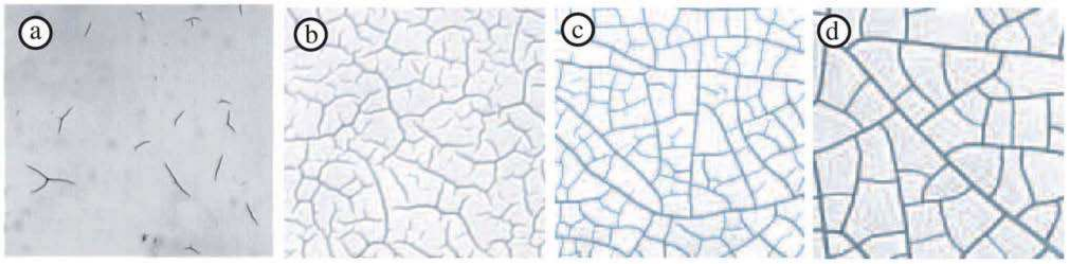

(b) Crack patterns in a film of colloidal particles desiccating on a rigid substrate, adapted from [LP11].

Figure 4.1: The images refer to three specimens of increasing thickness from left to right. In the extreme regimes, spontaneous nucleation in the bulk with $2\pi/3$ junctions, one evident length scale (left) dominate over the successive appearance of hierarchical running cracks before fragmentation (right). Images adapted from [LN00], [LP11].

are also studied in [LN00] using the same threshold law for cracking and debonding. In this case, nucleation is ruled by the homogeneous time-dependent degradation of the two thresholds for cracking and debonding. In [Lia03] is proposed a pseudo-dynamic model for the propagation of pre-existing cracks based upon a Griffith condition written with a crack-tip velocity-dependent toughness. Griffith's scalar condition and the XFEM technique limit the ability to investigate complex patterns, ruling out any possible branching and intersection of cracks. Consequently, only regular, not intersecting cracks are represented. In [CMP09], nucleation is obtained with a threshold criterion on the local stress, propagation using Griffith condition along a path selected by enforcing pure Mode I conditions at the crack tip.

In this Chapter, we intend to explore numerically the stages of nucleation, propagation and path selection for film and debonding cracks. In order to solve Problem 3.9, we adopt a regularized approximation of the energy functional extending that proposed in [Bou00], where it is shown that a suitable elliptic regularized problem converges to a mathematically well-posed weak formulation of a brittle fracture problem. Section 4.1 is devoted to the illustration of the regularized approximation via a gradient damage

model, see also [Pha+10]. The latter is exploited in Section 4.2 to state the regularized evolution problem which is numerically implemented to approximate Problem 3.9. Such approximation, besides being useful from a computational standpoint, offers a rich mechanical interpretation, as is briefly discussed at the end of the section. Finally, Section 4.3 is dedicated to illustrate some numerical experiments. In the first set we consider the case of cracking of a narrow strip under equi-biaxial load. These experiments are also used to validate the code against the closed form solutions obtained in Chapter 2. Then, more complex crack patterns are explored considering a circular wafer subject to equi-biaxial loads. Next, we perform a numerical experiment inspired from a real-life example of cracking of a shrinking thin vinyl sticker bonded to an aluminum panel, providing a qualitative comparison of the numerical crack pattern to the observed one. Then, inspired by experimental observations by [Mar+13], we provide the first elements of analysis of an interesting scenario in which a strong coupling between thin film cracking and debonding causes the selection of an optimal distance in a pattern constituted by two parallel cracks separated by a debonded region.

4.1 The regularized energy

The issue in dealing numerically with energies such as (3.33) resides in the difficulty of finding and representing the crack set Γ and its irreversible evolution. This requires the ability to approximate any possibly discontinuous function (the crack set), allowed jump anywhere within the computational domain, as well as its length, their evolution based on the unilateral energy minimality (3.37a).

The numerical formulation of Problem 3.9 extends that originally proposed in [Bou00], where it is shown that a suitable regularized elliptic problem converges to a mathematically well-posed weak formulation of the brittle fracture problem. The latter, in turn, is shown to be equivalent to the strong brittle fracture problem as proposed in [FM98]. The main idea, underlying the notion of approximation, involves in the introduction of a smooth additional scalar variable $\alpha \in H^1(\omega)$ and a small parameter η, both responsible of tracking the crack set Γ as well as its length. The inspiration for these results, thanks to the analogies between the strong Griffith problem in brittle fracture and the strong Mumford-Shah problem in image segmentation [MS89], comes from the approximation proposed originally by [AT92] (see also [AT90], [Bra98]). The novel element with respect to the problem in computer vision is the irreversible evolution of the crack field resulting in the unilaterality of the underlying minimization principle.

The extension of [Bou07] for the definition of the regularized energy is straightforward. It amounts to restricting the original energy functional to the two-dimensional case, and adding the two continuous perturbations associated to the elastic foundation and the debonding terms. In fact, in the limit reduced energy of Equation 3.33, displacement discontinuities are due only to transverse cracks, the debonding term does not require regularization and its associated problem is solved explicitly enforcing first order optimality conditions which reduce to the threshold criterion (3.35).

The non-dimensional regularized energy E_η defined over $H^1(\omega;\mathbb{R}^2) \times H^1(\omega) \times L^\infty(\omega;\{0,1\})$, approximating (3.33), is taken as follows:

$$E_\eta(u,\alpha,\Delta) := \frac{1}{2}\int_\omega a(\alpha)A(e(u)-e_0)\cdot(e(u)-e_0)\,dx + \frac{1}{2}\int_\omega \kappa u\cdot u\,(1-\chi_\Delta)\,dx + c_w\int_\omega\left(\frac{w(\alpha)}{\eta}+\eta|\nabla'\alpha|^2\right)dx + \int_\omega \gamma\,\chi_\Delta\,dx \quad (4.1)$$

where the stiffness function $a(\alpha)A$ and the dissipation function $w(\alpha)$ read:

$$a(\alpha) = \left((1-\alpha)^2+k_\eta\right), \qquad w(\alpha)=\alpha. \quad (4.2)$$

Note the linear dependence of the dissipation function $w(\alpha)$ upon α which entails the existence (starting from a sound state with $\alpha = 0$) of a truly elastic phase, with $\alpha = 0$ everywhere, before localization take place. The mechanical properties of energies of the type of (4.1) and for different choices of the constitutive functions (4.2) are analyzed in [Pha+10].

In order to correctly estimate the transverse fracture energy, the normalization constant c_w has to be chosen as $c_w = 4\int_0^1\sqrt{w(\alpha)} = 8/3$; see [Bra98].

In the bulk energy, the function $a(\alpha)$ determines stress softening in the neighborhood of a crack, the stiffness $a(\alpha)A$ drops to $k_\eta A$ in correspondence to a crack ($\alpha = 1$) and is $(1+k_\eta)A$ away from cracks. Hence, $k_\eta A \ll 1$ is the residual stiffness at a cracked point, it is needed to ensure coercivity of the energy with respect to $u \in H^1(\Omega)$.

The notion of approximation of (3.33) by (4.1) can be understood in the sense of Γ-convergence. The elements of the convergence proof are essentially given in [Cha04], in the case without substrate energy ($\Delta = \emptyset$, $\kappa = 0$) and $w(\alpha) = \alpha^2$. The statement can be adapted to the case $\Delta \neq \emptyset$, $\kappa \neq 0$ observing that the additional terms are a continuous perturbation of the functional considered in [Cha04] with respect to which Γ-convergence is stable (see *e.g.* [Bra98]). The extension to more general energies including the case $w(\alpha) = \alpha$ is done in [Bra98] for scalar elasticity and can be generalized without major issues to vectorial elasticity. Note also that, up to the debonding effect, the energy functional (3.33) is equivalent to a vectorial Mumford-Shah functional [MS89], where the role of the "fidelity term" is played here by the elastic foundation.

Γ-convergence further provides the term-by-term convergence of (4.1) to (3.33). In particular the first term in (4.1) converges to the elastic energy of the film (the stiffness $a(\alpha)$ converging to one in the sound domain and to zero in correspondence to cracks). The second term in (4.1) converges to the bonding layer's energy. The third term in (4.1) converges to the length of transverse cracks, *i.e.* the transverse fracture surface energy; finally the last term converges to the surface energy of debonding (the dependence upon η is via the displacement field u).

A functional of the type (4.1), while falling within the class of the elliptic approximations of free discontinuity problems as proposed in [AT90], [AT92], [Bra98], enjoys –at fixed η– an independent mechanical interpretation. It is shown in [Pha+10] that upon requiring additional *constitutive* hypotheses upon the functions $a(\alpha)$, $w(\alpha)$ and their derivatives, other than the sufficient requirements for Γ-convergence (given *e.g.* in

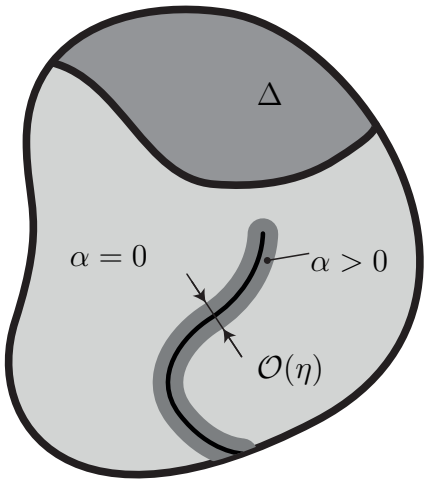

(a) In the regularized model, cracks are represented by the localization of the damage field α within bands of width of order of the internal damage length η. Debonded regions Δ do not need regularization and are computed explicitly from first order stability conditions.

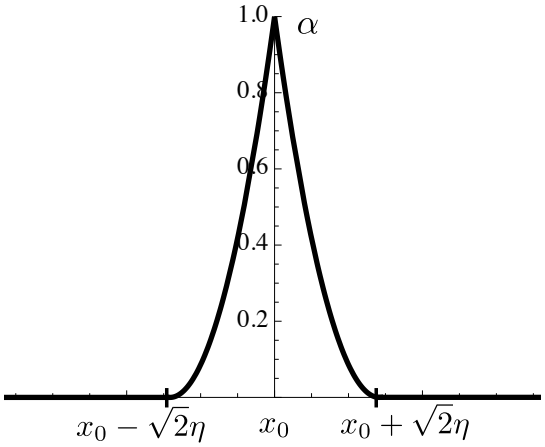

(b) The one-dimensional optimal damage profile for a crack at x_0, constructed with the law (4.2) with $k_\eta = 0$. Damage is positive on a band of width $s\sqrt{2}\eta$, see [Pha+10]

Figure 4.2: In the regularized model cracks are represented by the narrow band in which damage localizes Figure 4.2(a). The profile along a transverse one-dimensional section is shown in Figure 4.2(b).

[AT90], [AT92], [Bra98]), then the regularized energy has to be interpreted as a nonlocal gradient damage functional whose internal length is η, α being the damage field. The choice (4.2) satisfies such additional requirements, hence the energy (4.1) is formally equivalent and qualitatively different from the elliptic approximation in [AT92] since it embodies the new physical phenomenology of possibly irreversible damage processes.

In this sense, discontinuous Griffith models of brittle fracture arise as asymptotic limit models associated to a particular class of nonlocal gradient damage functionals, as their internal length scale (here η) tends to zero. Consequently, the heuristic idea of smeared approximation of fracture surfaces by localized damage is consistent both from a physical and mathematical standpoint.

The additional parameters, with respect to Griffith's functional (3.33), appearing in (4.1) are the internal length scale η and the residual stiffness k_η. The latter ensures coercivity of the energy (hence existence of minimizers when α reaches the value 1). It has to be an infinitesimal with respect to η, *i.e.* $\lim_{\eta\to 0} k_\eta/\eta = 0$. In the numerical experiments it is fixed to a reasonably small value, as a compromise between numerical stability and the correct estimation of the energy. A large value of k_η, indeed, produces a spurious systematic overestimation of the stiffness in the cracked regions, leading to the overestimation of the associated elastic energy and the underestimation of the released energy.

Localization of damage into narrow bands is related to the value of the internal length η, discriminating between regimes of diffused damage and fracture. As studied in detail in [Pha+10] for a one-dimensional bar under traction, for sufficiently long bars the localization of damage in narrow bands of thickness of order η (see Figure 4.2(b)) is a consequence of the selection of solutions by a stability principle. In this regime, the size effect renders unstable solutions with diffused damage. On the other hand, for short bars, solutions with homogeneous diffused damage are observed, thanks to their stability. Since we focus on the phenomena associated to fracture, the value of η is kept much smaller than the characteristic diameter of the computational domain, so that localization is privileged over diffuse damage. Its value is specified in each of the presented experiments.

4.2 The regularized formulation

The static problem. The regularized energy (Equation (4.1)) is suitable for the numeric solution of the static and quasi-static evolution problems. Consequently, the static problem 3.8 is approximated by the solution, at a given load intensity, of:

$$\min\{E_\eta(u,\alpha,\Delta): \quad u\in H^1(\omega;\mathbb{R}^2),\ \alpha\in H^1(\omega),\ 0\le\alpha\le 1,\ \Delta\subseteq\omega\}$$

The quasi-static evolution problem. A natural approach to numerically solve the quasi-static evolution Problem (3.9) is to construct a linear interpolation of the solutions at discrete time steps along a time horizon $[0,T]$. Defining $t_i : 0 = t_0 \le t_i \le t_n = T$,

for $n \in \mathbb{N}^+$, the quasi-static evolution is approximated by the following constrained minimization problem:

$$\min \left\{ E_\eta(u^i, \alpha^i, \Delta^i) : \quad u^i \in H^1(\omega; \mathbb{R}^2), \right. \\ \left. \alpha^i \in H^1(\omega),\ \alpha^{i-1} \leq \alpha^i \leq 1,\ \Delta^{i-1} \subseteq \Delta^i \subseteq \omega \right\}, \text{for } i \in \mathbb{N}^+ \quad (4.3)$$

The proof of the convergence of the regularized evolution problems is given in [Gia05] for the case of scalar elasticity, assuming that at each time one performs a *global* minimization of the regularized energy.

The numerical implementation of the global minimization, both for static and quasi-static problems, still presents major issues due to its non-convexity with respect to the triple (u, α, Δ). In one-dimension methods exist, based on dynamic programming, that are guaranteed to converge to global minimizers of the total energy. Of course, this is at the cost of versatility as these do not generalize easily to the multi-dimensional case. An example of application of such algorithms in a verification test for a problem of variational fracture of thin films under out-of-plane loads is given, in one-dimension and for a non-convex energy, in [MBK13]. Our approach is suited to the numerical simulation of two-dimensional problems in situations where complicated crack and debonding geometries are expected.

We rely on the necessary first order optimality conditions enforcing the weak form of Euler-Lagrange equations on u and α, for admissible test fields verifying the growth condition. Hence, we expect to converge to critical points of the energy E_η. However, taking advantage of the separate convexity of E_η with respect to u, α and Δ, it is guaranteed to converge either to a (local or global) minimizer or a saddle point.

It is well known that such an algorithm applied to a non-convex energy may not converge to a *global* minimizer, but only to a critical point. In the case of the uncoupled problems (transverse fracture or debonding only), this can me mitigated by implementing a *backtracking algorithm* relying on a necessary condition for optimality with respect to the time evolution in the same spirit as [Bou00]. This allows to construct an evolution satisfying necessary conditions for global minimality. In the current situation, when the competition takes place between three terms in the energy, a similar optimality condition can be written, but the construction of an evolution satisfying it is not as straightforward. Moreover, as it highlighted in the sequel, the solution of the problem based upon order one stability conditions has an additional mechanical interpretation. Hence we choose not to enforce necessary conditions for global minimality through a backtracking algorithm.

First order optimality conditions yield the following system of coupled variational problems:

$$u-\text{problem: } D_u E_\eta(u, \alpha, \Delta)(\hat{u}) = 0, \qquad \forall \hat{u} \in H^1(\omega; \mathbb{R}^2) \quad (4.4a)$$

$$\Delta-\text{problem: } D_\Delta E_\eta(u, \alpha, \Delta)(\hat{\Delta} - \Delta) \geq 0, \qquad \forall \hat{\Delta} \supseteq \Delta_{i-1} \quad (4.4b)$$

$$\alpha-\text{problem: } D_\alpha E_\eta(u, \alpha, \Delta)(\hat{\alpha} - \alpha) \geq 0, \qquad \forall \alpha_{i-1} \leq \hat{\alpha} \in H^1(\omega) \quad (4.4c)$$

, where

$$
\begin{aligned}
D_u E_\eta(u,\alpha,\Delta)(\hat{u}) &= \int_\omega \big((1-\alpha)^2 A(e(u)-e_0)\cdot e(\hat{u}) + \kappa u\cdot\hat{u}\,(1-\chi_\Delta)\big)\,dx \\
D_\Delta E_\eta(u,\alpha,\Delta)(\hat{\Delta}) &= \int_\omega \Big(\gamma - \frac{\kappa}{2}u\cdot u\Big)\,\chi_{\hat{\Delta}}\,dx \\
D_\alpha E_\eta(u,\alpha,\Delta)(\hat{\alpha}) &= \int_\omega \left(-(1-\alpha)A(e(u)-e_0)\cdot(e(u)-e_0) + \frac{c_w}{\eta}\right)\hat{\alpha}\,dx \\
&\quad + \int_\omega c_w\,\eta\nabla'\alpha\cdot\nabla'\hat{\alpha}\,dx
\end{aligned}
$$

To solve this system at each time-step we extend the alternate minimization algorithm used in [BFM08] for two and three dimensional elasticity without the presence of the bonding layer, to the present three-field case. We solve iteratively each subproblem with respect to the corresponding field, leaving the other two fixed to the previously available values. We resume in Algorithm 1 the numerical scheme. More precisely, we first solve in this way the $u-\Delta$ subproblem (elasticity-debonding) until convergence at fixed α (lines 7–13, Algorithm 1) and than iterate solving the α-problem (lines 14–16, Algorithm 1). The u-problem (*i.e.* the mechanical equilibrium) at fixed α and Δ is a linear unconstrained variational equation.

The solution of Problem (4.4b) at fixed u and α (*i.e.* the debonding criterion) is explicit and local in space. Considering the irreversibility condition on the debonding set, the condition (4.4b) simply gives $\chi_\Delta(x)=1$ if either the displacement exceeds the critical threshold at the point x or if it is already debonded.

The α-problem at fixed u and Δ (*i.e.* the fracture criterion) is a linear, bound constrained, variational inequality.

The regularized functional is finally discretized by piecewise linear finite elements. Provided that the characteristic diameter of the discrete elements h is $o(\eta)$, the convergence of the discretized functionals to the regularized energy is proved in [BC94], [Bou02] in the case of scalar elasticity. The physical domain ω is discretized with an unstructured conforming triangulation by a Delaunay algorithm and the discretization of the fields is done by standard finite elements of class $\mathcal{P}^1$ on the fixed mesh. The discrete approximation of E_η is constructed by projection onto a discrete space of piecewise linear functions [Cia78]. Classical results (see *e.g.* [BC94], [Bou02]) ensure Γ-convergence of $E_{\eta,h}$ to E_η as $h \searrow 0$ and compactness of minimizers, provided that $h \ll \eta$. Unstructured meshes are preferred to structured ones as the latter are known to induce anisotropies of the Hausdorff metric, hence a spuriously anisotropic toughness in the weak limit problem as $(h,\eta)\searrow 0$, see [Neg99]. The computational mesh is uniformly fine (the mesh is such that $h \ll \eta$) in order to capture and represent the steep gradients within the localization band. A coarse mesh produces a systematic overestimation of the dissipated surface energy, the first order interpolation error due to the discretization being of the order h/η, as it can be seen in the construction of the lower bound inequality in the finite element approximation result, see *e.g.* [BFM08, Chapter 8].

A note on the implementation. The problem of mechanical equilibrium (Equation (4.4a)) is a linear, unconstrained variational equality which we solve using standard iterative Krylov Subspace Solvers, the linear steps being solved with a preconditioned conjugated gradient algorithm. On the other hand, the fracture problem (Equation (4.4c)) is a linear, constrained, variational inequality which we solve using the bound-constrained Newton Trust-Region solver provided by the optimization toolbox `TAO` [Mun+12]. Parallel data representation and linear algebra are based on the `PETSc` toolkit [Bal+12].

Init: $u_0, \alpha_0, \chi_0 \leftarrow 0$, $\mathrm{tol} = 10^{-4}$; /* Sound, unloaded */
for $i = 1 : n$ **do**
  $u_i, \alpha_i, \chi_i \leftarrow u_{i-1}, \alpha_{i-1}, \chi_{i-1}$; /* Initial guess: solution at previous TS */
  $\alpha_i^{\mathrm{old}} \leftarrow \alpha_i$;
  repeat /* Alternate minimizations */
    $\chi_i^{\mathrm{old}} \leftarrow \chi_i$;
    repeat /* Solve for (u, χ) */
      u_i solution of (4.4a) with $\alpha = \alpha_i$, $\chi = \chi_i$; /* Linear elastic solver */
      $\chi_i \leftarrow \chi_{i-1}$;
      $\chi_i(x) \leftarrow 1$ if $|u_i(x)| > u_c$ /* Debonding: solve (4.4b) with $\alpha = \alpha_i$ */
      $\mathrm{err}_\chi = \sup(\chi_i - \chi_i^{\mathrm{old}})$;
      $\chi_i^{\mathrm{old}} \leftarrow \chi_i$
    until $\mathrm{err}_\chi = 0$;
    α_i solution of (4.4c) with $u = u_i$, $\chi = \chi_i$; /* Constrained solver for α */
    $\mathrm{err}_\alpha = \|\alpha_i - \alpha_i^{\mathrm{old}}\|_\infty$;
    $\alpha_i^{\mathrm{old}} \leftarrow \alpha_i$
  until $\mathrm{err}_\alpha \leq \mathrm{tol}$;
end

Algorithm 1: Algorithm for the solution of the quasi-static time-discrete evolution problem with transverse fracture and debonding. At each time step t_i, minimization in (u,χ) and α is performed until convergence. For the sake of conciseness, we replace here χ_Δ by χ.

4.2.1 Mechanical interpretation of the regularized model with local minimization

The regularized energy (4.1) falls within the class of the Ambrosio-Tortorelli approximations of free discontinuity problems and is an instance of a non-local damage functional. Indeed, the functions $w(\alpha), a(\alpha)$ besides satisfying the hypotheses required for the Γ-convergence approximation result (see [Bra98]), verify the additional constitutive assumptions that allow us to identify $a(\alpha)$ as stiffness function, $w(\alpha)$ as a dissipation function and $\alpha(x)$ as a damage function, see [Pha+10]. The parameter η is the internal characteristic length of the damage functional, and in this sense it has to be thought as a material parameter: its value discriminates the regimes of diffuse damage for values of η comparable to the size of the structure and localized damage (*i.e.* fracture) for

small values of η compared to the size of the structure. The evolutions associated to the computed solutions of (4.3), numerically obtained enforcing the order one necessary *local* optimality conditions, are consistent with the notion of irreversible evolution of energetically stable states, *i.e.* of unilateral local minimizers of the total energy. In this sense, transitions between states take place in correspondence to the loss stability of the energy-minimizing states. Although a study of the stability properties of the energy $E(u, \alpha, \Delta)$ of Equation (4.1) depending upon the parameters $(\kappa, \nu, \gamma, \eta)$ is beyond the scope of this work, we provide an interpretation of the critical loads in the one-dimensional traction test of a slender strip in Section 4.3.1.

The introduction of the additional length scale η determines the boundedness of the set of admissible stresses corresponding to the sound solution. Denoting by $\sigma = a(\alpha)A\left(e(u) - e_0\right)$ the (non-dimensional) stress tensor in the film, equation (4.4c) implies that an elastic state where $\alpha = 0$ is admissible only if

$$A^{-1}\sigma \cdot \sigma \leq \frac{3}{8\eta(1 + k_\eta)}. \tag{4.6}$$

The inequality above gives an explicit relation between the internal length η and the elastic limit stress σ_c in the film, showing that $\sigma_c \propto 1/\sqrt{\eta}$.

4.3 Numerical experiments

We perform three sets of numerical experiments to illustrate the capabilities of the formulation in simple cases. We focus on multiple cracking and possible debonding of a slender strip, of a disk and on cracking of a geometrically complex domain. The first set of experiments is also intended to verify the numerical code against the closed form solutions presented in Chapter 2, (see also [Leó+13d]). The second set of experiments shows the capability of capturing geometrically complex two-dimensional crack patterns. The third experiment provides a qualitative comparison with a real-life example inspired by the multiple cracking of a vinyl lettering panel. Lastly, we introduce a numerical experiment in which we observe the appearance of a coupled front of two parallel cracks plus debonding which selects an optimal spacing. This emerging distance is related to the internal elastic length scale. Such patterns have been reported by [SW03] and later isolated by [Mar+].

In what follows, we consider the systems loaded by an inelastic isotropic strain $e_0 = tI_2$ increasing linearly with time.

4.3.1 Multiple cracking and debonding of a slender strip

We perform a set of verification experiments for the problem of multifissuration and delamination of a one-dimensional stiff film bonded to a substrate. Let us consider a slender brittle elastic body, its reference domain being $\omega : \{x \in [0, x_0 L] \times [0, x_0 a]\}$, with $a \ll L$. To get an exact reference solution, the problem may be conveniently approximated by the one-dimensional model considered in Chapter 2, provided that

$a \ll \ell_e$, where $\ell_e = \kappa^{-1/2}$ is the characteristic length of the elastic problem. The condition $a \ll \ell_e$ implies that the stress field, under an equi-biaxial imposed inelastic strain, is essentially uniaxial.

The computational domain is of unit length and height $a = 2 \cdot 10^{-2}$, it consists of approximately $7 \cdot 10^3$ degrees of freedom. The average mesh size is $h = 2 \cdot 10^{-3}$, the value of $\eta = 2 \cdot 10^{-2}$ is held fixed for the three experiments, the ratio η/h is 10 and in the quasi-static simulation we consider load up to $T = 11.0$. Note that as long as $\eta \ll \ell_e$ no coupling arises at the length scale of η between the damage localization bands and the elastic displacement field which varies over a length scale of order ℓ_e.

We perform numerical experiments based on the closed form evolutions analyzed in Chapter 2. Recall that the analytical computations are obtained by a *global* minimization statement whereas the numerically computed solutions presented here satisfy first order local optimality conditions and are not necessarily global minimizers.

Transverse fracture experiment In Figure 4.4 we represent the outcome of a transverse fracture experiment. The non-dimensional parameters characterizing the experiment are: $\kappa = 36.0$ and $\gamma = 10 \cdot 10^4$. The chosen stiffness ratio κ corresponds to an internal characteristic elastic length scale $\ell_e = 1/6$, hence $\eta/\ell_e = 0.12$. The sound elastic energy branch loses stability at $t = 4.81$, see Figure 4.4(c), the system jumps towards the cracked state with one transverse crack in the center of the domain. This releases elastic energy at the expense of the surface energy, as it can be seen in the energy chart in Figure 4.4(c). As the load increases further, the system undergoes the elastic loading phase of the two segments. At $t = 7.46$ the loss of stability of this state leads to the appearance of two add-cracks, each at the middle of the segments. The snapshot of the last loading step is shown in Figure 4.4(a), the profile of the displacement and fracture fields is shown in Figure 4.4(b). The computed energy branches are seamlessly superposed to the analytical ones. Nonetheless, as it is observed in the space-time chart in Figure 4.4(d), critical times at which cracking happens differ between the numerical experience and the analytic computation due to the global *vs.* local setting of minimization. As expected, the critical loads corresponding to the local minimization criterion systematically overestimate those satisfying the global criterion.

The critical fracture loads are interpreted under the light of the considerations sketched in Section 4.2.1. Using a one-dimensional model, the critical load for the purely elastic domain is computed analytically using Equation (4.6). Indeed, for the elastic solution ($\alpha = 0$), the stress σ as a function of the load may be easily computed analytically, recall Equation (2.6). Substituting this expression into Equation (4.6), one finds that purely elastic solutions are admissible for loadings not greater than

$$t_c(\kappa, \eta) := \frac{\sqrt{3/8}}{\sqrt{\eta\,(1 + k_\eta)}} \frac{1}{\left(1 - \operatorname{sech}\left(\frac{\sqrt{\kappa}}{2}\right)\right)}. \tag{4.7}$$

The critical load for the equilibrium, sound, elastic solution is plotted in Figure 4.3 as a function of the stiffness ratio κ for $\eta = 0.02$. It is a monotonic function of κ decreasing

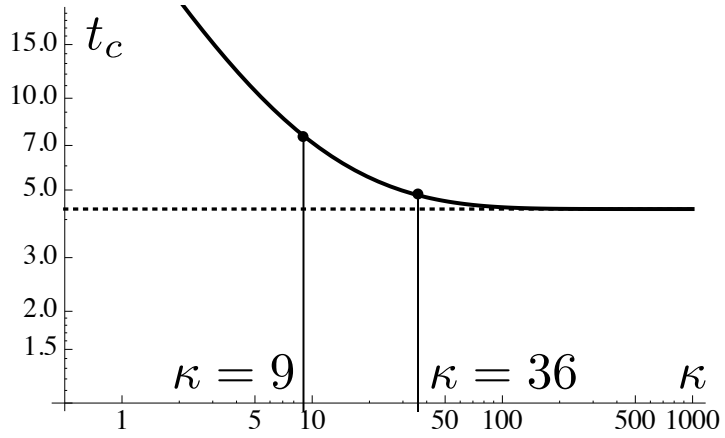

Figure 4.3: Critic loads of the transverse fracture experiments are compared to the elastic limit (Equation (4.6)) computed with the stability condition (4.4c) and plotted against the relative stiffness κ. The plot is for $\eta = 0.02$. The asymptote $\kappa \to \infty$ corresponds to the limit case of a long film with homogeneous stress. For $\kappa \to 0$ the critic load $t_c \to \infty$, this corresponds to the limit case of system in which no energy is stored in the bonding layer and the film freely accommodates the inelastic strain.

from $+\infty$ for $\kappa \to 0^+$ to $\sqrt{3/8\,\eta(1+k_\eta)}$ for $\kappa \to \infty$. In the same figure, we display with black dots the critical load captured by the numerical experiment. The first transverse fracture appears for the strip of stiffness ratio $\kappa = 36.0$ for $t = 4.81$. It creates two uncracked strips of half-length that, recalling the definition of κ, have an equivalent stiffness ratio $\kappa/4 = 9$. Both these two strips further break into two parts at the second critical load $t = 7.46$. Both critical loads coincide, within a small error, with the critical loads of the elastic solution given by Equation (4.7) for κ equal to 36 and 9, respectively (see Figure 4.3). Indeed, as done in [Pha+10] for the case of a bar in traction, it may be shown that for sufficiently long strips the elastic limit also coincides with the stability limit of the solution without damage localizations (*i.e.* fractures). When exceeding this limit, the fundamental undamaged solution becomes unstable. At this load, the numerical algorithm based on alternate minimizations detects new descent directions and reaches a new (stable) solution branch, implying newly added cracks. Note that after the first transverse crack, the first order stability properties of the two cracked segments are almost insensitive of the half crack localizations at the boundaries. This does not hold asymptotically when inducing further fragmentation, upon increasing the load and producing small segments whose characteristic elastic length is comparable to the internal length η associated to the damage localization. This regime is not explored in the present work and left for further investigation. In all the experiments the internal length of the damage process η is kept smaller than the elastic length $\ell_e = \kappa^{-1/2}$.

Debonding experiment Figure 4.5 refers to a debonding experiment with the same equivalent stiffness $\kappa = 36.0$ as the preceding case (and hence the same elastic length

$\ell_e = 1/6$) and a lower toughness ratio $\gamma = 0.50$. The sound elastic bonded branch is followed by the debonding phase whose onset is at $t = 2.25$. Elastic energy is continuously released at the expense of the debonding surface energy. The total energy asymptotically approaches the limit energy of the completely debonded film $E_\infty = L\gamma$. The computed energy coincide with the analytical ones and also the evolution are identical. In fact, unlike the perfectly bonded transverse cracking experiment, both in the numerical and closed form computations, the evolution of debonding relies only on first order optimality conditions, see Chapter 2.2.2. A snapshot of the last time step is displayed in Figure 4.5(a), the displacement and debonding fields are shown in Figure 4.5(b). The debonded domain is symmetric with respect to the axes of the film. In the debonded domain, the displacement is linear and accommodates the imposed inelastic strain, the energy vanishes therein. We remark that in spite of the lack of uniqueness of the displacement field in the debonding problem (recall from Section 2.2.2 that all states with equal debonded length have equal energy, irrespective of the location of the debonded region), numerical computations seem to favor symmetric solutions. The space-time chart in Figure 4.5(d) illustrates the evolution showing the bonded domain for a given load intensity.

Coupled experiments Experiments in Figures 4.6 and 4.7 show the interplay between the two failure modes. In these two experiments, the system exhibits one (resp. three) transverse cracks prior to peripheral debonding. The evolutions are obtained choosing $\kappa = 36.0$ ($\ell_e = 1/6$) and $\gamma = 2.2$ (resp. $\kappa = 64.0$ *i.e.* $\ell_e = 1/8$, and $\gamma = 3.1$). The corresponding energy chart and state diagrams are shown in Figures 4.6(c) and 4.7(c). A higher order effect is observed at the onset of debonding for the second coupled experiment due to the boundary layer induced in the neighborhood of the middle crack due to local softening. This breaks the symmetry of the boundary conditions for the two segments. The effect is visible in the space-time evolution and in the debonding and elastic energy terms in Figure 4.7(d), although not noticeable at the global level of the total energy.

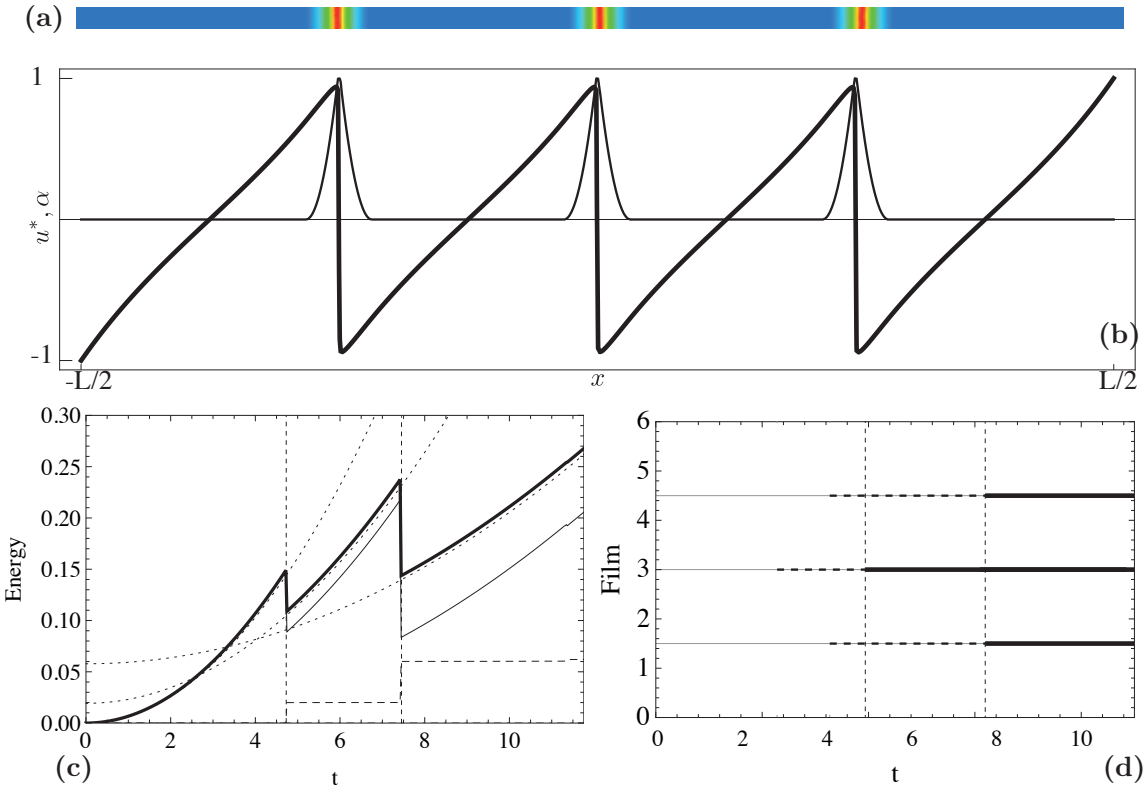

Figure 4.4: Top: snapshot of the fracture field at $t = T$ for the perfectly bonded transverse fracture experiment. Cracks are equidistributed and represented by the localization of the damage field α. The values of $\alpha \in [0, 1]$ are mapped onto a "inverted-hot" color table, blue corresponding to $\alpha = 0$ (sound material), red corresponding to $\alpha = 1$ (fully developed fracture). Middle: displacement and fracture field along the axis $[-L/2, L/2] \times \{0\}$ for $t = T_{max}$. The displacement field $u^*(x) = u(x)/\max_{x\in\omega} u(x)$ is normalized and displayed with a thick solid line. The fracture field α is shown with a thin black stroke. Bottom: in the energy chart (left) the total energy is plotted in bold line, the energy transverse fracture energy with a dashed line and the elastic energy with a thin solid line. Grid lines indicate the critic loads for transverse cracking. The total energy of the closed form solutions of Section 2.2.3 is plotted with a dotted line. In the space-time evolution diagram (right), the domain ω is represented on the vertical axis and the load on the horizontal axis. Solid black horizontal lines indicate the position of cracks during the evolution.

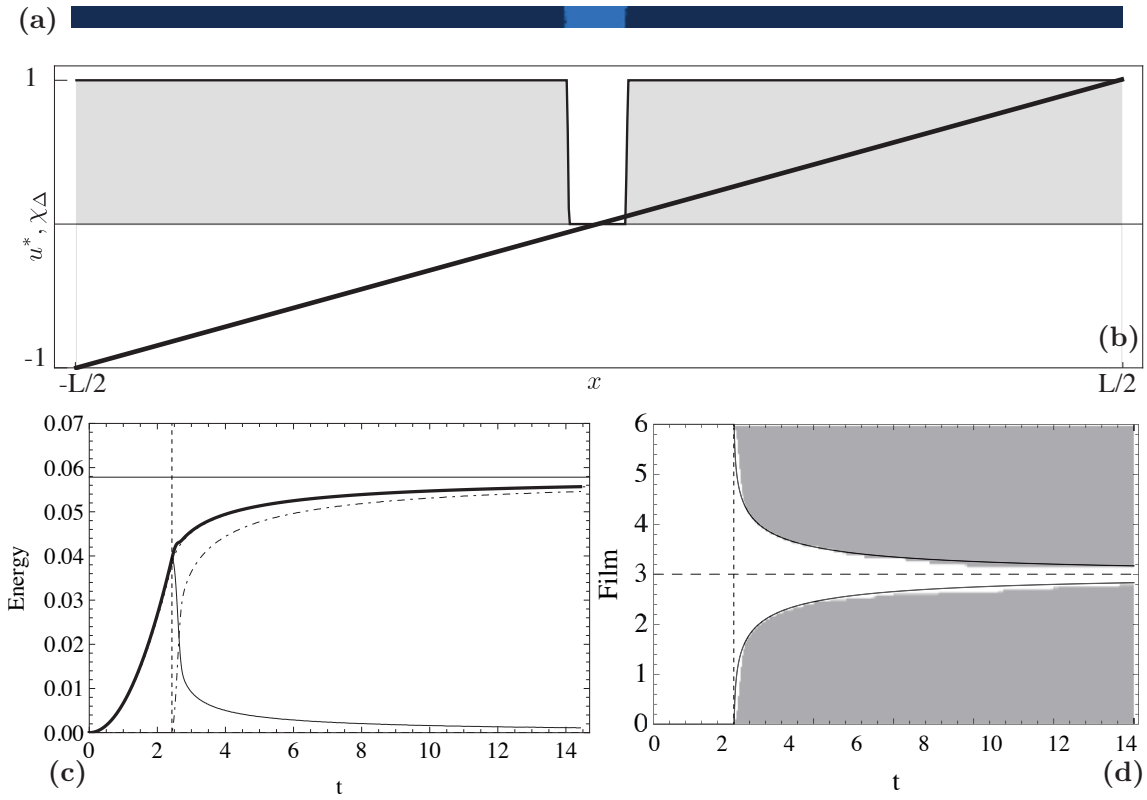

Figure 4.5: Top: Fracture and debonding fields at $t = T_{max}$ for the deboonding experiment. Debonding ($\chi_\Delta(x) = 1$ is the darker area) is symmetric about the two axes. Middle: The characteristic function of the debonded domain is shaded gray, displacement is plotted with a thick stroke. Note that, in debonded regions, the displacement in linear and accommodates the imposed strain. Bottom: energy chart (left) and evolution diagram (right). The asymptote in the energy chart corresponds to the limit energy of a completely debonded film. Debonding onset and its evolution coincide in both numeric and analytic computations as they are derived as consequences of the first order necessary condition for energy optimality. The thin black line in the space-time evolution plot (right) is the analytical solution to the debonding problem obtained, see 2.2.2.

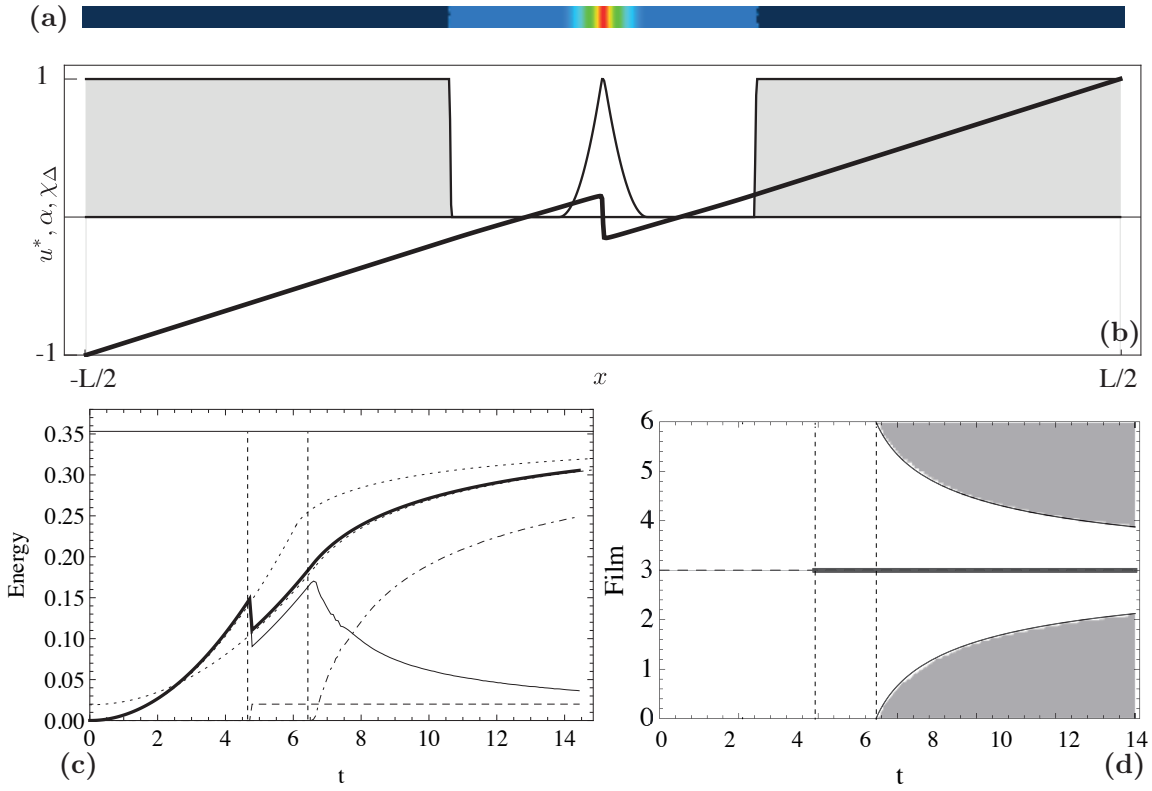

Figure 4.6: Top: fracture and debonding fields on the reference domain ω at $t = T_{max}$ for the first coupled experiment; we observe one transverse crack in the center and symmetric debonding starting from the boundaries. Middle: a single crack in the center of the film, the symmetric debonded region and the displacement field. Bottom: the analytic solution (global minimization) anticipates the appearance of the crack of the numerical experiment (local minimization). The debonding onset and evolution in both cases are equal.

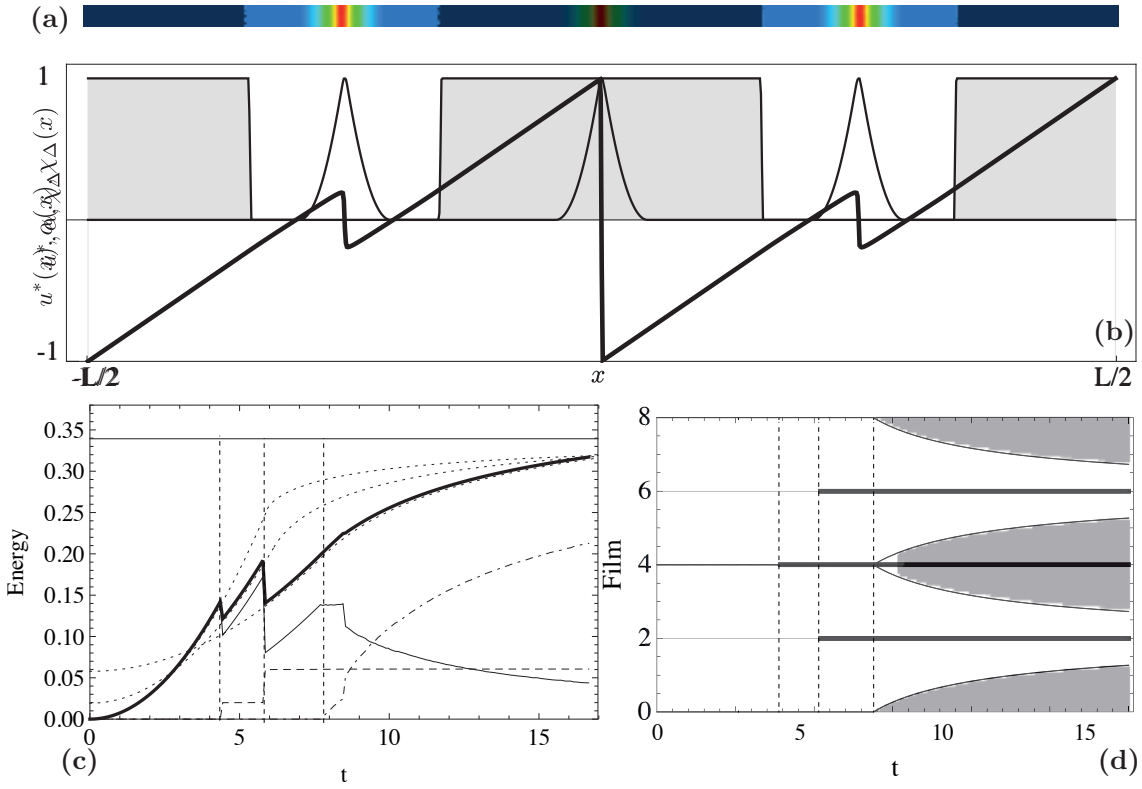

Figure 4.7: Top: fracture and debonding fields on the reference domain ω at $t = T_{max}$ for the second coupled experiment; we observe three equidistributed transverse cracks and debonding starting from the free boundaries of each segment. Middle: three equidistributed cracks (thin solid), debonded region (light gray shaded) and displacement field (thick solid). Bottom: energy chart and space-time evolution of the film. In (right) horizontal lines identify the position of the cracks: solid and dotted lines refer to the numerical experiment and the analytic solution, respectively. Note the higher order effect due to softening at the onset of debonding in the center, at $x = 4$.

4.3.2 Multiple cracking and debonding of a thin disk

We illustrate the ability to capture complex crack geometries and time-evolutions considering the problem of a homogeneously prestressed circular elastic wafer. We analyze qualitatively the outcome of the experiments showing its soundness on a mechanical basis and its coherence with mechanical intuition and commonly reported experimental observations.

The computational domain is of unit radius, each experiment is univocally identified by four non-dimensional parameters: the relative stiffness κ, the relative toughness γ, the Poisson ratio ν and the maximum load intensity T.

We introduce a non-homogeneity in order to explore more complex crack patterns around the sound elastic state. In the center of the wafer, we place a domain $\mathcal{D}_\eta$ of size of $\mathcal{O}(\eta)$ where we set $\alpha = 1$, see Figure 4.8(a).

Multiple cracking only The non-dimensional parameters for this experiment are $\kappa = 800.0$ ($\ell_e = 0.28$), $\gamma = 18.4, \nu = 0.3$ and $T = 7.54$. The wafer undergoes a first elastic loading phase during which the domain $\omega \setminus \mathcal{D}_\eta$ remains sound, identified in the energy chart of Figure 4.9 by the parabolic, elastic energy branch. As the load increases, nucleation is localized in the neighborhood of the domain $\mathcal{D}_\eta$. Sudden fracture occurs at $t = 4.0$: a network of cracks of finite length appears in a single loading step and a network of hexagonal polygons forms. We observe a non-axisymmetric solution to a problem with axisymmetric data, not surprising when dealing with bifurcation problems with nonconvex energies. Away from the boundaries, the cracks are structured in a network of six hexagons, all with the same characteristic diameter. We capture spontaneous nucleation of cracks within the domain, away from possible boundary non-homogeneities, with preference of $2\pi/3$-junctions over $\pi/2$-junctions. In this regime, the sound solution is stable until load intensities high enough to release sufficient energy to pay for the creation of the network of cracks, which, in the numerical experiment, consists in six hexagons. Fracture patterns with $2\pi/3$-junctions are observed in the experiments of [GK94], [San+07], [TA06]. More commonly, experiments on thin film fracture under isotropic and homogenous loads reports irregular *mud cracks* with $\pi/2$-junctions. This is supposedly related to a regime in which the material heterogeneities and imperfections dominate the nucleation phase letting a cracks appear at lower load levels. In fact, in the cited experimental references, the predominance of $2\pi/3$-junctions is prominent in regimes where cracking is less likely, or equivalently, when cracking appears for high (non-dimensional) load intensities, that is, for systems in which the film's thickness is close to the so-called critical thickness h_c. The latter quantity identifies the thickness below which no cracking is observed in the experimental conditions, *i.e.* at a given load. A shift, from $\pi/2$ to $2\pi/3$, of the distribution of the joint angles, is reported in [GK94] in the regimes where the thickness of the film h_f approaches h_c and in [Goe+10] along cyclic loading tests which favour crack reorganization and *maturation*.

Note that when cracks intersect a free boundary (either the domain boundary $\partial\omega$ or an existing crack) form a right angle, instead of the $2\pi/3$ angles observed in the spontaneous nucleation in the bulk of the sound domain. This is the case for all six

intersections with the edge of the wafer. Indeed, under homogeneous loads near a free boundary, the direction of maximum stress is parallel to that boundary and elastic energy release per unit of crack length is maximized by a crack advancing perpendicularly to it. As soon as cracks are close enough to be able to interact, they turn and produce the same phenomenology observed for the intersection of a crack with a free boundary. In Figures 4.8(b) and 4.8(c) we observe a crack turning to approach the existing crack at an angle of $\pi/2$.

As the load intensity increases further, new cracks are created by subdivision of the polygons. New isolated cracks appear forming joints at $\pi/2$ with pre-existing cracks of free boundaries, and new $2\pi/3$-joints form, see Figures 4.8(d)-4.8(f). The crack pattern becomes tighter, all polygons having the same characteristic size. As the polygons become smaller, new joints at sound points are less likely to appear and straight joints become predominant.

Multiple cracking and debonding Reducing the toughness of the bonding layer to $\gamma = 5.6$, all other conditions held fixed, highlights the interplay between transverse cracking and debonding. The evolution of the elastic sound phase and the first stages of cracking are the same as in the previous experiment, as it can be seen in the energy chart of Figure 4.11. Since polygons have different sizes, unlike in the one-dimensional experiment, debonding does not appear simultaneously at the boundary of each polygon. At $t = 5.0$ the largest cells start debonding from the outer boundary. As the load increases further, smaller polygons undergo debonding. At $t = T$ all polygons have debonded and the diameter of the bonded regions is the same in all polygons. In this experiment, like in the one-dimensional slender strip, we observe a size effect due to the existence of an intrinsic characteristic length scale. The latter is revealed by the fracture processes. Indeed, the competition between the surface energies fixes the maximum diameter (at a given load) of the domain that can be completely bonded. This quantity is a decreasing function of the load and it determines a threshold distinguishing two phenomenologically different regimes: that of multiple cracking and that of extensive debonding. Cracking will occur as long as the size of the subdomains identified by the cracks is smaller than the maximum diameter of the domain that can be completely bonded. With the increase of the load and sequential cracking, debonding is triggered in correspondence to subdomains where this threshold is exceeded. Debonding is hence energetically favorable and releases energy continuously with the increasing load, no additional transverse cracks appear and the energy is only released through debonding. In the energy chart (Figure 4.11), the transverse fracture surface energy stays constant after the onset of debonding. In this sense, the experiments presented here are *weakly* coupled, for multiple cracking and debonding do not occur simultaneously in order to release the stored elastic energy but the latter follows the former, the transition between the two phenomena being determined by the size effect. Analytic proofs of this qualitative argument have been given in one dimension in Chapter 2.

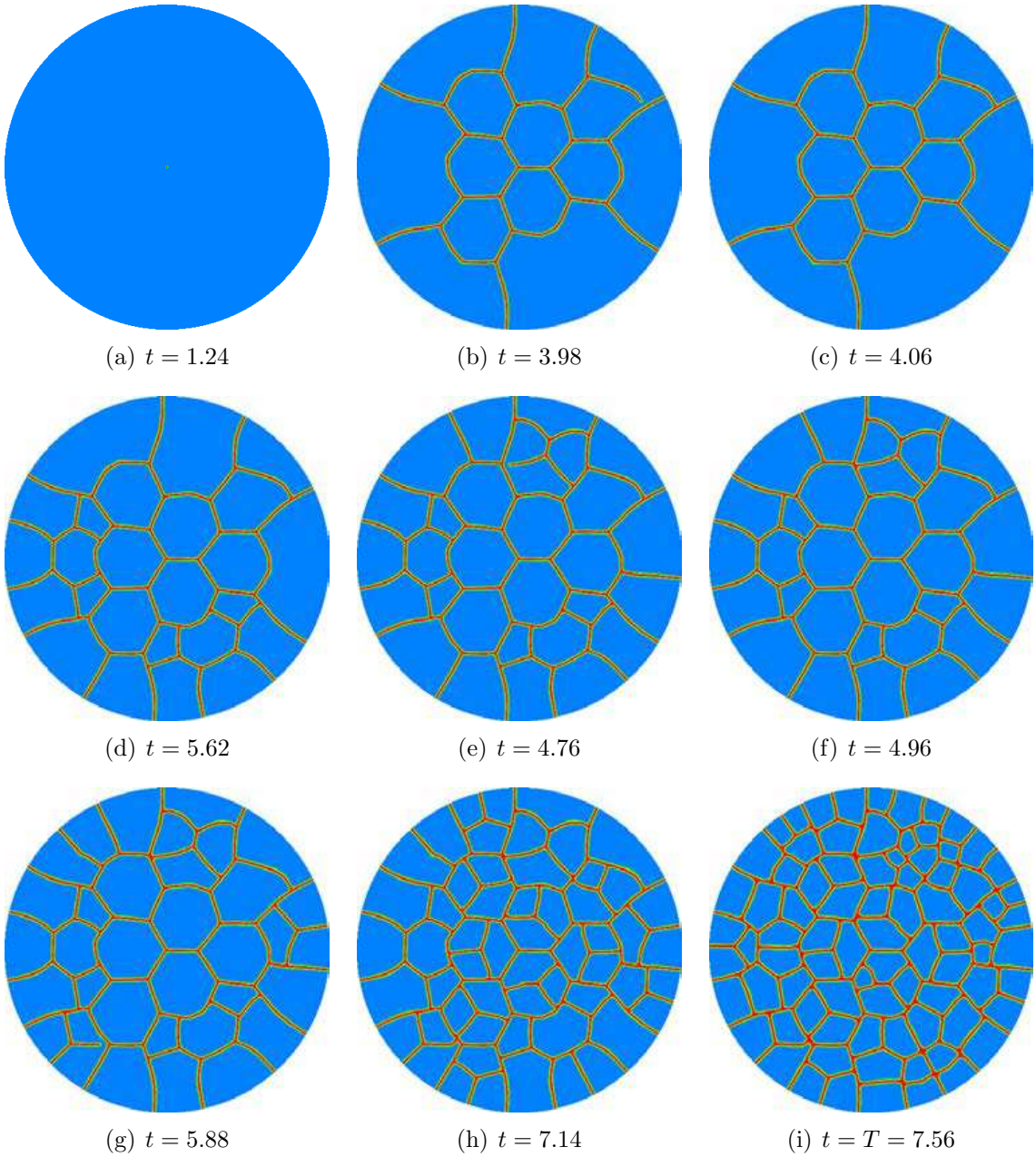

(a) $t = 1.24$ (b) $t = 3.98$ (c) $t = 4.06$

(d) $t = 5.62$ (e) $t = 4.76$ (f) $t = 4.96$

(g) $t = 5.88$ (h) $t = 7.14$ (i) $t = T = 7.56$

Figure 4.8: Snapshots of the fracture field in the wafer experiment under uniform load. The first fracture pattern consists of periodic hexagonal cells while for higher loadings, new cracks intersect preexisting boundaries at a right angle.

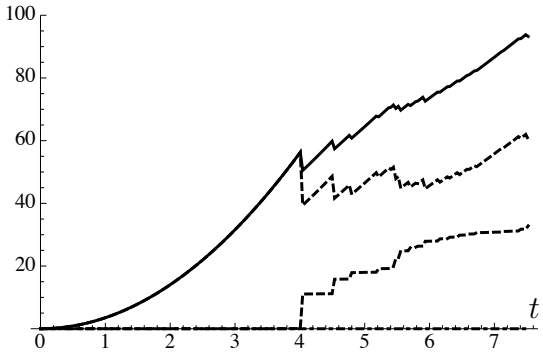

Figure 4.9: Energy chart for the transverse fracture wafer experiments, the corresponding snapshots are shown in Figures 4.8. Total, elastic, and surface energies are plotted with thick solid, thin solid, and dashed lines, respectively. A network of six hexagonal cracks appears at $t = 4.0$.

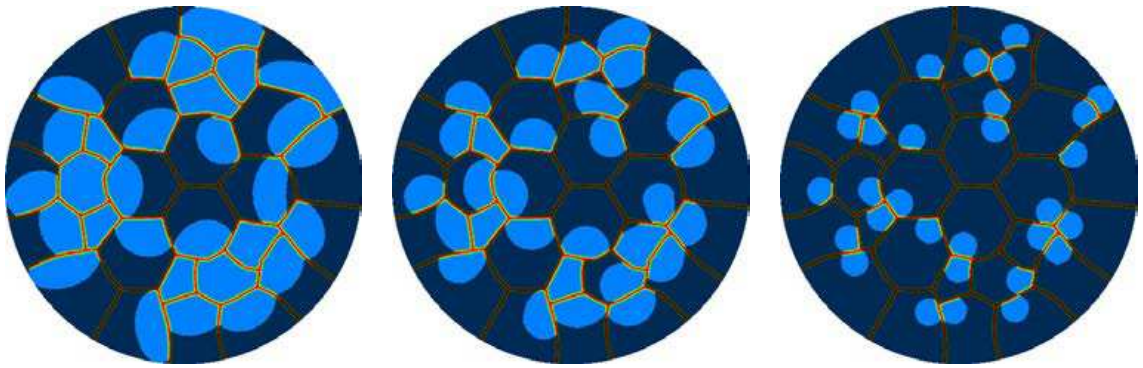

(a) $t = 5.44$ (b) $t = 7.14$ (c) $t = T = 7.56$

Figure 4.10: Combined fracture and debonding experiment of a wafer. Dark areas identify debonded regions whose first onset is at the boundaries of the largest cells, for $t = 5.00$. At the last time step all cells have undergone debonding, in each of these, the diameter of the bonded domain is the same.

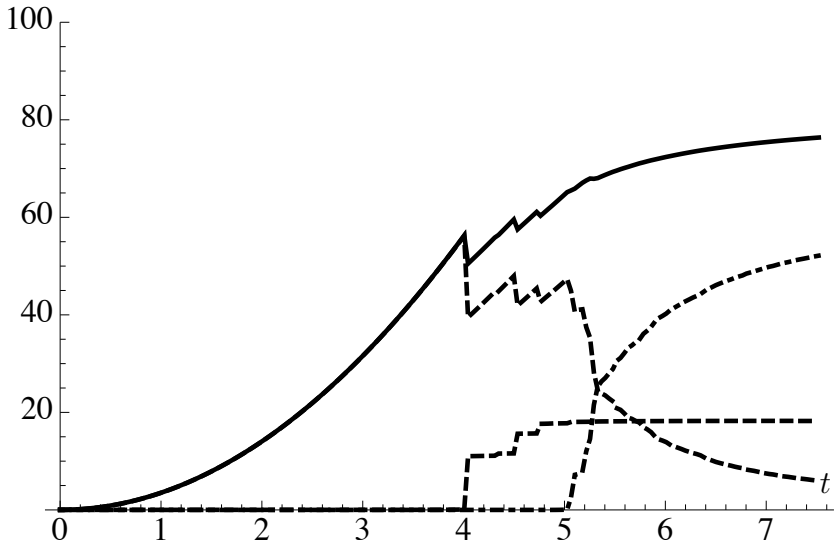

Figure 4.11: Energy chart for the coupled fracture and debonding wafer experiment, the corresponding snapshots are shown in Figures 4.10. The evolution of the initial stages of cracking is the same as in the transverse fracture experiment, see Figure 4.9. After the onset of debonding at $t = 5.0$ in no other cracks form and the fracture energy remains constant.

4.3.3 Vinyl lettering on a metal substrate

This numerical experiment is inspired by a real-life example, given by the stickers identifying research labs at the École Polytechnique in Palaiseau, France. A thin vinyl sticker is bonded to a metal panel and exposed to atmospheric conditions. Among other effects, the incident radiation from the sun generates inelastic mismatch strains leading to transverse cracking and possibly debonding. The inelastic stresses are due to shrinkage of the sticker, evidenced by the trace of glue left on the panel. A few panels relative to numbers in the range "401"–"408", all of the same material and subject to similar loading conditions, show recurring crack patterns. One picture is reproduced in Figure 4.14. From the analysis of the current state, we infer some qualitative informations about the evolution of the cracking process. The succession of cracks in time can be related to the opening of crack lips: wider apertures indicate cracks appeared at earlier stages of loading. Peripheral debonding is present but limited to a tiny region. Comparing the cracks of all stickers (not shown here), the robustness of crack patterns is striking. The first cracks are the ones at the center of the number "4", nucleating from the weak geometric singularities. Within the number "0", the first four cracks appear in the lower and upper lobes. After, cracks open in the two longest vertical sides. The stem of the number "1" exhibits almost equidistributed cracks, the extreme aspect ratio producing almost one-dimensional solutions. Foot's and head's serifs are responsible of stress concentration and favor the appearance of cracks whereas slender segments show almost equidistributed cracks.

We perform a numerical experiment meshing a domain corresponding to the number "401". Material parameters as well as numerical parameters are the same for all digits and, in order to proscribe debonding, we set a high value for the toughness ratio $\gamma = 2 \cdot 10^4$. We decide for simplicity not to include the effect of debonding in the numerical experiment. Consequently the only parameters identifying the experiment are the relative stiffness $\kappa = 17.68$ (the corresponding elastic length is $\ell_e = 0.056$), the Poisson ratio $\nu = 0.3$ and the internal length $\eta = 72 \cdot 10^{-4}$. The characteristic diameter of the triangular elements is $h = 12 \cdot 10^{-4}$ and the ratio h/η is 6. The digits "4", "0", "1" consist of (1.6, 0.6, 0.3)$\cdot 10^6$ dofs respectively. We do not model the circadian loading and impose a uniform equi-biaxial inelastic strain increasing linearly with time. Figure 4.12 shows the energy evolution and Figure 4.13 successive snapshots of the crack field on the reference configuration. The first cracks appear at the intersection of the stem and the crossbar of the number "4" nucleating at the weak geometric singularities, see Figure 4.13(a). A triple junction is first created by three cracks originating at the North-East, North-West and South-West corners. Subsequently a third crack nucleating at the South-East corner intersects the free edge just created at a right angle. The same pattern is observed for the vinyl sticker. In Figure 4.13(c) the stem and crossbar of the number "4" are cracked at the center and respectively two and one cracks are produced at their intersection with the diagonal segment. In the numeric experiment, six cracks appear simultaneously in the number "0", two in each lobe (upper and lower) and one horizontal crack at the center of each of the two side arches. The crack pattern is symmetric. Here, the aspect ratio of the domain plays an important role and, as the width-to-height ratio increases, the

cracks on the side arches are favored over those on the lobes. For the same load intensity, the number "1" shows three cracks at the serifs and two in the stem. The cracks at the serifs are favored by the sudden thickness variation and match the observed pattern. At higher loadings, periodicity of the cracks becomes prominent (Figure 4.13(d)) and secondary cracks (orthogonal to the former) appear (Figures 4.13(e-f)). A comparison of the observed patterns and our numerical experiments is shown in Figure 4.14.

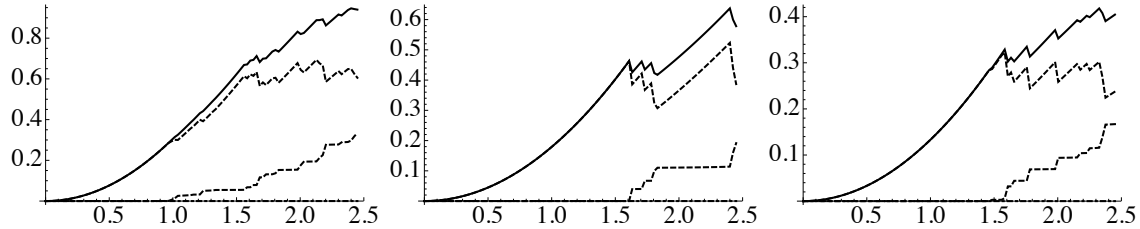

Figure 4.12: Energy charts for the subdomains corresponding to the digits "4", "0", and "1".

Figure 4.13: Computed crack pattern at (a) $t = 1.05$, (b) $t = 1.25$, (c) $t = 1.65$, (d) $t = 1.88$, (e) $t = 2.15$, (f) $t = 2.48$

(a) Cracked lettering at École Polytechnique, Palaiseau, France. A vinyl sticker is bonded to an aluminum substrate and exposed to the Sun which causes tensile stresses and subsequent cracking.

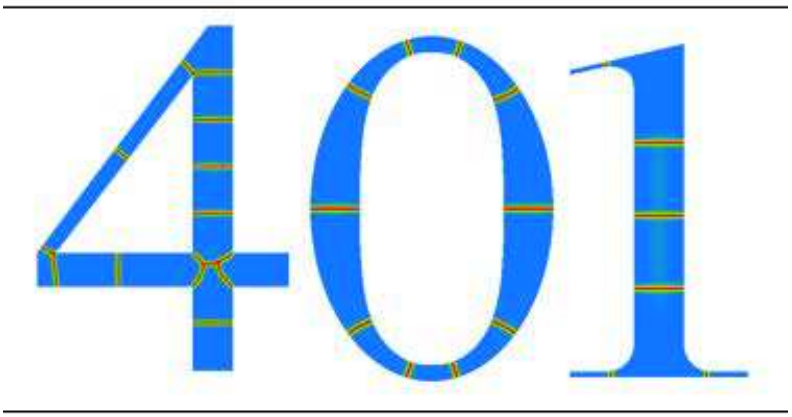

(b) Numerical experiment inspired by the real life example. We reproduce the main qualitative features of the observed crack pattern: nucleation at weak singularities, multiple cracking in the smooth domain, periodic fissuration of slender segments. The imposed load corresponds to $t = 1.75$.

Figure 4.14: Qualitative comparison of the crack pattern obtained in the numerical experiment to that observed. Proscribing debonding, the free parameters are, other than the Poisson ratio, the relative stiffness κ and the load intensity.

4.3.4 *Ouverture*: a strongly coupled two-dimensional pattern

As last example, we provide some elements of analysis of an interesting scenario in which a strong coupling between transverse fracture and debonding produces a pattern, proper to the two-dimensional setting, that shows a novel phenomenology related to the existence of the internal length scale. In fact, the cooperation of debonding and transverse cracking renders possible the release of stored elastic energy in a regime in which neither isolated propagation of channeling cracks nor extended debonding is energetically favorable. It is indeed their coupling, across distances that are long compared to the thickness of the film system, that produces a stable propagating front consisting of two transverse cracks separated by a debonded region. These patterns have been systematically reproduced by [SW03]. More recently, a single motif of the propagating coupled front is isolated and robustly reproduced in [Mar+13]. This pattern has been obtained for film systems that are stable, at a given load, with respect to channel cracking, by progressively reducing the debonding toughness. This is, recalling the expression of the non-dimensional parameters (3.34), by reducing γ in a thin film system for which the value of κ does not allow for channeling cracks, under the given load. We expect that such coupling be captured by our reduced model (3.9) as a phenomenon related to the existence of the internal length scale ℓ_e.

Preliminary results show that, indeed, with the proposed reduced model we are able to:

- Show that the parallel, straight propagation of the coupled front is possible for a given spacing $\bar{d}$. An estimation based on energy stationarity, namely:

$$-\frac{\partial}{\partial l}P_t(l,d) = \frac{\partial}{\partial l}S_t(l,d)$$

  can be solved to obtain $\bar{d}$. Here $P_t(l,d)$ is the elastic energy associated to two cracks of length l separated by a debonded region of width d. The associated energy release rate is computed analytically as a boundary value problem by differentiation with respect to the domain [DD81].

- Capture the regime of material parameters in which such pattern is observed in the experimental setting. For the solution $\bar{d}$ found above, the relative toughness has to verify $\gamma \leq 1$, that is, this coupled regime can be found only in the case of low adhesion, as in the experiments.

- Estimate the critic load for the propagation. The onset of the propagation is dominated by localized debonding, an estimation of the boundary displacement provides an estimation of the lower bound for the critic load, namely:

$$t_c \gtrsim \sqrt{\gamma}.$$

- Place this regime within its natural limits of channeling cracks propagation and extensive debonding. The energy estimate gives a solution in the low adhesion

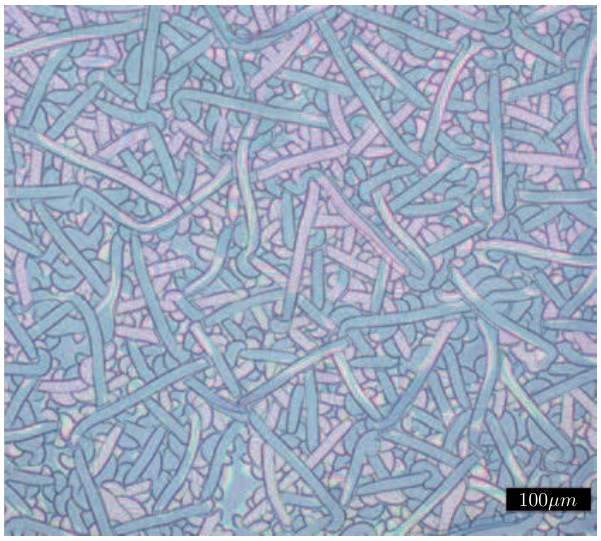

(a) Coupled propagation of transverse cracks and debonding produces a front of parallel propagating cracks with debonding in between. An optimal distance emerges robustly [Mar+13]. Similar patterns are also obtained by [SW03].

(b) A single motif of a coupled propagating front, isolated by [Mar+13].

Figure 4.15: A regime exists in which the cooperation between transverse cracks and debonding produces a stable self-organized propagating front which shows an optimal distance.

regime for loads t such that $0 \leq t < \sqrt{2\gamma} < \sqrt{2}$. This means that this regime can be observed for loads unable to trigger neither extensive debonding nor isolated channel cracking. Numerical experiments show indeed that such propagation mode is observed in the regime:

$$\sqrt{\gamma} \leq t \leq \sqrt{2\gamma},$$

that is for loads above the localized debonding threshold, and below the extended debonding threshold.

- Obtain a numerical estimation equilibrium distance, coherent to the order of magnitude suggested by laboratory experiments. In terms of internal length units ℓ_e, the equilibrium distance (see Figure 4.16(b)) is of order $(10 \div 20)$-ℓ_e. This entails the existence of three separated length scales in the numerical experiment, namely $\eta \ll \ell_e \ll L$. A screenshot of a computed evolution is shown in Figure 4.16. The pattern has shown to be insensitive to variations of the initial conditions, namely the initial length l_0 and spacing of the initial two cracks d_0, see Figure 4.16(a).

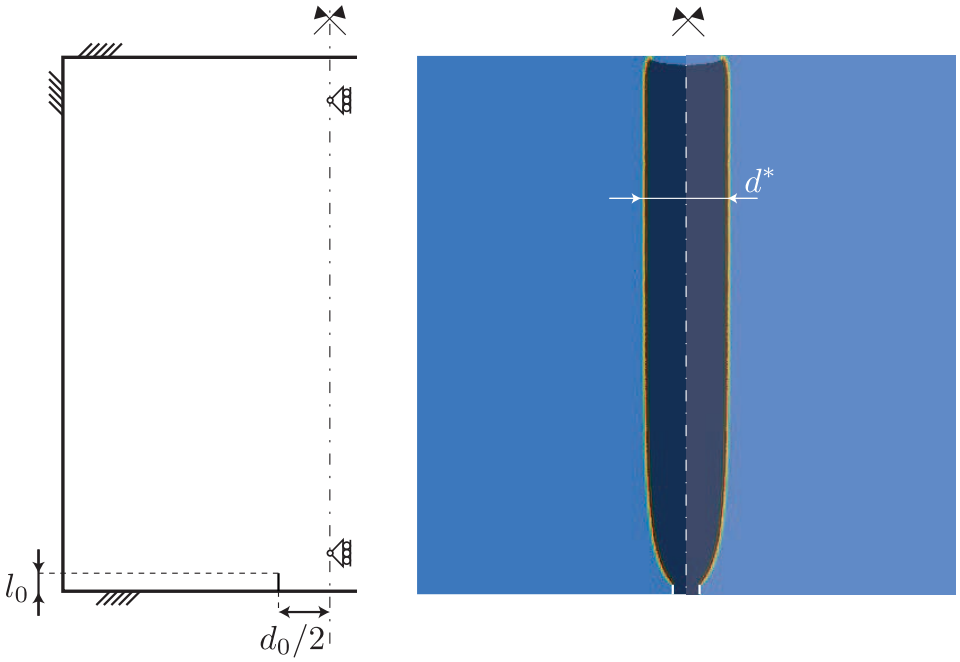

(a) The schematics of the experiment. We solve on a symmetric domain, since straight propagation is observed also in numerical experiments on the full domain.

(b) The final crack pattern. The strong coupling between transverse cracks and debonding manifests the optimal distance d^*.

Figure 4.16: Schematics and outcome of the numerical experiment, whose parameters are: $d_0 = 0.05, l_0 = 0.02, \ell_e = 0.015, \gamma = 0.45$. The computed patterns are insensitive of d_0 (both from above and below the optimal distance d^*), l_0, and also essentially insensitive of the boundary conditions.

4.4 Conclusions of the chapter

We have shown several numerical experiments based on the application of the two-dimensional model of transverse fracture and debonding of a bonded film, obtained by the asymptotic study presented in Chapter 2, to the case of vectorial elasticity. Notwithstanding the strong simplifications, the proposed model seems to be able to recover the main qualitative effects observed in experiments and provide a first unified framework to perform numerical experiments of the coupled transverse fracture and debonding problem without any a priori hypotheses on the crack shape.

The experiments performed on the thin strip, shown in Section 4.3.1, validate the numerical code against the closed form solutions studied in Chapter 2. We are able to capture numerically the properties, established analytically, of transverse fractures and debonded regions and of their mutual interplay. The computed evolutions show sequential, cascade, appearance of periodic cracks in the film, the onset of debonding

at the free boundaries, and provide coupled evolutions consisting in a cascade of cracks prior to the onset of debonding in each of the split segments.

We provide a quantitative explanation of the critical loads for transverse cracking encountered in the numerical experiments. Such critical loads manifest the richness of the underlying gradient damage model used in the numerical approximation of the brittle fracture problem. Such regularized model introduces the notion of a critical stress above which the sound body cannot be in equilibrium. This, in turn, drives the localization of damage into fractures. Consequently, fractures are a consequence of the loss of stability of the current state which jumps into a new stable state. Along this transition, the elastic energy released is dissipated to create new cracks. An interesting regime exists for small values of the elastic characteristic length ℓ_e, not shown here, in which a sound bar attains its critical state (*i.e.* $\sigma = \sigma_c$) for very high loads. It ensues a sudden, *i.e.* not sequential, formation of a periodic crack pattern, its spacing depending on the characteristic length scales of the system. The bifurcation of the initial state is ruled by the convexity properties of the energy. This regime, which is clearly not existent in the case considered in Chapter 2, deserves further investigation, profiting from the availability of analytical (and semi-analytical) tools for a complete study.

The fully two-dimensional experiment on a circular wafer, presented in Section 4.3.2, shows the capabilities of our approach to capture complex patterns, both with respect to their geometry and to the time evolution. We recover, coherently with mechanical intuition, many of the features observed in laboratory experiments regarding the evolution of cracks in such complex systems. Cracks approaching free boundaries and existing fractures form right junctions, whereas those nucleating at sound points within the bulk of the body form equi-triangular star shaped junctions, *i.e.* cracks join at $2\pi/3$. In this situation, cracks arrange into an hexagonal network, the size of the cells being function of the internal length scales. This is qualitatively coherent with laboratory observations which show that a regime exist where the nucleation of a periodic network, of a clearly distinguishable length scale, showing $2\pi/3$-junctions is preferred over the propagation of isolated running cracks. Analogously to the one-dimensional case, the computed evolutions consist in a first phase of multiple transverse cracking followed by extensive debonding from the boundaries. This is the manifestation in two-dimensions of the size effect discussed in Chapter 2. It is interesting at this point, to perform a more detailed study of the correlation between the characteristic length scale and that of the manifested periodic crack pattern. Unlike in the $1D$ case, this can reasonably be done only numerically. Also the other regime, that dominated by isolated running cracks, is under current numerical investigation.

A third set of numerical experiments is inspired by a real life example. We perform a fracture experiment of a geometrically complex lettering panel. In this case, the visual comparison is of striking fidelity. The robust crack patterns observed in real life are well captured, in addition we compute a temporal evolution that seems coherent to what the analysis of the pictures suggests.

A totally new regime, observed in laboratory experiments, is also isolated in the numerical experiments. It consists in a strongly coupled fracture and debonding front. Promising preliminary results open the way for the semi-analytical and numerical study

of a completely new regime, inexistent in one-dimension, that determines a wide set of fracture patterns such as stable parallel cracks, oscillating fractures and single or multiple spiraling cracks. In all these cases the fundamental ingredient seems to be, once again, a size effect that fixes an optimal distance for the propagation of the coupled front. The internal elastic length scale of the proposed model seems to be right one to capture this complex scenario. However, new challenges arise in the mechanical modeling. They are essentially linked to the existence, in laboratory experiments, of a characteristic *velocity* of propagation. The latter is low, not attributable to dynamic effects, and provided by some other physical mechanisms. Ongoing studies are dedicated to the investigation of a possible diffusive or poro-elastic couplings, susceptible to determine the velocity of propagation of the front.

Conclusions and perspectives

We have studied the phenomena of fracture and debonding in thin film systems in the framework of variational mechanics. The reference system is a three-dimensional brittle-elastic layer consisting in a thin film bonded to a rigid substrate by an intermediate layer.

The study of the elastic case without fractures, Section 3.1, allows us to proceed to a parametric study of the different regimes arising as asymptotic limits, depending upon the order of magnitude of the ratios of geometrical and mechanical parameters. Among all limit models, one interesting regime emerges. A non-trivial coupling of energies associated to two different elastic mechanisms, namely membrane deformations in the film and shear in the middle layer, determines an asymptotic regime in which a characteristic length scale emerges, just hidden in the three-dimensional equations. This limit regime is indeed proper to a wide class of three-dimensional systems. In this sense, we find a class of equivalence for elastic multilayer systems, which in the limit, behave as a linear membrane upon an elastic foundation. In the preliminary observation of the natural phenomenology, the existence of such length scale was estimated to be of primary importance in order to understand the complex mechanisms of multiple fissuration and debonding. This particular regime calls for further investigation in order to study the interplay between fracture mechanisms and elasticity.

We proceed in Section 3.3 to deepen the study of one instance of this equivalence class, *i.e.* the particular case of a thin stiff film bonded to a rigid substrate by a compliant bonding layer. We now consider also fracture. Based on energetic considerations, we identify a regime in which a possible interplay exists between cracks in the film and cracks within the bonding layer. The study of the brittle fracture problem in the setting of variational fracture mechanics provides a rigorous framework to investigate the nucleation and the evolution of complex crack patterns, both in space and time. This allows us to derive the properties of crack surfaces, based on an energy optimality principle, instead of postulating them. By prescribing a scaling law on the relevant quantities (namely, thicknesses, stiffnesses and toughnesses), we perform an asymptotic study as the small parameters tend to their natural limit. We obtain a limit, two-dimensional model which accounts for the interplay between elasticity and fracture, both in the film and in the bonding layer. Moreover, the asymptotic analysis characterizes the nature of cracks surfaces: fractures in the film are transverse and cut the entire thickness of the layer, whereas fractures in the bonding layer are planar regions across which no stress is transferred between the film and the underlying substrate. In the limit two-dimensional

model, the former are curves and the latter are surfaces, *i.e.* they have codimension 1 and 0 respectively. This study rigorously justifies the choice of such limit model in the past literature, previously made only on the basis of mechanical intuition. Finally, we state the static and evolution problems. The latter allows to study the evolution of irreversible fractures under increasing loads.

The rate-independent, irreversible, asymptotic model is rich. Already in dimension one, which is studied in depth in Chapter 2, it captures many features observed in these systems: periodicity of cracks in the film, peripheral debonding and sequential cascade appearance of cracks. The exploration of the fundamental features of the equilibrium states culminates in the univocal determination of the evolution of a one-dimensional film under increasing load: it necessarily consists in n sequential, cascade, periodic cracks and *then* simultaneous peripheral debonding in each segment. This is the way in which the size effect associated to the internal length scale, is revealed in one-dimension: it essentially discriminates between two mutually exclusive phases, one of periodic fissuration and one of extensive debonding.

We propose in Chapter 4 to apply the asymptotic results to the case of two-dimensional vector elasticity and perform numerical experiments. The nature of the two failure modes naturally demands for a different numerical treatment. We approximate the energy of the brittle elastic body by a regularized gradient damage model. This approximation renders the problem treatable from the numerical standpoint and is justified both from a mathematical and a mechanical point of view. Moreover, the gradient damage approximation is richer than the original brittle fracture model. Its implications are discussed in some detail in the set of numerical experiences devoted to the verification of the numerical model against the one-dimensional analytic solutions. Fully two dimensional experiments confirm the capabilities of the proposed formulation to capture the appearance of complex crack patterns whose essential features are in agreement with those observed in laboratory experiments. From the few numerical simulations performed, many different regimes arise: that dominated by possible local inhomogeneities and macroscopic effects at the scale of the structure, leading to nucleation at the singularities and successive bisections by channeling cracks; that in which the elastic characteristic length scale is revealed by fractures arranged in a network of quasi-periodic polygons, showing the emergence of macroscopic self-organized patterns; that of coupled and simultaneous propagation of a fracture and debonding front, opening the way for the interpretation of other geometrically involved crack patterns. The advantage of the proposed numerical approach is that it makes it possible to perform experiments that encompass the full evolution of fractures and all the stages of cracking, studying the effects of the film's and interface's properties separately, or jointly, via the four non-dimensional parameters that identify one single experiment.

At this point, a necessary further step has to be taken, after that of the observation of the natural phenomena and subsequent theoretical abstraction. Indeed, now, the quantitative comparison with experimental evidence is foreseen, allowing to corroborate the first elements of qualitative investigation already performed. Our results, indeed, rely on several strong assumptions which may be difficult to reproduce experimentally. Nonetheless, the small number of non-dimensional parameters to be identified in the

proposed model can turn helpful in the experimental comparison. It is further to be assessed which, and to what extent, other physical mechanisms may possibly play an important role.

From a more general standpoint, the asymptotic approach (and not the asymptotic techniques!) plays a foremost role throughout the whole work. It has indeed allowed us to reveal the existence of an internal elastic length scale for a class of elastic systems, and the nature of crack surfaces in brittle multilayers, that is the essential properties of the systems in our concerns. Aware of the power of this approach, care must be taken when, in the mechanical modeling, *new* characteristic scales and "small parameters" are introduced. Their presence, or lack thereof, has indeed to be seen already as the result of a suitable asymptotic process, which determines implicitly an order relation between the different scales. This applies, for instance, when we introduce the damage length scale η (associated to the width of regularized cracks) through the gradient damage model regularizing the limit two-dimensional brittle system. This successive construction of asymptotic models implies an order relation between the small parameter ε of the geometric and constitutive scaling law, and the internal length of the damage model η. This order relation is not anodyne since in general "asymptotic limits do not commute". Precisely, it means that $\varepsilon \ll \eta$. Moreover, attention should payed in situations where the internal characteristic length scale ℓ_e becomes small, possibly comparable to η, due *e.g.* to successive film cracking. Indeed, while for "large" ℓ_e cracking in the film and in the bonding layer responds essentially to first order stability conditions, when ℓ_e is "small" transverse cracks are essentially dominated, not by first order, but by *second* order stability conditions. This interesting behavior deserves further investigation. The same caution is expected for the advocated introduction, at the end of Chapter 4, of a time scale to take account of the velocity of the propagating coupled transverse cracks and debonding front. In fact, the underlying fracture model is itself quasi-static, in other words, it is a limit model for suitably "slow" loads in more general rate-dependent process. This latter regime is radically different and still much less known than the quasi-static limit. Hence, the introduction of a time scale could have a profound impact in the physics of the model, *i.e.* it may be a *singular perturbation*. Nonetheless, preliminary results, not presented here, show that a mechanically reasonable diffusion process associated to crack advance that modifies locally the material properties (like in corrosive cracks) is a *regular perturbation* of the model presented here: it does not alter the phenomenology associated to fracture (*i.e.* the crack pattern is the same) but manifests the propagative character of the front at finite velocity. In conclusion, the variational approach to the analysis of fracture and debonding of a thin film system presented here, as an instance of an *irreversible*, *rate-independent* problem with a *singular perturbation*, motivates to tackle other problems arising in different fields of solid mechanics. One of possible interest is that of phase transformation in alloys. Indeed, valuable results, both from a theoretical and numerical standpoint, have been obtained in this domain with the use of energetic theories, based on the introduction of mesoscopic internal variables accounting for the presence and features of the different phases. Here, inelastic behavior resulting in the formation of micro-structures, hysteretic response and the consequent multi-scale coupling, manifest a very appealing scenario for future investigation.

❧

Appendix A

Scientific contribution

Part of the material presented in this work has been proposed to the scientific community in papers in international peer reviewed journals and proceedings of international conferences. We list here these contributions.

Papers in peer reviewed journals

[Leó+13a] A. A. León Baldelli et al. "A variational model for fracture and debonding of thin films under in-plane loadings". In: *(submitted for review)* (2013).

[Leó+13d] A. A. León Baldelli et al. "Fracture and debonding of a thin film on a stiff substrate: analytical and numerical solutions of a one-dimensional variational model". In: *Continuum Mechanics and Thermodynamics* 25.2-4 (May 2013), pp. 243–268. ISSN: 0935-1175.

Contributions in peer reviewed conference proceedings

[Leó+11] A. A. León Baldelli et al. "Étude de la multifissuration e délamination par l'approche variationnelle à la mécanique de la fracture". In: *10e Colloque National en Calcul des Structures*. Giens, 2011, pp. 1–8.

[Leó+12] A. A. León Baldelli et al. "Multifissuration and Debonding of Thin Films . Analytic and Numeric 1D Solutions Via a Variational Approach". In: *The 23rd International Congress of Theoretical and Applied Mechanics*. Vol. 1. August. Beijing, PRC, 2012.

[Leó+13b] A. A. León Baldelli et al. “Complex crack patterns: transverse fractures and delamination in thin film systems”. In: *Third International Conference on Computational Modeling of Fracture and Failure of Materials and Structures*. Vol. 43. June. Prague, 2013.

[Leó+13c] A. A. León Baldelli et al. “Delamination and fracture of thin films: a variational approach.” In: *Direct and variational methods for nonsmooth problems in mechanics*. Amboise, 2013.

Bibliography

[AB08a] B. Audoly and A. Boudaoud. "Buckling of a stiff film bound to a compliant substrate—Part I: Formulation, linear stability of cylindrical patterns, secondary bifurcations". In: *Journal of the Mechanics and Physics of Solids* 56.7 (July 2008), pp. 2401–2421. ISSN: 00225096.

[AB08b] B. Audoly and A. Boudaoud. "Buckling of a stiff film bound to a compliant substrate—Part II: A Global Scenario for the Formation of the Herringbone pattern". In: *Journal of the Mechanics and Physics of Solids* 56.7 (July 2008), pp. 2422–2443. ISSN: 00225096.

[AB08c] B. Audoly and A. Boudaoud. "Buckling of a stiff film bound to a compliant substrate—Part III: Herringbone solutions at large buckling parameter". In: *Journal of the Mechanics and Physics of Solids* 56.7 (July 2008), pp. 2422–2443. ISSN: 00225096.

[ABZ07] N. Ansini, J.-F. Babadjian, and C. I. Zeppieri. "The Neumann Sieve Problem and Dimensional Reduction: a Multiscale Approach". In: *Mathematical Models and Methods in Applied Sciences* 17.05 (May 2007), pp. 681–735. ISSN: 0218-2025.

[ACM97] L. Ambrosio, A. Coscia, and G. D. Maso. "Fine Properties of Functions with Bounded Deformation". In: *Archive for Rational Mechanics and Analysis* 139.3 (Oct. 1997), pp. 201–238. ISSN: 0003-9527.

[AFP00] L. Ambrosio, N. Fusco, and D. Pallara. *Functions of Bounded Variation and Free Discontinuity Problems*. Oxford: Oxford University Press, 2000.

[AJB02] J. M. Ambrico, E. E. Jones, and M. R. Begley. "Cracking in thin multi-layers with finite-width and periodic architectures". In: *International Journal of Solids and Structures* 39.6 (Mar. 2002), pp. 1443–1462. ISSN: 00207683.

[All91a] G. Allaire. "Homogenization of the Navier-Stokes equations in open sets perforated with tiny holes II: Non-critical sizes of the holes for a volume distribution and a surface distribution of holes". In: *Archive for Rational Mechanics and Analysis* 113.3 (1991), pp. 261–298. ISSN: 0003-9527.

[All91b] G. Allaire. "Homogenization of the Navier-Stokes equations in open sets perforated with tiny holes I. abstract framework, a volume distribution of holes". In: *Archive for Rational Mechanics and Analysis* 113.3 (1991), pp. 209–259. ISSN: 0003-9527.

[AM00] R. Abdelmoula and J.-J. Marigo. "The effective behavior of a fiber bridged crack". In: *Journal of the Mechanics and Physics of Solids* 48.11 (Nov. 2000), pp. 2419–2444. ISSN: 00225096.

[Amb89] L. Ambrosio. "A compactness theorem for a new class of functions of bounded variation". In: *Boll. Un. Mat. Ital. B* 7.4 (1989), pp. 857–881.

[AMV] R. Alessi, J.-J. Marigo, and S. Vidoli. "Nucleation of cohesive cracks in gradient damage models coupled with plasticity". In: *Submitted for publication* ().

[Ans04] N. Ansini. "The nonlinear sieve problem and applications to thin films". In: *Asymptotic Analysis* 39 (2004), pp. 113–145.

[AR07] G. Allaire and A.-L. Raphael. "Homogenization of a convection–diffusion model with reaction in a porous medium". In: *Comptes Rendus Mathematique* 344.8 (Apr. 2007), pp. 523–528. ISSN: 1631073X.

[AT90] L. Ambrosio and V. M. Tortorelli. "Approximation of functionals depending on jumps by elliptic functional via Γ-convergence". In: *Communications on Pure and Applied Mathematics* 43.8 (Dec. 1990), pp. 999–1036. ISSN: 00103640.

[AT92] L. Ambrosio and V. M. Tortorelli. "On the approximation of Free Discontinuity Problems". In: *Bollettino dell'Unione Matematica Italiana* 7.6-B (1992), pp. 105–123.

[Bab06] J.-F. Babadjian. "Quasistatic evolution of a brittle thin film". In: *Calculus of Variations and Partial Differential Equations* 26.1 (Jan. 2006), pp. 69–118. ISSN: 0944-2669.

[Bal+12] S. Balay et al. *PETSc Users Manual*. Tech. rep. June. Argonne National Laboratory, 2012.

[Bar62] G. I. Barenblatt. "The Mathematical Theory of Equilibrium Cracks in Brittle Fracture". In: ed. by G. K. F. H. v. d. D. H.L. Dryden Th. von Kármán and L. Howarth. Vol. 7. Advances in Applied Mechanics. Elsevier, 1962, pp. 55–129.

[BC13] V. Balbi and P. Ciarletta. "Morpho-elasticity of intestinal villi". In: *Journal of the Royal Society, Interface / the Royal Society* 10.82 (May 2013), p. 20130109. ISSN: 1742-5662.

[BC94] G. Bellettini and A. Coscia. "Discrete approximation of a free discontinuity problem". In: *Numerical Functional Analysis and Optimization* 15.3-4 (Jan. 1994), pp. 201–224. ISSN: 0163-0563.

[BCD98] G. Bellettini, A. Coscia, and G. Dal Maso. "Compactness and lower semicontinuity properties in SBD(Ω)". In: *Mathematische Zeitschrift* 228.2 (June 1998), pp. 337–351. ISSN: 0025-5874.

[BDG99] A. Braides, G. Dal Maso, and A. Garroni. "Variational Formulation of Softening Phenomena in Fracture Mechanics: The One-Dimensional Case". In: *Archive for Rational Mechanics and Analysis* 146.1 (Apr. 1999), pp. 23–58. ISSN: 0003-9527.

[Ber+02] O. Bernard et al. "Mechanical and microstructural characterisation of oxide films damage". In: *Materials Science and Engineering A* 335.1-2 (Sept. 2002), pp. 32–42. ISSN: 09215093.

[Beu92] J. Beuth. "Cracking of thin bonded films in residual tension". In: *International Journal of Solids and Structures* 29.13 (Jan. 1992), pp. 1657–1675. ISSN: 00207683.

[BF01] A. Braides and I. Fonseca. "Brittle Thin Films". In: *Applied Mathematics and Optimization* 44.3 (Jan. 2001), pp. 299–323. ISSN: 0095-4616.

[BFF02] K. Bhattacharya, I. Fonseca, and G. Francfort. "An Asymptotic Study of the Debonding of Thin Films". In: *Archive for Rational Mechanics and Analysis* 161.3 (Feb. 2002), pp. 205–229. ISSN: 0003-9527.

[BFL02] G. Bouchitte, I. Fonseca, and G. Leoni. "A Global Method for Relaxation in $W^{1,p}$ and in SBV^p". In: *Archive for Rational Mechanics and Analysis* 165 (2002), pp. 187–242.

[BFM08] B. Bourdin, G. A. Francfort, and J.-J. Marigo. "The Variational Approach to Fracture". In: *Journal of Elasticity* 91.1-3 (2008), pp. 5–148. ISSN: 0374-3535.

[BG05] M. Ben Amar and A. Goriely. "Growth and instability in elastic tissues". In: *Journal of the Mechanics and Physics of Solids* 53.10 (Oct. 2005), pp. 2284–2319. ISSN: 00225096.

[BK96] J. Beuth and N. Klingbeil. "Cracking of thin films bonded to elastic-plastic substrates". In: *Journal of the Mechanics and Physics of Solids* 44.9 (Sept. 1996), pp. 1411–1428. ISSN: 00225096.

[BM06] M. Bialas and Z. Mroz. "Crack patterns in thin layers under temperature loading. Part I: Monotonic loading". In: *Engineering Fracture Mechanics* 73.7 (2006), pp. 917–938. ISSN: 00137944.

[BM07] M. Bialas and Z. Mroz. "An energy model of segmentation cracking of thin films". In: *Mechanics of Materials* 39.9 (2007), pp. 845–864. ISSN: 01676636.

[Bou00] B. Bourdin. "Numerical experiments in revisited brittle fracture". In: *Journal of the Mechanics and Physics of Solids* 48.4 (Apr. 2000), pp. 797–826. ISSN: 00225096.

[Bou02] B. Bourdin. "Image segmentation with a finite element method". In: *ESAIM: Mathematical Modelling and Numerical Analysis* 33.2 (Aug. 2002), pp. 229–244. ISSN: 0764-583X.

[Bou07] B. Bourdin. "Numerical implementation of the variational formulation for quasi-static brittle fracture". In: *Interfaces and Free Boundaries* (2007), pp. 411–430. ISSN: 1463-9963.

[Bra98] A. Braides. *Approximation of free-discontinuity problems*. Springer, 1998.

[Bre83] H. Brezis. *Analyse fonctionelle*. Masson, 1983.

[CB89] P. G. Ciarlet and F. Bourquin. "Modeling and justification of eigenvalue problems for junctions between elastic structures". In: *Journal of Functional Analysis* 87.2 (Dec. 1989), pp. 392–427. ISSN: 00221236.

[CB97] K. M. Crosby and R. M. Bradley. "Fragmentation of thin films bonded to solid substrates: Simulations and a mean-field theory". In: *Physical Review E* 55.5 (1997), pp. 6084–6091.

[CC00] B. Cotterell and Z. Chen. "Buckling and cracking of thin films on compliant substrates under compression". In: *International Journal of Fracture* (2000), pp. 169–179.

[CdR93] H. Colina, de Arcangelis L, and S. Roux. "Model for surface cracking." In: *Physical review. B, Condensed matter* 48.6 (Aug. 1993), pp. 3666–3676. ISSN: 0163-1829.

[CE03] T.-C. Chiu and F. Erdogan. "Debonding of graded coatings under in-plane compression". In: *International Journal of Solids and Structures* 40.25 (Dec. 2003), pp. 7155–7179. ISSN: 00207683.

[CFM09] A. Chambolle, G. A. Francfort, and J.-J. Marigo. "When and how do cracks propagate?" In: *Journal of the Mechanics and Physics of Solids* 57.9 (2009), pp. 1614–1622. ISSN: 00225096.

[CFM10] A. Chambolle, G. A. Francfort, and J.-J. Marigo. "Revisiting Energy Release Rates in Brittle Fracture". In: *Journal of Nonlinear Science* 20.4 (Apr. 2010), pp. 395–424. ISSN: 0938-8974.

[Cha+00] M. Charlotte et al. "Revisiting brittle fracture as an energy minimization problem: comparison of Griffith and Barenblatt surface energy models". In: *Damage and Fracture* (2000).

[Cha03] A. Chambolle. "A Density Result in Two-Dimensional Linearized Elasticity, and Applications". In: *Archive for Rational Mechanics and Analysis* 167.3 (May 2003), pp. 211–233. ISSN: 0003-9527.

[Cha04] A. Chambolle. "An approximation result for special functions with bounded deformation". In: *Journal de Mathématiques Pures et Appliquées* 83.7 (July 2004), pp. 929–954. ISSN: 00217824.

[Cia78] P. G. Ciarlet. *The Finite Element Method for Elliptic Problems*. Classics i. Philadelphia: SIAM, 1978.

[Cia88] P. G. Ciarlet. *Mathematical Elasticity Volume I: Three-Dimensional Elasticity*. Vol. 25. 5. Elsevier Science Publishers, May 1988, p. 451.

[Cia90] P. G. Ciarlet. "A new class of variational problems arising in the modeling of elastic multi-structures". In: *Numerische Mathematik* 57.1 (Dec. 1990), pp. 547–560. ISSN: 0029-599X.

[Cia97] P. G. Ciarlet. *Mathematical Elasticity Volume II: Theory of Plates*. Amsterdam: North-Holland, 1997.

[CK92] H. Choi and K.-S. Kim. "Analysis of the spontaneous interfacial decohesion of a thin surface film". In: *Journal of the Mechanics and Physics of Solids* 40.1 (Jan. 1992), pp. 75–103. ISSN: 00225096.

[CL96] P. Ciarlet and V. Lods. "Asymptotic analysis of linearly elastic shells. I. Justification of membrane shell equations". In: *Archive for rational mechanics and analysis* 136.2 (Dec. 1996), pp. 119–161. ISSN: 0003-9527.

[CLM96] P. G. Ciarlet, V. Lods, and B. Miara. "Asymptotic analysis of linearly elastic shells. II. Justification of flexural shell equations". In: *Archive for Rational Mechanics and Analysis* 136.2 (Dec. 1996), pp. 163–190. ISSN: 0003-9527.

[CMP09] Y. Cohen, J. Mathiesen, and I. Procaccia. "Drying patterns: Sensitivity to residual stresses". In: *Physical Review E* 79.4 (Apr. 2009), p. 046109. ISSN: 1539-3755.

[Cox52] H. L. Cox. "The elasticity and strength of paper and other fibrous materials". In: *British Journal of Applied Physics* 3.3 (Mar. 1952), pp. 72–79. ISSN: 0508-3443.

[Dac04] B. Dacorogna. *Introduction to the Calculus of Variations*. London: Imperial College Press, 2004. ISBN: 0486673669.

[Dac92] B. Dacorogna. *Direct Methods in the Calculus of Variations*. Vol. 72. 3. 1992, pp. 239–239. ISBN: 9780387357799.

[DD81] P. Destuynder and M. Djaoua. "Sur une Interprétation Mathématique de l'Intégrale de Rice en Théorie de la Rupture Fragile". In: *Mathematical Methods in the Applied Sciences* 3.1 (Aug. 1981), pp. 70–87. ISSN: 01704214.

[DL72] G. Duvaut and J.-L. Lions. *Les inéquations en mécanique et physique*. Dunod, 1972, p. 387.

[DMP12] M. David, J.-J. Marigo, and C. Pideri. *Homogenized Interface Model Describing Inhomogeneities Located on a Surface*. Vol. 109. 2. Mar. 2012, pp. 153–187. ISBN: 1065901293745.

[DO04] G. Del Piero and D. R. Owen. *Multiscale Modeling in Continuum Mechanics and Structured Deformations*. Springer Wien New York, 2004.

[DT01] G. Del Piero and L. Truskinovsky. "Macro- and micro-cracking in one-dimensional elasticity". In: *International Journal of Solids and Structures* 38.6-7 (Feb. 2001), pp. 1135–1148. ISSN: 00207683.

[DT02a] G. Dal Maso and R. Toader. "A Model for the Quasi-Static Growth of Brittle Fractures: Existence and Approximation Results". In: *Archive for Rational Mechanics and Analysis* 162.2 (Apr. 2002), pp. 101–135. ISSN: 0003-9527.

[DT02b] G. Dal Maso and R. Toader. "A Model for the Quasi-Static Growth of Brittle Fractures: Existence and Approximation Results". In: *Archive for Rational Mechanics and Analysis* 162.2 (Apr. 2002), pp. 101–135. ISSN: 0003-9527.

[DTE88] M. Drory, M. Thouless, and A. Evans. "On the decohesion of residually stressed thin films". In: *Acta Metallurgica* 36.8 (Aug. 1988), pp. 2019–2028. ISSN: 00016160.

[Dug60] D. Dugdale. "Yielding of steel sheets containing slits". In: *Journal of the Mechanics and Physics of Solids* 8.2 (May 1960), pp. 100–104. ISSN: 00225096.

[Dun69] J. Dundurs. "Edge-bonded dissimilar orthogonal elastic wedges". In: *Journal of Applied Mechanics* 36 (1969).

[EDH88] A. G. Evans, M. D. Drory, and M. S. Hu. "The cracking and decohesion of thin films". In: *Journal of Materials Research* 3.05 (Jan. 1988), pp. 1043–1049. ISSN: 0884-2914.

[EM06] M. A. Efendiev and A. Mielke. "On the Rate-Independent Limit of Systems with Dry Friction and Small Viscosity". In: *Journal of Convex Analysis* 13.1 (2006), pp. 151–167.

[Eva89] H. Evans. "Cracking and spalling of protective oxide layers". In: *Materials Science and Engineering: A* 120-121 (Nov. 1989), pp. 139–146. ISSN: 09215093.

[FI13] M. Focardi and F. Iurlano. "Ambrosio-Tortorelli approximation of cohesive fracture models in linearized elasticity". In: (2013), pp. 1–16.

[FJM06] G. Friesecke, R. D. James, and S. Müller. "A Hierarchy of Plate Models Derived from Nonlinear Elasticity by Gamma-Convergence". In: *Archive for Rational Mechanics and Analysis* 180.2 (Jan. 2006), pp. 183–236. ISSN: 0003-9527.

[FL03] G. Francfort and C. J. Larsen. "Existence and convergence for quasi-static evolution in brittle fracture". In: *Communications on Pure and Applied Mathematics* 56.10 (Oct. 2003), pp. 1465–1500. ISSN: 0010-3640.

[FM98] G. Francfort and J.-J. Marigo. "Revisiting brittle fracture as an energy minimization problem". In: *Journal of the Mechanics and Physics of Solids* 46.8 (Aug. 1998), pp. 1319–1342. ISSN: 00225096.

[FS09] L. B. Freund and S. Suresh. *Thin Film Materials. Stress, Defect Formation and Surface Evolution*. Cambridge University Press, 2009, p. 770. ISBN: 9780521529778.

[Fuk+99] N. Fukugami et al. "Density measurement of thin glass layers for gas barrier films". In: *Journal of Vacuum Science & Technology A: Vacuum, Surfaces, and Films* 17.4 (1999), p. 1840. ISSN: 07342101.

[GCL89] E. Giorgi, M. Carriero, and A. Leaci. "Existence theorem for a minimum problem with free discontinuity set". In: *Archive for Rational Mechanics and Analysis* 108.4 (1989), pp. 195–218. ISSN: 0019-9710.

[Gia05] A. Giacomini. "Ambrosio-Tortorelli approximation of quasi-static evolution of brittle fractures". In: *Calc. Var. Partial Dif.* 22.2 (2005), pp. 129–172.

[GK94] A. Groisman and E. Kaplan. "An Experimental Study of Cracking Induced by Desiccation ." In: *Europhysics Letters* 25.6 (1994), pp. 415–420.

[GMM09] L. Goehring, L. Mahadevan, and S. W. Morris. "Nonequilibrium scale selection mechanism for columnar jointing." In: *Proceedings of the National Academy of Sciences of the United States of America* 106.2 (Jan. 2009), pp. 387–92. ISSN: 1091-6490.

[Goe+10] L. Goehring et al. "Evolution of mud-crack patterns during repeated drying cycles". In: *Soft Matter* 6.15 (2010), p. 3562. ISSN: 1744-683X.

[Gri21] A. A. Griffith. "The Phenomena of Rupture and Flow in Solids". In: *Philosophical Transactions of the Royal Society of London* 221 (1921), pp. 163–198.

[Han02] U. A. Handge. "Analysis of a shear-lag model with nonlinear elastic stress transfer for sequential cracking". In: *Journal of Materials Science* 37 (2002), pp. 4775–4782.

[HS91] J. W. Hutchinson and Z. Suo. "Mixed mode cracking in layered materials". In: *Advances in Applied Mechanics* 29 (1991), pp. 63–191.

[HS93] S. Ho and Z. Suo. "Tunneling Cracks in Constrained Layers". In: *Journal of Applied Mechanics* 60.4 (1993), p. 890. ISSN: 00218936.

[HSB96] T. Hornig, I. Sokolov, and A. Blumen. "Patterns and scaling in surface fragmentation processes". In: *Physical Review E* 54.4 (Oct. 1996), pp. 4293–4298. ISSN: 1063-651X.

[Hsu01] C.-H. Hsueh. "Analyses of Multiple Film Cracking in Film/Substrate Systems". In: *Journal of the American Ceramic Society* 84.12 (Dec. 2001), pp. 2955–2961. ISSN: 00027820.

[Hua+03] R. Huang et al. "Channel-cracking of thin films with the extended finite element method". In: *Engineering Fracture Mechanics* 70.18 (Dec. 2003), pp. 2513–2526. ISSN: 00137944.

[Hut96] J. W. Hutchinson. "Stresses and Failure Modes in Thin Films and Multilayers". In: *Thin Films* October (1996).

[Irw58] G. R. Irwin. "Fracture". In: *Elasticity and Plasticity*. Ed. by S. Flugge. Springer-Verlag, 1958.

[JHK90] H. M. Jensen, J. W. Hutchinson, and K. Kyung-Suk. "Decohesion of a cut prestressed film on a substrate". In: *International Journal of Solids and Structures* 26.9-10 (Jan. 1990), pp. 1099–1114. ISSN: 00207683.

[Kit11] S. Kitsunezaki. "Crack growth in drying paste". In: *Advanced Powder Technology* 22.3 (May 2011), pp. 311–318. ISSN: 09218831.

[Kit99] S. Kitsunezaki. "Fracture patterns induced by desiccation in a thin layer". In: *Physical Review E* 60.6 Pt A (Dec. 1999), pp. 6449–64. ISSN: 1063-651X.

[KMR05] M. Kocvara, A. Mielke, and T. Rubicek. "A Rate-Independent Approach to the Delamination Problem". In: *Mathematics and Mechanics of Solids* 11.4 (Jan. 2005), pp. 423–447. ISSN: 1081-2865.

[Let+04] Y. Leterrier et al. "Mechanical integrity of transparent conductive oxide films for flexible polymer-based displays". In: *Thin Solid Films* 460.1-2 (July 2004), pp. 156–166. ISSN: 00406090.

[Let+10] Y. Leterrier et al. "Models for saturation damage state and interfacial shear strengths in multilayer coatings". In: *Mechanics of Materials* 42.3 (Mar. 2010), pp. 326–334. ISSN: 01676636.

[LHE95] D. Leung, M. He, and A. Evans. "The cracking resistance of nanoscale layers and films". In: *Journal of Materials Research* 10.07 (Mar. 1995), pp. 1693–1699. ISSN: 0884-2914.

[Lia03] J. Liang. "Evolving crack patterns in thin films with the extended finite element method". In: *International Journal of Solids and Structures* 40.10 (May 2003), pp. 2343–2354. ISSN: 00207683.

[Lio73] J.-L. Lions. *Perturbations Singulieres dans les Problemes aux Limites*. Berlin, Heidelberg, New York: Springer-Verlag, 1973. ISBN: 3540062645.

[LN00] K. Leung and Z. Néda. "Pattern formation and selection in quasistatic fracture". In: *Physical review letters* 85.3 (July 2000), pp. 662–5. ISSN: 0031-9007.

[LP11] V. Lazarus and L. Pauchard. "From craquelures to spiral crack patterns: influence of layer thickness on the crack patterns induced by desiccation". In: *Soft Matter* 7.6 (2011), p. 2552. ISSN: 1744-683X.

[Mar+] J. Marthelot et al. "Crescent and spiral cracks paths in thin films: when delamination cooperates with crack propagation". In: *(in preparation)* ().

[Mar+13] J. Marthelot et al. "Ruine de films minces par coopération entre rupture et délaminage". In: *Congrés Français de Mécanique*. Bordeaux, 2013, pp. 1–3.

[MBK13] A. Mesgarnejad, B. Bourdin, and M. Khonsari. "A variational approach to the fracture of brittle thin films subject to out-of-plane loading". In: *Journal of the Mechanics and Physics of Solids* (May 2013), pp. 1–32. ISSN: 00225096.

[Mea87] P. Meakin. "A simple model for elastic fracture in thin films". In: *Thin Solid Films* 151.2 (Aug. 1987), pp. 165–190. ISSN: 00406090.

[MFT05] G. D. Maso, G. A. Francfort, and R. Toader. "Quasistatic Crack Growth in Nonlinear Elasticity". In: *Archive for Rational Mechanics and Analysis* 176.2 (Feb. 2005), pp. 165–225. ISSN: 0003-9527.

[MHC01] O. Millet, A. Hamdouni, and A. Cimetière. "A classification of thin plate models by asymptotic expansion of non-linear three-dimensional equilibrium equations". In: *International Journal of Non-Linear Mechanics* 36.1 (Jan. 2001), pp. 165–186. ISSN: 00207462.

[MI13] G. D. Maso and F. Iurlano. "Fracture models as Γ-limits of damage models". In: *Communications on Pure and Applied Mathematics* 12.4 (2013).

[Mia94] B. Miara. "Jusitification of the asymptotic analysis of elastic plates, I. The linear case". In: *Asymptotic Analysis* 9 (1994), pp. 47–60.

[Mie05] A. Mielke. "Evolution of rate-independent systems". In: *Handbook of Differential Equations: Evolutionary Differential Equations*. October 2004. 2005.

[MM06] J.-J. Marigo and N. Meunier. "Hierarchy of One-Dimensional Models in Nonlinear Elasticity". In: *Journal of Elasticity* 83.1 (Mar. 2006), pp. 1–28. ISSN: 0374-3535.

[MS89] D. Mumford and J. Shah. "Optimal approximations by piecewise smooth functions and associated variational problems". In: *Communications on Pure and Applied Mathematics* 42.5 (July 1989), pp. 577–685. ISSN: 00103640.

[MT04] J.-J. Marigo and L. Truskinovsky. "Initiation and propagation of fracture in the models of Griffith and Barenblatt". In: *Continuum Mechanics and Thermodynamics* 16.4 (May 2004), pp. 391–409. ISSN: 0935-1175.

[MTL00] A. Mielke, F. Theil, and V. I. Levitas. *A variational formulation of rate-independent phase transformations using an extremum principle*. 2000.

[Mun+12] T. Munson et al. *TAO 2.1 Users Manual*. Tech. rep. Mathematics and Computer Science Division, Argonne National Laboratory, 2012.

[Nag+93] M. Nagl et al. "The tensile failure of nickel oxide scales at ambient and at growth temperature". In: *Corrosion Science* 35.5-8 (Jan. 1993), pp. 965–977. ISSN: 0010938X.

[NE93] M. M. Nagl and W. T. Evans. "The mechanical failure of oxide scales under tensile or compressive load". In: *Journal of Materials Science* 28.23 (Dec. 1993), pp. 6247–6260. ISSN: 0022-2461.

[Neg99] M. Negri. "The anisotropy introduced by the mesh in the finite element approximation of the mumford-shah functional". In: *Numerical Functional Analysis and Optimization* 20.9-10 (Jan. 1999), pp. 957–982. ISSN: 0163-0563.

[Ngu00] Q. S. Nguyen. *Stability and nonlinear solid mechanics*. Wiley, 2000. ISBN: 978-0-471-49288-7.

[NM96] R. Nahta and B. Moran. "Film cracking and debonding in a coated fiber". In: *International Journal of Fracture* 79.4 (1996), pp. 351–372. ISSN: 0376-9429.

[Pha+10] K. Pham et al. "Gradient Damage Models and Their Use to Approximate Brittle Fracture". In: *International Journal of Damage Mechanics* 20.4 (Nov. 2010), pp. 618–652. ISSN: 1056-7895.

[PM10a] K. Pham and J.-J. Marigo. "Approche variationnelle de l'endommagement : I. Les concepts fondamentaux". In: *Comptes Rendus Mécanique* 338.4 (Apr. 2010), pp. 191–198. ISSN: 16310721.

[PM10b] K. Pham and J.-J. Marigo. "Approche variationnelle de l'endommagement : II. Les modèles à gradient". In: *Comptes Rendus Mécanique* 338.4 (Apr. 2010), pp. 199–206. ISSN: 16310721.

[PMM11] K. Pham, J.-J. Marigo, and C. Maurini. "The issues of the uniqueness and the stability of the homogeneous response in uniaxial tests with gradient damage models". In: *Journal of the Mechanics and Physics of Solids* 59.6 (June 2011), pp. 1163–1190. ISSN: 00225096.

[PT98] G. del Piero and L. Truskinovsky. "A one-dimensional model for localized and distributed failure". In: *Le Journal de Physique IV* 08.PR8 (Nov. 1998), pages. ISSN: 1155-4339.

[Rhe+01] Y.-w. Rhee et al. "Contact-induced Damage in Ceramic Coatings on Compliant Substrates: Fracture Mechanics and Design". In: *Journal of the American Ceramic Society* 84.5 (May 2001), pp. 1066–1072. ISSN: 00027820.

[Ric68a] J. R. Rice. "A Path Independent Integral and the Approximate Analysis of Strain Concentration by Notches and Cracks". In: *Journal of Applied Mechanics* 35.2 (1968), pp. 379–386. ISSN: 00218936.

[Ric68b] J. R. Rice. "Mathematical Analysis in the Mechanics of Fracture". In: *Fracture: an Advanced Treatise*. Ed. by H. Liebowitz. Vol. 107. B2. New York, NY: Academic Press, 1968, pp. 191–311.

[RK04] T. Roubíček and M. Kružík. "Microstructure evolution model in micromagnetics". In: *Zeitschrift für angewandte Mathematik und Physik* 55.1 (Jan. 2004), pp. 159–182. ISSN: 0044-2275.

[RSZ09] T. Roubíček, L. Scardia, and C. Zanini. "Quasistatic delamination problem". In: *Continuum Mechanics and Thermodynamics* 21.3 (July 2009), pp. 223–235. ISSN: 0935-1175.

[San+07] E. Santanach Carreras et al. "Avoiding "mud" cracks during drying of thin films from aqueous colloidal suspensions." In: *Journal of colloid and interface science* 313.1 (Sept. 2007), pp. 160–8. ISSN: 0021-9797.

[Sán80] E. Sánchez-Palencia. *Non-Homogeneous Media and Vibration Theory*. Springer, 1980.

[San82] E. Sanchez-Palencia. "On the asymptotics of the fluid flow past an array of fixed obstacles". In: *International Journal of Engineering Science* 20.12 (Jan. 1982), pp. 1291–1301. ISSN: 00207225.

[SF93] R. Stringfellow and L. Freund. "The effect of interfacial friction on the buckle-driven spontaneous delamination of a compressed thin film". In: *International Journal of Solids and Structures* 30.10 (Jan. 1993), pp. 1379–1395. ISSN: 00207683.

[SL11] P. Szymczak and A. J. Ladd. "The initial stages of cave formation: Beyond the one-dimensional paradigm". In: *Earth and Planetary Science Letters* 301.3-4 (Jan. 2011), pp. 424–432. ISSN: 0012821X.

[SM12] P. Sicsic and J.-J. Marigo. “From Gradient Damage Laws to Griffith’s Theory of Crack Propagation”. In: *Journal of Elasticity* (Oct. 2012). ISSN: 0374-3535.

[SS92] J. Sánchez-Hubert and E. Sánchez-Palencia. *Introduction aux méthodes asympotiques et à l’homogénéisation*. Masson, 1992.

[SSF00] V. B. Shenoy, A. F. Schwartzman, and L. B. Freund. “Crack patterns in brittle thin films”. In: 1 100 (2000), pp. 1–17.

[Suo01] Z. Suo. “Fracture in Thin Films”. In: *Encyclopedia of Materials: Science and Technology (Second Edition)*. Ed. by E.-C. K. H. J. Buschow et al. Second Edi. Oxford: Elsevier, 2001, pp. 3290–3296. ISBN: 978-0-08-043152-9.

[SW03] M. Sendova and K. Willis. “Spiral and curved periodic crack patterns in sol-gel films”. In: *Applied Physics A: Materials Science & Processing* 76.6 (Apr. 2003), pp. 957–959. ISSN: 0947-8396.

[TA06] K. Toga and B. Alaca. “Junction formation during desiccation cracking”. In: *Physical Review E* 74.2 (Aug. 2006), p. 021405. ISSN: 1539-3755.

[Tho+11] M. D. Thouless et al. “Periodic cracking of films supported on compliant substrates.” In: *Journal of the mechanics and physics of solids* 59.9 (Sept. 2011), pp. 1927–1937. ISSN: 0022-5096.

[TOG92] M. Thouless, E. Olsson, and A. Gupta. “Cracking of brittle films on elastic substrates”. In: *Acta Metallurgica et Materialia* 40.6 (June 1992), pp. 1287–1292. ISSN: 09567151.

[TPI00] H. Tada, P. C. Paris, and G. R. Irwin. *The Stress Analysis of Cracks Handbook, Third Edition*. Three Park Avenue New York, NY 10016-5990: ASME, Jan. 2000. ISBN: 0791801535.

[VMA99] A. G. Varias, I. Mastorakos, and E. C. Aifantis. “Numerical simulation of interface crack in thin films”. In: (1999), pp. 195–207.

[Win67] E. Winkler. *Die Lehre von der Elasticität und Festigkeit*. 1867, p. 388.

[XH00] Z. C. Xia and J. W. Hutchinson. “Crack patterns in thin films”. In: *Journal of the Mechanics and Physics of Solids* 48 (2000), pp. 1107–1131.

[YH03] H.-H. Yu and J. W. Hutchinson. “Delamination of thin film strips”. In: *Thin Solid Films* 423.1 (Jan. 2003), pp. 54–63. ISSN: 00406090.

[YSE92] T. Ye, Z. Suo, and A. Evans. “Thin film cracking and the roles of substrate and interface”. In: *International Journal of Solids and Structures* 29.21 (Jan. 1992), pp. 2639–2648. ISSN: 00207683.

[YTN98] M. Yanaka, Y. Tsukahara, and N. Nakaso. “Cracking phenomena of brittle films in nanostructure composites analysed by a modified shear lag model with residual strain”. In: *Journal of Materials Science* 33.8 (Apr. 1998), pp. 2111–2119. ISSN: 0022-2461.